Universitat d'Alacant
Universidad de Alicante

DYNAMIC VISUAL SERVOING OF ROBOT MANIPULATORS: OPTIMAL FRAMEWORK WITH DYNAMIC PERCEPTIBILITY AND CHAOS COMPENSATION

Javier Pérez Alepuz

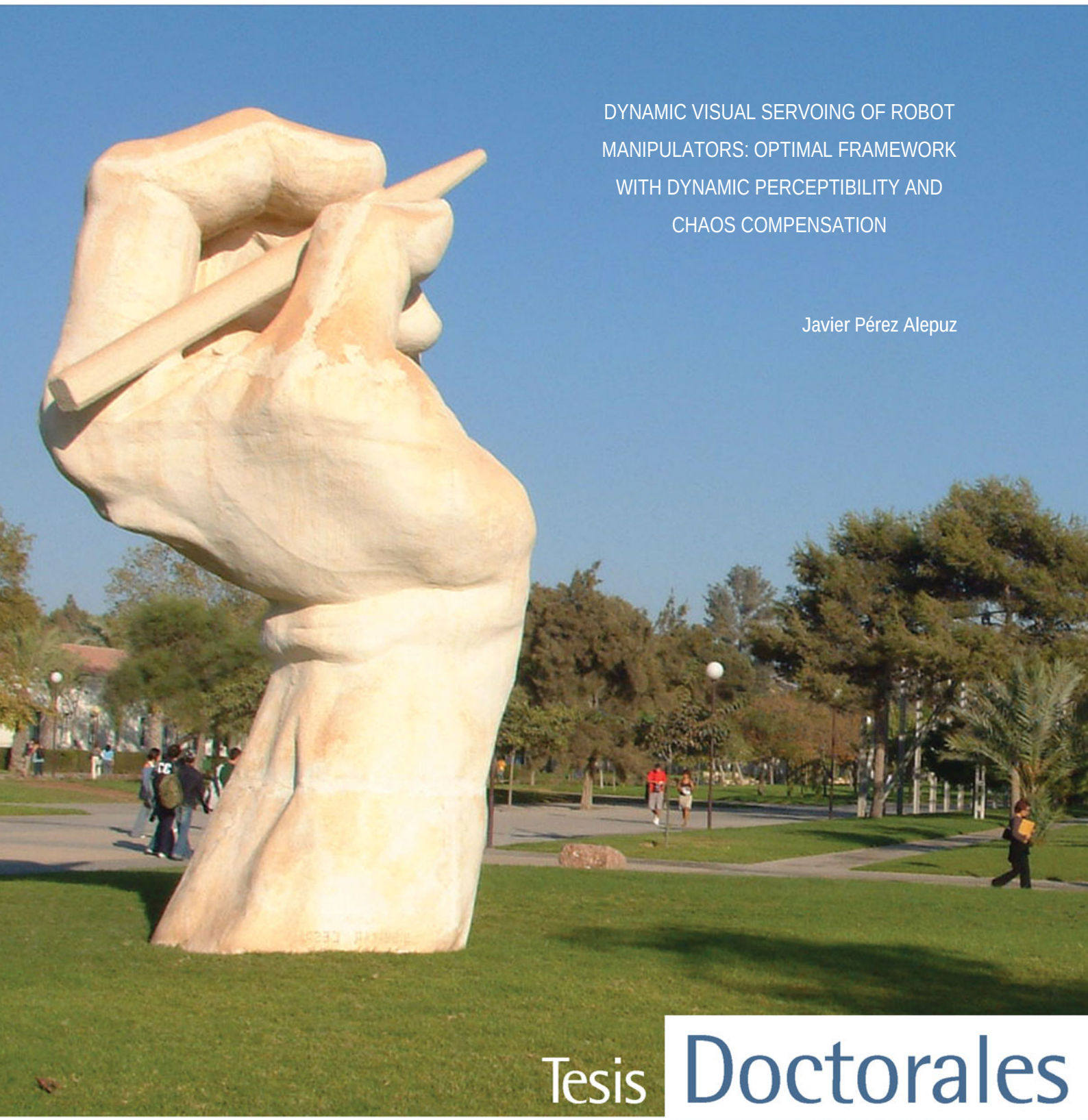

Tesis Doctorales

www.eltallerdigital.com

UNIVERSIDAD de ALICANTE

Universitat d'Alacant
Universidad de Alicante

DYNAMIC VISUAL SERVOING OF ROBOT MANIPULATORS: OPTIMAL FRAMEWORK WITH DYNAMIC PERCEPTIBILITY AND CHAOS COMPENSATION

Javier Pérez Alepuz

Tesis doctoral

Alicante, septiembre 2017

Universitat d'Alacant
Universidad de Alicante

University Institute for Computing Research
University of Alicante Polytechnic School

DYNAMIC VISUAL SERVOING OF ROBOT MANIPULATORS: OPTIMAL FRAMEWORK WITH DYNAMIC PERCEPTIBILITY AND CHAOS COMPENSATION

Javier Pérez Alepuz

Thesis presented for obtaining the
DOCTORAL DEGREE BY THE UNIVERSITY OF ALICANTE

MENCIÓN DE DOCTOR INTERNACIONAL
Doctorate in Computer Engineering

Supervised by:
Jorge Pomares Baeza
Gabriel Jesús García Gómez

Acknowledgments

This Thesis would not have been possible if it was not for all the wonderful people that surround me. It is incredible to realize how many people are involved in my life and I would like to thank them here:

To **Fernando Torres**, head of the AUROVA group; and to all the group members, for being there.

To my supervisor and friend **Jorge Pomares**, without whose help I would not have been able to finish this project. I really appreciate his guidance and understanding during the past years, and I felt the two of us made the perfect team.

To my co-supervisor and friend **Gabriel Jesús García,** for having the patience for teaching me hundreds of his 101 courses about every known topic. Our constant quarrels only hiding my eternal respect and admiration for him.

To my dearest friends who are nearby: **Ivan and Elena**, for making me a little smarter, constantly pushing me to see the world outside of the box, and widening my understanding of things. **Damián**, for his solid friendship, forgiving me every time I leave him stranded in the courses we take together. **María**, for always having nice words about me and tolerating me even when she knows I am *infected*. **Uki**, just for tolerating me. I know I can be a bit wearying at times. **Aiman**, for being so smart and solving all my electrical problems. **Ángel**, for waiting for me when I get behind. **Virginia and Kereck**, for making the transition through my graduate degree so much fun and so awesome. **Marcelo**, for ruining my diets. **Carlos**, for always being willing to give me his advice. **Andrés**, for teaching me so much about ridiculous stuff. Nerd.

Also, special thanks to **Reza Emami**, who welcomed me to do research with him and his team in Sweden. It truly was a memorable experience. And to all the

friends I made up there: **Maryam**, the childhood friend I never had and always needed. **Sandra**, and her kindness. **Teresa**, and her craziness. Also, Panta. **Tobias**, who knows so much about fancy stuff and does everything so much better than me. (I kick his butt at ping pong and bowling, though). **Leonard**, one of the best guys to have around. **Vijay**, and all his movies. **Mathias**, my Star Wars pal. Even if I didn't know more about you, I'd still like you.

To all my friends across the pond, whom I wish I could see more often: **Daniella**, the first real English teacher I ever had and my favorite Canadian mom. It was fun (and confusing) to start speaking English with you. **Sara**, for all her help with English related issues. She's also the best sword fighting badass I know, only she chose the wrong weapon over lightsabers. Lightsabers make everything better. **Emily and Joseph**, my *Smash Bros.* buddies. I really miss those games. **Joy and Jeff**, my adoptive American parents. I even have a certified diploma approved by cats. I love my adoptive family. **Katie**, and her aglets. **Mariel**, and her unicorns.

And last but not least, the family that is nearest to me: To **Marian**, my best cousin. To **Toni**, always willing to give me a hand anytime I ask him for help. To my **sister**, and her unconditional support no matter what crazy idea I have in mind, always pointing me in the right direction. She also gave me cutest niece, my young padawan. To my **father**, who keeps telling everyone how proud he is of me, even though I know it's just a stratagem for me to keep fixing things around his house. Also to my **father and sister**, I love you both so much. To my **mother**, who never got to see this project of mine fulfilled in life, but did get to see so many others. Thanks to her I am the person I am today. Wherever you are, I will keep trying to make you proud, and I will always carry you in my heart.

…and to the rest of the people that I probably forgot.

You guys rock,

Javi

Abstract

This Thesis presents an optimal framework with dynamic perceptibility and chaos compensation for the control of robot manipulators. The fundamental objective of this framework is to obtain a variety of control laws for implementing dynamic visual servoing systems. In addition, this Thesis presents different contributions like the concept of dynamic perceptibility that is used to avoid image and robot singularities, the framework itself, that implements a delayed feedback controller for chaos compensation, and the extension of the framework for space robotic systems.

Most of the image-based visual servoing systems implemented to date are indirect visual controllers in which the control action is joint or end-effector velocities to be applied to the robot in order to achieve a given desired location with respect to an observed object. The direct control of the motors for each joint of the robot is performed by the internal controller of the robot, which translates these velocities into joint torques. This Thesis mainly addresses the direct image-based visual servoing systems for trajectory tracking. In this case, in order to follow a given trajectory previously specified in the image space, the control action is defined as a vector of joint torques. The framework detailed in the Thesis allows for obtaining different kind of control laws for direct image-based visual servoing systems. It also integrates the dynamic perceptibility concept into the framework for avoiding image and robot singularities. Furthermore, a delayed feedback controller is also integrated so the chaotic behavior of redundant systems is compensated and thus, obtaining a smoother and efficient movement of the system. As an extension of the framework, the dynamics of free-based space systems is considered when determining the control laws, being able to determine trajectories for systems that do not have the base attached to anything. All these different steps are described throughout the Thesis.

This Thesis describes in detail all the calculations for developing the visual servoing framework and the integration of the described optimization techniques. Simulation and experimental results are shown for each step, developing the controllers in an FPGA for further optimization, since this architecture allows to reduce latency and can be easily adapted for controlling of any joint robot by simply modifying certain modules that are hardware dependents. This architecture is modular and can be adapted to possible changes that may occur as a consequence of the incorporation or modification of a control driver, or even changes in the configuration of the data acquisition system or its control. This implementation, however, is not a contribution of this Thesis, but is necessary to briefly describe the architecture to understand the framework's potential.

These are the main objectives of the Thesis, and two robots where used for experimental results. A commercial industrial robot: Mitsubishi PA10, and another planar three-degrees-of-freedom robot. This last one's design and implementation has been developed in the research group where the Thesis is written.

Resumen

La Tesis presenta un framework óptimo con perceptibilidad dinámica y compensación de caos para el control de robots manipuladores. El objetivo fundamental de este framework es obtener una variedad de leyes de control para implementar sistemas de control visual dinámicos. Además, esta Tesis especifica diferentes contribuciones como son el concepto de perceptibilidad dinámica usada para evitar singularidades en imagen y articulares, el framework mismo, que implementa un delayed feedback controller para la compensación de caos y la extensión del framework para sistemas robóticos espaciales.

La mayoría de los sistemas de control visual basados en imagen implementados hasta la fecha son indirectos, significando que la acción de control son velocidades a aplicar en las articulaciones o en el extremo del robot para conseguir un posicionamiento con respecto al objeto observado. El control directo de los motores para cada articulación es llevado a cabo por el controlador interno del robot, que traduce estas velocidades en pares articulares. Esta Tesis principalmente afronta el control visual directo basado en imagen para el seguimiento de trayectorias. En este caso, para seguir una trayectoria previamente especificada en el espacio imagen, la acción de control es definida como un vector de pares articulares. El framework detallado en la Tesis permite obtener diferentes leyes de control para sistemas de control visual directo basado en imagen. También integra el concepto de perceptibilidad dinámica dentro de dicho framework para evitar singulares articulares y en imagen. Además, un delayed feedback controller es también integrado para compensar el comportamiento caótico de sistemas redundantes y así obtener un movimiento más suave y eficiente del sistema. Como extensión del framework, la dinámica de sistemas espaciales de base flotante es considerada a la hora de obtener las leyes de control, siendo posible determinar

trayectorias para sistemas que no tienen la base anclada a ningún sitio. Todos estos diferentes pasos son descritos a lo largo de la Tesis.

La Tesis describe en detalle todos los cálculos para desarrollar el framework de control visual y la integración de las diferentes técnicas de optimización descritas. Resultados en simulación y experimentales se muestran para cada paso, desarrollando los controladores en una FPGA para mayor optimización, ya que éste tipo de arquitecturas permiten reducir latencias y pueden ser fácilmente adaptables para controlar cualquier robot articular simplemente modificando ciertos módulos que dependen del hardware. Esta arquitectura es modular y se puede adaptar a los cambios que pueden ocurrir como consecuencia de la incorporación o modificación de un controlador, o incluso a los cambios en la configuración del sistema de adquisición de datos o su estrategia de control. Esta implementación, no es sin embargo contribución de esta Tesis, pero se hace necesario describir brevemente la arquitectura para entender el potencial del framework.

Éstos son los objetivos principales de la Tesis, donde dos robots fueron usados para los resultados experimentales. Un robot comercial: Mitsubishi PA10, y otro robot planar de tres grados de libertad, siendo éste último diseñado e implementado en el grupo de investigación donde la Tesis ha sido escrita.

Index

1 Introduction

This Chapter details the main motivations for the development of this Thesis, defining the performed research belonging to different research projects. This Chapter also presents the main contributions to the field of direct visual servoing systems that are detailed throughout the Thesis.

Lastly, the organization of this Thesis is presented, indicating what topic is addressed for each Chapter.

1.1 Motivation

Computer vision systems of today are integrated in a big number of industrial applications as a way for detecting defects in production lines, object/pattern recognition, and surface scanning method, among other uses. Within these industrial applications, it is important to highlight visual servoing systems for robotic manipulators guidance. The main goal of visual servoing systems is the use of computer vision as a method for guidance of robots. These control systems are fed with the information acquired by one or several cameras, in a way that such controller determines the control actions for moving the manipulator during its task. As described throughout the Thesis, visual servoing systems are extensively widespread, not only in research laboratories, but also in a wide range of applications, from industrial robotics to service robotics. One of the aspects that favored the growth of visual servoing systems, its diffusion and extension of its applications is the increase of capture and processing capabilities of today's cameras, as well as the equipment used for processing data. This has allowed for computing bigger amount of information in less time, avoiding possible delays, and guiding the robot in a smooth manner. Despite the efforts from the last decade for improving different aspects in the development of these visual servoing

systems, even nowadays a great number of opened lines of research exist, where some like the improvement of the behavior of those denominated direct visual servoing systems should be noted. These controllers are different with respect the indirect or kinematic ones for the fact that take into account the robot's dynamics. The control action of direct visual servoing systems computes the joint torques to be applied to the guided manipulator. This way, the internal feedback loop of the motors is eliminated and thus, the employed feedback is used for directly generate the currents or joint torques to apply to the robot during the tracking. The Thesis presents an optimal control-based framework for defining direct image-based visual servoing laws. The proposed image-based controllers allow for not only perform positioning, but also the tracking of trajectories by employing 2-D information from the feedback. As described throughout the Thesis, the framework allows for generating different control laws with different dynamic characteristics and accuracies. Furthermore, this framework allows for unifying direct image-based visual servoing systems for trajectory tracking.

Another aspect this Thesis addresses is the detection and avoidance of singularities when a visual servoing tracking is being performed. It is well known that situations where a robot's Jacobian has no inverse exist. In other words, it is singular. When this happens, velocities computed for the joints are infinite, situation that in real life cannot happen since the motors can only give a limited torque. For this reason, singular situations need to be studied with the goal of avoiding them. Singularities usually correspond to the limits in the workspace or when two or more links are aligned. They cause loss of degrees of freedom, in other words, positions in the 3-D space where the end-effector of the manipulator cannot reach. The bibliography usually applies the concept of manipulability in an attempt to detect such singularities, or even develop strategies for avoiding them. Something similar to this happens when the singularities appears in the image space. Image-based visual servoing systems employ the concept of interaction matrix that relates the variation with respect to the time of extracted visual features

with the camera's relative velocity that observes such features. For image singularities, certain movements of the camera – situated at the robot's end-effector – cannot be perceived by using extracted features. The perceptibility is a scalar function that provides information about the possibility of the vision system to perceive the motion within its field of view by using only kinematics information. The concept of perceptibility has been previously proposed as a measurement of closeness to image singularities. This Thesis defines the concept of dynamic perceptibility. This concept constitutes an extension to perceptibility to take into account the employed robot's dynamic characteristics.

The last main section of the Thesis performs the extension of previously defined developments for the guidance of spacecraft and floating-base space manipulators. This research is the result of abroad stays in the Onboard Space Systems group at Luleå University of Technology, Division of Space Technology (Kiruna, Sweden), the first one from June 15th to September 17th, 2015 funded by the Doctoral School at the University of Alicante; and the second one from April 14th to July 13th, 2016 funded by a scholarship from the Generalitat Valenciana.

All above described the main components of the Thesis overall. However, the research does not only intend to implement new algorithms for avoiding existing limitations, but also to evaluate their impact when applied in real environments. For this, all different controllers were implemented by using the proposed software and hardware architecture for the control of two robots. One industrial robot Mitsubishi PA10 and a three-degrees-of-freedom robot developed and built by the research group in which this Thesis was written.

1.2 Thesis' framework

The first project where this Thesis worked on was "Visual-tactile-force guided control dexterous manipulation of rigid and elastic objects" (Manipulación diestra de objectos rígidos y elásticos con guiado mediante control visual-táctil-fuerza) funded by Ministerio de Economía y Competitividad (DPI2012-32390) and FEDER

funds. The objective of the project was the research of visual servoing and grasp-manipulation techniques oriented to their combined implementation for their application to industrial or service robotic tasks. This way, the intention is that proposed solutions can be successfully used on industrial environments for the manipulation of dangerous products or substances for humans, as well as today's environments with position or force restrictions. For some of these tasks, there is not always a knowledge of the object or substance to manipulate. For this reason, two systems are needed. A first visual perception system that allows for recognizing the object to be manipulated and supervised for any movement's trajectory, and a second robotic system that allows for both grasping and manipulation tasks. The intention is to imitate humans' manipulability capabilities and articular precision for tasks such grasping and contact perceptibility of objects (rugosity and surface shape), or tactile coordination for the turning of such objects. The Thesis' contribution to the project is the development of image-based visual servoing systems for the guidance of robotic manipulators. The main load of research fall in the optimization of such controllers for the implementation of control laws for direct visual servoing.

A second project where the Thesis worked on was "Embedded visual servoing robot manipulators by using FPGA reconfigurable hardware" (Control visual embebido de robots manipuladores utilizando hardware reconfigurable FPGA [GRE12-17]), funded by the Vicerrectorado de Investigación, Desarrollo e Innovación from the University of Alicante. The objective of this project was the research of visual servoing techniques embedded on FPGAs. For this, the different possibilities of connection between a fast-camera and a FPGA were studied. The use of an FPGA for image processing and compute the calculations needed for the control law require a free-flowing communication with the camera. Direct visual servoing systems require high-speed response components that improve the controller's precision by diminishing the feedback loop delay. In addition to the implementation of a direct controller on a FPGA for accelerating the image

processing, the project also allowed to add determinism to the computation of the control law, permitting to obtain an exact time iteration computation. Therefore, the Thesis allows for addressing the design of direct visual servoing systems that are then implemented on FPGAs.

Lastly, the research and developments carried out on the Thesis are being applied to the project "Multisensorial robotic system with dual manipulation for human-robot assistance tasks" (Sistema robótico multisensorial con manipulación dual para tareas asistenciales humano-robot [DPI2015-68087-R]) funded by Ministerio de Economía y Competitividad and FEDER funding. This project deals with the design, construction, control and programming of a robotic torso aiming to serve as assistance for manipulation tasks for people that present some sort of motor disability to help them with their quotidian tasks. For this, the torso employs two manipulator arms with two robotic hands at their end-effectors. Human-robot collaboration in one single environment for providing assistance demands a safe highly sensitive robotic system with sensorial functionalities. Furthermore, the system must be able to adapt itself to the environment for providing services and/or assistance and react in the face of specific situations, like collisions or unexpected changes in the environment. This project develops a multisensorial robotic system with these characteristics. This way, the robot must be able to adapt to changing, non-structured, dynamic environments while taking care of the human-robot interaction. For this reason, a vision-force-tactile-based system is included into the robotic manipulation system that allows for integrating the perceptive capabilities needed for the manipulation of unknown objects or that are not previously modeled. The Thesis focuses on the application of the visual servoing framework for guiding manipulators during the task.

1.3 Thesis' structure

Once the motivation and framework of the Thesis have been described, this Section briefly describes the way the Thesis is structured. Figure 1.1 shows a

diagram of the different chapters. After this first introductory chapter, a theoretical framework is described in Chapter 2. This theoretical framework includes a state of the art for visual servoing systems, paying special attention to image-based visual servoing systems, and allows for progressively focus on the contributions to the situation of the field today.

The three following chapters constitute the main core of the Thesis. The third chapter details the proposed direct visual servoing framework based on optimal control. Chapter 4 proposes the concept of dynamic perceptibility, including such concept in the framework defined in Chapter 3. Lastly, Chapter 5 extends the optimal control framework for guiding spacecraft and floating-base space robots.

The Thesis finishes with a chapter of conclusions in which the contribution, conclusions and future works are described.

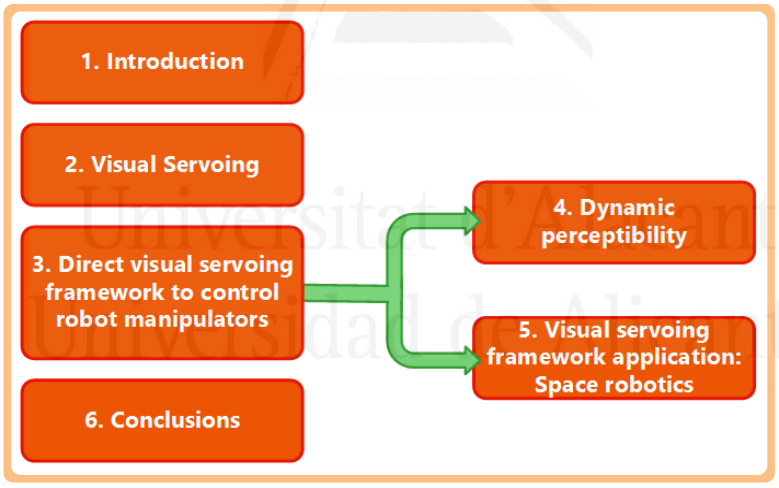

Figure 1.1. Thesis' structure

1.4 Thesis' goals

Finishing this introductory chapter, the objectives and main contributions carried out by the Thesis are described next.

The main goal of the Thesis is the development of a framework for defining new direct visual servoing control laws as well as their extension to spacecrafts

and floating-base space robots. This main objective can be itemized into the following points:

- Direct visual servoing research. Study of existing visual servoing laws of today and definition of a direct image-based visual servoing system for trajectories tracking.
- Design of a framework based on optimal control for defining direct image-based visual servoing laws with chaos compensation. Study of dynamic characteristics and precision of different generated dynamic controllers and their comparison with existing ones.
- Definition of the concept of dynamic perceptibility as a criterion that takes kinematics and dynamics characteristics into account for detection of image and robot singularities.
- Integration of the concept of dynamic perceptibility and dynamic manipulability into the proposed framework for avoiding singularities when the direct visual servoing is employed.
- Research and implementation of controllers for the guidance of spacecraft and space manipulators by using visual feedback.
- Extension of the direct image-based visual servoing framework for floating-based robots, allowing for the tracking of trajectories by considering not only the specific characteristics of such systems but also orbital dynamics.

1 Introducción

Este capítulo detalla las principales motivaciones para el desarrollo de esta Tesis, definiendo las investigaciones realizadas pertenecientes a diferentes proyectos de investigación. Este capítulo presenta también las principales contribuciones al campo de los sistemas de control visual directo que se detallan a lo largo de la Tesis. Por último, se presenta la organización de esta Tesis, indicando qué tema se aborda para cada Capítulo.

1.1 Motivación

Los sistemas de visión artificial de hoy en día están integrados en un gran número de aplicaciones industriales como una forma de detectar defectos en las líneas de producción, reconocimiento de objetos/patrones y métodos de exploración de superficies, entre otros usos. Dentro de estas aplicaciones industriales, es importante resaltar los sistemas de control visual para la manipulación de manipuladores robotizados. El objetivo principal de los sistemas de control visual es el uso de visión por computador como un método para guiar a los robots. Estos sistemas de control se alimentan con la información adquirida por una o varias cámaras, de tal manera que dicho controlador determina las acciones de control para mover el manipulador durante su tarea. Como se describe en la tesis, los sistemas de servo visual están ampliamente extendidos, no sólo en los laboratorios de investigación, sino también en una amplia gama de aplicaciones, desde la robótica industrial hasta la robótica de servicio. Uno de los aspectos que favoreció el crecimiento de los sistemas de control visual, su difusión y extensión de sus aplicaciones es el aumento de las capacidades de captura y procesamiento de las cámaras actuales, así como el equipo utilizado para el

procesamiento de datos. Esto ha permitido computar una mayor cantidad de información en menos tiempo, evitar posibles retrasos y guiar al robot de una manera suave. A pesar de los esfuerzos de la última década para mejorar diferentes aspectos en el desarrollo de estos sistemas de control visual, aún hoy en día existe un gran número de líneas abiertas de investigación, donde algunos como la mejora del comportamiento de los denominados sistemas de control visual directos. Estos controladores son diferentes con respecto a los indirectos o cinemáticos por el hecho de tener en cuenta la dinámica del robot. La acción de control de los sistemas de control visual directo calcula los pares de las articulaciones que se van a aplicar al manipulador guiado. De esta manera, se elimina el bucle interno de retroalimentación de los motores y, por tanto, se utiliza la realimentación empleada para generar directamente las corrientes o pares de torsión que se aplican al robot durante el seguimiento. La Tesis presenta un framework óptimo basado en el control para definir leyes de control visual directo basado en imagen. Los controladores basados en imágenes propuestos permiten no sólo realizar el posicionamiento, sino también el seguimiento de trayectorias empleando información bidimensional de la retroalimentación. Como se describe a lo largo de la Tesis, el framework permite generar diferentes leyes de control con diferentes características dinámicas y precisiones. Además, este framework permite la unificación de sistemas de control visuales directos basados en imagen para el seguimiento de trayectorias. Otro aspecto abordado en esta Tesis es la detección y elusión de las singularidades cuando se está realizando un seguimiento visual. Es bien sabido que las situaciones en las que el Jacobiano de un robot no tiene inversa existen. En otras palabras, es singular. Cuando esto sucede, las velocidades calculadas para las articulaciones son infinitas, situación que en la vida real no puede suceder ya que los motores sólo pueden dar un par limitado. Por esta razón, las situaciones singulares deben ser estudiadas con el objetivo de evitarlas. Singularidades por lo general corresponden a los límites en el espacio de trabajo o cuando dos o más enlaces están alineados. Causan pérdida de grados de libertad,

es decir, posiciones en el espacio 3-D donde el efector final del manipulador no puede alcanzar. La bibliografía generalmente aplica el concepto de manipulabilidad en un intento de detectar tales singularidades, o incluso desarrollar estrategias para evitarlas. Algo similar a esto sucede cuando las singularidades aparecen en el espacio de la imagen. Los sistemas de control visual basados en imágenes emplean el concepto de matriz de interacción que relaciona la variación con respecto al tiempo de las características visuales extraídas con la velocidad relativa de la cámara que observa tales características. Para las singularidades de la imagen, ciertos movimientos de la cámara - situados en el efector final del robot - no pueden ser percibidos usando las características extraídas. La perceptibilidad es una función escalar que proporciona información acerca de la posibilidad de que el sistema de visión perciba el movimiento dentro de su campo de visión usando solamente información cinemática. El concepto de perceptibilidad se ha propuesto previamente como una medida de la proximidad a las singularidades de la imagen. Esta Tesis define el concepto de perceptibilidad dinámica. Este concepto constituye una extensión de la perceptibilidad para tener en cuenta las características dinámicas del robot empleado.

La última sección principal de la Tesis realiza la extensión de desarrollos previamente definidos para el guiado de vehículos espaciales y manipuladores espaciales de base flotante. Esta investigación es el resultado de las estancias en el extranjero en el grupo Onboard Space Systems de Luleå University of Technology, División de Tecnología Espacial (Kiruna, Suecia), la primera del 15 de junio al 17 de septiembre del 2015, financiado por la Escuela de Doctorado de la Universidad de Alicante; y la segunda del 14 de abril al 13 de julio de 2016, financiada por una beca de la Generalitat Valenciana.

Todo lo anterior describe globalmente los principales componentes de la Tesis. Sin embargo, la investigación no sólo tiene la intención de implementar nuevos algoritmos para evitar las limitaciones existentes, sino también para evaluar su impacto cuando se aplica en entornos reales. Para ello, se implementaron todos los

diferentes controladores utilizando la arquitectura de software y hardware propuesta para el control de dos robots. Un robot industrial Mitsubishi PA10 y un robot de tres grados de libertad desarrollado y construido por el grupo de investigación en el que se escribió esta Tesis.

1.2 Marco de la Tesis

El primer proyecto en el que se desarrolló esta tesis fue "Manipulación visual de objetos rígidos y elásticos con guiado mediante control visual-táctil-fuerza", financiado por el Ministerio de Economía y Competitividad (DPI2012-32390) y fondos FEDER. El objetivo del proyecto fue la investigación de control visual y técnicas de manipulación de agarre orientadas a su aplicación combinada para su aplicación a tareas industriales o de servicio robótico. De esta manera, la intención es que las soluciones propuestas se puedan utilizar con éxito en entornos industriales para la manipulación de productos o sustancias peligrosas para seres humanos, así como ambientes de hoy con restricciones de posición o fuerza. Para algunas de estas tareas, no siempre hay un conocimiento del objeto o sustancia a manipular. Por esta razón, se necesitan dos sistemas. Un primer sistema de percepción visual que permita reconocer el objeto a ser manipulado y supervisado para cualquier trayectoria de movimiento, y un segundo sistema robótico que permita tareas de agarre y manipulación. La intención es imitar las capacidades de manipulación de los seres humanos y la precisión articular para tareas tales como la percepción de agarre y contacto de los objetos (rugosidad y forma superficial) o la coordinación táctil para el giro de tales objetos. La contribución de la tesis al proyecto es el desarrollo de sistemas de control visuales basados en imágenes para guiar a los manipuladores robóticos. La carga principal de la investigación cae en la optimización de tales controladores para la implementación de leyes de control para el control visual directo.

Un segundo proyecto en el que se trabajó la tesis fue "Manipuladores de robot de servo visual integrados mediante el uso de hardware reconfigurable FPGA"

(Control visual embebido de robots manipuladores utilizando hardware FPGA reconfigurable [GRE12-17]), financiado por el Vicerrectorado de Investigación, Desarrollo e Innovación de La Universidad de Alicante. El objetivo de este proyecto fue la investigación de técnicas de servo visual integradas en FPGAs. Para ello, se estudiaron las diferentes posibilidades de conexión entre una cámara rápida y un FPGA. El uso de un FPGA para el procesamiento de imágenes y computar los cálculos necesarios para la ley de control requieren una comunicación fluida con la cámara. Los sistemas de control visual directo requieren componentes de respuesta de alta velocidad que mejoran la precisión del controlador al disminuir el retardo del bucle de realimentación. Además de la implementación de un controlador directo en un FPGA para acelerar el procesamiento de imágenes, el proyecto también permitió agregar determinismo al cálculo de la ley de control, permitiendo obtener un cálculo de iteración de tiempo exacto. Por lo tanto, la Tesis permite abordar el diseño de sistemas de control visual directo que luego se implementan en FPGAs.

Por último, las investigaciones y desarrollos realizados en la Tesis se están aplicando al proyecto "Sistema robótico multisensorial con manipulación dual para tareas asistenciales-robot humano" [DPI2015-68087-R]) financiado por el Ministerio de Economía y Competitividad y fondos FEDER. Este proyecto se ocupa del diseño, construcción, control y programación de un torso robótico con el objetivo de servir de ayuda a las tareas de manipulación de personas que presentan algún tipo de discapacidad motora para ayudarles en sus tareas cotidianas. Para ello, el torso emplea dos brazos manipuladores con dos manos robotizadas en sus efectores finales. La colaboración entre humanos y robots en un único entorno para proporcionar asistencia requiere un sistema robótico altamente sensible y seguro con funcionalidades sensoriales. Además, el sistema debe ser capaz de adaptarse al entorno para prestar servicios y/o asistencia y reaccionar frente a situaciones específicas, como colisiones o cambios inesperados en el entorno. Este proyecto desarrolla un sistema robótico multisensorial con estas

características. De esta manera, el robot debe ser capaz de adaptarse a entornos cambiantes, no estructurados y dinámicos mientras se ocupa de la interacción humano-robot. Por esta razón, un sistema basado en la visión-fuerza-táctil está incluido en el sistema de manipulación robótica que permite integrar las capacidades perceptivas necesarias para la manipulación de objetos desconocidos o que no han sido modeladas previamente. La tesis se centra en la aplicación de la estructura de servo visual para guiar a los manipuladores durante la tarea.

1.3 Estructura de la Tesis

Una vez descrita la motivación y el marco de la tesis, esta sección describe brevemente la estructura de la tesis. La Figura 1.1 muestra un diagrama de los diferentes capítulos. Después de este primer capítulo introductorio, se describe un marco teórico en el Capítulo 2. Este marco teórico incluye un estado del arte para sistemas de control visual, prestando especial atención a los sistemas de control visual basados en imágenes y permite enfocar progresivamente las contribuciones a la situación actual del campo.

Los tres capítulos siguientes constituyen el núcleo principal de la Tesis. El tercer capítulo detalla el framework de control visual directo propuesto basado en un control óptimo. El Capítulo 4 propone el concepto de perceptibilidad dinámica, incluyendo dicho concepto en el framework definido en el Capítulo 3. Por último, el Capítulo 5 extiende el framework de control óptimo para guiar naves espaciales y robots espaciales de base flotante.

La Tesis concluye con un capítulo de conclusiones en el que se describen las contribuciones, conclusiones y trabajos futuros.

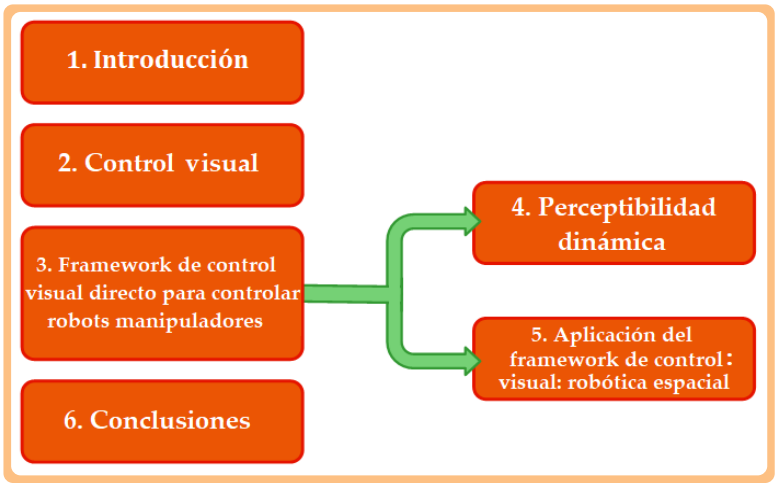

Figura 1.1. Estructura de la Tesis

1.4 Objetivos de la Tesis

Al finalizar este capítulo introductorio, se describen a continuación los objetivos y principales contribuciones realizadas por la Tesis.

El objetivo principal de la tesis es el desarrollo de un framework para definir nuevas leyes directas de control visual, así como su extensión a naves espaciales y robots espaciales de base flotante. Este objetivo principal se puede detallar en los siguientes puntos:

- Investigación en control visual directo. Estudio de las actuales leyes de control visual de hoy en día y definición de un sistema de control visual directo basado en imagen para el seguimiento de trayectorias.
- Diseño de un framework basado en un control óptimo para definir leyes de control visual directo basado en imagen con compensación de caos. Estudio de características dinámicas y precisión de diferentes controladores dinámicos generados y su comparación con los existentes.
- Definición del concepto de perceptibilidad dinámica como criterio que toma en cuenta las características cinemáticas y dinámicas para la detección de singularidades de imagen y robot.

- Integración del concepto de perceptibilidad dinámica y manipulación dinámica en el framework propuesto para evitar singularidades cuando se emplea el control visual directo.
- Investigación e implementación de controladores para la guía de vehículos espaciales y manipuladores espaciales mediante el uso de retroalimentación visual.
- Ampliación del framework de control visual directo basado en imagen para robots con base flotante, permitiendo el seguimiento de trayectorias considerando no sólo las características específicas de tales sistemas, sino también la dinámica orbital.

2 Visual servoing

This chapter presents an in-depth review of the state of the art of visual servoing studying the concepts more related with this thesis and indicating those points where the contributions are focused. To that end, this chapter begins with an introductory section describing the fundamental characteristics of visual servoing systems and outlines which system is going to be used in the Thesis. Section 2.2 presents the different typologies presented by visual servoing systems as dependent on the location of the visual system. Section 2.3 describes the primary and most common classifications for visual servoing systems (position-based and image-based). Section 2.4 details another important classification that differentiates visual servoing systems according to their control loop action (indirect visual servoing and direct visual servoing). Section 2.5 describes the different base configurations and briefly explain what implies the use of such configurations. Section 2.6 shows a brief implementation for all configuration strategies, extending the image-based visual servoing implementation since is the one used in the Thesis. The system is implemented by using an indirect control scheme with the objective of indicating the main notation.

2.1 Introduction

The term *visual servoing* is employed in the literature to reference the use of computer vision to control the movement of a robot. One of the first works where the term visual servoing is employed was (Hill & Park, 1979) that proposed the use of a closed loop control strategy wherein visual information was introduced in the feedback. The main components of a visual servoing system are those represented in Figure 2.1, detailed within a generic application for tracking and manipulation.

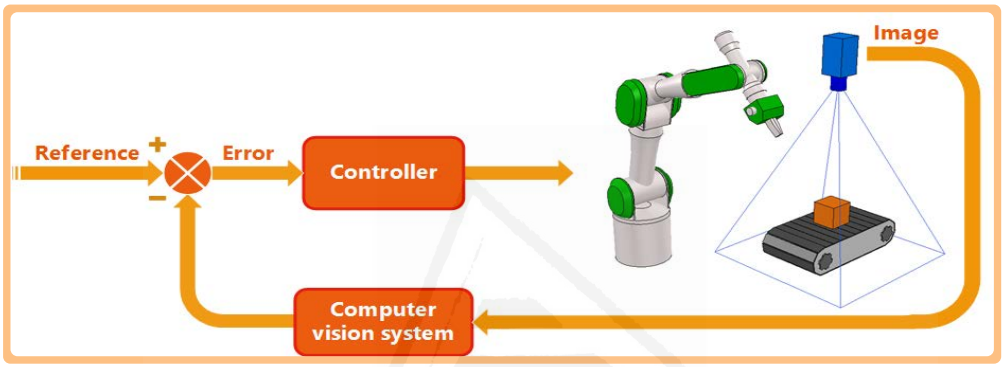

Figure 2.1. Visual servoing generic scheme

The main elements that appear in Figure 2.1, defined:

- *Reference:* Specifies the final joint configuration the robot needs to achieve. The used reference depends on whether a position-based controller is used (the reference to be achieved is a 3-D position) or an image-based controller is used (the reference is a set of desired visual features).
- *Controller*: Performs the robot's guidance by using visual information until it reaches the given reference value. For the case shown in Figure 2.1, the controller guides the robot until it grasps the object. The type of controller depends on—among other things—whether the control performed is position-based, image-based, and if the control is direct or indirect. The main characteristics of these controllers are specified in sections 2.3.1 and 2.3.2.

- *Computer vision system:* This box represents the feedback of the visual servoing system and takes care of extracting the visual information required to guide the robot. In the case of an image-based controller, this component only extracts the visual information. However, when a position-based controller is used, this box determines the 3-D position of the object involved in the task from that extracted visual information. For the example indicated in Figure 2.1, it continually captures the image of the object the robot is intended to grasp.

2.2 Classification according to camera position

Visual information can be acquired by a camera mounted directly on the robot manipulator (in which the movement of the robot causes movement in the camera), or the camera can be mounted somewhere in the working area in such a way that enables observation of the robot's movement from a stationary pose. These configurations (represented in Figure 2.2), are called *eye-in-hand* and *eye-to-hand* configurations, respectively. When a camera is employed at the end-effector of the robot, objects in the working space exist within the robot's visual field and have a constant relationship between the camera's coordinate system and the end-effector of the robot. When an external camera is used, the relationship between the camera's pose and the pose of the coordinate system situated at the base of the robot is fixed. On the other hand, with an external camera there is no constant relationship between the camera's pose and the robot end-effector's pose. This Thesis employs an *eye-in-hand* configuration throughout, so the object from which the features are extracted is within the camera's field of view. This also means the relationship between the camera's coordinate system and the robot's end-effector will therefore remain constant during a given task.

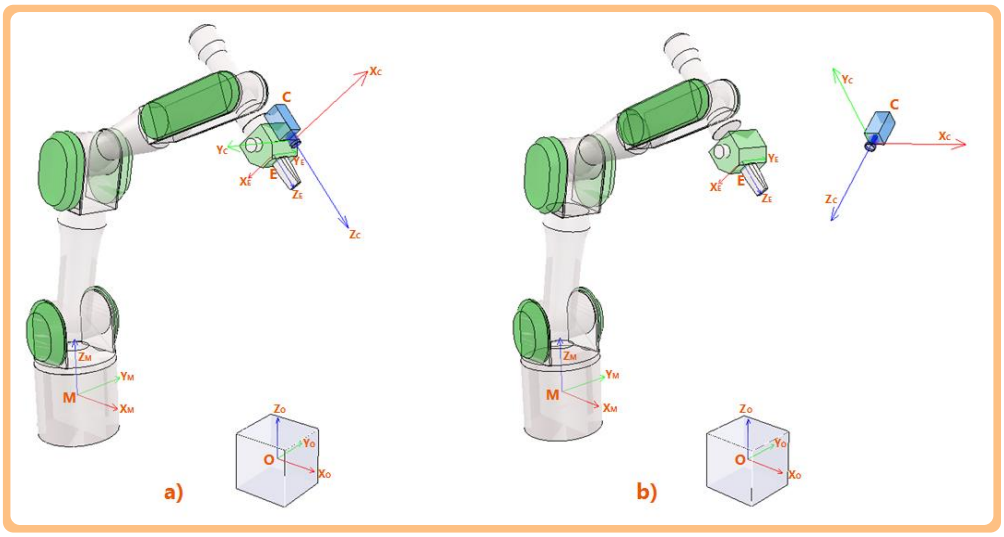

Figure 2.2. Possible camera configurations. a) Camera at the robot's end-effector (eye-in-hand). b) External camera (eye-to-hand).

No matter the configuration of the camera singularities may occur when performing a task. These singularities might happen at a joint or image level, due to the characteristics of the system being employed. Basically, joint singularities happen when there is a point in the workspace where the robot loses its ability to move the end effector in some direction no matter how it moves its joints. It typically occurs when two of the robot's joints line up, making them redundant. On the other hand, image singularities happen when the controller cannot determine a movement of the end-effector in the 3-D space with the information provided by the vision sensor. As previously stated, the objective of a visual servoing system is to perform the robot's positioning by employing computer vision. This Thesis develops visual servoing strategies for the guidance of a robot while avoiding both joint singularities and image singularities. The main contribution of the Thesis within this field have been published in (Alabdo, Perez, García, Pomares, & Torres, 2015; Perez, Alabdo, Pomares, Garcia, & Torres, 2016).

2.3 Classification according to workspace

A classification system for visual servoing systems based on position and image is established in (Sanderson & Weiss, 1980), which described the very first image-based visual servoing system. This next section provides an overview of the different visual servoing system types in existing literature according to the workspace where the visual servoing control is being performed.

2.3.1 Position-based visual servoing

Within the field of position-based visual servoing systems, it is worth mentioning some classic works like (Allen, Yoshimi, & Timcenko, 1991) until more recent ones like (Huang et al., 2017). Besides these two works, it is worth mentioning other remarkable ones like (Park, Kwon, & Ha, 2012) and (Wilson, Williams, & Bell, 1996) that describe the use of vision for a robot's positioning with respect to an object whose position was previously determined.

Position-based systems are those where the reference of the control system is a desired tridimensional position and orientation $\boldsymbol{p}^C, \boldsymbol{\varphi}^C$ (as shown in Figure 2.3).

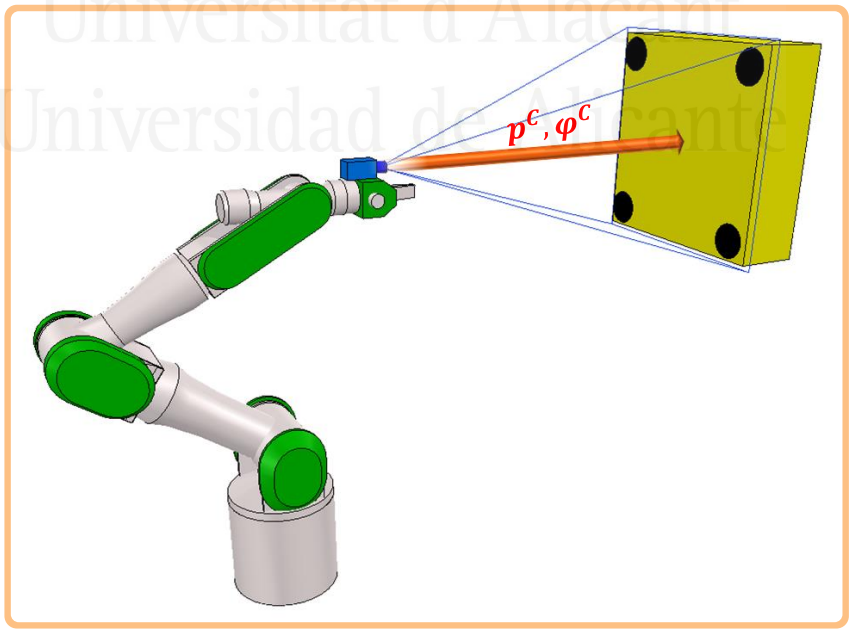

Figure 2.3. Position-based visual servoing system.

When dealing with reconstruction tasks based on point-type primitives,, it is worth mentioning the contribution of (Dementhon & Davis, 1995) consisting of an iterative technique that allows for quick estimation of the pose of an object from four or more non-coplanar points or from four coplanar points (Oberkampf, DeMenthon, & Davis, 1993). Others authors like those of (David, DeMenthon, Duraiswami, & Samet, 2004) developed a modification of this algorithm that allows for the direct correspondence between and determination of a pose from the points used as reference features. The use of multiple cameras allows for reconstructing by consensus the pose of an object as seen from each of the different cameras (Jorstad, Burlina, Wang, Lucarelli, & DeMenthon, 2008). Additionally, it is possible to find works aiming toward localization estimation by using segments as primitives. Along these lines, remarkable studies like (Horaud, Dornaika, & Lamiroy, 1997) propose an adaptation of the algorithm found in (Dementhon & Davis, 1995) for the segments extraction case.

The same way, important research was done in (Cervera, Berry, & Martinet, 2001; Cervera & del Pobil, 2002; Prats, Martínez, Sanz, & del Pobil, 2008) about stereoscopic systems and their use in position-based visual servoing systems as well as the inclusion of 3-D features in image-based visual systems. Although it is well known that these visual servoing systems allow for obtaining a trajectory very close to the line between then initial and desired pose, nowadays the problem of convergence and robustness is still being studied (Park et al., 2012; Wang, Thunberg, & Hu, 2012). Studies by the authors of (Thuilot, Martinet, Cordesses, & Gallice, 2002) deal with the problem of missing the object during position-based visual servoing tasks, for which the authors generate a trajectory that always maintains the object within the camera's field of view in an iterative manner. Works like (Lippiello, Siciliano, & Villani, 2003, 2007) focused on the development of position-based visual servoing systems by using multi-camera systems for tracking moving objects. Nowadays, position-based controllers are not only applied to manipulator robots on a ground level, but also in other environments

such as controlling different degrees of freedom of aerial vehicles (Mahony, Kumar, & Corke, 2012) or controlling robotic manipulators in outer space (Dong & Zhu, 2015). Position-based visual servoing allows the robot to correctly carry out the given control task. It does, however, have several drawbacks. For a position-based strategy be completely reliable, the camera must be perfectly calibrated (Espiau, 1994) since those intrinsic parameters are used to compute a pose from a set of measurements, and 3-D models of the objects and pose estimation algorithms must also be absolutely perfect (Janabi & Marey, 2010) since both sources of information are merged to estimate the pose of the target. As previously indicated, this has not been the approach employed for this Thesis as it aims to use an image-based architecture that does not require reconstructing the tridimensional location of the object involved with a given task.

2.3.2 Image-based visual servoing

Image-based visual servoing systems are those where the reference is determined in the image space and shown as a semi-transparent representation of the object as in Figure 2.4 and Figure 2.5.

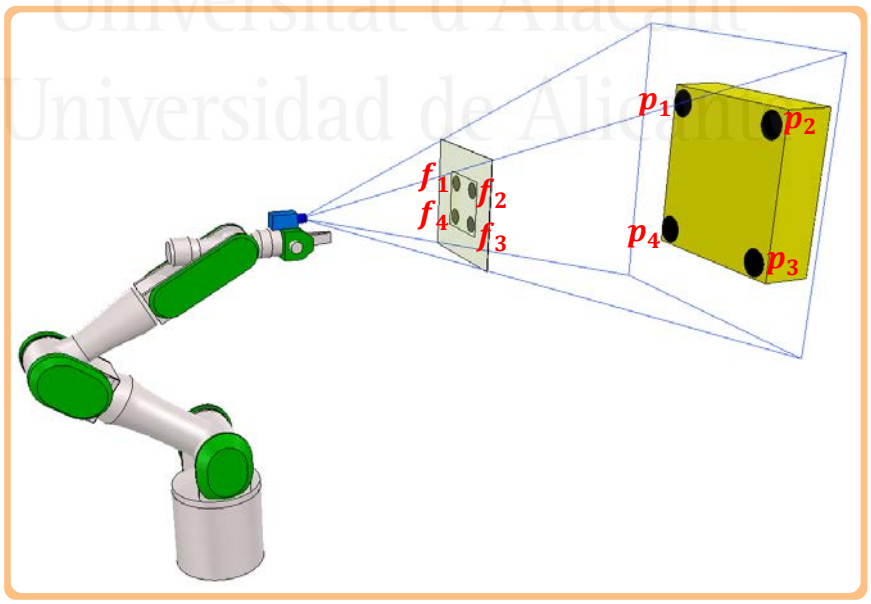

Figure 2.4. Image-based visual servoing system. Initial features.

In Figure 2.4, points $\boldsymbol{p}_1, \boldsymbol{p}_2, \boldsymbol{p}_3$ and $\boldsymbol{p}_4$ are projected at the initial position $\boldsymbol{s} = [\boldsymbol{f}_1, \boldsymbol{f}_2, \boldsymbol{f}_3, \boldsymbol{f}_4]$, with the goal of converging the initial position to the desired one, $\boldsymbol{s}_d$, where $\boldsymbol{s}_d = [\boldsymbol{f}_{1d}, \boldsymbol{f}_{2d}, \boldsymbol{f}_{3d}, \boldsymbol{f}_{4d}]$ is the projection of points $\boldsymbol{p}_1, \boldsymbol{p}_2, \boldsymbol{p}_3$ and $\boldsymbol{p}_4$ at the desired position as shown in Figure 2.5.

This last strategy is the one used in this Thesis. Although the literature that reviews image-based visual servoing is quite extensive, works like (Chaumette & Hutchinson, 2006) and (Chaumette & Hutchinson, 2007) perform a review of the main lines of research and problems related to indirect image-based controllers. This section cites those lines of research related to this Thesis in order to highlight its contributions.

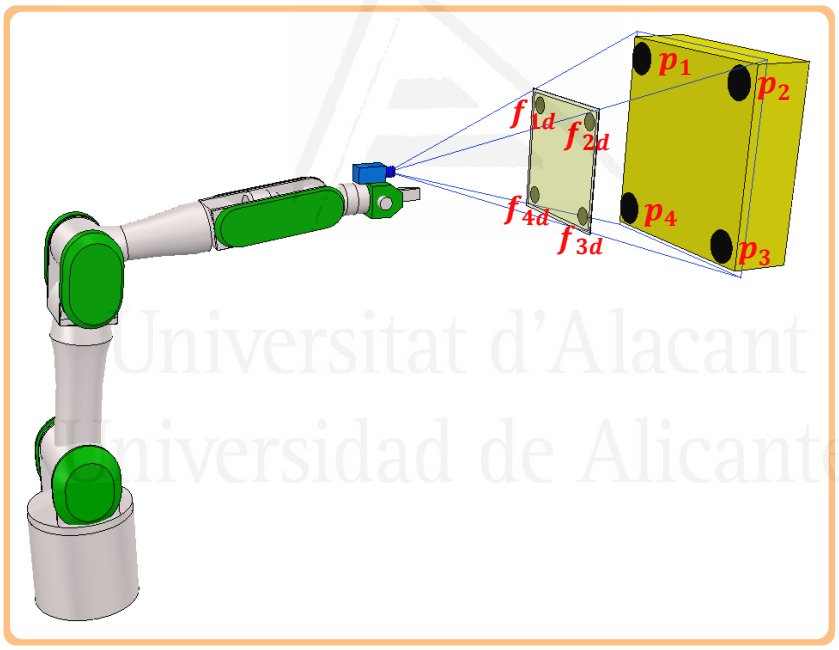

Figure 2.5. Image-based visual servoing system. Desired features.

One of the elements that most affects the behavior of image-based visual servoing controllers is the interaction matrix, which is employed by the controller and depends on several parameters. The interaction matrix, $\mathbf{L}_s$, is employed by the image-based visual servoing controllers for relating velocities in a tridimensional point with velocities of a corresponding point in the image space. When

considering an external camera that is observing a point situated at the end-effector of a moving robot, the interaction matrix provides information about how the features change in the image space when the end-effector moves:

$$\begin{bmatrix} \dot{f}_x \\ \dot{f}_y \end{bmatrix} = \mathbf{L}_s\left(\boldsymbol{p}_E^C\right) \cdot \begin{bmatrix} \boldsymbol{v}_{tE}^C \\ \boldsymbol{w}_E^C \end{bmatrix} \tag{2.1}$$

where $\boldsymbol{p}_E^C$ is a point in 3-D space that moves with a rotational velocity $\boldsymbol{w}_E^C\left(\dot{\alpha}_E^C, \dot{\beta}_E^C, \dot{\gamma}_E^C\right)$, as well as with a translational velocity $\boldsymbol{v}_{tE}^C\left(\dot{x}_{tE}^C, \dot{y}_{tE}^C, \dot{z}_{tE}^C\right)$, both with respect to the camera's coordinate frame. Furthermore, $\left(\dot{f}_x, \dot{f}_y\right)$ are the coordinates of the features extracted from the image.

In general, if $\boldsymbol{p}^C$ is considered to be the pose of a point of an object observed by the camera in a space dimension of size j, $\boldsymbol{v}^C = [\boldsymbol{v}_t^C \quad \boldsymbol{w}^C]$ is the point's velocity with respect to the camera's reference frame (comprised of the translational and rotational velocity). A vector with k features observed in the image (measured in pixels) is represented by $\boldsymbol{s}$. Also, a vector represented by $\dot{\boldsymbol{s}}$ is the variation of those features in the image. The interaction matrix is represented by $\mathbf{L}_s$ and undergoes the following transformation:

$$\dot{\boldsymbol{s}} = \mathbf{L}_s \cdot \boldsymbol{v}^C \tag{2.2}$$

The expression that allows for computing this interaction matrix is obtained by developing the previous expression:

$$\dot{\boldsymbol{s}} = \frac{\partial \boldsymbol{s}}{\partial \boldsymbol{r}} \cdot \frac{\partial \boldsymbol{r}}{\partial t}, \dot{\boldsymbol{s}} = \begin{bmatrix} \dot{f}_{1x} \\ \dot{f}_{1y} \\ \vdots \\ \dot{f}_{kx} \\ \dot{f}_{ky} \end{bmatrix} = \begin{bmatrix} \frac{\partial f_{1x}}{\partial \boldsymbol{r}_1} & \cdots & \frac{\partial f_{1x}}{\partial \boldsymbol{r}_j} \\ \vdots & \ddots & \vdots \\ \frac{\partial f_{ky}}{\partial \boldsymbol{r}_1} & \cdots & \frac{\partial f_{ky}}{\partial \boldsymbol{r}_j} \end{bmatrix} \cdot \boldsymbol{v}^C \tag{2.3}$$

As can be seen in Equation (2.3), the number of columns in the interaction matrix changes depending on the task (with consideration to a dimensional space of size j).

The value of the interaction matrix for the case where the extracted features are points has been determined in many previous works one of which is (Chaumette & Hutchinson, 2006). In any case, following the previously employed notation, this interaction matrix acquires the following value:

$$\dot{\boldsymbol{s}} = \begin{bmatrix} \frac{f_u}{z_p^C} & 0 & -\frac{(f_x-u_0)}{z_p^C} & -\frac{(f_x-u_0)(f_y-v_0)}{f_v} & \frac{(f_x-u_0)^2+f_u^2}{f_u} & -\frac{f_u(f_y-v_0)}{f_v} \\ 0 & \frac{f_v}{z_p^C} & -\frac{(f_y-v_0)}{z_p^C} & -\frac{(f_y-v_0)^2+f_v^2}{f_v} & \frac{(f_x-u_0)(f_y-v_0)}{f_u} & \frac{f_v(f_x-u_0)}{f_u} \end{bmatrix} \cdot \begin{bmatrix} \dot{x}_t^C \\ \dot{y}_t^C \\ \dot{z}_t^C \\ \dot{\alpha}^C \\ \dot{\beta}^C \\ \dot{\gamma}^C \end{bmatrix} \quad (2.4)$$

In the interaction matrix appear certain parameters that can be extracted from a pin-hole model of a camera represented by Figure 2.6. Given a point $\boldsymbol{p}^M$ from the 3-D space in a world's coordinate frame, $\boldsymbol{p}^M(x_p^M, y_p^M, z_p^M)$ and $\boldsymbol{p}^S(x_p^S, y_p^S)$ is its projection in the image space; the projection $\boldsymbol{p}^S$ in the image space of the point $\boldsymbol{p}^M$ is obtained by an intersection of the line that joins $\boldsymbol{p}^M$ and the optical center of the camera $\mathbf{C}$ with the image space. The distance between the optical center $\mathbf{C}$ and the image space is called the focal distance, or simply "the focal", f. The point that is obtained as a result of the intersection of the principal axis z_C (a perpendicular line to the image plane that goes through the optical center $\mathbf{C}$), and the image plane is called principal point. This principal point (u_0, v_0) represents two of the intrinsic parameters of the camera. In order to obtain them, the camera must be precisely calibrated, either in a previous phase of the task is undertaking or through an online calibration. The focal, f, is another of the intrinsic parameters that must be considered when modeling a real camera. As previously described, this is the distance between the camera's reference frame and the image plane. Usually, the focal distance is grouped with other two parameters that represent the pixel size: (s_x, s_y). This way, the intrinsic parameters of the camera can be modeled with the set $\xi = \{f_u, f_v, u_0, v_0\}$, when $f_u = f \cdot s_x$ and $f_v = f \cdot s_y$.

Suppose it is the case that the vision system is able to extract k characteristic points from an image. In this case, the set of features is comprised by several points in the image expressed in pixels, $\boldsymbol{s} = \{f_i, i \in 1..k\}$ and the resulting interaction matrix can be generalized for several points in the following way:

$$\mathbf{L}_s = \begin{bmatrix} \mathbf{L}_{s1} \\ \mathbf{L}_{s2} \\ \vdots \\ \mathbf{L}_{sk} \end{bmatrix} \tag{2.5}$$

where $\mathbf{L}_{si}$ is the interaction matrix for an image feature point.

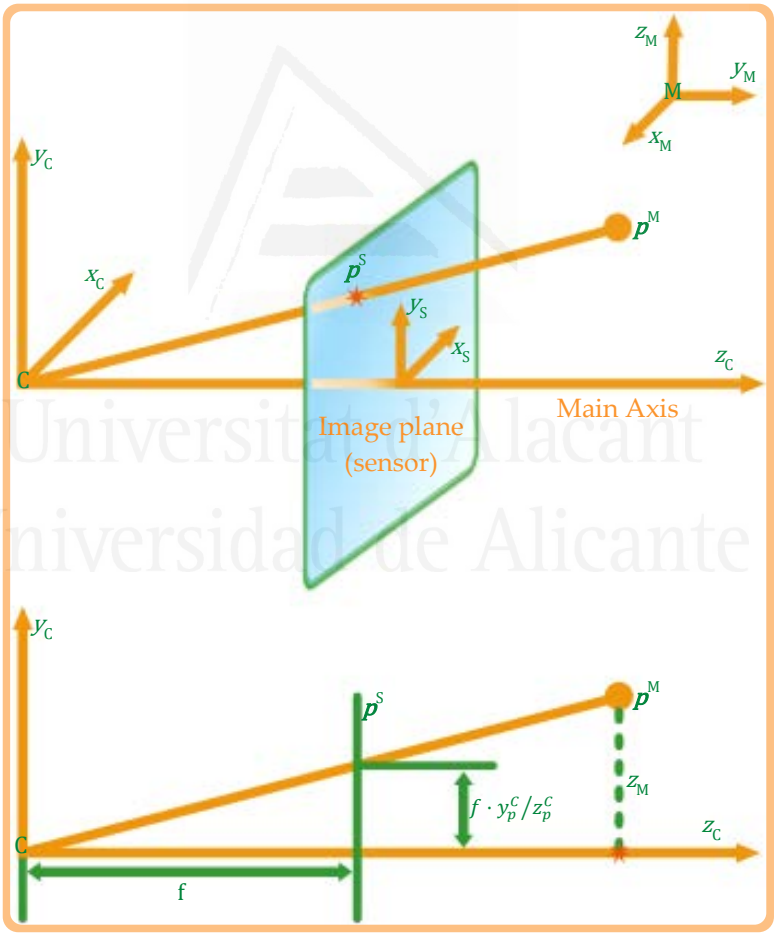

Figure 2.6. Intrinsic camera parameters

The studies of different authors like (Chaumette, 1998; Nematollahi & Janabi, 2009) deal with singularity problems, robustness, and stability in image-base

visual servoing systems with regard to previous works. These last authors study the stability and convergence of these systems and indicate different situations that can promote a local minimum. Later, Chaumette and Hutchinson (Chaumette & Hutchinson, 2006) review stability problems. In order to avoid these singularity and local minimum problems, the work developed by (Marchand, Chaumette, & Rizzo, 1996) proposed the inclusion of secondary tasks that guaranteed convergence within a main task. With the objective of avoiding these problems in mind, it is worth mentioning the work of Corke and Hutchinson (Corke & Hutchinson, 2001) related to partitioned visual servoing. These works propose a control strategy that treats different degrees of freedom in the task separately to guarantee convergence before different situations arise like those indicated in (Xie, Li, Tu, & Perron, 2009). In this regard, the Thesis deals with image singularities by developing the dynamic perceptibility concept, and then using it to optimize the movement of the robot (Alabdo et al., 2015; Perez et al., 2016). A definition of the concept of a task-function approach controller that takes into account the unilateral restrictions like the manipulator's joint limits is described in (Mansard, Khatib, & Kheddar, 2009). When dealing with stability problems, it is worth mentioning those that stem from dealing with a redundant robot (Agravante, Claudio, Spindler, & Chaumette, 2017). In this case, it is not only necessary to correctly perform the end-effector guidance but also to solve the redundancy by establishing the most appropriate joint configuration for each situation. This is the case in the work (N. Garcia, Perez, Sabater, Morales, & Badesa, 2011) where redundant robots were employed simultaneously. Also, some dynamic visual control systems for redundant robots with chaos compensation have been developed to avoid robotic chaotic behaviors with new architectures that improve systems maintainability and traceability (Pomares, Jara, Perez, & Torres, 2015; Pomares, Perea, & Torres, 2014; Pyragas, 2006). The use of 2.5-D visual servoing for guiding redundant robots while studying Lyapunov-based stability can be found in (Fang, Behal, Dixon, & Dawson, 2002). The visual servoing system developed in this Thesis will also guide

a redundant robot. This way, it proposes a new strategy for adjusting the redundant joint behavior during trajectory tracking in the image space. This approach permits solving this redundancy and will also be extended to direct visual servoing.

Some research projects—with the aim of improving the robot's behavior—propose combining visual information with other sensors. For example, hybrid visual/force servoing systems propose simultaneous control of different directions. One direction is controlled by employing visual information and the other by using force control (G. J. Garcia, Corrales, Pomares, & Torres, 2009; Siciliano, Villani, Lippiello, & De Santis, 2010). A robot that can be redundant with respect to the described task in the image space will be employed in this Thesis.

Within the field of image-based visual servoing systems, a commonly held requirement is to keep any extracted visual features within the camera's field of view during the entire visual servoing task (Chesi, Hashimoto, Prattichizzo, & Vicino, 2004; Mezouar & Chaumette, 2002; Schramm & Morel, 2006; Wang, Lang, & de Silva, 2009). One way to avoid missing features as much as possible is to use panoramic cameras, which is the case in works like (Cervera, Garcia, Martinez, Nomdedeu, & del Pobil, 2008; Hadj, Mezouar, Martinet, & Chaumette, 2008; Mariottini & Prattichizzo, 2008; Tahri, Mezouar, Andreff, & Martinet, 2009). There are also other approaches like (G. J. Garcia et al., 2009; Mezouar & Chaumette, 2003; Schramm & Morel, 2006) that employ trajectory tracking techniques instead of fixed desired visual features. This latter approach will be used in this Thesis, since the problem in visual servoing is formulated as tracking a time-dependent trajectory

2.4 Classification according to control strategy

2.4.1 Indirect visual servoing

This first classification is defined while keeping in mind a classical implementation of the controller as shown in Figure 2.7. These classic controllers also belong to the group called indirect controllers.

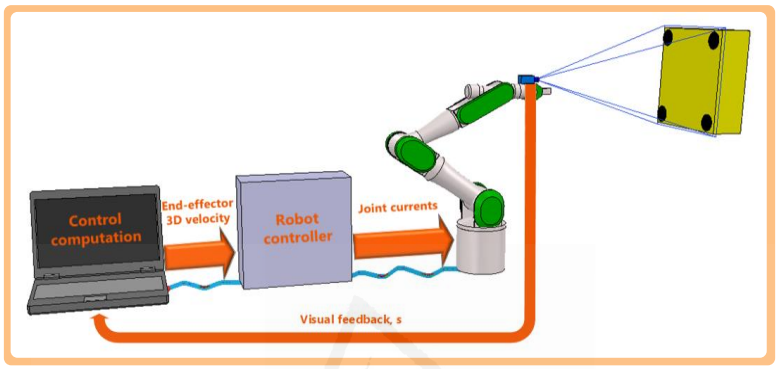

Figure 2.7. Representation of an indirect visual servoing system

In this case, the control action is specified as velocities to be applied at the robot's end effector and do not take robot dynamics into account. When applying an indirect controller to a task only kinematic aspects of the robot are taken into account.

2.4.2 Direct visual servoing

In direct controllers the control action is usually given as torques applied directly to the joints as shown in Figure 2.8.

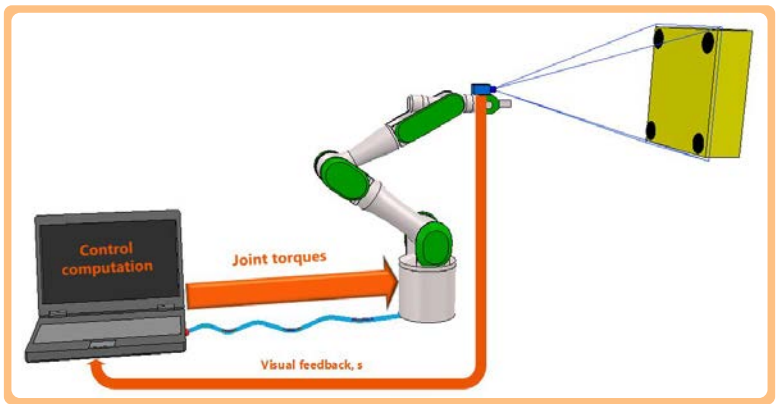

Figure 2.8. Representation of a direct visual servoing system

For each type of visual servoing system described in this section, Section 2.6 details the main research projects related to this doctoral Thesis.

2.5 Classification according to base configuration

Visual servoing systems have mainly been used in industry for faster processing and handling, but after the vast improvements in technology in recent years new opportunities for applying these strategies to the space industry are slowly appearing. However, there are different general considerations when controlling an object in zero gravity that are taken for granted when dealing with systems attached to the ground. Generally speaking, the system will be describing an orbital trajectory while performing a task, and therefore new moments and inertias have to be considered when controlling it. Because of the orbital trajectory, the reference frame is usually taken as the center of mass of the heaviest object (usually, a planet).

There are various ways of classifying the way robot manipulators mounted on satellites are used, such as by their final purpose or how the base functions. Regarding the base spacecraft, there are two types of operations that are considered and studied in (Dubowsky & Papadopoulos, 1993). This classification is important since this Thesis works with one of these operations. Chapter 5 describes several contributions to the field that relate the use of visual control strategies to space manipulators mounted on satellites.

2.5.1 Fixed base

Systems with a fixed base are those that are attached to a fixed point in 3-D space with respect to the origin reference point, and they may have any possible orientation. In other words, if an empty room is considered as the 3-D workspace, a robot with a fixed base could be assembled on the ground as shown in Figure 2.9, attached to the wall as represented in Figure 2.10, or be on the ceiling as in Figure 2.11.

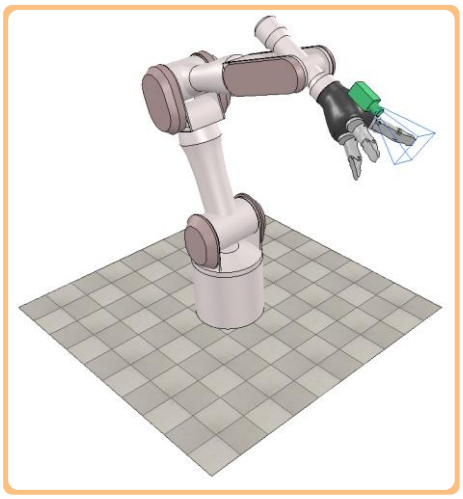

Figure 2.9. Mitsubishi PA10 robot with a Jaco hand from Kinova Robotics with a vision system at its end-effector.

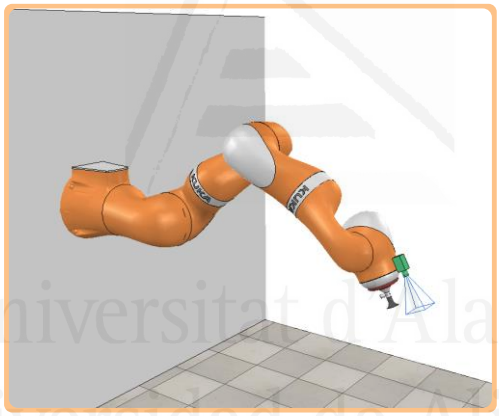

Figure 2.10. Kuka LBR iiwa 14 R820 robot from KUKA Laboratories GmbH with a Baxter vacuum cup from Rethink Robotics with a vision system at its end-effector.

In any case, the inertia and momentum exerted on the base of the robot are absorbed by the environment from which they are attached. The only difference is the gravitational vector that affects the behavior of the robot in a different way. The position in which the robot is ultimately installed depends on the robot configuration, the task to be performed, and other considerations.

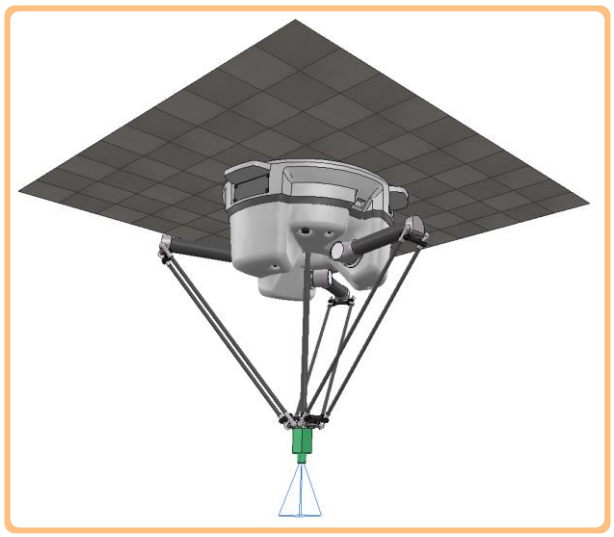

Figure 2.11. ABB IRB360 from ABB Robotics with a vision system.

2.5.2 Mobile base

Systems with a mobile base are able to act based on the environment and move the system along one or more axis in 3-D space. The ways in which a system moves around are many, such as legs, wheels, propellers or a combination of several of those (Siegwart, Nourbakhsh, & Scaramuzza, 2011). When dealing with legged robots people may automatically think about a humanoid or an animal-shaped robot, but the truth is that many robots have been inspired by insects. Building any legged robot is not easy task. Figure 2.12 shows the humanoid that may be the most famous robot developed by Honda (Hirai, Hirose, Haikawa, & Takenaka, 1998); the most recent models are known as ASIMO (Sakagami et al., 2002).

Providing legs to a robot has been proven to be a difficult task. Looking at nature, legs provide many advantages when compared to other locomotive mechanisms. Robots can navigate through different environments while being able to jump or step over obstacles, providing a high degree of adaptation to the surface. They can also change their center of mass, an extremely useful ability in irregular, changing, or unstable environments. As technology develops, other

Figure 2.12. a) Predecessor of ASIMO, the P3. b) ASIMO robot.
Source: http://www.flickr.com/photos/machu/39761200/

humanoid robots have been developed (such as the NAO robot shown in Figure 2.13), and have been used to do research from walking (Strom, Slavov, & Chown, 2010) to human interaction (Han, Campbell, Jokinen, & Wilcock, 2012; Shamsuddin et al., 2012) by using vision systems.

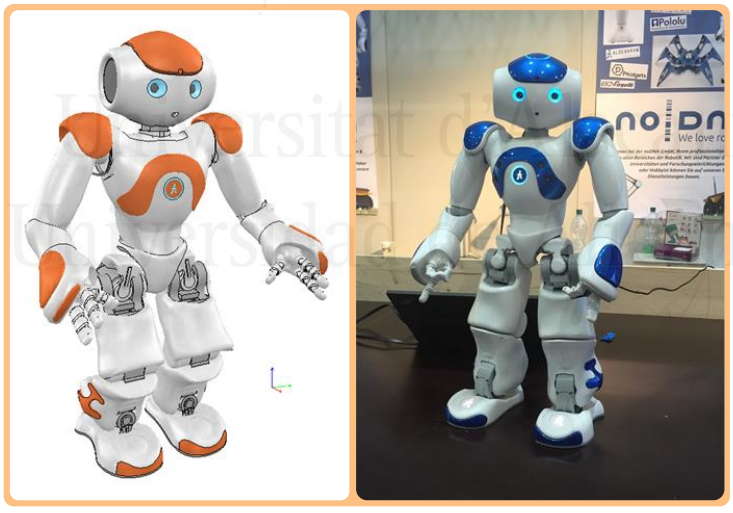

Figure 2.13. Nao robot from Aldebaran Robotics.

At the same time, improvements in computation capacity allow for the development of more complex systems (for example, with more degrees of freedom). This is the case of insectoid robots like the hexapod (Mishra, Ghosh, Goyal, Thakor, & Kukreja, 2016; Sun & Gao, 2016) shown in Figure 2.14.

Figure 2.14. Mishra's printed hexapod

Despite all the advantages that legs might offer, wheels are the most widespread approach when building a mobile robot. Generally speaking, a wheel only requires one motor whereas a leg requires two or more motors (depending on the complexity of the locomotive system), so one degree of freedom is easier and cheaper to implement. When dealing with a standard type of wheels, there are several ways of controlling the movement of a robot. For example, turning opposite wheels on the same axis at different rates (an example of the this is the robot Summit XL shown in Figure 2.15) or orienting the axis that attach paired

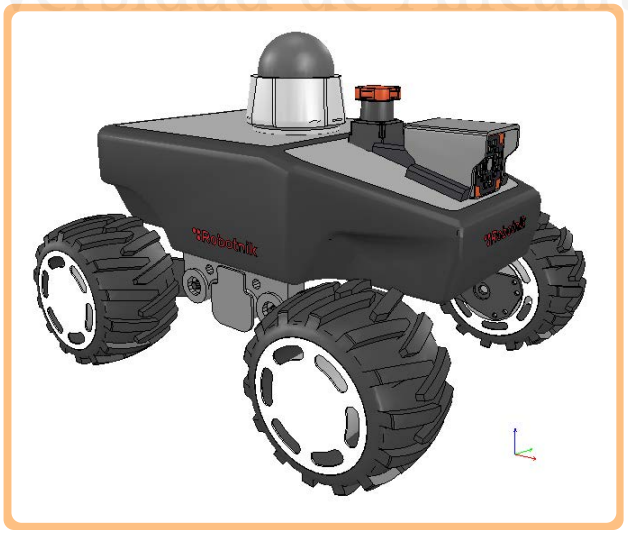

Figure 2.15. Summit XL from Robotnik

wheels in different directions (like real cars do today), but this strategy requires an extra actuator and a slightly more complex mechanical configuration.

Another after-effect of new computation capabilities is the proliferation of the widely known multi-copters (Bourquardez et al., 2009; Mahony et al., 2012; Ozawa & Chaumette, 2011). Figure 2.16 shows an example of a multi-copter with four propellers, also known as a quadcopter.

Figure 2.16. Parrot quadcopter with a vision system

For the previous systems, a gravity vector affects them directly by pushing them into the center of the earth; thus, they walk, ride, or fly over the ground.

2.5.3 Free-floating base

The next level of mobility comes into play when dealing with free-floating cases, where the base is completely free and floating in the workspace with no attitude control. It is freely reacting to the movements exerted on it, and—in the case of this Thesis—the manipulator attached to it. Examples for this category of base include underwater systems with neutral buoyancy capabilities as shown in Figure 2.17 or systems orbiting around the earth with no actuation capabilities as shown in Figure 2.18. Because of the orbital trajectory, the reference frame is

usually taken as the center of mass of the heaviest object (a planet is usually considered). The contributions of the Thesis are focused on this topic, developing image-based visual servoing systems that work in zero-gravity.

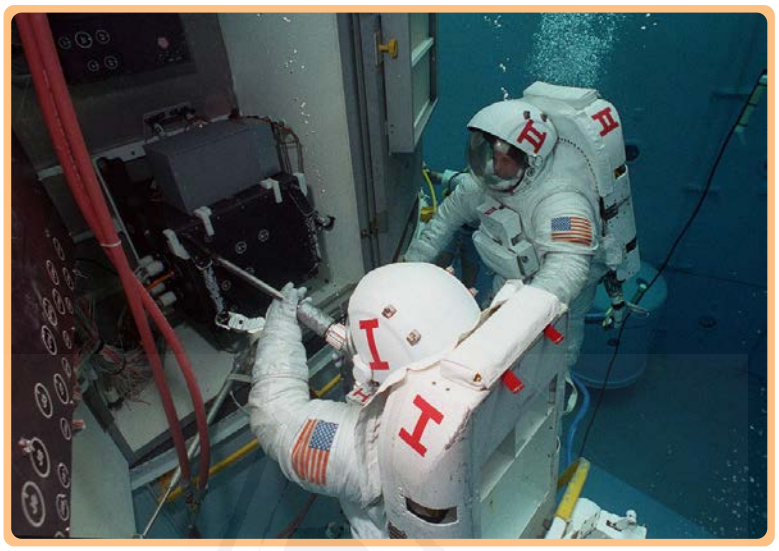

Figure 2.17. Neutral Buoyancy Simulator Hubble WFPC replacement; astronauts working in a neutral buoyancy environment. Source: https://commons.wikimedia.org/wiki/File:Neutral_Buoyancy_Simulator_Hubble_WFPC_replacement.jpg

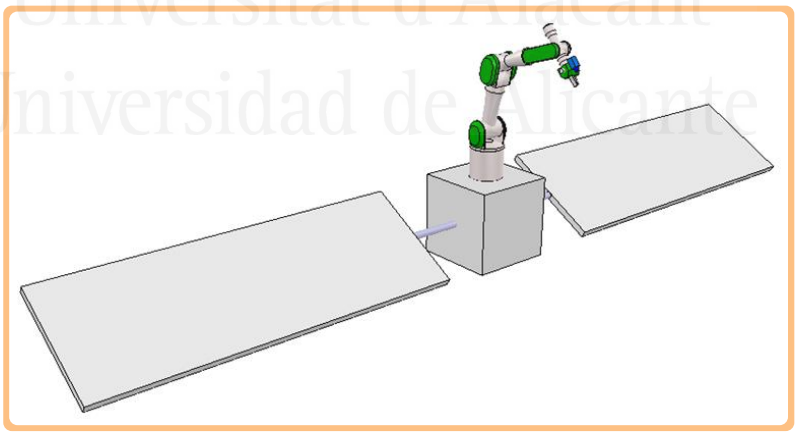

Figure 2.18. Free-floating spacecraft system where the base is not controlled.

2.5.4 Free-based case

The free-based case (also known as a free-flying case for systems that fly in the earth's atmosphere) includes those where the base is actively controlled, and thus

the system's attitude and position can be modified with the actuators to position and orient the system. Essentially, all free-floating systems can be transformed into free-based systems by equipping them with appropriate actuators. In this way, for example, Figure 2.19 shows how an astronaut working in a neutral buoyancy environment can be equipped with a Manned Maneuvering Unit to be able to move around.

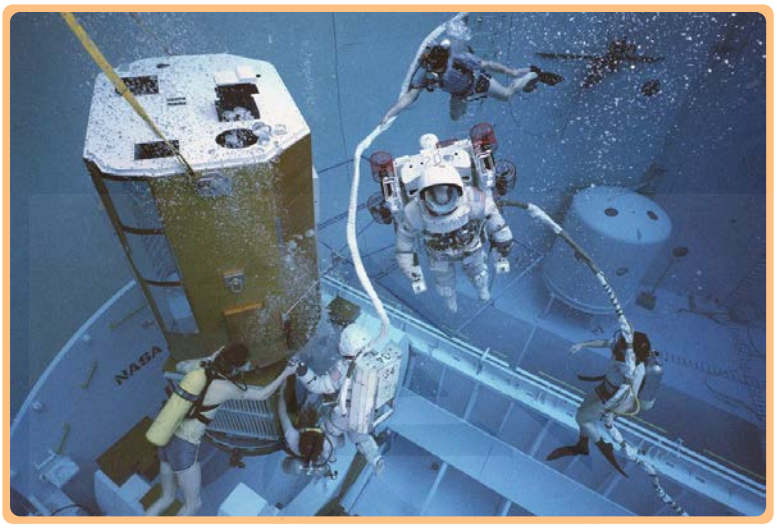

Figure 2.19. Neutral buoyancy simulator, Solar Max Testing; astronaut practicing with a Manned Maneuvering Unit. Source: https://www.flickr.com/photos/nasamarshall/8618645187

Another possibility could be to equip a free-floating satellite with thrusters and reaction wheels to be able to control the system, as is shown in Figure 2.20.

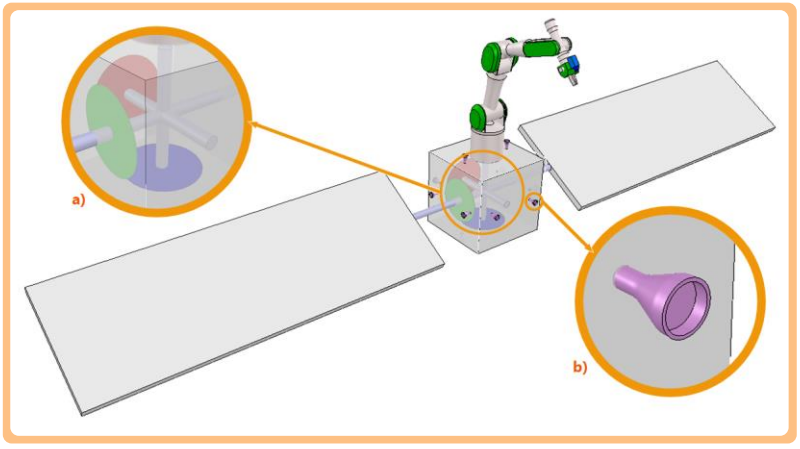

Figure 2.20. Free-based system where the base is controlled by: a) Reaction wheels; b) Thrusters

The configuration of the actuators shown in Figure 2.20 is only an example to illustrate one possible way of controlling translational and attitude control actions on a spacecraft. There are actually many other ways of actuating a spacecraft. Furthermore, within one specific propulsion system there are different configurations and techniques that change the behavior or the actuated system, and thereby change the control. Some satellite missions employ gravity gradient stabilization or magnetic control techniques for controlling the attitude of a satellite, but these approaches are only used due to their simplicity and their low cost. The main problem they have is their low precision when orienting a spacecraft since they depend on external factors like a gravitational field or the condition of a geomagnetic field (Silani & Lovera, 2005). The attitude control system shown in Figure 2.20 is a type known as reaction wheels, which is more expensive but has been proven to be highly effective for attitude control and has been used for all kinds and sizes of satellites. The reaction wheel system consists of spinning rotational mechanical devices used to store rotational energy called flywheels. The spinning is achieved by an electrical motor attached to the flywheel which creates angular momentum, thus reorienting the spacecraft. The number and configuration of flywheels needed for a three-axis satellite attitude control is still being debated (Ismail & Varatharajoo, 2010). It has been concluded that the power intake for the attitude control system can be minimized by selecting the minimum torque configuration with respect to a specific mission. Reaction wheels are especially useful when the spacecraft must be rotated in very small increments and have been used with almost a 100% success rate in space missions.

2.6 Classifications for all configuration strategies

2.6.1 Indirect position-based visual servoing

In this kind of configuration, the input for the controller is the difference between the desired location of the observed object and the estimated one from the features extracted by the vision system. In order to reconstruct the 3-D pose of the

object involved in the task ($\boldsymbol{p}^C, \boldsymbol{\varphi}^C$), the system needs a model of the working space as well as a calibrated model of the camera employed in the vision system. In this type of visual servoing, the system reference is the desired pose of the robot or the existing object in the working space.

Figure 2.21 represents a basic scheme for a position-based controller. This particular arrangement corresponds to an indirect controller, and its first level of feedback is provided by the joint controllers. The second level of feedback corresponds to visual feedback, and the scheme demonstrates the need for reconstructing the 3-D pose of the object involved with the task.

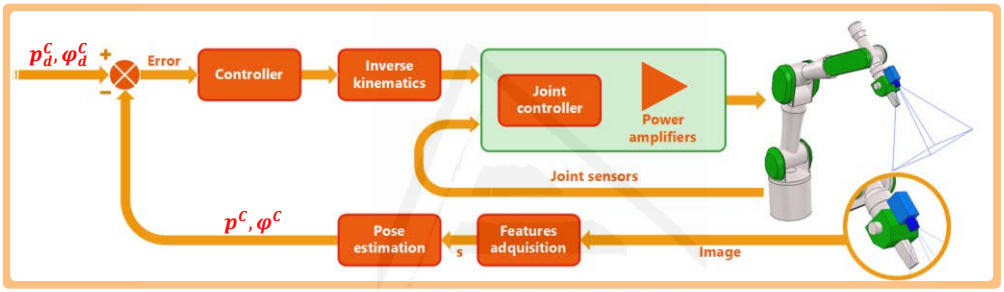

Figure 2.21. Indirect position-based controller.

2.6.2 Indirect image-based visual servoing

When an image-based visual servoing system is employed, the controller generates control actions so that the visual features obtained from the images converge progressively toward the desired features. Figure 2.22 shows the scheme of an indirect image-based controller. As shown, a feature extraction process (four points in the image, in this case) is performed for the control loop's feedback. This differs from position-based controllers in that it is not necessary to calculate the 3-D pose involved in the task. This way, the control is performed directly in the image space. Since some of the contributions of this Thesis are applied to this concept, this section describes the main considerations for implementation of indirect image-based visual controllers.

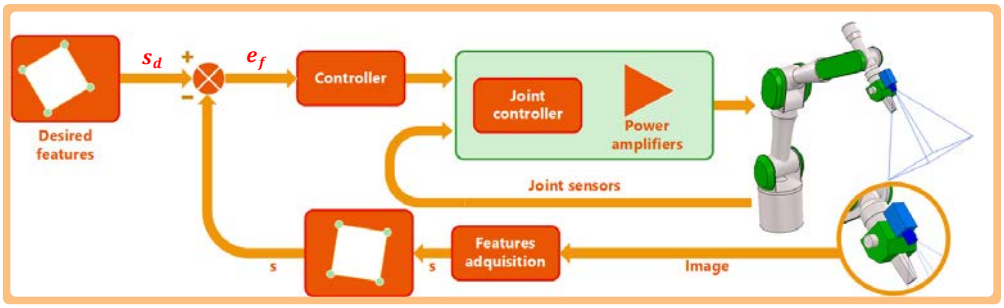

Figure 2.22. Indirect image-based controller.

This section describes the main considerations to take into account when implementing an indirect image-based controller when the extracted visual features are a set of points. This set of points is represented with the variable $\boldsymbol{s}$. The visual controller must apply the control actions in such a way that set $\boldsymbol{s}$ progresively reaches the value of the desired features $\boldsymbol{s}_d$. In this way, an error function is defined. The objective is to progressively reduce such errors:

$$\boldsymbol{e}(\boldsymbol{r},t) = \hat{\mathbf{L}}_s^{+}(\boldsymbol{s}(\boldsymbol{r},t) - \boldsymbol{s}_d) \tag{2.6}$$

The error function $\boldsymbol{e}$, indicated in Equation (2.6) represents the error that is progressively reduced in tridimensional space. This error is obtained from the error measured in the image space $\boldsymbol{e}_s(\boldsymbol{r},t) = \boldsymbol{s}(\boldsymbol{r},t) - \boldsymbol{s}_d$ and depends on the camera pose $\boldsymbol{r}$ and the time t. The relationship between the image and position errors is the estimation of the pseudoinverse of the interaction matrix. The inverse can be used under the assumption that the matrix is square, not singular; therefore, the inverse exists. For this to happen, the number of features extracted from the image must be three, so the image Jacobian or interaction matrix is 6x6.

If the interaction matrix has more rows than columns, the following pseudoinverse is used:

$$\mathbf{L}_s^{+} = \left(\mathbf{L}_s^{\mathrm{T}} \cdot \mathbf{L}_s\right)^{-1} \cdot \mathbf{L}_s^{\mathrm{T}} \tag{2.7}$$

If the interaction matrix has more columns than rows, the used pseudoinverse has the following value:

$$\mathbf{L}_s^+ = \mathbf{L}_s^T \cdot \left(\mathbf{L}_s \cdot \mathbf{L}_s^T\right)^{-1} \tag{2.8}$$

$\hat{\mathbf{L}}_s$ represents an estimate of the interaction matrix, since it depends of the distance between the camera and the object. On many occasions, this depth parameter is considered constant (equals to the final desired position). Furthermore, the intrinsic parameters are not calculated with complete accuracy, but are an approximation.

The objective of the visual servoing strategy is to reduce the task function exponentially, so it follows:

$$\dot{\boldsymbol{e}} = -\lambda \cdot \boldsymbol{e} \tag{2.9}$$

where $\lambda > 0$. Also, since $\boldsymbol{e}$ depends on the pose of the camera, $\boldsymbol{r}$, and time, t, its derivative can be expressed the following way:

$$\dot{\boldsymbol{e}} = \left(\frac{\partial \boldsymbol{e}}{\partial \boldsymbol{r}}\right)\boldsymbol{v}^c + \frac{\partial \boldsymbol{e}}{\partial t} \tag{2.10}$$

where $\boldsymbol{v}^c$ is the camera velocity, and $\frac{\partial \boldsymbol{e}}{\partial t}$ represents the error variations due to the movement of the observed object. From the definition of a task function, it can be stated that $\frac{\partial \boldsymbol{e}}{\partial r}$ is defined in the following way:

$$\frac{\partial \boldsymbol{e}}{\partial \boldsymbol{r}} = \hat{\mathbf{L}}_s^+ \mathbf{L}_s \tag{2.11}$$

From the Equations (2.9) and (2.10), the following expression for the camera velocity can be obtained:

$$\boldsymbol{v}^c = \left(\frac{\partial \hat{\boldsymbol{e}}}{\partial \boldsymbol{r}}\right)^+ \cdot \left(-\lambda \boldsymbol{e} - \frac{\partial \hat{\boldsymbol{e}}}{\partial t}\right) \tag{2.12}$$

where:

- $\left(\frac{\partial \hat{e}}{\partial r}\right)$ can be equals to the identity matrix:

$$\frac{\partial \hat{e}}{\partial r} = \hat{\mathbf{L}}_s^{+}\hat{\mathbf{L}}_s = \mathbf{I}_6 \tag{2.13}$$

- $\frac{\partial \hat{e}}{\partial t}$ is an estimation of the object's movement in the image.

Next, this Thesis presents some experiments that exemplify several visual servoing tasks and show their behavior. A six-degree-of-freedom Mitsubishi PA10 has a camera situated at the end-effector of the robot and has to perform a positioning task with respect to a desired pattern of features in the field of view. Figure 2.23 shows the beginning of the experiment, where the system is in a joint configuration such that the camera sees the pattern of features as represented by the green circles. The system also knows in advance the desired position of the features when the given task is finished. These features are represented as red asterisks in Figure 2.23.

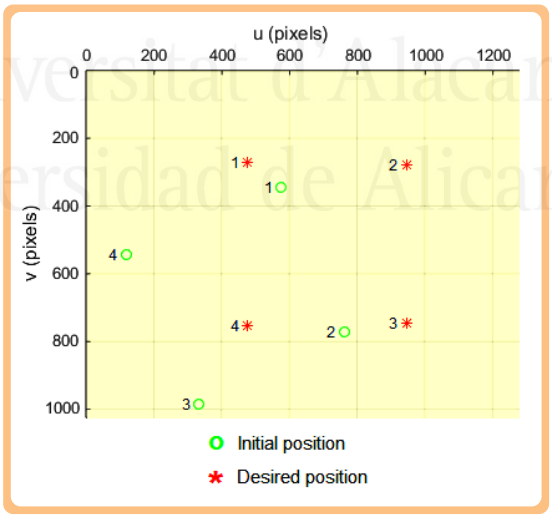

Figure 2.23. Experiment 1. Initial and desired positions of four features in 3-D space as seen in the image space of the camera.

Figure 2.24 depicts the evolution of the visual features during the visual servoing task. As before, the experiment starts with the camera pointing at the

pattern in a way that sees the features in a configuration represented by the green circles. The indirect visual servoing strategy correctly determines that the general movement of the points is towards the desired position, but—as is clear—the trajectory is not entirely straight. This could be because the distance between the camera and the pattern is fixed within the control law and the intrinsic parameters of the camera are not exactly correct. However, the real features do converge to the desired ones. This represents how robust this strategy can be, given that even with errors in several aspects of the system the control law works properly and the desired position is achieved. If the system was to be perfectly calibrated, the trajectory of the pattern would be straight lines.

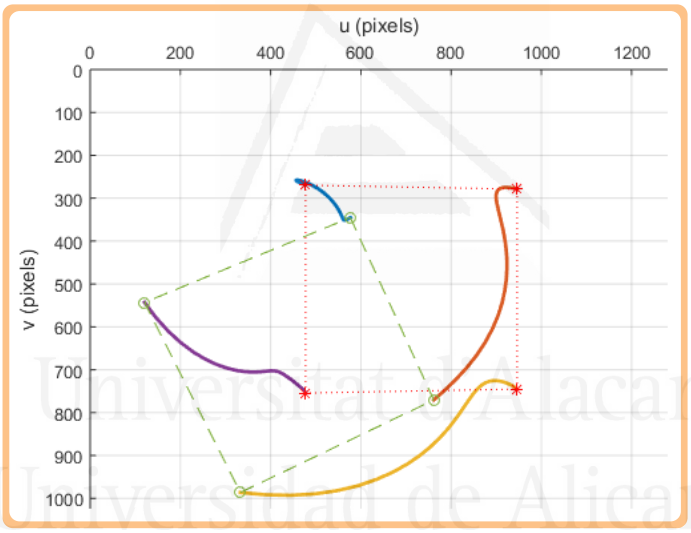

Figure 2.24. Experiment 1. Evolution of the features during the experiment.

This experiment performs a simple proportional control law. Figure 2.25 represents the Cartesian velocity of the camera in the 3-D space. At the beginning of the experiment, the error in the image makes the robot move the camera proportionally fast to the desired position. As the pattern seen by the camera gets closer to the desired one by the system, the velocity starts decreasing until the observed features match the desired ones and then the robot holds that position.

Figure 2.26 represents the value of the image error $\boldsymbol{e}_s$ during the work. As in Figure 2.25, at the beginning of the experiment, there is a large error for almost all the coordinates. This causes the system to react quickly and converge to a null error quickly when it starts moving. As the system reaches the desired position, the small error makes the robot move more slowly, thus slowly reducing the remaining error but nevertheless always towards zero.

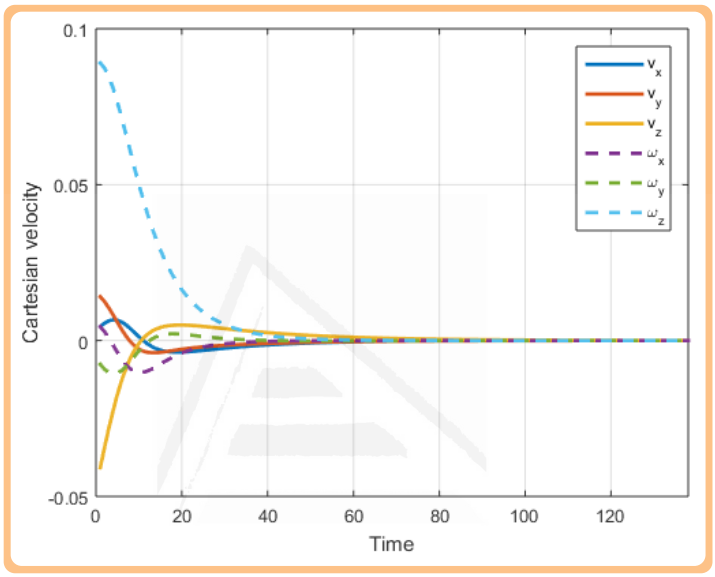

Figure 2.25. Experiment 1. Cartesian velocity of the camera in 3-D space with respect to time.

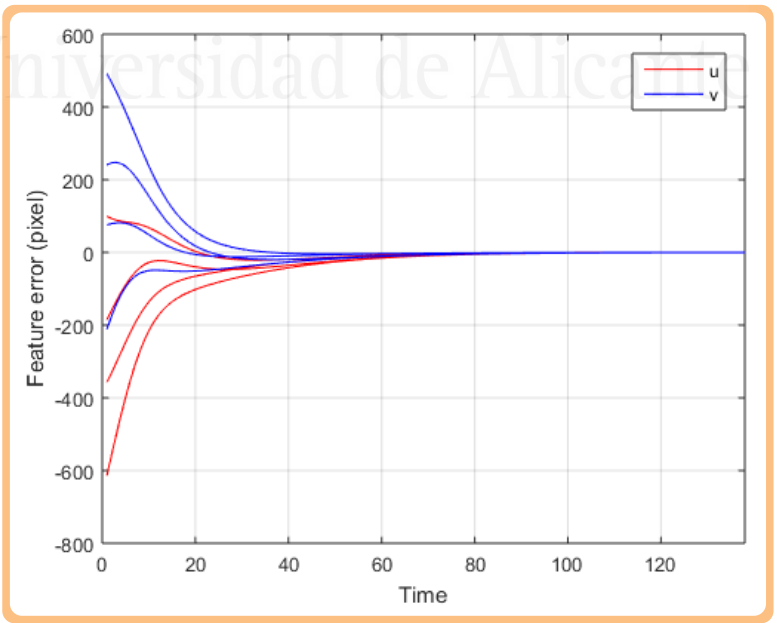

Figure 2.26. Experiment 1. Feature error in the image space with respect to time.

For the second experiment, the camera is situated closer to the pattern than the desired position. This is represented by Figure 2.27 and depicts a movement involving depth.

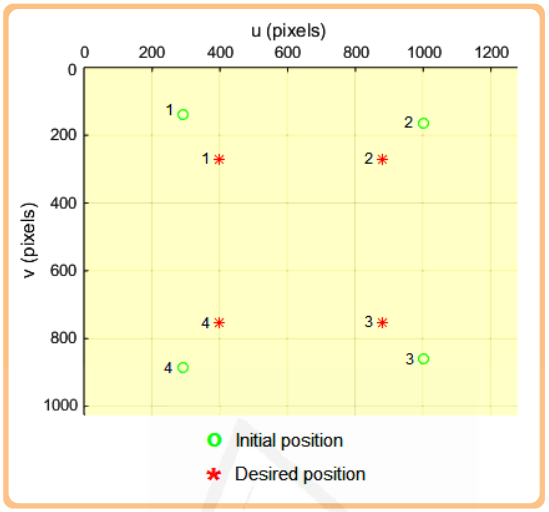

Figure 2.27. Experiment 2. Initial and desired position of four features in 3-D space as seen in the image space of the camera.

Again, Figure 2.28 depicts the evolution of the features during the experiment and represents a movement of the end-effector backwards, achieving a movement in depth.

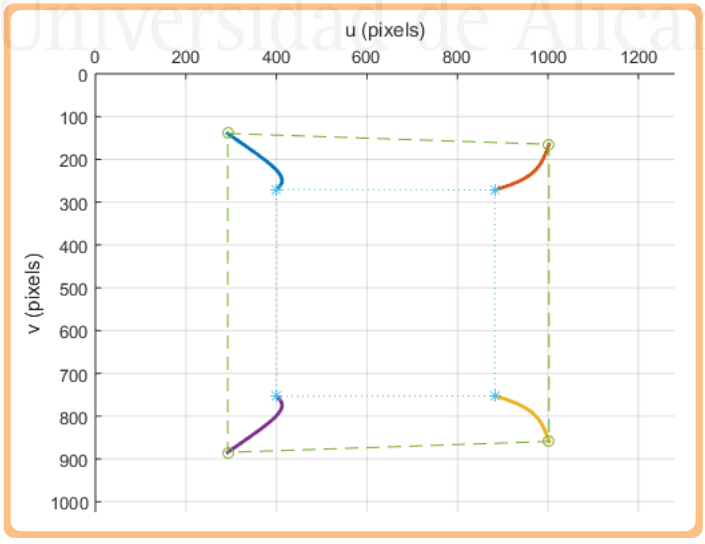

Figure 2.28. Experiment 2. Evolution of the features during the experiment.

Figure 2.29 represents the evolution of the Cartesian velocity, showing that the camera slows down the more it reaches de desired position.

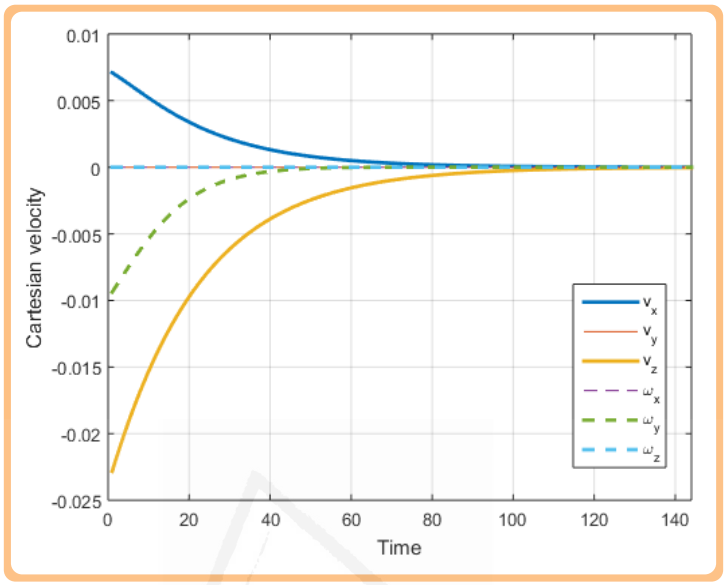

Figure 2.29. Experiment 2. Cartesian velocity of the camera in 3-D space with respect to time.

At the same time, the error converges to zero as shown in Figure 2.30, proving the success of the task.

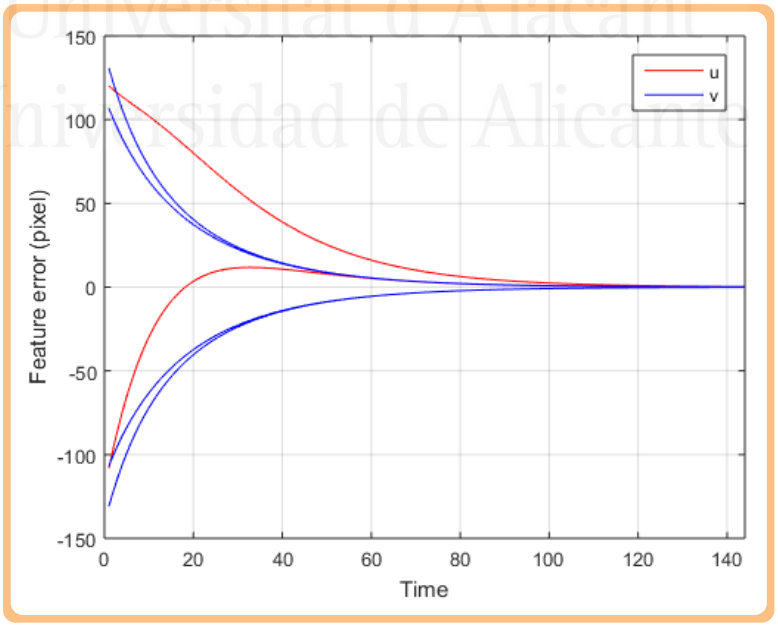

Figure 2.30. Experiment 2. Feature error in the image space with respect to time.

Figure 2.31 is a representation of the evolution of the camera pose during the experiment, showing soft and controlled movements.

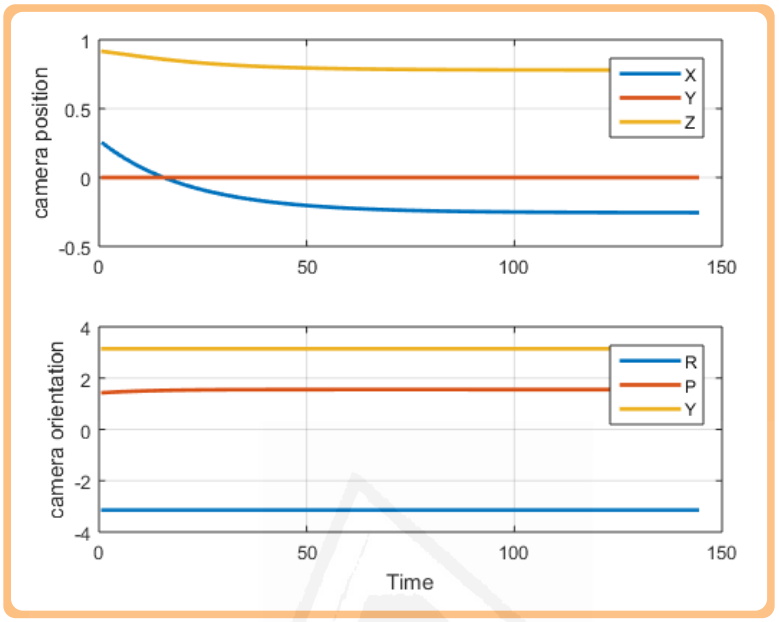

Figure 2.31. Experiment 2. Pose evolution of the camera with respect to time.

The next experiment shows an example of a visual singularity, where the desired features are rotated 180 degrees in respect to the real features as shown in Figure 2.32.

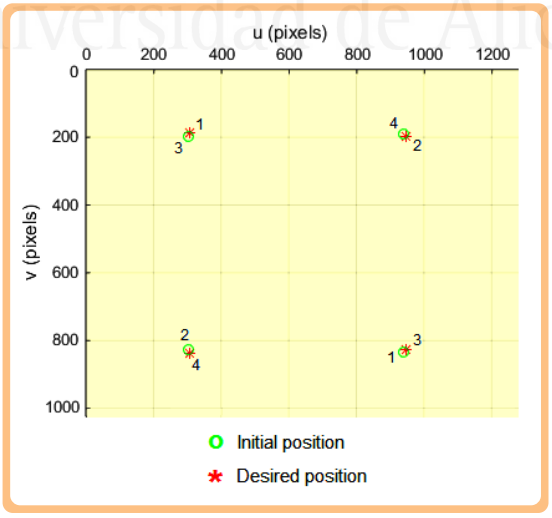

Figure 2.32. Experiment 3. Initial and desired position of four features in 3-D space as seen in the image space of the camera.

When dealing with a situation like this, the control strategy determines that the movement in the image space should be similar to the one shown in Figure 2.33, but this can only be achieved when the end effector holding the camera retracts from the pattern. The arrows from Figure 2.33 indicate the direction the features should move in order to match the desired ones. The only end-effector trajectory that satisfies this condition would be to move the robot's end-effector backwards and thereby eventually failing due to workspace limitations. This can be seen in the first iterations of the experiment in Figure 2.34, where the features move towards the center. At some point, they move to one side of the image, but this could be because of the influence of the movement of the camera due to the robot's joint configuration. Nevertheless, the end effector keeps moving away to obtain the correct pattern, thus making the square smaller until the experiment fails because of the limitations of the robot's working space.

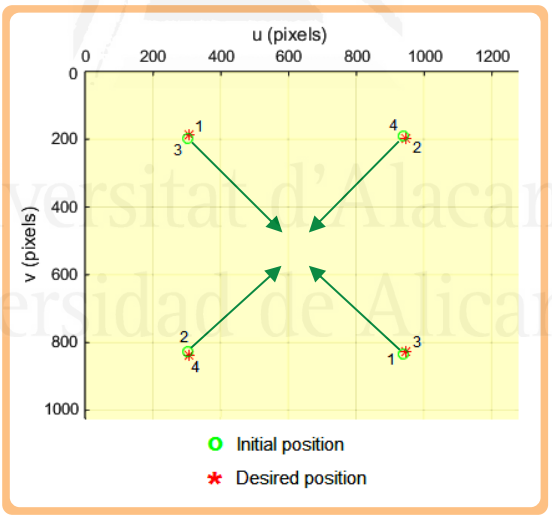

Figure 2.33. Experiment 3. Theoretical direction of the features to match the desired features.

As Figure 2.35 shows, the camera starts moving faster as the error in the image increases—but in the wrong direction—until the system crashes, proving the instability of the experiment.

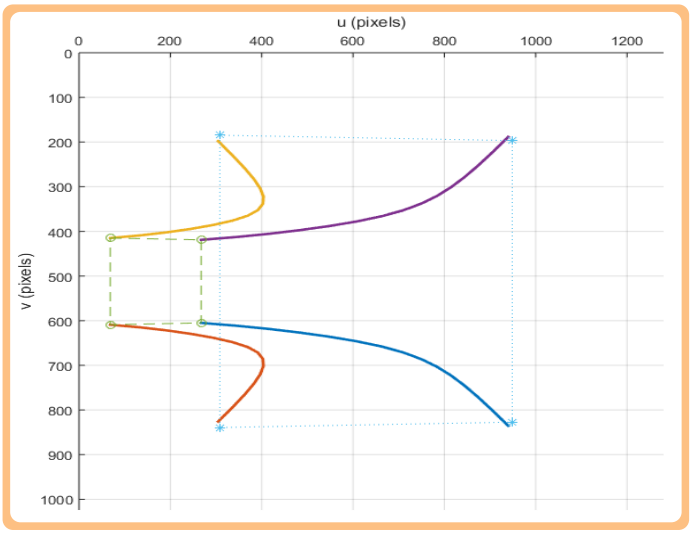

Figure 2.34. Experiment 3. Evolution of the features during the experiment.

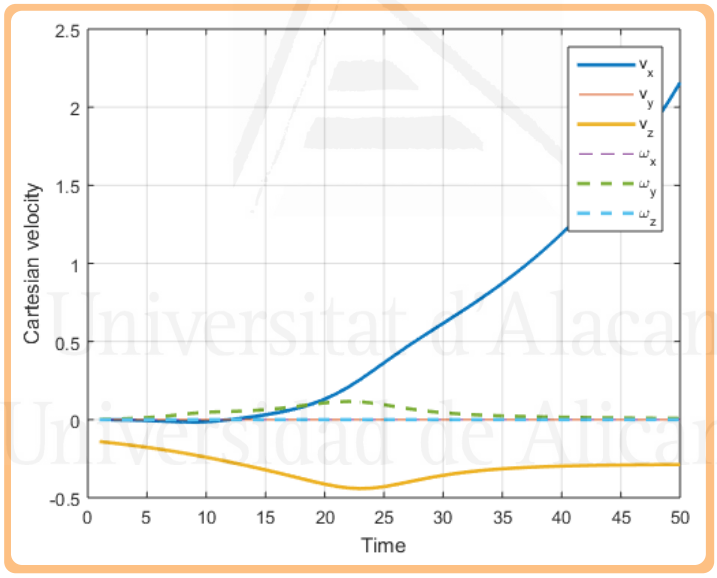

Figure 2.35. Experiment 3. Cartesian velocity of the camera in 3-D space with respect to time.

Another demonstration of how the system is unstable is the evolution of the error with respect to the time. The system shows clear signs of instability as seen in Figure 2.36, where the error in u pixels increases quickly and the error in v remains between 400 and 600 during the experiment, never converging to 0.

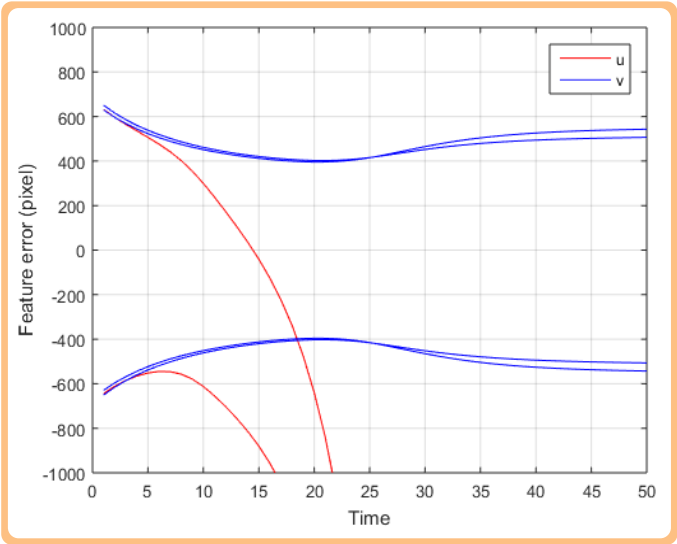

Figure 2.36. Experiment 3. Feature error in the image space with respect to time.

2.6.3 Direct position-based visual servoing

This section outlines the main characteristics of direct position-based visual servoing systems. As stated before, indirect visual servoing systems determine the velocity applied to the robot's end effector or joint velocities in order to position the camera with respect to the reference object. To do this, the internal robot controller is used and translates these velocities into torques and forces for the joints. By employing a direct control scheme like the one in Figure 2.37, the internal feedback control loop for the servomotors is removed and the visual information is used to directly generate the currents or torques to be applied to the motors of the robot's every joint.

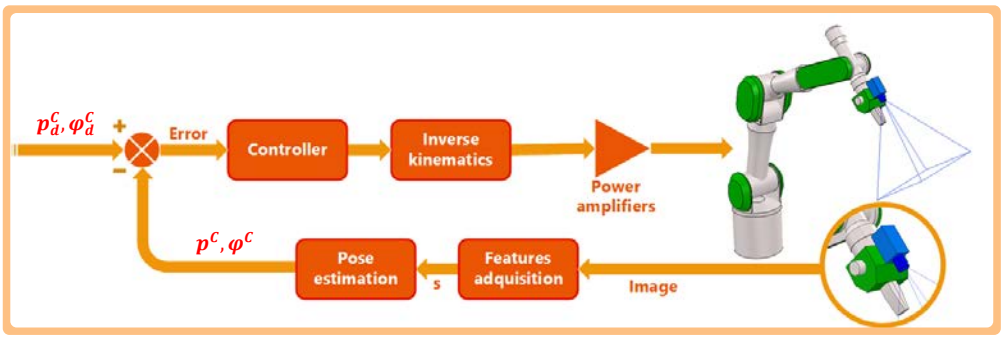

Figure 2.37. Direct position-based controller.

These controllers integrate not only the robot's kinematics, but also its dynamic behavior. The result is a faster controller that reacts better to changes in the reference parameter or to movements in the observed object. Figure 2.37 depicts how a desired tridimensional pose is used as the reference parameter.

2.6.4 Direct image-based visual servoing

Finishing out the classification of visual servoing systems, Figure 2.38 indicates the main components of a direct image-based visual servoing system. For this configuration, the reference is a set of desired visual features; that is, those to be observed once the task is over. The error $\boldsymbol{e}_s$ specified in the image space is the input for the controller. This error determines the necessary joint torques (or current to be applied to each motor) that moves the robot so the extracted features converge into the desired ones.

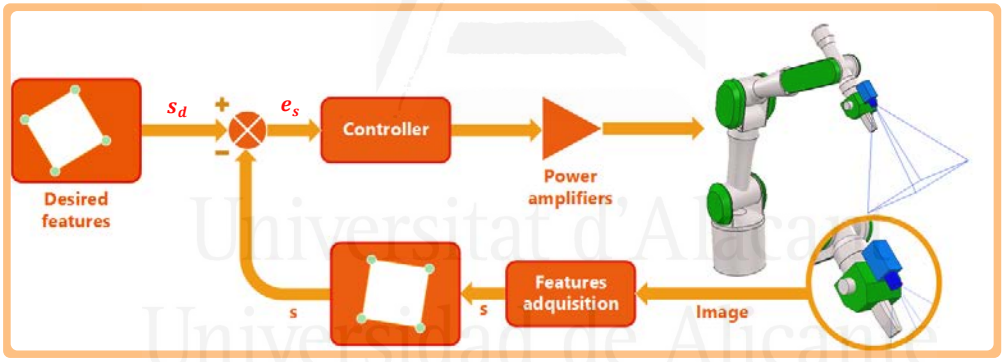

Figure 2.38. Direct image-based controller.

After the appearance of these first visual servoing systems in early 1980's, their evolution has been slow. However, new developments appeared during the last couple of decades, mainly due to the higher processing capabilities of new computers and computer vision systems that allow for processing a scene at a higher frequency. One of the main lines of research in this field is that developed by (Chaumette, 1990) consisting of applying the task function (Samson, Espiau, & Borgne, 1991) when using information captured by a camera. From that point on, a notable number of authors began to be interested in different aspects of visual

servoing. The following references present an overview of the main lines of recent research within the field of visual servoing systems (Chaumette & Hutchinson, 2006, 2007; Chesi & Hashimoto, 2010; Wang, 2016). Since a great deal of this Thesis' contributions are applied to this type of visual servoing, the state of the art of the controllers is described in more detail here.

It is possible to find some researchers who have worked on direct image-based visual servoing systems with the objective of improving response times and stability compared to indirect control strategies. It is also worth mentioning that some authors have developed designs of visual servoing systems based on passive properties (Soria, Roberti, Carelli, & Sebastián, 2008). Further, there are implementations of direct control algorithms that consider the manipulator's dynamics (Kelly, Cervantes, Alvarez-Ramirez, Bugarin, & Monroy, 2008) and employ Lyapunov's theory to analyze the system's stability. As indicated before, direct visual servoing systems allow for obtaining joint forces and torques directly. This removes the delay produced by the internal robot controller. The result is quicker and more precise control, since the time between movement instructions is reduced and allows the robot to react quicker when presented with sudden changes in the trajectory. Existing works in the field describe dynamic visual servoing for a robot. In most cases, these robots have just a few degrees of freedom. One of the first visual servoing works where the dynamics are taken into account is performed by (Miyazaki & Masutani, 1990). The controller proposed by (Miyazaki & Masutani, 1990) approximates a controller based on the transposed Jacobian, a technique developed for the first time in (Takegaki & Arimoto, 1981). (Pomares, Corrales, Garcia, & Torres, 2011) describe a direct visual servoing strategy for tracking an image, and consider the fact that the visual references for each instant of tracking depend on the time. The majority of direct visual servoing systems utilize an estimated dynamic model or one that is known in advance. It is also important to mention the works of (Cheah, Hou, Zhao, & Slotine, 2010) and (Li & Cheah, 2012) which implement an adaptive direct visual servoing controller

that is able to perform the task correctly even with errors in the dynamic model or task parameters (such as the depth or distance between the camera and the observed object). In general, for both direct and indirect visual servoing controllers, their stability was only demonstrated locally; in other words, it has only been demonstrated in a closed environment with a certain desired configuration. However, a work was published recently that tries to achieve a demonstration of global stability for direct visual servoing thanks to task sequencing (Li & Cheah, 2013).

This Thesis describes a new framework based on optimal control to define new dynamic visual controllers to carry out the guidance of any serial link structure. The proposed general method employs optimal control to obtain the desired behavior in the joint space based on an indicated cost function which determines how the control effort is distributed over the joints. The proposed approach allows the development of new direct visual controllers for any mechanical joint system with redundancy. This Thesis also shows experimental results and verifications on a real robotic system for some derived controllers obtained from the control framework, some of them implemented using Field Programmable Gate Arrays (FPGAs) (Perez et al., 2016).

The reduction in cost of FPGAs, their increasing capabilities, and the possibility of improving the performance of sensor processing tasks with specific hardware technologies have all increased their application and use in new fields related to control. The current capabilities of FPGAs enable the use of specific hardware technologies which can be employed to implement embedded control systems (García et al., 2014). FPGAs have already been used with success in different systems, such as the development of a higher-degree polynomial profile generator for CNC and in robotics applications (Osornio, de Jesús Romero, Herrera, & Castañeda, 2009), in the control of robotic arms (Kung & Shu, 2005), in neural network-based controllers (Muthuramalingam, Himavathi, & Srinivasan, 2008), and mechatronic systems (MacCleery & Kassas, 2008), among others. FPGAs

and their partial re-configurability provide additional useful properties to control systems (e.g. processing, interface, testing, configuration capabilities, etc.).

In terms of implementation of these kinds of systems, FPGAs allows for obtaining a dedicated parallel architecture that can be adapted in runtime to the system's needs. Within the field of visual servoing systems, there are only a few prior implementations that integrate FPGAs in some element of the visual servoing system. The majority of the delays in these systems are due to image processing tasks. This is why there are some works such as (Liyanage & Krouglicof, 2014) that optimize the image capture process through hardware implementation allowed by FPGAs. Additionally, it is possible to find embedded indirect visual servoing systems that integrate image processing and control (Hu, Chang, & Yang, 2011). However, it is not possible to find frameworks for the direct visual control of robot manipulators with varying degrees of freedom as described throughout the Thesis (Alabdo et al., 2015).

2.7 Conclusions

This chapter outlined the state of the art for visual servoing systems and provided an overview of visual servoing itself. Next, it undertook a classification scheme according to several criteria: the position of the camera in a visual servoing system, the workspace that can be position-based or image-based, and the direct or indirect control strategy. It followed with the different possible base configurations for the different robotic systems (fixed, mobile, free-floating, and free-based), ending with a description of the characteristics of the different permutations between the workspace and control strategies. More specific descriptions are detailed for indirect image-based visual servoing systems, since they are the ones that are mostly extended. Nevertheless, the Thesis' contributions will be focused on direct image-based visual servoing systems.

The next chapters of the Thesis are structured in a way that Chapter 3 describes in detail a direct image-based visual servoing system, describing an optimal control strategy for redundant robots. The control strategy is then improved taking the manipulability into consideration and extending it with a chaos compensation approach, finalizing with some experimental results. Once the control works well, the Thesis aims for optimizing the control strategy. This leads to Chapter 4, that introduces the concept of dynamic perceptibility that is later applied for controlling trajectories for two types of robot by using an FPGA. Some experimental results are shown at the end of the chapter. At this point, the Thesis described an optimal control with chaos compensation, so the next step is to teste it in an environment that requires high robustness. Chapter 5 extends the direct image-based visual servoing systems to space technology, extending the control framework developed in previous chapters for spacecrafts and free-floating base systems (those orbiting around a planet with no attitude control). It finishes with some experimental results showing the behavior of the system.

3 Direct visual servoing framework for controlling robot manipulators

This chapter presents the description and implementation of a generic visual servoing framework for controlling robot manipulators. For this, the chapter starts with an introductory section indicating strategies for controlling redundant manipulators and the different challenges the systems have to face. Second 3.2 presents the optimal visual servo control for such manipulators, describing their kinematics and dynamics characteristics and the implementation of the optimal servo control for repetitive image trajectories. Section 3.3 describes the problem of chaotic joint behavior for redundant manipulators and its resolution with a feedback time-delay chaos compensation term in the visual servoing controller. Section 3.4 details the implementation of the framework taking into account the manipulability and chaos compensation into the control action. Lastly, some experiments are presented to show the potential and good results when applying such framework to obtain different control action for a redundant manipulator. The Chapter finishes with some conclusions.

3.1 Introduction

Recently, new industrial robot manipulators include kinematic redundant structures in order to face complex and/or multiple tasks in unstructured and/or dynamic environments. This redundancy provides robotic systems with a large number of degrees of freedom performing complex joint structures. These mechanical structures both overcome intrinsic limitations of the mechanical construction and provide more flexibility during the tasks' performance. In the field of manufacturing processes, requirements such as the complexity of geometric shapes, the accuracy needed in the finished piece and the high speed required for the machining processes have focused the use of redundant joint structures (Andolfatto, Lavernhe, & Mayer, 2011; Song, Wang, Xiao, Wang, & Hong, 2012). However, controlling a redundant system during this type of tasks involves not only the correct end-effector motion, but also the achievement of correct joint-stabilization movements. This chapter presents a new optimal control framework for redundant joint structures where the task to be performed is specified in the image space. The classical image-based controllers determine the required camera velocities in order to position the robot with respect a reference object (Chaumette & Hutchinson, 2006). Using this last approach, the internal robot controller computes the joint torques in order to achieve the previously mentioned camera velocities. However, the framework proposed in this section to perform the control of the joint structure guidance is based on direct visual servoing. By means of direct visual servoing, the internal control loop of servo motors is removed and the visual servo control is employed to stabilize the robot (Pomares, Corrales, Garcia, & Torres, 2011). The result is a faster and more accurate control that reacts more quickly to abrupt changes in the image trajectories. Moreover, the approach presented in this Thesis is based on an optimal control framework and it is employed to control redundant joint structures taking the robot dynamics into account. This way, this control approach considers the optimization of the motor signals or torques sent to the

mechanical system during visual control tasks. Using this framework, several new direct visual controllers can be obtained for any mechanical system with redundancy, which offers a useful unification methodology. A precision study of different controllers derived from the framework is presented. The main contributions of this control framework have been published in (Pomares, Jara, Perez, & Torres, 2015).

The control of redundant mechanical systems has been a topic research in the last years, where many authors have proposed different control algorithms based on dynamics. It is worth pointing out the work presented by Khatib (Khatib, 1983), which proposed a dynamic control scheme for redundant robots using the pseudo-inverse of the Jacobian matrix. Other works such as these presented by Xian (Xian, De Queiroz, Dawson, & Walker, 2004) and Zergeroglu (Zergeroglu, Dawson, Walker, & Setlur, 2004), are based on a nonlinear controller which ensured an asymptotic tracking in the Cartesian space. Tatlicioglu (Tatlicioglu, Braganza, Burg, & Dawson, 2009) and Lin (Lin, 2004) presented the application of another kind of controllers such adaptive and optimal control in the path planning. Other recent approaches are focused in neural network technology because of their learning capabilities and parallel computing. In this field, most of the contributions are in charge of compensating both the nonlinearities (Nakanishi, Cory, Mistry, Peters, & Schaal, 2008) and structured/unstructured uncertainties of the system (Kumar, Borm, Panwar, & Chai, 2012). The above commented approaches are based on position, orientation and/or velocity control in the path tracking. However, as it is previously indicated, the proposed framework employs image information for the robot guidance. Therefore, the use of this framework allows us to derive new visual controllers to track complex shapes in the image space using any redundant joint structure, guaranteeing that the correct joint motion is obtained.

In applications such as laser-cutting, the redundant machine must often track repetitive or quasi-repetitive trajectories. This can produce a non-periodic joint

motion or chaotic behavior. As it is shown in the results section, a chaotic behavior in the joint space can be obtained while using a classical visual servoing system. In this case, the robot end-effector tracks the image trajectory correctly but an unpredictable and non-periodic motion is generated in the joint space. This non-repeatability in the joint space limits the practical applications of the visual controller. In previous works (Pomares, Perea, & Torres, 2014), the authors have integrated chaos compensation in classical dynamic visual controllers in order to obtain a periodic joint trajectory when the robot end-effector also tracks a periodic image trajectory. This last aspect guarantees a smoother joint behavior and increases the safety by obtaining predictable trajectories. In this chapter, the chaos controller is also integrated in the proposed framework. Therefore, the new controllers derived from the framework also include chaos compensation. Section 3.5 presents some experimental results where a precision study is included in order to evaluate the new direct visual controllers.

3.2 Optimal visual control for redundant robot manipulators

This section shows the proposed control framework to guide redundant robots using visual information. In order to accurately explain the control framework, this section is divided into five subsections. Firstly, the kinematics and dynamics formulation of a robot is defined. Secondly, the visual servoing concepts employed in the framework are described. Afterwards, the optimal control approach applied for visual servoing is explained. Next, the image trajectory to be tracked is described as a task constrain. Finally, the required modifications of the control framework for redundancy resolution and chaos control are presented.

3.2.1 Kinematics and dynamics of the joint structure

The differential kinematics of a joint structure with n degrees of freedom establishes the relationship between the joint velocities and the corresponding end-effector velocity. This relationship can be given as follows:

$$\dot{\boldsymbol{r}} = \mathbf{J}_r(\boldsymbol{q})\dot{\boldsymbol{q}} \tag{3.1}$$

where $\boldsymbol{r} \in \Re^{\eta}$ is the pose of the camera located at the robot end-effector, being η the dimension of the space where the path tracking is performed, $\dot{\boldsymbol{r}}$ is the Cartesian end-effector velocity, $\boldsymbol{q} \in \Re^{nx1}$ is a vector of generalized joint coordinates where n is the number of joints, $\dot{\boldsymbol{q}} \in \Re^{nx1}$ represents the joint velocities, and $\mathbf{J}_r(\boldsymbol{q})$ is the manipulator Jacobian matrix.

Regarding the dynamics, the well-known model of a serial n-link rigid mechanism, in absence of friction, can be written as:

$$\boldsymbol{\tau} = \mathbf{M}(\boldsymbol{q})\ddot{\boldsymbol{q}} + \mathbf{C}(\boldsymbol{q}, \dot{\boldsymbol{q}}) + \boldsymbol{g}(\boldsymbol{q}) \tag{3.2}$$

where $\ddot{\boldsymbol{q}} \in \Re^{nx1}$ is the joint accelerations, $\mathbf{M}(\boldsymbol{q}) \in \Re^{nxn}$ is the symmetric positive definite manipulator inertia matrix, $\mathbf{C}(\boldsymbol{q}, \dot{\boldsymbol{q}}) \in \Re^{nx1}$ denotes the vector of centripetal and Coriolis forces, and $\boldsymbol{g}(\boldsymbol{q}) \in \Re^{nx1}$ is the gravitational force. Finally, $\boldsymbol{\tau} \in \Re^{nx1}$ is the vector of applied motor commands (i.e. torques or forces). In order to simplify this equation, we can write the dynamics as follows:

$$\mathbf{M}(\boldsymbol{q})\ddot{\boldsymbol{q}} = \boldsymbol{\tau} + \mathbf{F}_{cg}(\boldsymbol{q}, \dot{\boldsymbol{q}}) \tag{3.3}$$

where $\mathbf{F}_{cg}(\boldsymbol{q}, \dot{\boldsymbol{q}}) = -\mathbf{C}(\boldsymbol{q}, \dot{\boldsymbol{q}}) - \boldsymbol{g}(\boldsymbol{q})$.

3.2.2 Visual servo control

Visual servo control techniques (Sanderson & Weiss, 1980) allow for the guidance of a joint robot using visual information, typically using an eye-in-hand configuration where a camera is held by the mechanism end-effector. The relationship between velocities in camera image space, $\dot{\boldsymbol{s}}_r$, and end-effector velocity, $\dot{\boldsymbol{r}}$, is represented by:

$$\dot{\boldsymbol{s}}_r = \mathbf{L}_s(\boldsymbol{s})\dot{\boldsymbol{r}} \tag{3.4}$$

where $\mathbf{L}_s(\boldsymbol{s})$ is the interaction matrix. From this relation and Equation (3.1), the image space velocity $\dot{\boldsymbol{s}}_r$ can be related to joint space velocity $\dot{\boldsymbol{q}}$ by means of the following relationship:

$$\dot{\boldsymbol{s}}_r = \mathbf{L}_s(\boldsymbol{s}) \cdot \mathbf{J}_r(\boldsymbol{q})\dot{\boldsymbol{q}} = \mathbf{L}_J(\boldsymbol{q}, \boldsymbol{s})\dot{\boldsymbol{q}} \tag{3.5}$$

where $\mathbf{L}_J = \mathbf{L}_J(\boldsymbol{q}, \boldsymbol{s})$ is the Jacobian matrix mapping joint space to image space. This matrix relates differential changes in joint configuration of the robot to differential changes in the observed image feature parameters.

The image acceleration or second time derivative of $\boldsymbol{s}_r$ is obtained by differentiating Equation (3.5) with respect to the time:

$$\ddot{\boldsymbol{s}}_r = \mathbf{L}_J\ddot{\boldsymbol{q}} + \dot{\mathbf{L}}_J\dot{\boldsymbol{q}} \tag{3.6}$$

The variable $\ddot{\boldsymbol{s}}_r$ denotes the reference image accelerations of the proposed controller based on image space.

3.2.3 Optimal control approach

The dynamic model of a serial-link robot represented by Equation (3.2) has been used in different approaches to control a robotic system for tracking (Pomares et al., 2014). Following this idea, the approach proposed by Udwadia (Udwadia, 2003) gave a new perspective about tracking based on optimal control for nonlinear mechanical systems. This approach will be used in this Thesis in order to perform the visual tracking of a redundant joint structure.

Basically, the control approach suggested by Udwadia (Udwadia, 2003) supposes a system with m constrains (holonomic and/or non-holonomic) which represent the task for the robot to be described. The time derivate of these constraints is represented by the following equation:

$$\mathbf{A}(\boldsymbol{q}, \dot{\boldsymbol{q}}, t)\ddot{\boldsymbol{q}} = \boldsymbol{b}(\boldsymbol{q}, \dot{\boldsymbol{q}}, t) \tag{3.7}$$

where $\mathbf{A}(\boldsymbol{q}, \dot{\boldsymbol{q}}, t) \in \Re^{mxn}$ and $\boldsymbol{b}(\boldsymbol{q}, \dot{\boldsymbol{q}}, t) \in \Re^{mx1}$ are the matrix and the vector obtained, respectively. The optimal controller treats to minimize the control torques of the mechanical system while performing a specific task taking into account the following function cost:

$$\boldsymbol{\Omega}(t) = \boldsymbol{\tau}^T \mathbf{W}(t) \boldsymbol{\tau} \tag{3.8}$$

where $\mathbf{W}(t) \in \Re^{nxn}$ is a time-dependent weight matrix. The function control that minimizes $\boldsymbol{\Omega}(t)$ of the mechanical system based on the dynamics model expressed in Equation (3.3) while performing the task described in Equation (3.7) is given by (for the sake of clarity the time and joint dependences are not indicated):

$$\boldsymbol{\tau} = \mathbf{W}^{-1/2}\left(\mathbf{A}\mathbf{M}^{-1}\mathbf{W}^{-1/2}\right)^{+} \cdot \left(\boldsymbol{b} + \mathbf{A}\mathbf{M}^{-1}\mathbf{F}_{cg}\right) \tag{3.9}$$

where $\mathbf{M}$ is the inertia matrix and the symbol + denotes the pseudo-inverse for a general matrix. As it can be seen in Equation (3.9), the matrix $\mathbf{W}$ is an important depending variable in the control law and determines how the control effort is distributed over the joints.

Equation (3.6), which describes the image task of the redundant robot, can be expressed into the form of Equation (3.7):

$$\mathbf{L}_J \ddot{\boldsymbol{q}} = \ddot{\boldsymbol{s}}_r - \dot{\mathbf{L}}_J \dot{\boldsymbol{q}} \tag{3.10}$$

This way, the task constrains are defined by the following relationships:

$$\begin{aligned} \mathbf{A} &= \mathbf{L}_J \\ \boldsymbol{b} &= \ddot{\boldsymbol{s}}_r - \dot{\mathbf{L}}_J \dot{\boldsymbol{q}} \end{aligned} \tag{3.11}$$

Therefore, with this definition of $\mathbf{A}$ and $\boldsymbol{b}$, the optimal control will minimize the torques of the joint structure while performing a tracking in the image space.

The final control law can be obtained replacing these variables into the function that minimizes the motor signals described by Equation (3.9):

$$\boldsymbol{\tau} = \mathbf{W}^{-1/2}\left(\mathbf{L}_J\mathbf{M}^{-1}\mathbf{W}^{-1/2}\right)^{+} \cdot \left(\ddot{\boldsymbol{s}}_r - \dot{\mathbf{L}}_J\dot{\boldsymbol{q}} - \mathbf{L}_J\mathbf{M}^{-1}\mathbf{F}_{cg}\right) \tag{3.12}$$

As it can be seen, the visual controller represented by (3.12) depends implicitly on the weighting matrix $\mathbf{W}$ and different values of this matrix can simplify the product $\left(\mathbf{L}_J\mathbf{M}^{-1}\mathbf{W}^{-1/2}\right)^{+}$ and consequently, the control law. Additionally, different visual servoing control laws can be obtained with different values of $\mathbf{W}$, performing a new optimal control framework for the visual tracking of redundant joint structures.

3.2.4 Task description using an image trajectory

The optimal control approach described in the previous subsection will be employed to track an image trajectory taking into account the robot dynamics. As shown, the tracked trajectory is defined and expressed as a set of constraints following Equation (3.7) (see Equation (3.11)). In this subsection, the definition of the reference control $\ddot{\boldsymbol{s}}_r$ is described considering an eye-in-hand camera system which extracts a set of k image feature points.

Let $\boldsymbol{s} = \left[f_{1x}, f_{1y}, f_{2x}, f_{2y}, \ldots, f_{kx}, f_{ky}\right]^{\mathrm{T}} \in \Re^{2k}$ be a vector of the k extracted image feature points, the task description as constraint is given by the following equation in the image space:

$$(\ddot{\boldsymbol{s}}_d - \ddot{\boldsymbol{s}}) + \mathbf{K}_D(\dot{\boldsymbol{s}}_d - \dot{\boldsymbol{s}}) + \mathbf{K}_P(\boldsymbol{s}_d - \boldsymbol{s}) = 0 \tag{3.13}$$

where $\ddot{\boldsymbol{s}}_d$, $\dot{\boldsymbol{s}}_d$ and $\boldsymbol{s}_d$ are the desired image space accelerations, velocities and positions, respectively. $\mathbf{K}_P \in \Re^{2kx2k}$ and $\mathbf{K}_D \in \Re^{2kx2k}$ are proportional and derivative gain matrices, respectively. This equation can be expressed in regard to image error in the following way:

$$\ddot{\boldsymbol{s}}_d + \mathbf{K}_D\dot{\boldsymbol{e}}_s + \mathbf{K}_P\boldsymbol{e}_s = \ddot{\boldsymbol{s}}_r \tag{3.14}$$

where $\boldsymbol{e}_s$ and $\dot{\boldsymbol{e}}_s$ are the image error and the time derivative of the error respectively. As stated, the variable $\ddot{\boldsymbol{s}}_r$ denotes the reference image accelerations of our image space based controller. Replacing this variable into the dynamic visual servo controller, Equation (3.12), the control law is set by the following relationship:

$$\boldsymbol{\tau} = \mathbf{W}^{-1/2}\left(\mathbf{L}_J\mathbf{M}^{-1}\mathbf{W}^{-1/2}\right)^{+} \cdot \left(\ddot{\boldsymbol{s}}_d + \mathbf{K}_D\dot{\boldsymbol{e}}_s + \mathbf{K}_P\boldsymbol{e}_s - \dot{\mathbf{L}}_J\dot{\boldsymbol{q}} - \mathbf{L}_J\mathbf{M}^{-1}\mathbf{F}_{cg}\right) \qquad (3.15)$$

In Figure 3.1 a scheme with the main components of the proposed framework is shown. In order to demonstrate an asymptotic tracking of the control law described in Equation (3.15), some operations must be done. Firstly, the closed loop behavior is computed using Equation (3.3) as:

$$\begin{aligned}\mathbf{M}\ddot{\boldsymbol{q}} - \mathbf{F}_{cg} = {} & \mathbf{W}^{-1/2}\left(\mathbf{L}_J\mathbf{M}^{-1}\mathbf{W}^{-1/2}\right)^{+} \\ & \cdot \left(\ddot{\boldsymbol{s}}_d + \mathbf{K}_D\dot{\boldsymbol{e}}_s + \mathbf{K}_P\boldsymbol{e}_s - \dot{\mathbf{L}}_J\dot{\boldsymbol{q}} - \mathbf{L}_J\mathbf{M}^{-1}\mathbf{F}_{cg}\right)\end{aligned} \qquad (3.16)$$

Equation (3.16) can be simplified by pre-multiplying its left and right side by $\left(\mathbf{L}_J\mathbf{M}^{-1}\mathbf{W}^{-1/2}\right)\cdot\mathbf{W}^{1/2}$:

$$\mathbf{L}_J\ddot{\boldsymbol{q}} = \ddot{\boldsymbol{s}}_d + \mathbf{K}_D\dot{\boldsymbol{e}}_s + \mathbf{K}_P\boldsymbol{e}_s - \dot{\mathbf{L}}_J\dot{\boldsymbol{q}} \qquad (3.17)$$

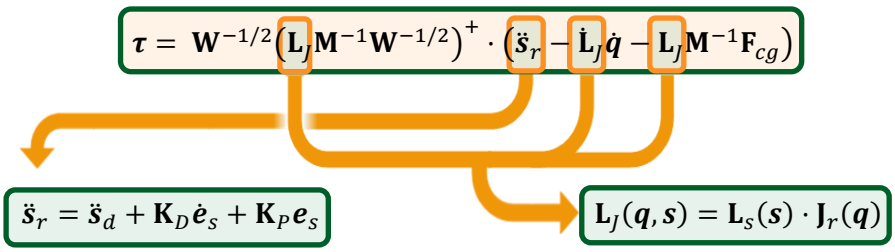

Figure 3.1. Scheme of the main components of the proposed framework.

W: weighting matrix to define new controllers

Using the relationship expressed in (3.6), it can be concluded that:

$$\ddot{\boldsymbol{e}}_s = -\mathbf{K}_D\dot{\boldsymbol{e}}_s - \mathbf{K}_P\boldsymbol{e}_s \tag{3.18}$$

Therefore, when $\mathbf{L}_J$ is full rank an asymptotic tracking is achieved of the visual servo controller expressed by Equation (3.15) in the tracking of an image trajectory.

3.2.5 Null-space resolution

In this Section, a redundant robot is considered to track the image trajectory and hence n > η, being η the dimension of where the path tracking is being performed. In this case, the visual controller must guarantee the correct motion of end-effector and joints, avoiding singularities and/or possible chaotic behavior. Therefore, it is needed a joint function which stabilizes the robot without affecting the task performed in the image space. One possibility to do that is by defining a desired behavior that is only applied in the null space of the visual controller indicated in Equation (3.12). As it is shown in this last equation, the task space is defined by $\mathbf{W}^{-1/2}\left(\mathbf{L}_J\mathbf{M}^{-1}\mathbf{W}^{-1/2}\right)^{+}$. Therefore, the term expressed as $\left[\mathbf{I} - \mathbf{W}^{-1/2}\left(\mathbf{L}_J\mathbf{M}^{-1}\mathbf{W}^{-1/2}\right)^{+}\left(\mathbf{L}_J\mathbf{M}^{-1}\mathbf{W}^{1/2}\right)\mathbf{W}^{1/2}\right]\cdot\boldsymbol{\tau}_1$ can be used to project the motor command $\boldsymbol{\tau}_1$ onto the null space of the dynamic visual servo task. Including this control in the proposed framework, the following control law can be obtained:

$$\begin{aligned}\boldsymbol{\tau} = {} & \mathbf{W}^{-1/2}\left(\mathbf{L}_J\mathbf{M}^{-1}\mathbf{W}^{-1/2}\right)^{+}\cdot\left(\ddot{\boldsymbol{s}}_r - \dot{\mathbf{L}}_J\dot{\boldsymbol{q}} - \mathbf{L}_J\mathbf{M}^{-1}\mathbf{F}_{cg}\right) + \mathbf{W}^{-1/2} \\ & \cdot\left[\mathbf{I} - \left(\mathbf{L}_J\mathbf{M}^{-1}\mathbf{W}^{-1/2}\right)^{+}\left(\mathbf{L}_J\mathbf{M}^{-1}\mathbf{W}^{1/2}\right)\right]\mathbf{W}^{1/2}\cdot\boldsymbol{\tau}_1\end{aligned} \tag{3.19}$$

Thus, the task accomplishment is independent of the joint-space stabilization done by $\boldsymbol{\tau}_1$. Setting $\boldsymbol{\tau}_1 = \mathbf{C} + \boldsymbol{g} + \boldsymbol{\tau}_0$, the Coriolis, centrifugal and gravitational forces can be compensated. Using this modification, the control law yields as follows:

$$\boldsymbol{\tau} = \mathbf{W}^{-1/2}\left(\mathbf{L}_J\mathbf{M}^{-1}\mathbf{W}^{-1/2}\right)^{+} \cdot \left(\ddot{\boldsymbol{s}}_r - \dot{\mathbf{L}}_J\dot{\boldsymbol{q}}\right) + \mathbf{C} + \boldsymbol{g} + \mathbf{W}^{-1/2} \cdot \left[\mathbf{I} - \left(\mathbf{L}_J\mathbf{M}^{-1}\mathbf{W}^{-1/2}\right)^{+}\left(\mathbf{L}_J\mathbf{M}^{-1}\mathbf{W}^{1/2}\right)\right]\mathbf{W}^{1/2} \cdot \boldsymbol{\tau}_0 \quad (3.20)$$

Next section will show the definition of the control signal required to compensate the chaotic joint behavior which can appear during the tracking of repetitive image trajectories.

3.3 Chaotic joint behavior in visual servoing tasks

As it is proved through the results section of this chapter, by using a visual servoing system a chaotic behavior can also be obtained in the joint space. In this case, the robot-end tracks the image trajectory correctly but an unpredictable and non-periodic motion is obtained in the joint space. There are different tasks which require that a robot-end describes a repetitive trajectory. For example, processes such as polishing, milling or cutting often require that the robot performs repetitive trajectories. However, the non-repeatability in the joint space limits the practical applications of the visual controller.

The Delayed Feedback Control (DFC) method, proposed by Pyragas (Pyragas, 1992), has been proved to be adequate to control chaotic systems. This method generates a control signal in order to synchronize the current state of the system and the one obtained delayed one period of the system (Pyragas, 2006). In this paper, the DFC method is employed to avoid the chaotic joint behavior of the defined dynamic visual servoing system. This last aspect guarantees a smoother joint behavior and increases the safety obtaining predictable trajectories. Furthermore, a method to adjust the parameters of the chaos controller is proposed and verified with the experimental results.

By using the controller presented in Section 3.2, there are experiments in which a chaotic joint motion is obtained during the tracking of repetitive image trajectories. In order to guarantee the applicability of the controller, a repetitive

path tracked by the robot-end must produce a periodic joint motion. To eliminate the chaotic joint behavior, a DFC will be integrated in the proposed framework. The main advantage of the DFC method against others such as the OGY method (Ott, Grebogi, & Yorke, 1990) is that it does not require a reference signal corresponding to the desired unstable periodic orbit (UPO). To implement the DFC method an exact model of the system dynamics or the form of the periodic orbit is not required (except for its period).

In general, when a chaotic behavior is obtained in the joint space, joint trajectories have a large number of UPOs embedded. These trajectories visit or access the neighborhood of each of these periodic orbits. Some of these UPOs may correspond to the desired system's performance. In order to obtain this desired performance, the DFC method generates a perturbation proportional to the difference between the current state of the system, $\boldsymbol{x}(t)$, (or a subset of the system state variables) and the state of the system delayed by one period of the UPO, $\boldsymbol{x}(t-\varepsilon)$ (Pyragas, 2006). The control action or perturbation of the DFC controller vanishes when the stabilization of the target orbit is achieved. Considering the robot dynamics presented in Equation (3.2), a direct visual servoing system with DFC compensation leads to the following control action:

$$\boldsymbol{\tau} = \mathbf{M}(\boldsymbol{q})\mathbf{L}_J{}^{+}\left(\ddot{\boldsymbol{s}}_r - \dot{\mathbf{L}}_J\dot{\boldsymbol{q}}\right) + \mathbf{M}(\boldsymbol{q})k\left(\boldsymbol{x}(t-\varepsilon) - \boldsymbol{x}(t)\right) + \mathbf{C}(\boldsymbol{q},\dot{\boldsymbol{q}}) + \boldsymbol{g}(\boldsymbol{q}) \qquad (3.21)$$

where k is a constant gain to be determined and ε is the feedback time-delay. The delay constant ε, is chosen to be equal to the period of the target UPO. By choosing an appropriate value of the control gain, k, the target UPO can be stabilized, i.e., the system trajectory converges to the ε periodic orbit. Using these values, the system under control automatically settles on the target periodic motion, and the stability of this motion is maintained with only small perturbations (Pyragas, 2006).

As it is indicated in (Liu, Li, & Zhang, 2007), to implement the DFC method in a redundant manipulator, joint velocity variables must be considered as the delayed subset of the system state variables (i.e. $\boldsymbol{x}(t) = \dot{\boldsymbol{q}}(t)$). This previous work computes the suitable values of k using numerical simulations (it does not consider the robot dynamics and does not employ image-based control). These simulations determine the values of k from which the computed largest Lyapunov exponent of the system is negative. These gain values are employed in the robot controller. However, these theoretical values of k do not compensate the chaotic robot behavior in practice. As it will be described, the measurement noise and uncertainties in different robot parameters cause that the theoretical values obtained using numerical simulations are not adequate to compensate the chaotic behavior. To avoid this problem, a method to adjust the value of k and ε is proposed and validated by using the experimental results.

3.4 Dynamic visual servo controllers derived from the control framework

Up to now, the control framework has been written depending on the weighting matrix $\mathbf{W}$. As stated, the choice of $\mathbf{W}$ plays an important role in the controller because it determines how the torques are distributed over the joints. Moreover, different values of this matrix can simplify the product $\left(\mathbf{L}_J\mathbf{M}^{-1}\mathbf{W}^{-1/2}\right)^+$ and consequently, the control law. Following, the new visual servoing control laws obtained from the choice of different values of $\mathbf{W}$ will be shown. A precision study of the derived controllers will be evaluated in the results section.

Considering $\mathbf{W} = \mathbf{M}^{-2}$ and replacing this value in the control framework expressed in Equation (3.20), the result yields:

$$\boldsymbol{\tau} = \boldsymbol{\tau}_{DFC} + \mathbf{M}\mathbf{L}_J^+ \cdot \left(\ddot{\mathbf{s}}_r - \dot{\mathbf{L}}_J\dot{\boldsymbol{q}}\right) + \mathbf{C} + \boldsymbol{g} + \mathbf{M} \cdot \left[\mathbf{I} - \mathbf{L}_J^+\mathbf{L}_J\right]\mathbf{M}^{-1} \cdot \boldsymbol{\tau}_0 \qquad (3.22)$$

This controller represents a direct visual servo control using inversion of the dynamic model of the joint structure.

Another value for the choice of $\mathbf{W}$ is $\mathbf{DM}^{-2}$, where $\mathbf{D}$ is a diagonal positive matrix. This matrix allows distributing the torques on the joints, and therefore, large weights cause small torques. Using this value for $\mathbf{W}$, the controller from Equation (3.20) results as follows:

$$\boldsymbol{\tau} = \boldsymbol{\tau}_{DFC} + (\mathbf{DM}^{-2})^{-1/2}\left(\mathbf{L}_J\mathbf{M}^{-1}(\mathbf{DM}^{-2})^{-1/2}\right)^{+}\left(\ddot{\mathbf{s}}_r - \dot{\mathbf{L}}_J\dot{\mathbf{q}}\right) + \mathbf{C} + \boldsymbol{g} + (\mathbf{DM}^{-2})^{-1/2} \cdot \left[\mathbf{I} - \left(\mathbf{L}_J\mathbf{M}^{-1}(\mathbf{DM}^{-2})^{-1/2}\right)^{+}\left(\mathbf{L}_J\mathbf{M}^{-1}(\mathbf{DM}^{-2})^{-1/2}\right)\right] \cdot (\mathbf{DM}^{-2})^{1/2} \cdot \boldsymbol{\tau}_0 \tag{3.23}$$

Applying the pseudo inverse as $\mathbf{Q}^{+} = \mathbf{Q}^{T}(\mathbf{Q} \cdot \mathbf{Q}^{T})^{-1}$ and simplifying this equation, the control law yields as:

$$\boldsymbol{\tau} = \boldsymbol{\tau}_{DFC} + \mathbf{MD}^{-1}\mathbf{L}_J^{T} \cdot \left(\mathbf{L}_J\mathbf{D}^{-1}\mathbf{L}_J^{T}\right)^{-1}\left(\ddot{\mathbf{s}}_r - \dot{\mathbf{L}}_J\dot{\mathbf{q}}\right) + \mathbf{C} + \boldsymbol{g} + \mathbf{MD}^{-1/2} \cdot \left[\mathbf{I} - \mathbf{D}^{-1/2}\mathbf{L}_J^{T}\left(\mathbf{L}_J\mathbf{D}^{-1}\mathbf{L}_J^{T}\right)^{-1}\mathbf{L}_J\mathbf{D}^{-1/2}\right] \cdot \mathbf{D}^{1/2}\mathbf{M}^{-1} \cdot \boldsymbol{\tau}_0 \tag{3.24}$$

Additionally, new controllers can be obtained using different values of $\mathbf{W}$. According to (Udwadia, 2003), an important value for $\mathbf{W}$, due to its physical interpretation, is $\mathbf{W} = \mathbf{M}^{-1}$, since it is consistent with the principle of d'Alembert. Furthermore, the use of $\mathbf{W} = \mathbf{I}$ simplifies the control law. In the next section the controllers obtained when $\mathbf{W} = \mathbf{M}^{-1}, \mathbf{W} = \mathbf{DM}^{-1}, \mathbf{W} = \mathbf{I}, \mathbf{W} = \mathbf{D}, \mathbf{W} = \mathbf{M}^{-2}$, and $\mathbf{W} = \mathbf{DM}^{-2q}$ are evaluated and compared with classical direct visual servoing like the proposed in previous works (Pomares et al., 2011a).

3.5 Experimental results

In this section, a set of experiments is presented to illustrate the precision performance of different direct visual servoing control laws obtained using the proposed framework. In order to evaluate the precision and properties of the generated controllers the eye-in-hand robot presented in Figure 3.2 is employed. A Photonfocus MV-D752-160 camera is considered, which acquires 340 images

every second with a resolution of 752x582 pixels. The robot has three rotational joints (q_1, q_2, q_3) whose actuators are four geared DC motors.

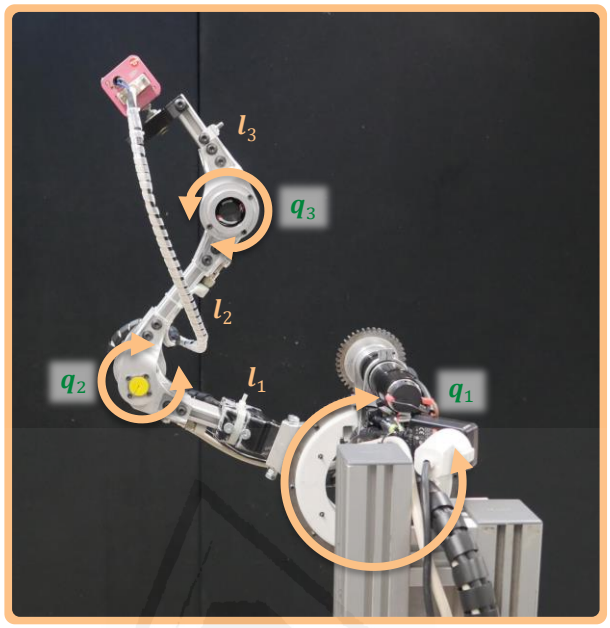

Figure 3.2. Robot employed in the experimental results.

The camera is supposed to be previously calibrated and the camera intrinsic parameters are $(u_0, v_0) = (298, 225)$ px, and $(f_u, f_v) = (1082.3, 1073.7)$ px (position of the optical center (u_0, v_0) and the focal length in the x and y directions, respectively). For the sake of clarity, the eye in hand camera is observing one visual feature performing a planar movement with respect to the robot at a distance of 1 m (k = 1). In all the experiments presented in this section, gain settings are $\mathbf{K}_P = 0.1 \cdot \mathbf{I}_{2x2}$ and $\mathbf{K}_D = 0.5 \cdot \mathbf{I}_{2x2}$ (the proportional and derivative matrices of the controller).

3.5.1 Chaos compensation

The system performance is evaluated in the next two subsections. The first one shows the chaotic joint behavior during the tracking of a repetitive trajectory in the image space. Furthermore, this first subsection describes the method to adjust the DFC part of the controller in order to obtain a periodic motion in the

joint space. The second subsection shows the controller behavior when different tracking velocities are considered.

In both cases, the desired trajectory to be tracked by the robot-end in the image space is defined by the equations:

$$\boldsymbol{s_d} = \begin{bmatrix} f_{xd} \\ f_{yd} \end{bmatrix} = \begin{bmatrix} 320 + 166\cos(\omega t + \pi/4) + 20\sin(\omega 5t) \\ 265 + 160\sin(\omega t + \pi/4) + 15\sin(\omega 5t) \end{bmatrix} \quad (3.25)$$

3.5.1.1. Parameters setup

Initially, a middle tracking velocity ($\omega = 1 rad/s$) and the controller indicated in Equation (3.25) is considered. Chaos control can be achieved by choosing appropriate value of the delay, ε, and of the adjustable weight, k. In order to observe the system behavior without chaos control ($k = 0$) a first experiment is presented in Figure 3.3. Figure 3.3.a shows the trajectory of the extracted image feature and Figure 3.3.b represents the tracking error module during the tracking.

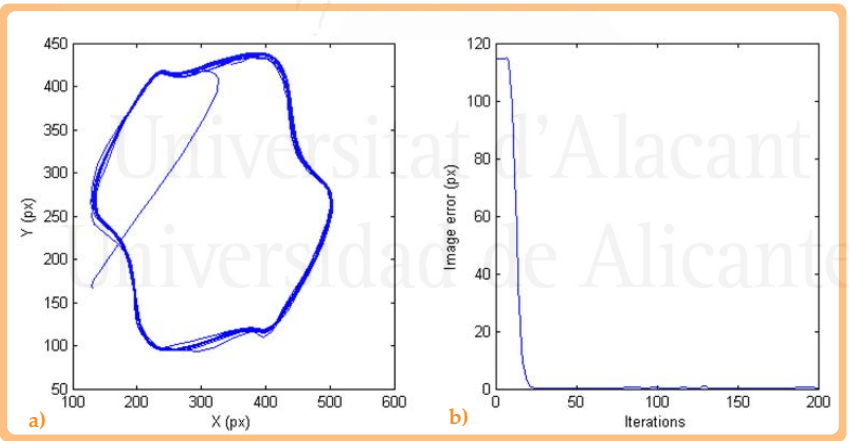

Figure 3.3. Behavior in the image space without chaos control.

a) Image trayectory. b) Image error module.

Using the previous indicated parameters, the image error remains low and the repetitive trajectory is correctly tracked in the image space. However, the joints have a non-repetitive behavior (see Figure 3.4).

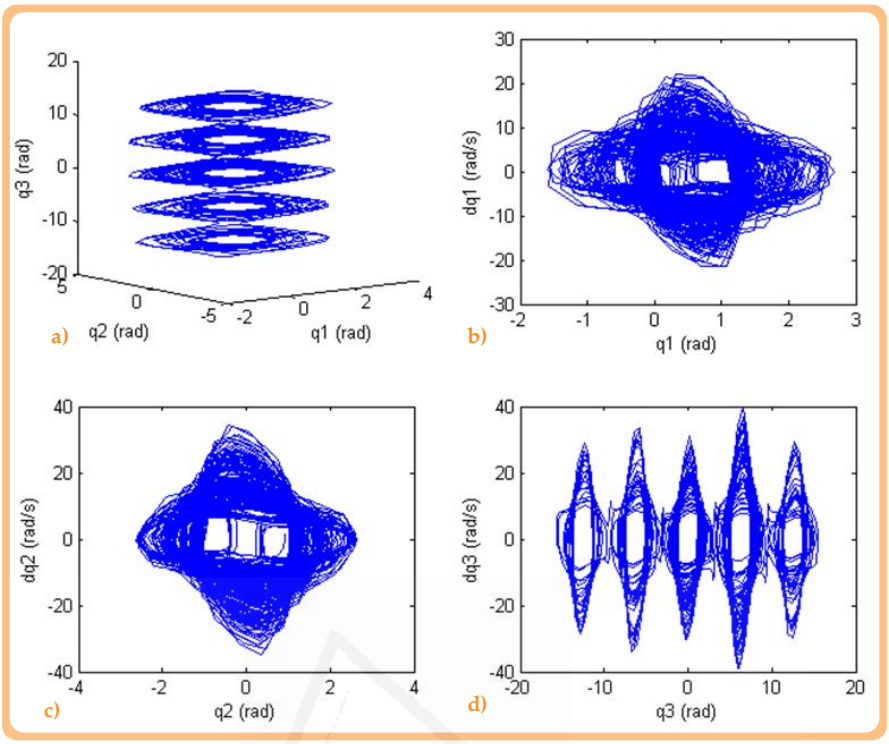

Figure 3.4. Phase portrait reconstructed from: a) q_1, q_2, q_3, b) $q_1, \dot{q}_1$, c) $q_2, \dot{q}_2$, d) $q_3, \dot{q}_3$. ($k = 0$).

The phase portraits represented in this last figure shows the chaotic behavior in the joint space. This aspect can also be observed in the largest Lyapunov exponent diagram illustrated in Figure 3.5.

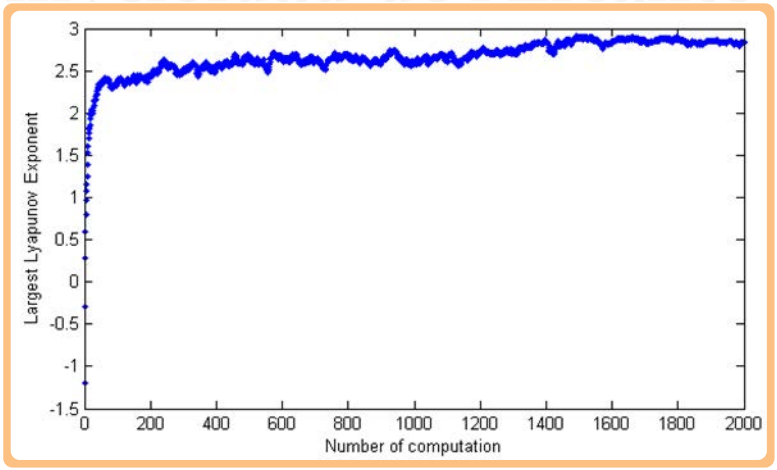

Figure 3.5. Largest Lyapunov exponent diagram (LLE = 2.83 > 0)

Figure 3.6 represents the torques obtained during the experiment. For the sake of clarity only the first 200 iterations are represented. Optimal values of k and ε provide stabilization of the desired UPO indicated by the choice of ε. These values depend on the control parameters and the chosen UPO. In order to determine these optimal values, the process described in the next paragraphs has been employed.

As previously indicated, the delay constant, ε, is chosen to be equal to the period of the target UPO. Therefore, the delay $\varepsilon = 2\pi$ seconds is initially considered and the optimal value of k must be determined. To obtain this value, the dependence between $|\boldsymbol{\Omega}| = |\dot{\boldsymbol{q}}(t-\varepsilon) - \dot{\boldsymbol{q}}(t)|$ and k must be computed (see Figure 3.7). To obtain this dependence, some variables must be defined. During the tracking of an image trajectory $\Omega_j q_i$ is defined as the difference $|\dot{\boldsymbol{q}}_i(t_j - \varepsilon) - \dot{\boldsymbol{q}}_i(t_j)|$, where t_j is the time at iteration j and the index i indicates thejoint under consideration. $|\boldsymbol{\Omega}_{j,\beta}\boldsymbol{q}_i|$ is the average value of the terms $\{\boldsymbol{\Omega}_j\boldsymbol{q}_i, \boldsymbol{\Omega}_{j+1}q_i \cdots \boldsymbol{\Omega}_{j+\beta}\boldsymbol{q}_i\}$. Finally, $|\boldsymbol{\Omega}_{j,\beta}|$ is defined as the average of the values of $|\boldsymbol{\Omega}_{j,\beta}\boldsymbol{q}_1|$, $|\boldsymbol{\Omega}_{j,\beta}\boldsymbol{q}_2|$, and $|\boldsymbol{\Omega}_{j,\beta}\boldsymbol{q}_3|$. In practice, in order to obtain Figure 3.7, a "setup phase" is employed. During this setup phase, the robot tracks the image trajectory while Figure 3.7 is being obtained. Throughout the tracking, the value of k is progressively increased, so that, for each value of k, the parameters $|\boldsymbol{\Omega}_{j,\beta}\boldsymbol{q}_1|$, $|\boldsymbol{\Omega}_{j,\beta}\boldsymbol{q}_2|$, $|\boldsymbol{\Omega}_{j,\beta}\boldsymbol{q}_3|$ and $|\boldsymbol{\Omega}_{j,\beta}|$ are determined during β iterations. Experimentally, 30 iterations are considered sufficient to stabilize the UPO (if possible). Therefore, $|\boldsymbol{\Omega}\boldsymbol{q}_i|$ is the value of $|\boldsymbol{\Omega}_{j,\beta}\boldsymbol{q}_i|$obtained for a given value of k during $\beta = 30$ iterations. $|\boldsymbol{\Omega}|$ is the average value of $|\boldsymbol{\Omega}\boldsymbol{q}_1|$, $|\boldsymbol{\Omega}\boldsymbol{q}_2|$ and $|\boldsymbol{\Omega}\boldsymbol{q}_3|$ for each value of k. Figure 3.7 represents the values of $|\boldsymbol{\Omega}\boldsymbol{q}_i|$ and $|\boldsymbol{\Omega}|$ depending on k. The lower value of $|\boldsymbol{\Omega}|$ is obtained when $k = 4.6$. This value will be employed in the DFC part of the controller to eliminate the chaotic behavior. In practice, it is not necessary to obtain the complete dependence between k and $|\boldsymbol{\Omega}|$. A gradient descent allows us to obtain the minimum value of $|\boldsymbol{\Omega}|$ and, therefore, the optimal k.

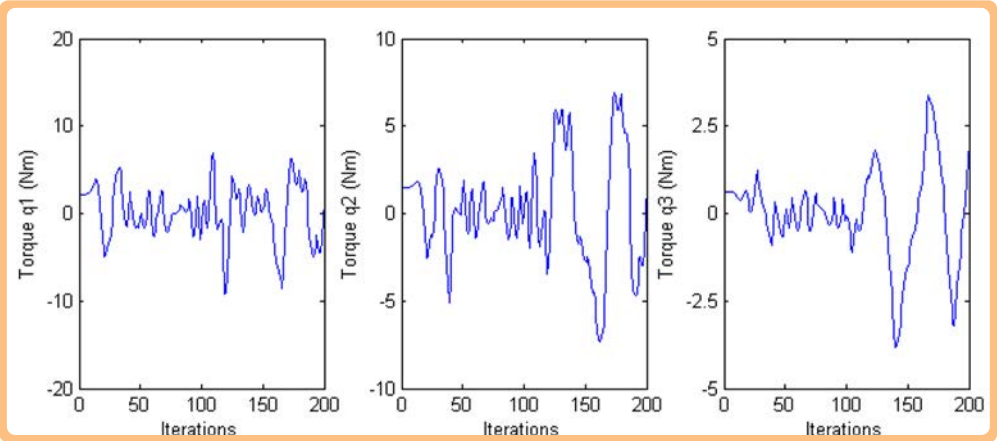

Figure 3.6. Torques during the tracking without chaos control $\omega = 1\ rad/s$.

In numerical simulations, it is possible to obtain theoretical values for k which make $|\boldsymbol{\Omega}|$ equals zero. However, these values do not assure that the stabilization of the UPO will be achieved in practice. This is due to the presence of measurement noise. Furthermore, uncertainties in different robot parameters influence the system with unmodeled delays. This aspect has motivated the developed experimental analysis to adjust the value of k.

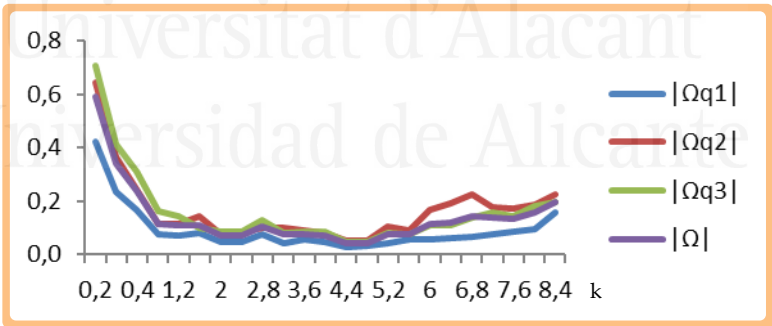

Figure 3.7. Experimental values of $|\Omega|$ depending of k.

In Figure 3.8, the absolute of the mean difference $|\boldsymbol{\Omega}|$ is represented depending on the value of ε (in this case, the value of k is fixed to 4.6). To obtain this figure, an increment $\Delta\varepsilon = \varepsilon - \varepsilon_0$ is added to the delay ε (fixed to 2π). The lower value is not obtained when $\Delta\varepsilon = 0$, as one would expect. In contrast to numerical simulations, the stabilization can be reached for a delay time larger

than 2π ($\varepsilon = 2\pi + 2\pi - \varepsilon_0$, where $2\pi/\varepsilon_0 = 1.01$). The previous indicated unmodeled delays explain this difference between theoretical values and the required values to eliminate the chaotic behavior in the real robot.

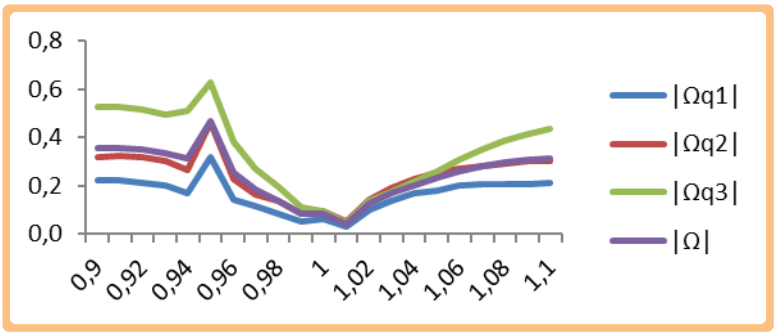

Figure 3.8. Experimental values of |Ω| depending of ε.

Figure 3.9 represents the results obtained considering the previous obtained weight, k, and delay, $\varepsilon = 2\pi + \Delta\varepsilon$. As Figure 3.9 shows, at the beginning of the experiment, the state of the system is not near the UPO selected by the choice of ε. Therefore, a large value of the difference between the delayed joint velocities and the current ones ($\boldsymbol{\Omega} = \dot{\boldsymbol{q}}(t-\varepsilon) - \dot{\boldsymbol{q}}(t)$) is obtained when starting the tracking process. After a transient of about 20 iterations, the UPO becomes stable and $|\boldsymbol{\Omega}| = |\dot{\boldsymbol{q}}(t-\varepsilon) - \dot{\boldsymbol{q}}(t)|$ remains low. These results are obtained with the previous indicated optimal values of k and ε. A small deviation of these parameter values leads to a higher value of $|\boldsymbol{\Omega}|$ and the UPO is not correctly stabilized.

By using the chaos control approach, the torques and image error module during the tracking are indicated in Figure 3.10 and Figure 3.11 respectively.

As it is shown in these figures, after a transient, the chaotic behavior is eliminated and the robot-end tracks the periodic image trajectory correctly. To perform the tracking, the robot joints describe smooth motions (the torques remain low).

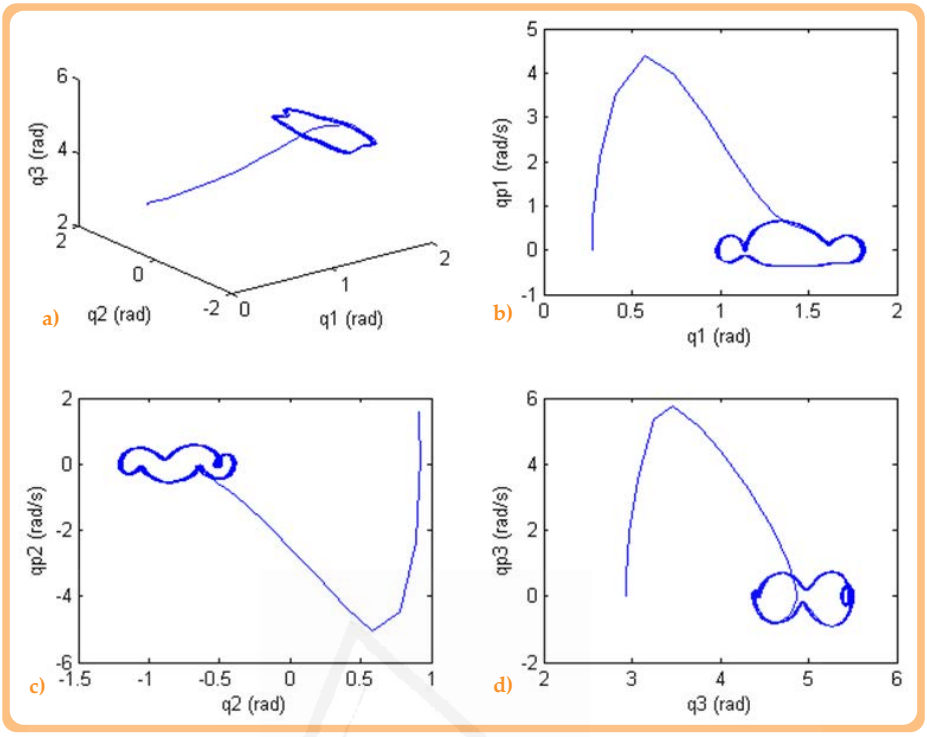

Figure 3.9. Phase portrait reconstructed from: a) q_1, q_2, q_3, b) $q_1, \dot{q}_1$, c) $q_2, \dot{q}_2$, d) $q_3, \dot{q}_3$. ($k = 4.6$).

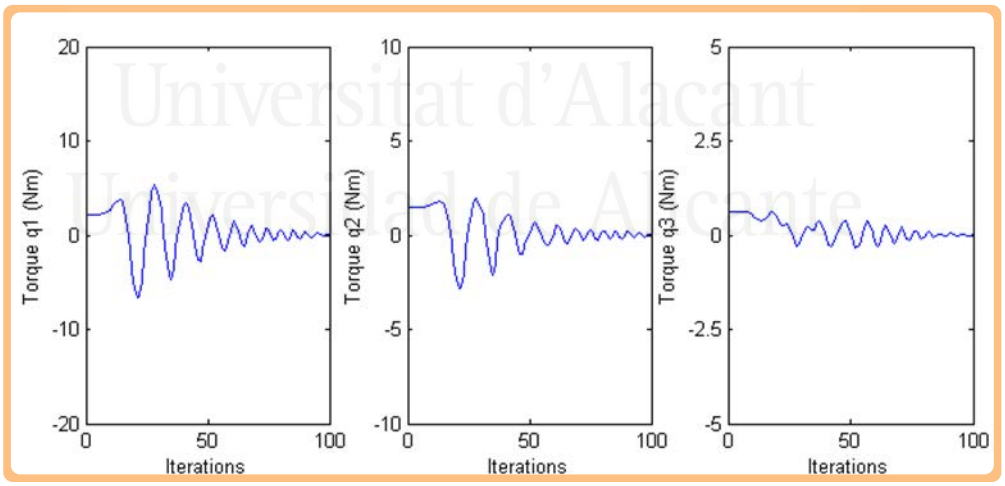

Figure 3.10. Torques during the tracking with chaos control $\omega = 1\ rad/s$.

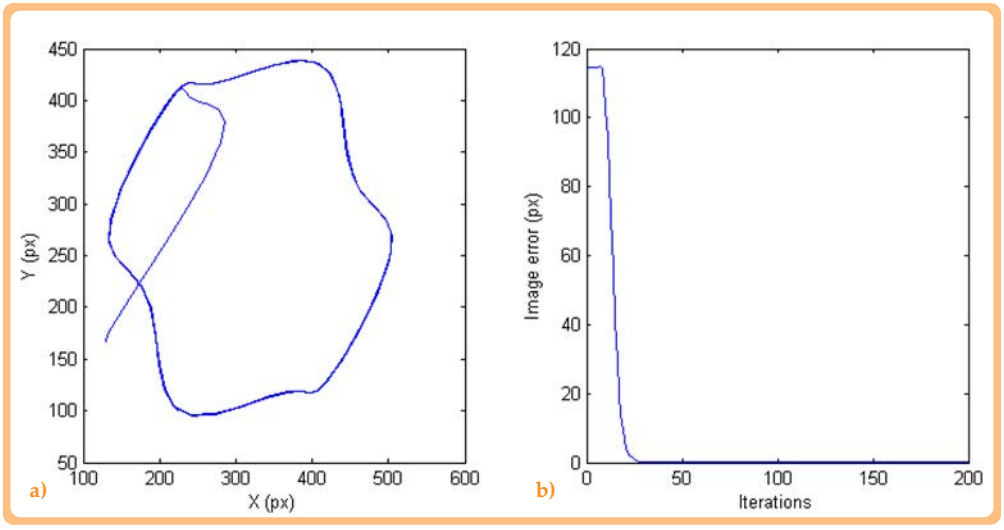

Figure 3.11. Behaviour in the image space with chaos control.

a) Image trayectory. b) Image error module.

Finally, the robot configurations during the tracking (without and with chaos control) are represented in Figure 3.12 (only 50 iterations are represented).

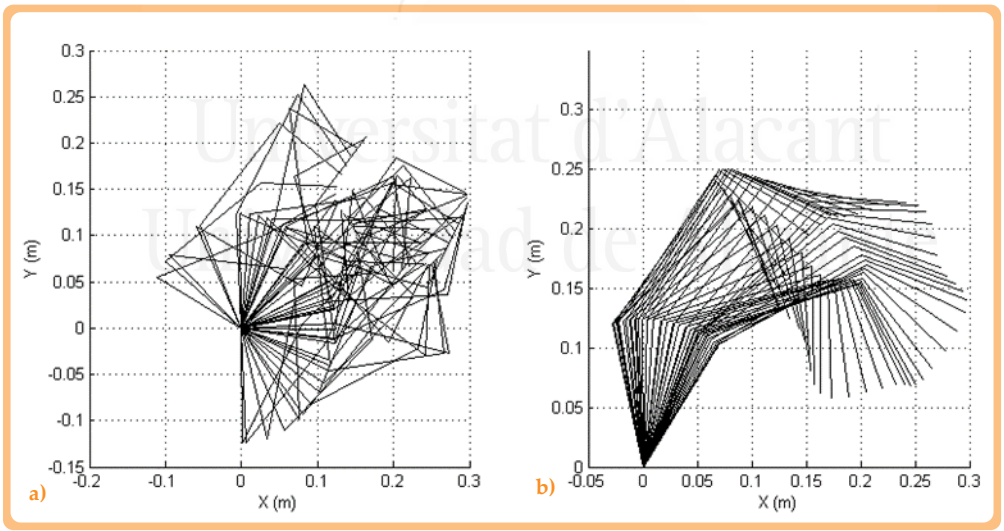

Figure 3.12. Robot configurations during the tracking.

a) Without chaos control. b) With chaos control

3.5.1.2 Tracking behavior

This section shows the performance of the visual controller in terms of image error in low and high-speed tracking tasks. In order to evaluate the correct behavior in different velocities, the torques generated by the controller (see Equation (3.22)) are also evaluated considering the weight $k = 4.6$ and the delay $\varepsilon = 2\pi + \Delta\varepsilon$ previously obtained. Firstly, the module of the image error ($\boldsymbol{s}_d - \boldsymbol{s}$) is represented in Figure 3.13 when the value of ω is equal to 0.5, 2 and 4 rad/s. As Figure 3.13 shows, the error remains low for the three velocities. As expected, the system has greater oscillations for higher velocities but, nevertheless, the robot performs the tracking for all of them correctly.

In order to evaluate the improvement of the system behavior, Figure 3.14 represents the obtained torques with and without chaos control. As it can be seen, lower torques are obtained when chaos control is applied and a smooth evolution is generated in the joint space compared to a system without chaos

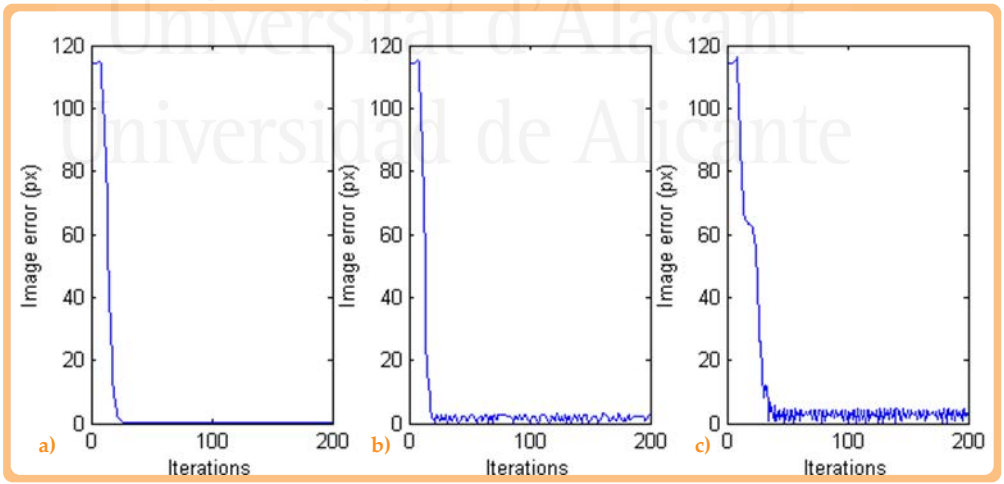

Figure 3.13. Image error with chaos control: a) $\omega = 0.5\ rad/s$, b) $\omega = 2\ rad/s$, c) $\omega = 4\ rad/s$

compensation, where not only the torques are higher to compensate the greater errors in the system, but also has a more inconsistent evolution, having big changes in direction of the movement.

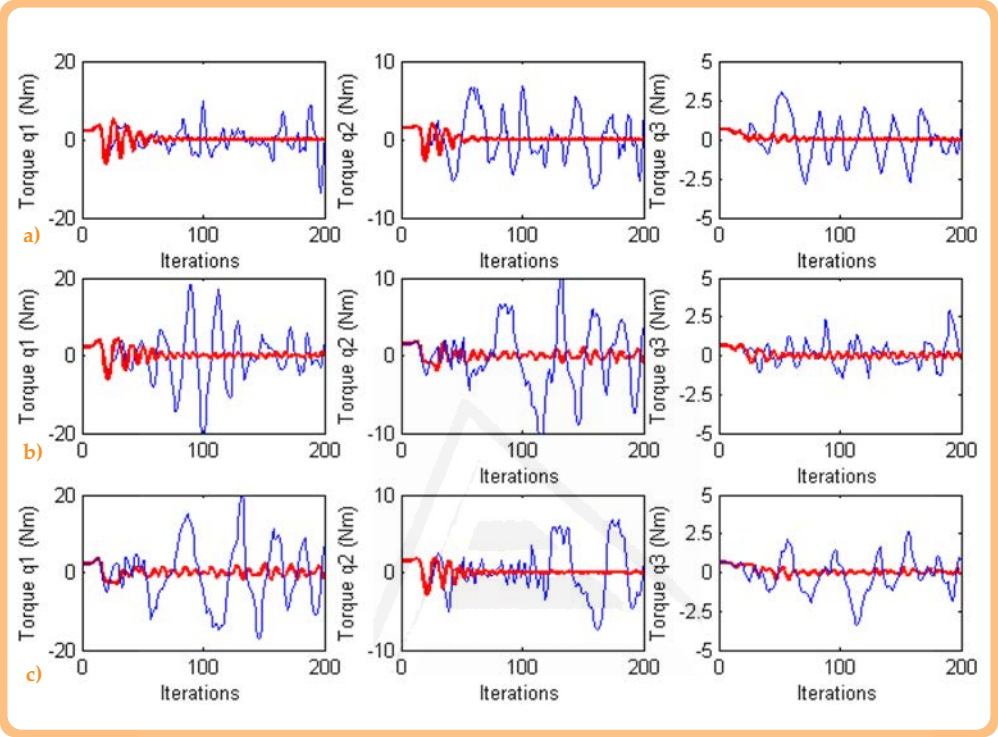

Figure 3.14. Torques during the tracking without chaos control (in blue) and with chaos control (in red): a) $\omega = 0.5\ rad/s$, b) $\omega = 2\ rad/s$, c) $\omega = 4\ rad/s$.

3.5.2 Experiment 2

In this section the obtained visual servoing control laws with chaos compensation are evaluated during the tracking of the periodic image trajectory defined by the following equations:

$$\boldsymbol{s}_d = \begin{bmatrix} f_{xd} \\ f_{yd} \end{bmatrix} = \begin{bmatrix} 320 + 166\cos(\omega t + \pi/4) \\ 265 + 160\sin(\omega t + \pi/4) \end{bmatrix} \tag{3.26}$$

where the parameter ω determines the tracking velocity.

Firstly, in order to evaluate the tracking system with chaos compensation a medium velocity is considered ($\omega = 1$ rad/s). Figure 3.15 represents in blue the

desired image trajectory obtained when $\mathbf{W} = \mathbf{M}^{-2}, \mathbf{W} = \mathbf{D}\mathbf{M}^{-2}, \mathbf{W} = \mathbf{M}^{-1}, \mathbf{W} = \mathbf{D}\mathbf{M}^{-1}, \mathbf{W} = \mathbf{I}$, and $\mathbf{W} = \mathbf{D}$. A correct behavior is obtained for all the controllers; however, it can be observed that the trajectory is more accurately tracked when $\mathbf{W} = \mathbf{M}^{-2}$ and $\mathbf{W} = \mathbf{M}^{-1}$. As previously indicated, when $\mathbf{W} = \mathbf{D}\mathbf{M}^{-2}, \mathbf{W} = \mathbf{D}$ or $\mathbf{W} = \mathbf{D}\mathbf{M}^{-1}$ the value of $\mathbf{D}$ allows us to indicate which joints will support high loads. In this experiment, the weight value corresponding to the first joint is twice the weight corresponding to the second and third joints.

Figure 3.16 represents the joint configurations of the robot during the tracking and Figure 3.17 represents the robot configurations considering $\mathbf{W} = \mathbf{M}^{-2}$ and without introducing the chaos controller.

Comparing both figures, it can be observed that using the proposed controllers the chaos behavior is compensated and a periodic joint trajectory is obtained during the tracking of the periodic image trajectory.

In order to show more clearly the tracking precision, Table 3.1 represents the mean error in pixels during the tracking of the previous indicated trajectory considering different tracking velocities. The mean image error obtained by using previous classical direct visual controllers is also included in this table. As it can be seen in Table 3.1, the image error is lower when $\mathbf{W} = \mathbf{M}^{-1}$ or $\mathbf{W} = \mathbf{M}^{-2}$ is employed. Furthermore, in these cases the performance is clearly improved with respect to the previous controllers (Pomares et al., 2011a).

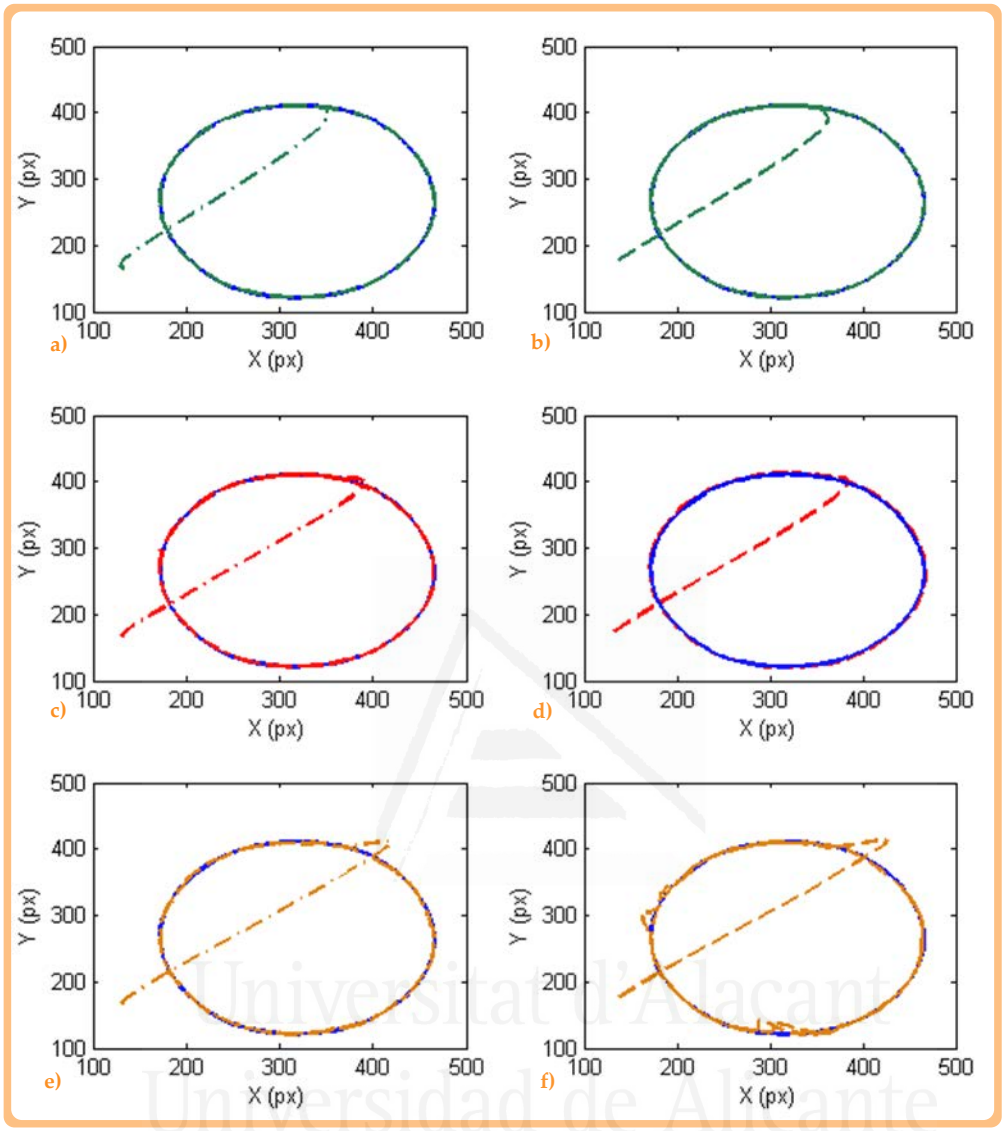

Figure 3.15. Experiment 2. Desired image trajectory (blue) and obtained image trajectories considering: a) $W = M^{-2}$. b) $W = DM^{-2}$. c) $W = M^{-1}$. d) $W = DM^{-1}$. e) $W = I$. f) $W = D$.

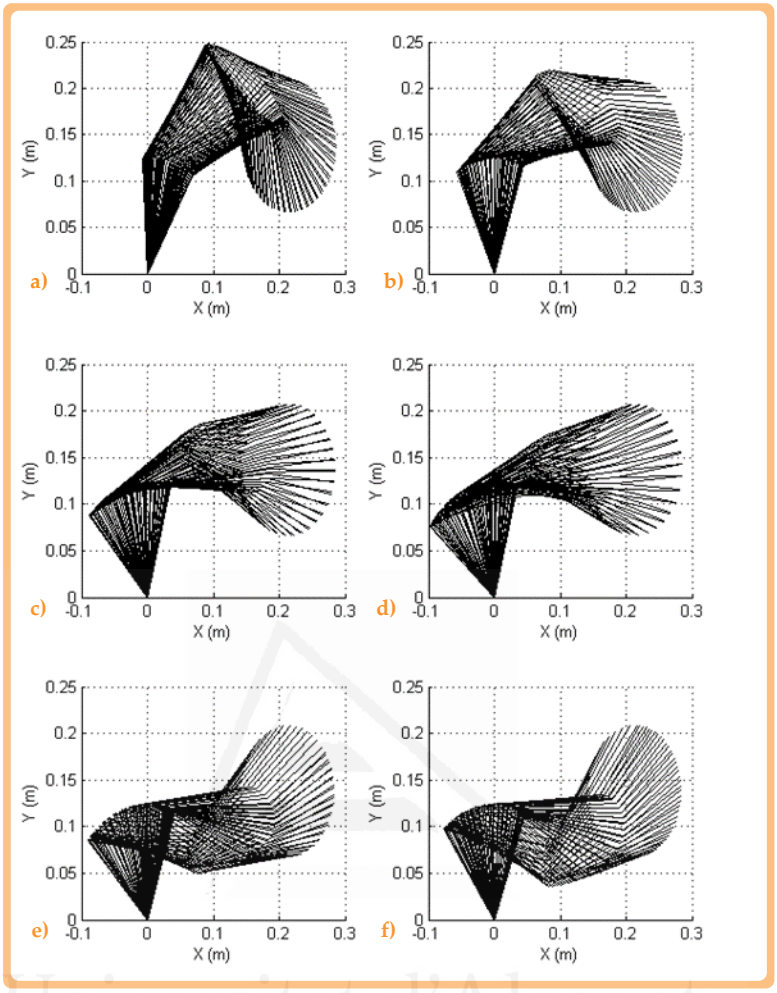

Figure 3.16. Experiment 2. Obtained 3D trajectory during the tracking considering a) $W = M^{-2}$. b) $W = DM^{-2}$. c) $W = M^{-1}$. d) $W = DM^{-1}$. e) $W = I$. f) $W = D$.

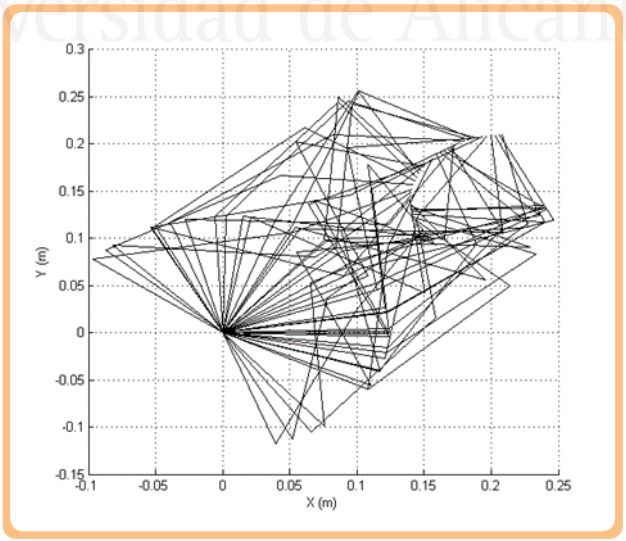

Figure 3.17. Experiment 2. Robot configurations during the tracking without chaos control ($W = M^{-2}$).

Table 3.1. Experiment 2. Mean image error (Pixels).

W	$\omega = 0.5$ rad/s	$\omega = 1$ rad/s	$\omega = 2$ rad/s
$\mathbf{M}^{-2}$	2.14	2.12	3.84
$\mathbf{DM}^{-2}$	2.12	2.43	3.74
$\mathbf{M}^{-1}$	2.12	2.95	2.39
$\mathbf{DM}^{-1}$	2.42	3.10	3.34
I	3.81	3.22	4.40
D	3.45	3.66	4.81
Previous direct visual controller	2.25	3.20	4.12

3.5.3 Experiment 3

In order to evaluate the tracking considering a more complex trajectory, all the controllers are tested during the tracking of a trajectory with abrupt changes (see Figure 3.18). In the experiments represented in this last figure, a medium tracking velocity is considered ($\omega = 1$ rad/s). As in the previous section, a correct tracking is achieved in the image space for all the six controllers and the best behavior is obtained when $\mathbf{W} = \mathbf{M}^{-2}$ or $\mathbf{W} = \mathbf{M}^{-1}$. As it was indicated in the previous section, the matrix $\mathbf{D}$ is a diagonal matrix and the weight value corresponding to the first joint is twice the weight corresponding to the second and third joints. In order to demonstrate the effect obtained by using this matrix, in Figure 3.19 the torques which were obtained when $\mathbf{W} = \mathbf{M}^{-2}$ and $\mathbf{W} = \mathbf{DM}^{-2}$ are represented. Comparing Figure 3.19.a and Figure 3.19.b, it can be observed that when $\mathbf{W} = \mathbf{DM}^{-2}$ lower torques in the first joint are obtained. Therefore, this diagonal matrix can be employed to distribute the torques and to diminish the effort in the desired joints.

Figure 3.20 represents the robot joint configurations achieved during the tracking in the 3D space. As it can be observed, the chaos is compensated (see

Figure 3.21) which represents the robot joints configurations when chaos control is not applied).

Finally, in order to indicate more clearly the precision and errors during the task, Table 3.2 indicates the mean error in pixels during the tracking considering different tracking velocities. From this table, similar conclusions can be extracted. The highest precision is obtained when $\mathbf{W} = \mathbf{M}^{-1}$ or $\mathbf{W} = \mathbf{M}^{-2}$. In contrast, when $\mathbf{W} = \mathbf{I}$ the controller is simpler and easier to implement. Additionally, the use of $\mathbf{W} = \mathbf{D}\mathbf{M}^{-2}, \mathbf{W} = \mathbf{D}$ or $\mathbf{W} = \mathbf{D}\mathbf{M}^{-1}$ also introduces small errors during the tracking but it allows us to indicate which joints will support high loads. Thus, the proposed framework can be employed to generate the controllers depending on the tracking requirements. Furthermore, the framework can be extended in order to generate new direct visual servo controllers with other properties depending the value of $\mathbf{W}$.

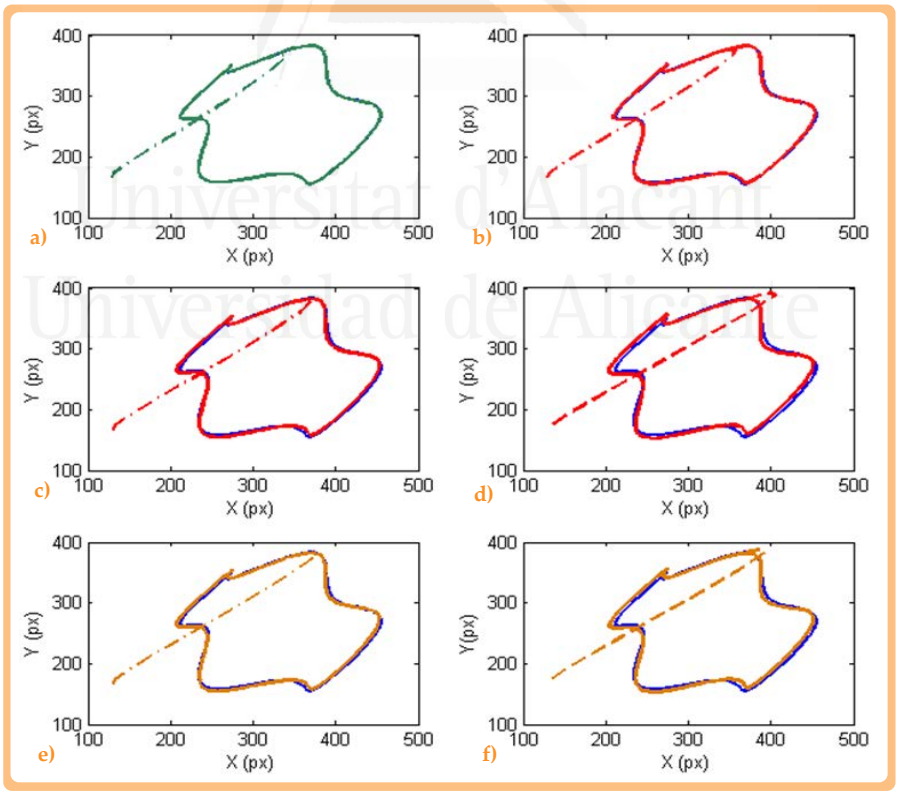

Figure 3.18. Experiment 3. Desired image trajectory (blue) and obtained image trajectories considering a) W = M^{-2}. b) W = DM^{-2}. c) W = M^{-1}. d) W = DM^{-1}. e) W = I. f) W = D.

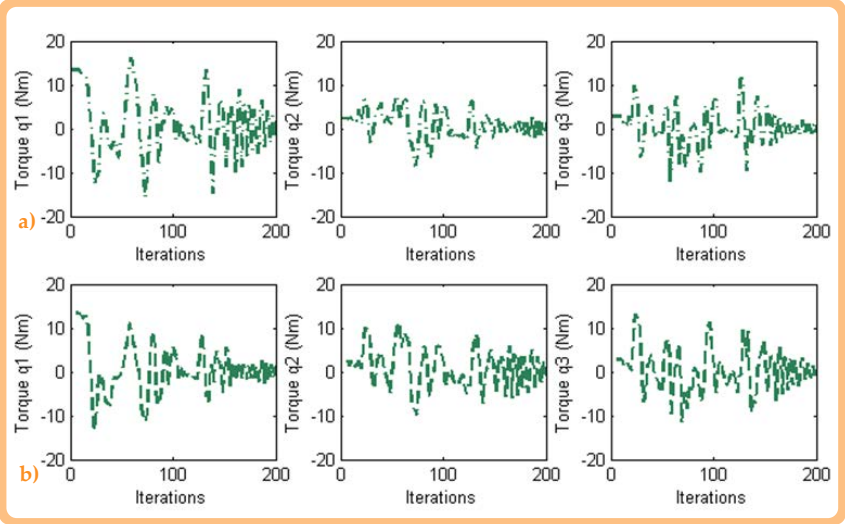

Figure 3.19. Experiment 3. Torques obtained during the experiment when a) $W = M^{-2}$. b) $W = DM^{-2}$.

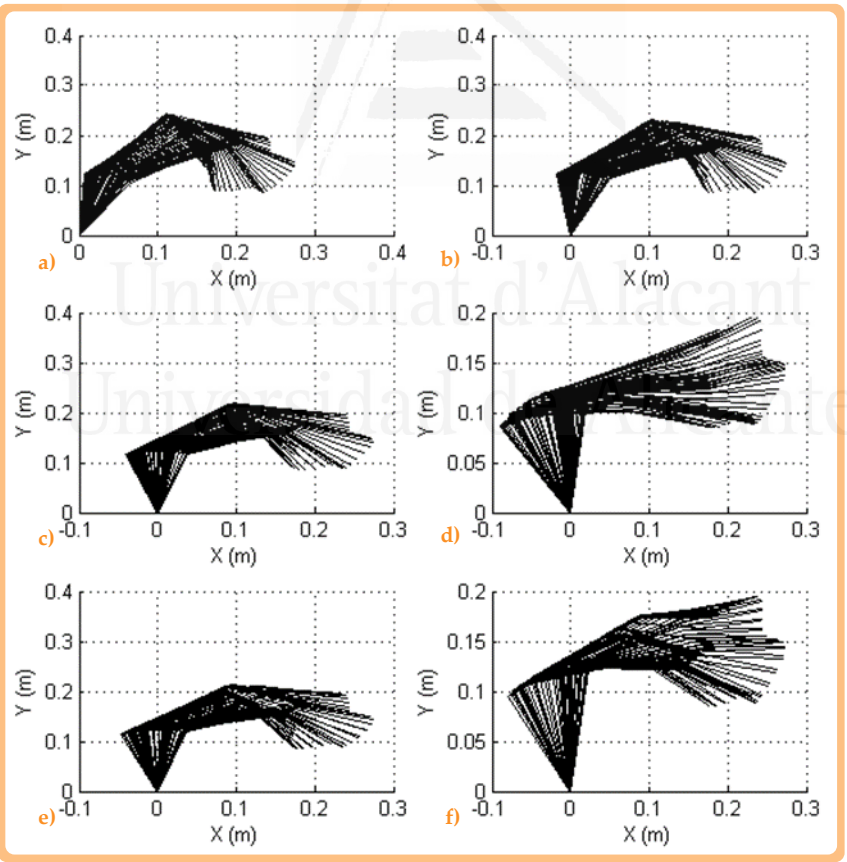

Figure 3.20. Experiment 3. Obtained 3D trajectory during the tracking considering a) $W = M^{-2}$. b) $W = DM^{-2}$. c) $W = M^{-1}$. d) $W = DM^{-1}$. e) $W = I$. f) $W = D$.

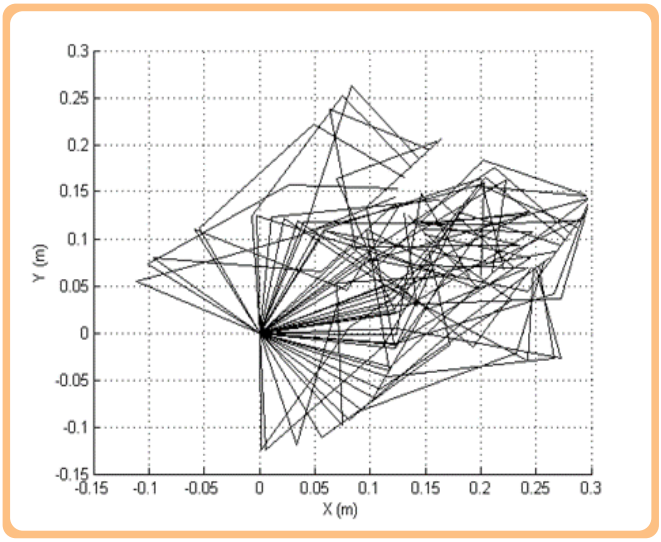

Figure 3.21. Experiment 3. Robot configurations during the tracking without chaos control (W = M^{-1}).

Table 3.2. Experiment 2. Mean image error (Pixels).

W	$\omega = 0.5$ rad/s	$\omega = 1$ rad/s	$\omega = 2$ rad/s
M^{-2}	1.54	1.95	3.00
DM^{-2}	2.41	2.63	3.55
M^{-1}	1.34	1.92	2.55
DM^{-1}	3.87	4.00	4.48
I	1.75	2.22	3.12
D	4.45	4.88	5.21
Previous direct visual controller	1.5	2.0	3.1

3.6 Conclusions

The use of an optimal control approach is presented in this chapter, allowing to define new dynamic visual controllers in order to carry out the guidance of any serial link structure with both redundant resolution and chaos

compensation. Making use of both the dynamic robot model and the definition of the image trajectory as task description, different image-based dynamic visual servoing systems are defined. The proposed approach allows derivation of previously known dynamic visual controllers, and permits the development of new ones for any mechanical system with redundancy.

The implementation of some derivate controllers on a three-degrees-of-freedom robotic system has been carried out. As stated, new controllers are generated by using the proposed framework. Each controller has different precision and behavior in both the task and joint space. Therefore, the proposed framework can be employed in order to generate new direct visual servoing controllers with the performance required for a given application.

Next chapter introduces the concept of dynamic perceptibility that is later applied for controlling trajectories for two types of robots by using an FPGA. Some experimental results are shown at the end of the chapter. Finally, Chapter 5 extends the direct image-based visual servoing systems to space technology, extending the control framework developed in previous chapters for spacecrafts and free-floating base systems (those orbiting around a planet with no attitude control).

4 Dynamic perceptibility

This Chapter presents the definition of the concept of dynamic perceptibility. Such concept considers the robot's dynamic characteristics as well as image characteristics for determining the movement capabilities of a given task. The Chapter starts with an introduction describing the most common issues that visual servoing has to deal with, robot or image singularities being one of them. Section 4.2 describes several concepts that can be used as singularity avoidance, and among them, the dynamic perceptibility proposed by this Thesis, defined to take into account several issues when determining the movement capabilities. Section 4.3 details the FPGA-based hardware architecture employed, while Section 4.4 defines the controller that is implemented in such architecture. Several experimental results are shown in Section 4.5 that demonstrates the correct behavior and advantages of using an FPGA-based architecture. The Chapter finishes with a section of conclusions.

4.1 Introduction

Manipulability is currently a well-known concept that measures the distance between the current configuration of a robot and the closest singular pose (Yoshikawa, 1985b). A high manipulability is required to assure the ability of the robot to move in arbitrary directions. Additionally, the concept of dynamic manipulability has been defined in order to take into account the robot dynamics (Yoshikawa, 1985a). However, when a direct visual servoing controller is defined, the control is carried out in the image space and additional considerations must be taken into account to perform the robot guidance. The image-based visual servoing systems employ the concept of interaction matrix which relates the time variation of the extracted visual features to the relative camera-object kinematics screw. The interaction matrix is singular if it contains the image measurements of three feature points that are collinear (Kung & Shu, 2005), or belong to a cylinder containing the camera optical center (Chaumette, Rives, & Espiau, 1993), or belong to a plane perpendicular to the camera optical axis and at least one set of image measurements satisfy (Papanikolopoulos, 1995). At image singularities, certain camera (end-effector) motions cannot be perceived by using the extracted image feature. The perceptibility is a scalar function that provides information about the possibility of the vision system to perceive the motion within its field of view only using kinematics information (Sharma & Hutchinson, 1997). The concept of perceptibility has been previously proposed as a measure of closeness to image singularities. In this chapter, the dynamic perceptibility concept is proposed in order to take into account the manipulator kinematics and dynamics. This new concept provides information about the system ability to track objects using an image-based direct visual servoing system and it has suitable properties for high-speed and high-precision motion control avoiding image singularities. The use of this parameter is a useful criterion to determine situations where the robot is close to a singularity (in the image or in the joint space). The dynamic perceptibility is integrated in the proposed controllers for robot and image singularity avoidance

(Alabdo, Pérez, García, Pomares, & Torres, 2015; Perez, Alabdo, Pomares, Garcia, & Torres, 2016).

Additionally, an optimal implementation of the proposed image-based visual controllers and the dynamic perceptibility concept is carried out by using an FPGA-based architecture. The use of FPGAs allows for using a specific technology of reprogrammable hardware for the implementation of visual servoing systems. The implementation of a direct visual servoing system embedded in an FPGA allows for improving these systems by reducing processing times and obtaining stable delays in the feedback. Also, the possibility of making partial reconfigurations allows for modifying sections of the logic implemented in the FPGA, adjusting them according to the functionality needed and the dynamics of the controllers, to the application to be developed. Therefore, the use of an FPGA allows for implementing a dedicated parallel architecture that can be adapted at runtime to the needs of the system.

In the field of visual servoing systems, there are just some implementations that integrate FPGAs in some element of the visual servoing system. Most of the delays from these systems happen when processing the images. This is the reason why some works like (Liyanage & Krouglicof, 2014) optimize the images capturing with the hardware capabilities that an FPGA allows. Also, (Wang et al., 2016) employs an FPGA for processing an image in real time for, afterwards, performing a positioning by using position-based visual servoing. However, in this last work, the control is not implemented in the FPGA. Another approximation in which an FPGA is used for a more efficient image processing and in real time is (Dhipa, Jeyakkannan, & Chandrasekar, 2015). A stereoscopic image processing speed is improved when parallelizing the process. Data and tasks are parallelized with segmented pipelines in an FPGA. Images from stereo pairs provide 3-D information for performing positioning tasks with position-based visual servoing. Additionally, it is possible to find embedded indirect visual servoing systems that integrate the image processing as well as the control (Hu, Chang, & Yang, 2011).

And FPGA was successfully used for achieving a robust control of an inverted pendulum by using an image co-processor based on FPGA in (Tu & Ho, 2011), and (Park & Jong Lee, 2003) presents a visual servoing system that consists on a computer vision system and a robot that moves a plate situated at the end-effector with a ball on it, so the ball performs a desired trajectory. Works initiated by (L Zhang, Slaets, & Bruyninckx, 2012) are extended to visual servoing systems in (Lin Zhang, Slaets, & Bruyninckx, 2014). This last work proposes an open architecture for visual servoing of robots. The architecture and related intellectual property (IP) cores are developed by a component-based design that interprets a robotic system by computation components, communication, configuration and coordination, together with a composition of these components and black boxes. The motor controller's IP core is designed as open hardware. Open software implies the use of OROCOS (Bruyninckx, 2001). The performance of the visual servoing is evaluated with the visual coupling of a Performer MK2 robot and a KUKA LWR robot. The modeling and parameters identification of a three-degrees-of-freedom robot is described in (Pérez, 2008). The implementation of an indirect visual servoing scheme and the acquisition/processing of the image is performed in an FPGA with the goal of accelerating the computation time. It is not possible however to find previous FPGA-based architectures that implement direct visual servoing systems for guiding robot manipulators by using visual information. The proposed controllers and the FPGA-based architecture are published in (Alabdo et al., 2015)

This chapter presents an optimal control framework for direct visual servoing robots which integrates the concept of dynamic perceptibility and its implementation in the FPGA-based architecture. The presented approach is based on optimal control framework described in Chapter 3, and is employed to control robots during the tracking of image trajectories taking into account the robot dynamics. Thus, this control approach considers the optimization of the motor signals or torques sent to the mechanical system during visual control tasks. The

dynamic perceptibility concept is integrated in the framework to avoid singularities. Using this framework, several new direct visual controllers can be derived. The correct behavior of both the controller and the FPGA-based architecture are evaluated with the two previous indicated robots (the Mitsubishi PA10 and the three-degrees-of-freedom COOPER robot).

This chapter is organized as follows: it starts describing the new developed concept of dynamic perceptibility after describing the already existing ones of manipulability, dynamic manipulability and perceptibility. The proposed FPGA-based architecture is described next, following with the development of the control system. Merging all together, an optimal framework on FPGA is detailed for obtaining all different control laws. The chapter finishes with some results that prove the correctness and valuable application of this FPGA-based framework.

4.2 Dynamic perceptibility

This section describes the dynamic perceptibility concept as a measure of the system ability to track objects using a direct visual controller. To explain this idea, previous similar concepts are reviewed in order to highlight the contribution of the dynamic perceptibility approach and its use in the direct visual servoing of robot manipulators.

4.2.1 Manipulability and dynamic manipulability

Manipulability is a well-known concept defined by Yoshikawa (Yoshikawa, 1985b) where the ability of positioning a robot manipulator is measured with a scalar value given by:

$$\omega = \sqrt{det[\mathbf{J}_r, \mathbf{J}_r^T]} \tag{4.1}$$

Considering a set of joint velocities with a unit form $\dot{\boldsymbol{q}}^T\dot{\boldsymbol{q}} = 1$, which lie on the surface of a hypersphere in the n-dimensional joint velocity space, and taking into account the differential kinematics, $\mathbf{J}_r$, of the manipulator that gives the

relationship between the joint velocities, $\dot{\boldsymbol{q}}$, and the corresponding end-effector velocity, $\dot{\boldsymbol{r}}$, the following relation can be obtained:

$$\dot{\boldsymbol{r}}^T[\mathbf{J}_r\mathbf{J}_r^T]^{-1}\dot{\boldsymbol{r}} = 1 \tag{4.2}$$

which is the equation of points on the surface of a m-dimensional ellipsoid in the end-effector velocity space. The volume of such ellipsoid is determined by Yoshikawa's scalar value. Figure 4.1 shows an example of how the scalar value of manipulability evolves for two types of trajectories, join and Cartesian space.

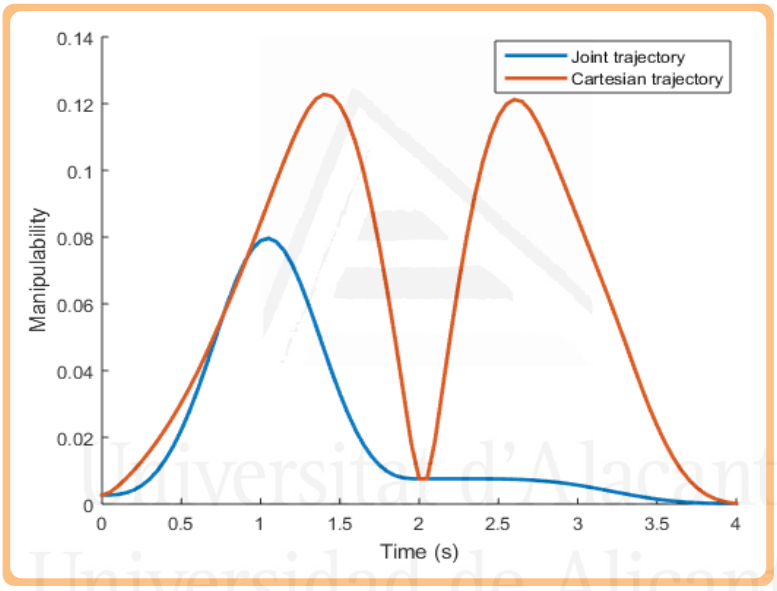

Figure 4.1. Evolution of the manipulability for a given joint and Cartesian trajectory.

Both trajectories start and finish at the same point in the 3D space, with a common middle point as shown in Figure 4.2. These three points are represented in Figure 4.1 at second 0, 2, and 4, where the manipulability for both trajectories match since the joint configuration of the robot is the same. Figure 4.2.a shows the joint trajectory carried out by the robot and can be seen how it moves close to the limit of the working area, with the arm almost completely extended, causing the low manipulability during the trajectory represented in blue in Figure 4.1, whereas Figure 4.2.b shows a Cartesian trajectory within the working area where the arm

can move comfortably, thus, high values of manipulability during the movement between common points for both trajectories, as shown in red in Figure 4.1.

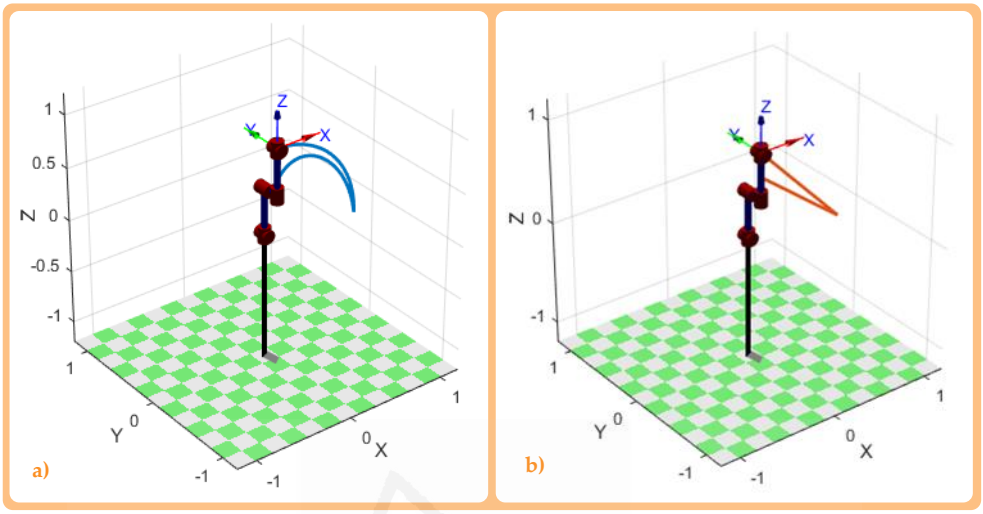

Figure 4.2. Representation of the two trajectories a) Joint space b) Cartesian space

At all times, the manipulability scalar value can be represented by an ellipsoid, being the area of such ellipsoid the capability of movement of the end-effector of the robot for a given pose. For example, Figure 4.3 shows different points of views of a pose where the manipulability reaches a maximum peak in the Cartesian trajectory, around second 1.4 of the experiment. For this particular pose, manipulability determines that the end-effector has a higher movement capability in the Y and Z axis than in the X axis, although since the ellipsoid is not flat.

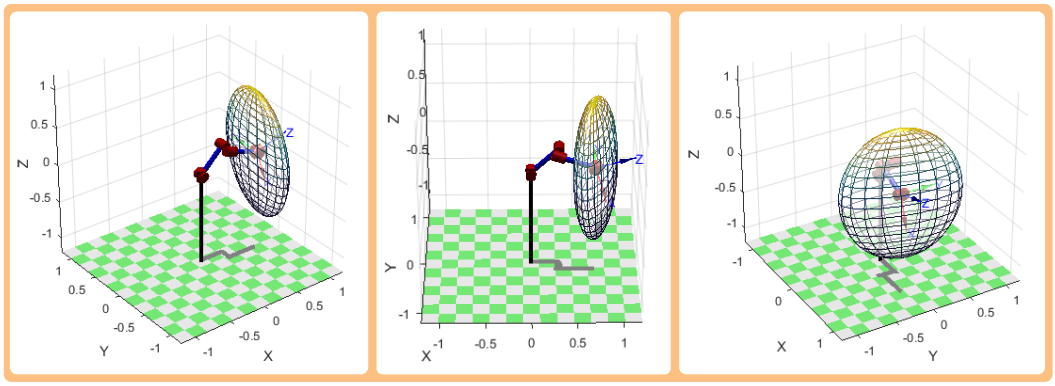

Figure 4.3. Different points of view of position with maximum value of manipulability

Figure 4.3.b shows that the robot can still move in the X axis, but risking a joint singularity as pictured in Figure 4.4 where the robot is completely stretched and the end-effector at the workspace limit, thus the ellipsoid being almost completely flat in the X axis.

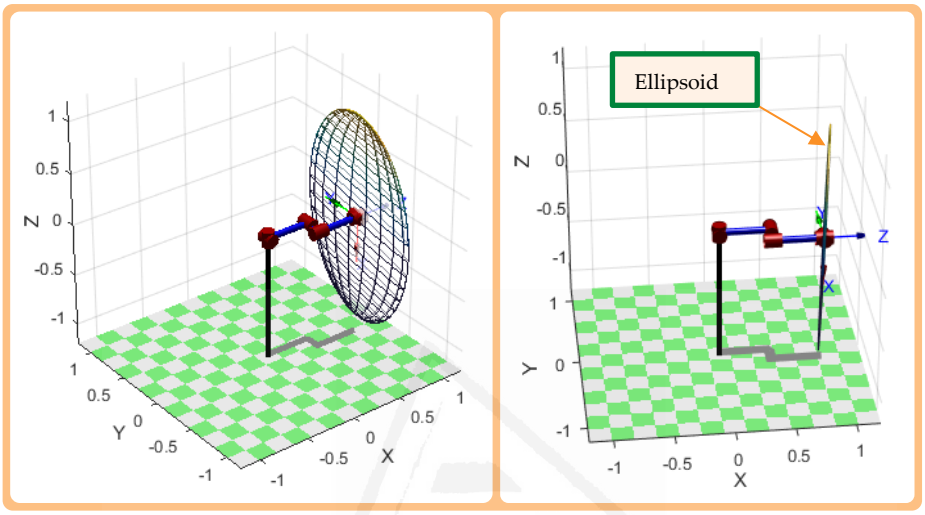

Figure 4.4. Joint singularity. Robot reached the workspace limit.

Developing the concept of manipulability, Yoshikawa later defined the concept of dynamic manipulability (Yoshikawa, 1985a), where the dynamics of the robot manipulator is taken into account when determining its manipulability scalar value:

$$\omega_d = \sqrt{det[\mathbf{J}_r(\mathbf{M}^T\mathbf{M})^{-1}\mathbf{J}_r^T]} \tag{4.3}$$

The robot dynamics is simplified ignoring the gravity term and assuming $\dot{\boldsymbol{q}} = 0$ to define the dynamic manipulability concept, therefore:

$$\boldsymbol{\tau} = \mathbf{M}\ddot{\boldsymbol{q}} \tag{4.4}$$

Considering a set of generalized joint forces with unit form $\boldsymbol{\tau}^T\boldsymbol{\tau} = 1$, the hypersphere defined by the dynamic manipulability can be defined as:

$$\ddot{\boldsymbol{r}}^T(\mathbf{J}_r\mathbf{M}^{-1}\mathbf{M}^{-T}\mathbf{J}_r^T)^{-1}\ddot{\boldsymbol{r}} = 1 \qquad (4.5)$$

Having the same trajectories from Figure 4.2 but this time applying the concept of dynamic manipulability, the graph shown in Figure 4.5 is obtained.

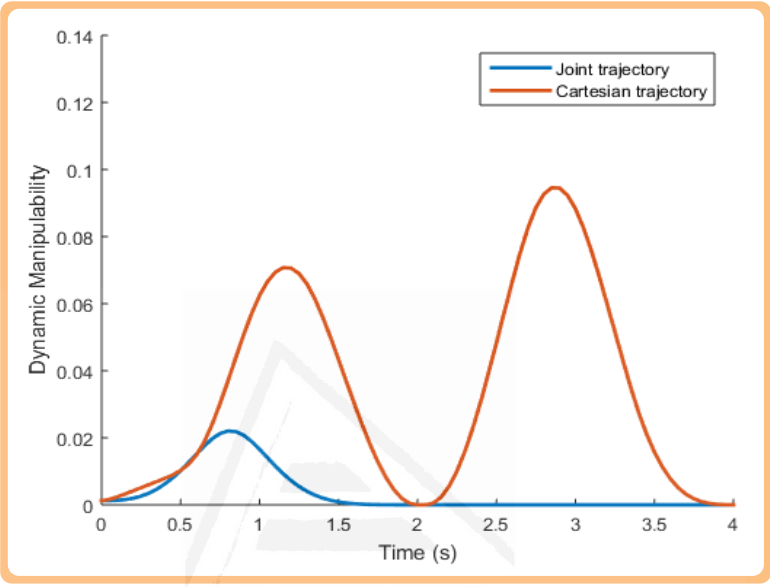

Figure 4.5. Evolution of the dynamic manipulability for a given joint and Cartesian trajectory.

When introducing the dynamics into the equation of manipulability, the system essentially has an extra constraint, thus the movement capability is slightly reduced. Comparing Figure 4.1 and Figure 4.5, when dealing with dynamic manipulability, the curves are reduced in height, meaning the robot has a higher limitation of the movement of the end-effector for a given pose. This is also captured when studying the ellipsoid at the highest value of dynamic manipulability in the Cartesian trajectory. Comparing Figure 4.3 and Figure 4.6, being the last one the representation of dynamic manipulability ellipsoid, this one is smaller than the previous one, confirming the movement capability reduction of the end-effector. It also has a different shape, indicating that the direction of the most ideal movement for a given pose changes.

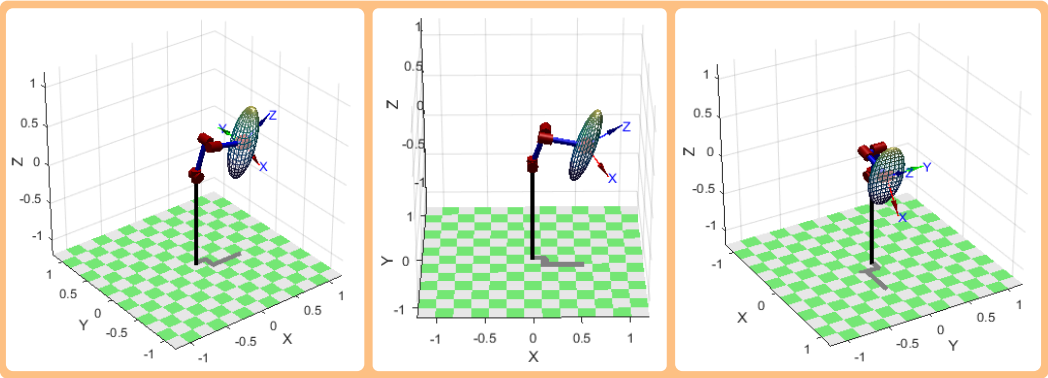

Figure 4.6. Different points of view of position with maximum value of dynamic manipulability

A singularity in the robot Jacobian is obtained when the robot is in a configuration in which certain end-effector velocities are not possible. The manipulability concept can be employed as a measure of the distance between the current configuration of the robot and the closest singular pose. A high manipulability is required to assure the ability of the robot to move in arbitrary directions.

4.2.2 Perceptibility and dynamic perceptibility

The concept of perceptibility determines the ability of the vision system to perceive the robot motion within its field of view when a visual servoing approach is employed to perform its guidance. When the vision system cannot observe the motion of the visual features, a singularity appears in the interaction matrix. As previously indicated, the perceptibility index allows the system to measure the closeness to image singularities (Sharma & Hutchinson, 1997). The perceptibility is a scalar function of the interaction matrix defined by the following expression:

$$\omega_p = \sqrt{det[\mathbf{L}_s, \mathbf{L}_s^T]} \tag{4.6}$$

As it is shown in Equation (4.6), perceptibility index only employs kinematic information. In contrast with the previous index the new concept of dynamic perceptibility is proposed in order to take into account the manipulator dynamics

when a direct visual control system is used to perform the robot guidance. To obtain the value of the dynamic perceptibility, the following two vectors are defined:

$$\tilde{\boldsymbol{\tau}} = \boldsymbol{\tau} - \mathbf{C} - \boldsymbol{g} = \mathbf{M}\ddot{\boldsymbol{q}} \tag{4.7}$$

$$\tilde{\dot{\boldsymbol{s}}} = \ddot{\boldsymbol{s}} - \dot{\mathbf{L}}_J \dot{\boldsymbol{q}} = \mathbf{L}_J \ddot{\boldsymbol{q}} \tag{4.8}$$

From Equations (4.7) and (4.8) the following relation can be obtained:

$$\tilde{\dot{\boldsymbol{s}}} = \mathbf{L}_J \mathbf{M}^{-1} \tilde{\boldsymbol{\tau}} \tag{4.9}$$

This last equation quantifies the relationship between applied torques and corresponding image accelerations, when just inertial effects are considered. The dynamic perceptibility, ω_{dp}, is a scalar function which measures the relationship of Equation (4.9) and can be obtained using the following expression:

$$\omega_{dp} = \sqrt{det\left[\mathbf{L}_J \mathbf{M}^{-1} \left(\mathbf{L}_J \mathbf{M}^{-1}\right)^T\right]} \tag{4.10}$$

The result of multiplying $\mathbf{L}_J \mathbf{M}^{-1} \left(\mathbf{L}_J \mathbf{M}^{-1}\right)^T$ is a 2k x 2k matrix. Since the image space has two dimensions, only the k 2x2 matrices that appear in the diagonal of the 2k x 2k matrix are needed. These matrices contain the information about the dynamic perceptibility for each visual feature. From these matrices it is possible to represent the k ellipses for each visual feature as represented in the experiments indicated in the results section. In order to illustrate the information obtained from the proposed dynamic perceptibility in contrast with the previous concepts, Figure 4.7 shows the obtained ellipsoids and ellipses considering manipulability, dynamic manipulability, perceptibility and dynamic perceptibility at the iteration 14 of the experiment, when the robot is close to a singularity. The ellipsoid in Figure 4.7.a represents the movement capability of the end-effector, where it is more desirable to move it forwards or backwards, instead of up or down. Figure

4.7.b represents the same information but taking into consideration the robot dynamics, and hence, obtaining a more restrictive ellipsoid. The ellipses shown in Figure 4.7.c and Figure 4.7.d represent the movement capability of every point in the pattern (a pattern composed of three image points is considered).

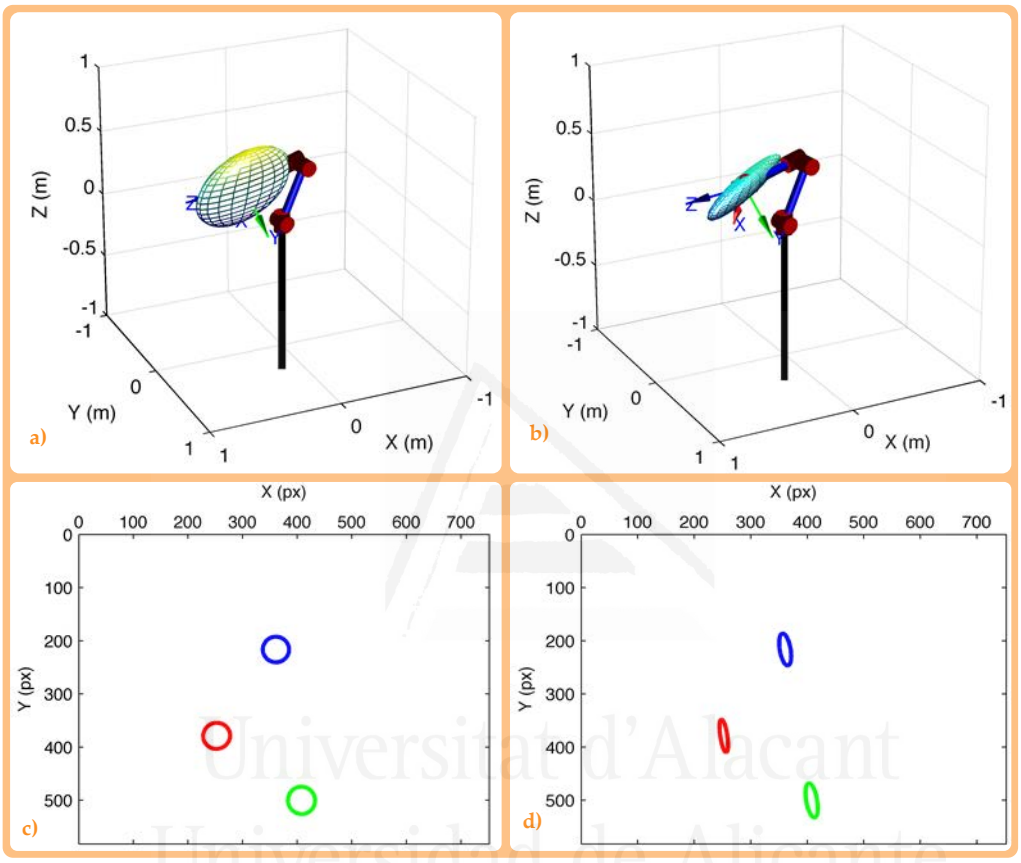

Figure 4.7. Example of dynamic perceptibility concept. a) Manipulability ellipsoid. b) Dynamic Manipulability ellipsoid. c) Perceptibility ellipses. d) Dynamic perceptibility ellipses.

The first ones are obtained only with information in the image space, that is why they are almost perfectly round. The second ones, on the other hand, take into consideration the robot dynamics, influencing the shape of the ellipses, concluding that, in the image space, it would be better to move the pattern up or down, instead of sideways.

4.3 FPGA-based architecture

This section describes the main components of the FPGA-based architecture employed to implement the controllers described in Chapter 3 and the proposed dynamic perceptibility (see Figure 4.8). This architecture will be evaluated for visual servoing two different robots. The first one is the industrial robot Mitsubishi PA10 and the second one is a three-degrees-of-freedom COOPER robot. To visual servoing both robots a PHOTONFOCUS MV-D752-160-CL-8 camera is installed at its end-effector. The camera is able to acquire and process 200 frames/sec using an image resolution of 752 x 582 pixels.

The FPGA board used is the KC705 evaluation board from Xilinx. This board is based on the Kintex-7 XC7K325T-2FFG900C FPGA. In order to read images from the camera, a commercial CameraLink receiver CLR-HSMC made by Terasic is employed. It uses the High Speed Mezzanine Card (HSMC) to interface with another motherboard hosting an HSMC/HSTC carrier such Altera's FPGA boards. An adapter board, KY-FMC2HSMC from KAYA INSTRUMENTS is used to enable connection of CLR-HSMC to the Xilinx FPGA board via LPC FMC expansion connector.

In order to test the proposed controller, the system was embedded in an FPGA. As shown in Figure 4.8, the embedded system design is made up of three principal parts (different background colors).

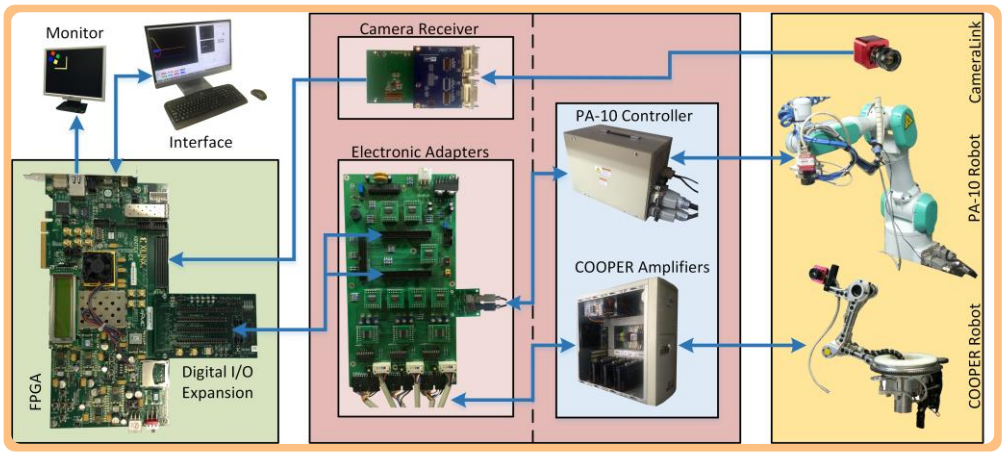

Figure 4.8. System components.

These parts consist of an FPGA board, electronic adapters, and both robot manipulators equipped with a high-speed camera located at their end-effectors. Also, a PC can be used as a terminal for parameters configuration and signals visualization.

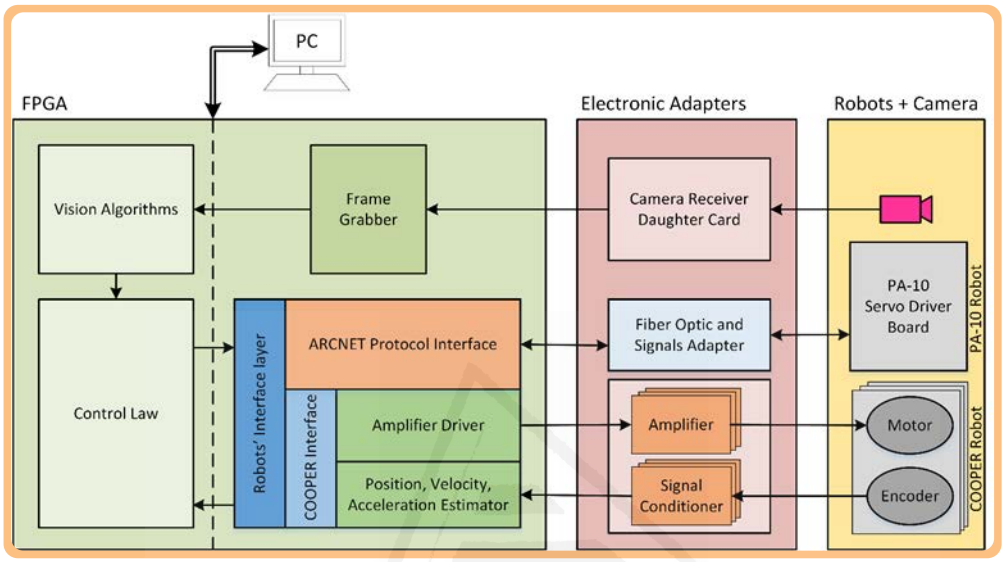

Figure 4.9. Hardware architecture of the embedded visual servoing system.

The software design was divided into sub-processes in order to get greater system flexibility. The functionality of each sub-process was implemented in an independent module. These modules are synchronized and executed in a parallel way, taking advantage of the FPGA architecture.

In the FPGA, four different modules have been implemented: Vision algorithms, Control law, Frame grabber and the robots interface layer. The first two modules are not hardware dependent. The Frame grabber module carries out the reading of the image data acquired by the camera. It depends on the protocol used by the chosen camera for the visual servoing application (in this case CameraLink). The second hardware-dependent module is the robots' interface layer. This layer provides the control law with the information required, independently of the controlled robot. To control the Mitsubishi PA10 robot, a communication interface is implemented (ARCNET protocol). In this case, all the

commands to the servo driver and all the information from the servo driver are obtained via ARCNET. This module generates the control commands (in format of 256 bytes packets) based on the data received from the Control Law module, and sends them to the servo driver to be executed in each control cycle. After transmitting the control commands to the servo driver, the current value and status of each axis of the robot are transmitted (returned) to the FPGA and interpreted by the ARCNET Protocol Interface module.

The three-degrees-of-freedom robot's motors are brushed 24V-DC motors from Maxon, equipped with optical quadrature encoders MR of type L, 3 channels. As it is represented in Figure 4.9, the FPGA board needs an intermediate amplifying stage to drive them directly. For that, the ADS50/5 amplifiers from Maxon were chosen. They allow a low level control of the motor's torque and current. The ADS50/5 take as input reference an analog voltage signal between -10V and +10V. A servo controller of this nature requires a -10V to +10V analog output channel, and an encoder input channel.

The rest of the modules that compose the proposed architecture are not hardware-dependent. They were divided by their functionality: vision and control.

4.4 Control system

In this section, the concept of dynamic perceptibility is integrated in the optimal framework described in Chapter 3. Additionally, this section describes the implementation of a visual servoing system with dynamic perceptibility in the FPGA architecture.

4.4.1 Image trajectory and dynamic perceptibility

Denoting $\mathbf{K}_P \in \Re^{2kx2k}$ as a proportional gain matrix and $\mathbf{K}_D \in \Re^{2kx2k}$ as a derivative matrix, where k is the number visual points, the reference acceleration in the image space for the direct visual controller can be expressed as:

$$\ddot{\boldsymbol{s}}_r = \ddot{\boldsymbol{s}}_d + \mathbf{K}_D(\dot{\boldsymbol{s}}_d - \dot{\boldsymbol{s}}) + \mathbf{K}_P(\boldsymbol{s}_d - \boldsymbol{s}) = \ddot{\boldsymbol{s}}_d + \mathbf{K}_D\dot{\boldsymbol{e}}_s + \mathbf{K}_P\boldsymbol{e}_s \tag{4.11}$$

where $\ddot{\boldsymbol{s}}_d$, $\dot{\boldsymbol{s}}_d$ and $\boldsymbol{s}_d$ are the desired image space accelerations, velocities and positions, respectively. Therefore, from (3.6) and (4.11), the following relation can be obtained:

$$\mathbf{L}_J\ddot{\boldsymbol{q}} = \ddot{\boldsymbol{s}}_d + \mathbf{K}_D\dot{\boldsymbol{e}}_s + \mathbf{K}_P\boldsymbol{e}_s - \dot{\mathbf{L}}_J\dot{\boldsymbol{q}} \tag{4.12}$$

By using the information provided by the ellipses determined by the dynamic perceptibility, the system must avoid situations where the robot is near a singularity. This is done by modifying the image error, $\boldsymbol{e}_s = \boldsymbol{s}_d - \boldsymbol{s}$. The trajectory is in the neighborhood of an image singularity when $\omega_{dp} < \omega_{dpt}$ (ω_{dp} is the current dynamic perceptibility and ω_{dpt} is a threshold value defined by the user). In this last case, the image error $\boldsymbol{e}_s = \boldsymbol{s}_d - \boldsymbol{s}$ of the controller is modified to force the robot motion in the direction of the largest eigenvector of each dynamic perceptibility ellipse:

$$\boldsymbol{e}_s = \boldsymbol{e}_s + \|\boldsymbol{e}_s\|\,\mathbf{AU} \tag{4.13}$$

where $\|\boldsymbol{e}_s\|$ is the norm of the image error and $\mathbf{A}$ is a proportional diagonal matrix that controls the amount of influence of the perceptibility for each visual feature. $\mathbf{U}$ is a diagonal matrix where the values of its diagonal are unitary vectors pointing in the direction of the largest eigenvector of each dynamic perceptibility ellipse for each visual feature.

The next subsection describes a direct image-based visual servoing in order to guide robotic arms using dynamic perceptibility and direct visual servoing.

4.4.2 Implementation of an FPGA-based visual servoing system with dynamic perceptibility

As described in Section 3.4.2 different controllers can be obtained from the proposed optimal framework considering different values for the weight matrix

$\mathbf{W}$. For example, when $\mathbf{W} = \mathbf{M}^{-2}$ the following controller is obtained without considering chaos control:

$$\boldsymbol{\tau} = \mathbf{M}\mathbf{L}_J^{+} \cdot \left(\ddot{\boldsymbol{s}}_r - \dot{\mathbf{L}}_J \dot{\boldsymbol{q}}\right) + \mathbf{C} + \boldsymbol{g} \tag{4.14}$$

This section describes the main considerations about the FPGA implementation of the direct visual controller indicated in Equation (4.14). The main components of the FPGA architecture were previously detailed in Section 4.3 and Figure 4.10 depicts the pipeline of the whole system. This scheme shows the parallelization designed to perform the visual servoing task accurately. This parallelization is especially useful to obtain a time-constrained response. This is the most important feature of the proposed architecture with respect to the traditional one: multi-purpose CPU. With this architecture, the visual servoing system becomes a real time system.

The vision module is composed of a set of five stages. It picks the images received by the frame grabber (Stage 1 in Figure 4.10) to extract the desired visual data. The vision algorithms are implemented in a pipeline (Stages 2-6 in Figure 4.10). Thus, every pixel received by the vision module is processed as soon as it arrives, without needing to store the whole image into a buffer and then having to wait to receive the full image to start the processing. Hence, latency of the complete system is reduced while considerable amount of storing resources and communication traffic are saved up.

Figure 4.10 demonstrates the timing diagram of the pipelined visual servoing cycle for the PA-10 robot, where the neck of the bottle is the ARCNET frame transmission time (5ms), so the camera frame rate was configured to be similar to such time (200 fps). Nevertheless, in the case of the COOPER robot, the calculated torques after the control stage in the pipeline are sent and applied directly to the robot motors amplifiers and, thus, the system can work at the maximum rate at which the camera can operates.

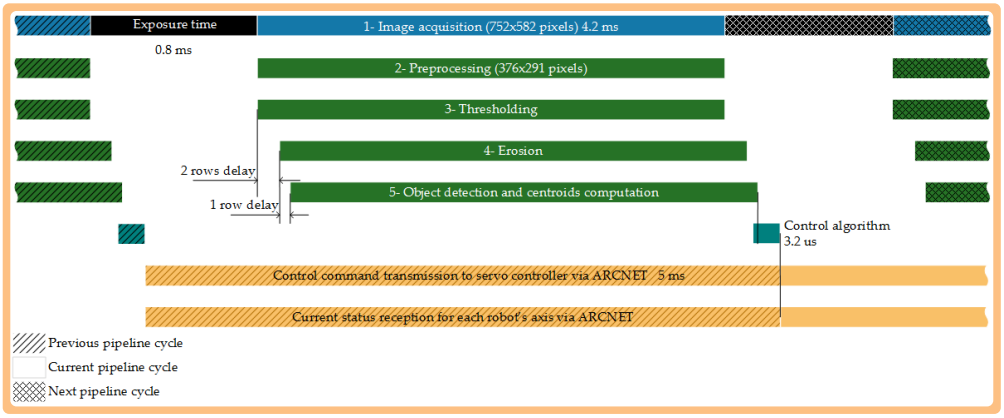

Figure 4.10. Pipeline of the whole system (PA-10).

4.4

To implement the control law proposed in Equation (4.14) using the FPGA architecture, with the correction described in Equation (4.13), an optimizing method based on parallel processing and pipeline technic is followed. Figure 4.11 shows the functional scheme of the implemented Control module coded in VHDL. Taking advantage of the FPGA parallelism capabilities, the independent terms are calculated at the same time, while the dependent ones have to wait till the correct inputs are ready. In this work, all the elements of the matrices ($\mathbf{L}_J$, $\mathbf{M}$, $\mathbf{C}$, etc.) are calculated simultaneously exploiting to the maximum the parallel execution capabilities (spatial parallelism) of FPGA devices. Therefore, by changing the degrees of freedom of the employed robot, computation time of the control algorithm will be unsubstantially affected. Nevertheless, the occupation of the FPGA hardware resources will increase exponentially, but in this work, an optimization method based on sharing the idle cores between various operations or execute them in pipeline is followed. Table 4.1 shows a summary of the resources used by the Xilinx's Kintex-7 FPGA board used in this work. This summary shows the FPGA resources occupation for the implementation of the control algorithm for both robots and the time required to execute it. The time consumed by the control algorithm is almost negligible when compared to the time elapsed in the rest of the system modules (see Figure 4.11). All the coded variables are expressed in double-precision binary floating-point format specified in the

IEEE-754 standard. This representation uses 1-bit for sign, 11-bits for exponent and 53-bits for fraction. The Xilinx LogiCORE IP Floating-Point Operator v5.0 is employed to perform all floating-point arithmetic on an FPGA device. This core can be customized for operation, word length, latency, and interface. This core supports operations like multiplication, addition/subtraction, division, comparison, etc. and is compliant with the IEEE-754 Standard and optimized for speed and latency. The operation is specified when the core is generated, so in this work, one core was generated for each operation. Thus, all the similar operations in the same matrix share the same operation core and so a lot of FPGA hardware is saved up and the implementation is optimized. Once the new torques are computed, they are sent to the robot via the ARCNET interface module. It takes 5ms, not only for sending the torques, but also to receive the data from the robot to compute position, velocity and acceleration for each joint.

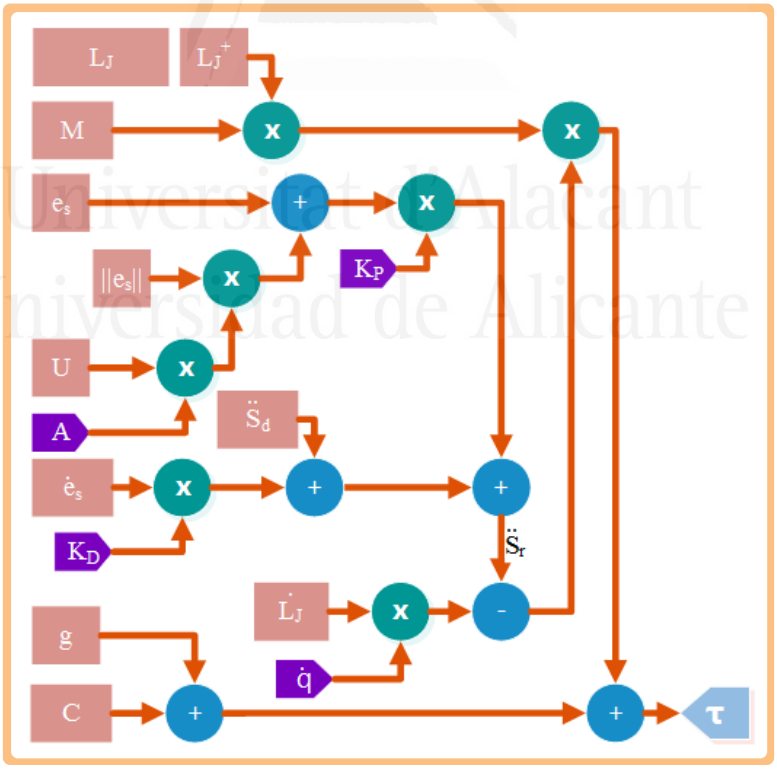

Figure 4.11. Control module scheme (PA-10).

Table 4.1. FPGA Resources Utilization for control algorithm and execution time

	Slices	LUTs	LUT-RAM	DSP Blocks	Execution time
3 dof robot	6525(12%)	19511(9%)	411(0.4%)	17(1.5%)	2.95 μs
PA10	20227(37%)	56581 (26%)	1849(1.8%)	62(5.5%)	3.2 μs

4.5 Optimal framework implementation in the FPGA architecture

As described in Chapter 3, this Section describes the implementation of the proposed optimal framework in the FPGA architecture. The first Section shows the main components and the execution time of the main approach without chaos compensation and the second one, this time with chaos compensation.

4.5.1 FPGA implementation without chaos control

The proposed optimal framework can be represented by using the following expression that depends on the weight matrix **W**:

$$\boldsymbol{\tau} = \mathbf{W}^{-1/2}\left(\mathbf{L}_J\mathbf{M}^{-1}\mathbf{W}^{-1/2}\right)^{+} \cdot \left(\ddot{\boldsymbol{s}}_r - \dot{\mathbf{L}}_J\dot{\boldsymbol{q}}\right) + \mathbf{C} + \boldsymbol{g} \tag{4.15}$$

The times scheme for the VHDL implementation of the framework is represented in Figure 4.12. The framework represented by Equation (4.15) is implemented thanks to FPGA embedded architecture. Also, an interface is developed that allows for monitoring the visual servoing task and, at the same time, provides the possibility of modifying diverse parameters and constants of the controllers implemented with the FPGA. One of the available parameters for the user at runtime is the adjustment of **W** matrix, without the need of recompiling the program in the FPGA.

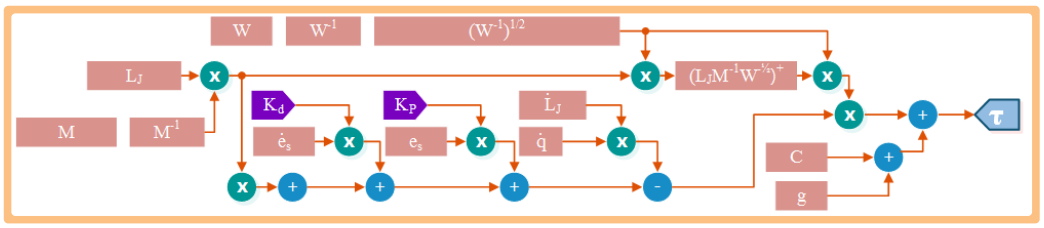

Figure 4.12. Execution times scheme at runtime for the design of direct visual servoing systems.

4.5.2 FPGA implementation with chaos control

An execution times scheme employed for the implementation of the optimal framework considering chaos compensation is described next. As previously stated, the framework calculations were implemented in a way that it allows for obtaining a series of direct visual servoing control laws by simply defining new values of the matrix **W**. The optimal framework with chaos compensation can be expressed as:

$$\boldsymbol{\tau} = \mathbf{M}k\left(\dot{\boldsymbol{q}}(t-\varepsilon) - \dot{\boldsymbol{q}}(t)\right) + \mathbf{W}^{-1/2}\left(\mathbf{L}_J\mathbf{M}^{-1}\mathbf{W}^{-1/2}\right)^{+} \cdot \left(\ddot{\boldsymbol{s}}_r - \dot{\mathbf{L}}_J\dot{\boldsymbol{q}}\right) + \mathbf{C} + \boldsymbol{g} \qquad (4.16)$$

Figure 4.13 shows the VHDL implementation scheme with the required times for the computation of all different terms of the controller. This way, the framework implemented in the FPGA allows for adjusting at runtime different behaviors when trajectory tracking for adapting it to every situation.

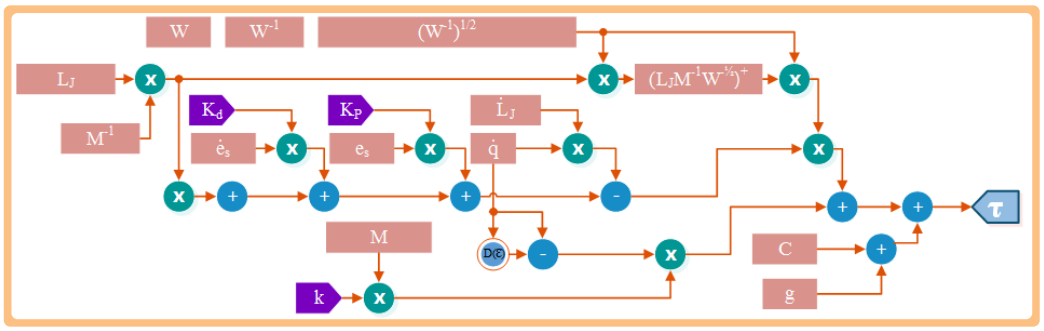

Figure 4.13. Execution times scheme at runtime for the design of direct visual servoing systems with chaos compensation

Furthermore, the adjustment of **W** allows for easily testing new controllers to find the more appropriate to the properties of the desired trajectory in the image.

4.6 Results

This section presents several experiments to illustrate the performance of the FPGA based visual servoing architecture. Furthermore, the value of the dynamic perceptibility concept proposed in this section is shown during these experiments. As the experiments show, this concept provides information about the system ability to track objects using a direct visual controller. This parameter is a useful criterion to determine situations where the robot is close to a singularity (in the image or in the joint space). The FPGA-based architecture and the proposed dynamic visual controller are tested with two robots: three-degrees-of-freedom COOPER robot and a Mitsubishi PA10 robot. First, an experiment with the COOPER robot is presented. Additionally, the redundancy of the Mitsubishi PA10 robot allows us to present the results obtained in more difficult tasks. In the experiment described in Section 4.6.2, the robot passes near to a robot singularity and in the one detailed in Section 4.6.3 the robot achieves an image singularity. Finally, Section 4.6.4 presents an experiment of the visual servoing system with chaos compensation. The use of the FPGA architecture allows for obtaining reduced and constant delays in the visual feedback. This aspect is important to better eliminate the joint chaotic behavior.

The considered camera intrinsic parameters are $(u_0, v_0) = (368, 290)$ px, and $(f_u, f_v) = (433, 433)$ px (position of the optical center (u_0, v_0) and the focal length in the X and Y directions, respectively). Calibration of both the camera intrinsic and extrinsic parameters relating the camera position to the robot end effector are left coarse. This was done intentionally to demonstrate the robustness of the control system. During this section, the control law presented in Equation 4.14 is named as DVS (Dynamic Visual Servoing) and the term DPVS (Dynamic Perceptibility-

based Visual Servoing) is used to refer when the error modification indicated in Equation (4.13) is applied.

4.6.1 Visual servoing of the three-degrees-of-freedom COOPER robot

This section describes an experiment that illustrates the implementation of the proposed architecture and controllers in the three-degrees-of-freedom COOPER robot. Due to the limitations of this robot and in order to avoid singularities, we will work in a 2D plane parallel to the scene for the initial tests. An image-based visual servoing task can be accomplished with three image points, but we need a robot with at least six degrees of freedom. For that, the three degrees of freedom of the robot are used and the end-effector will always move in the same plane and maintain the same distance to the image pattern used. A pattern of a white object situated on a black canvas is used. These experiments are not addressed to perform complex image processing tasks, but rather in demonstrating that this system is highly robust and re-configurable.

In order to implement this experiment, the robot is first positioned at the desired location. In this desired location, the object's center of gravity in the image space is stored as the desired image feature. The robot is then moved to a position named "initial position". Then, the DVS controller is used to achieve the desired image position from the initial one. In order to implement the controller indicated in Equation (4.15), the following constants are used: $\mathbf{K}_P = 0.7\mathbf{I}_{2x2}$, $\mathbf{K}_D = 0.3\mathbf{I}_{2x2}$.

Figure 4.14.a shows the evolution of the object's center of gravity in the image plane. The final position is reached using the controller without oscillations. Figure 4.14.b shows the trajectory followed by the robot end-effector in the positioning performed by the proposed controller. The robot moves the camera with a fairly straight trajectory, with no oscillations, and without missing the desired position. One of the figures that best represent the correct execution of a visual controller is Figure 4.15.a. It shows the evolution of the norm of the image error. This error, computed through the reference object center of gravity in the image space (for the

current and final position), is the error that the controller tries to minimize in consecutive iterations. The error decreases quickly in the initial iterations. Finally, Figure 4.15.b shows the output of the controller during the positioning task, that is, the torques sent to the motors of each robot joint. Approximately, after 2 seconds, the system reached the final position and sends torques close to 0.

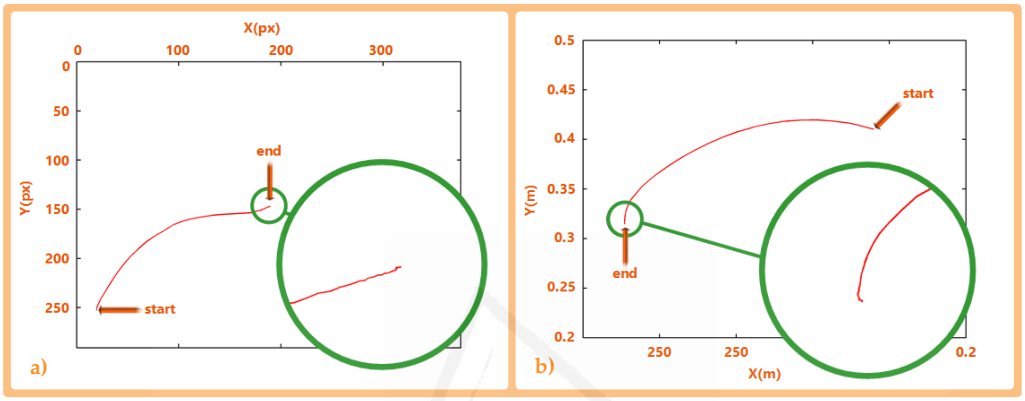

Figure 4.14. Experiment 1. 3 dof robot. a) Evolution of the object's center of gravity in the image plane. b) Evolution of the robot end-effector in the 3D Cartesian space.

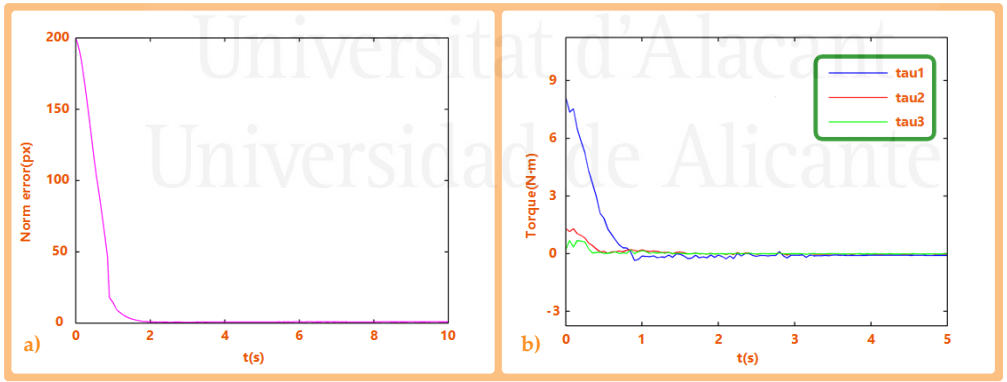

Figure 4.15. Experiment 1. 3 dof robot. a) Evolution of the norm of the error in the image. b) Evolution of the output of the system: Joint torques.

4.6.2 Visual servoing of a PA10 robot with a robot singularity

This section describes an experiment where the robot passes near a singularity when the DVS control law is used. In order to avoid this situation, the dynamic perceptibility concept will be employed to determine the adequate robot motion.

In this experiment, a set of three image points are considered as image features to perform the robot guidance. The value of the initial features extracted in the image are $\boldsymbol{s} = [\boldsymbol{f}_1 = (328, 175), \boldsymbol{f}_2 = (159, 345), \boldsymbol{f}_3 = (301, 532)]$ px and the desired ones are $\boldsymbol{s}_d = [\boldsymbol{f}_{1d} = (276, 191), \boldsymbol{f}_{2d} = (276, 391), \boldsymbol{f}_{3d} = (476, 391)]$ px. At the beginning of the experiment, the robot is located at (0.5963, -0.1501, -0.01435) m. Using the proposed DVS controller, the image trajectories indicated in Figure 4.16.a are obtained. This last figure represents not only the image trajectory but also the dynamic perceptibility ellipses obtained during the trajectory. As it can be seen, the ellipses present an irregular size when the robot is close to the singularity (this zone is indicated in Figure 4.16.a as "singularity risk" and a manipulability of 0.005 is obtained indicating that the robot singularity is nearby). These ellipses give a measure of the ability of performing end-effector accelerations in a given pose. Using this information in the modified dynamic controller DPVS ($\mathbf{A}$ = 0.012I3x3), the image trajectory represented in Figure 4.16.b is obtained. As it can be seen in this last figure, the obtained ellipses are more regular and their size and orientation are more constant during the experiment.

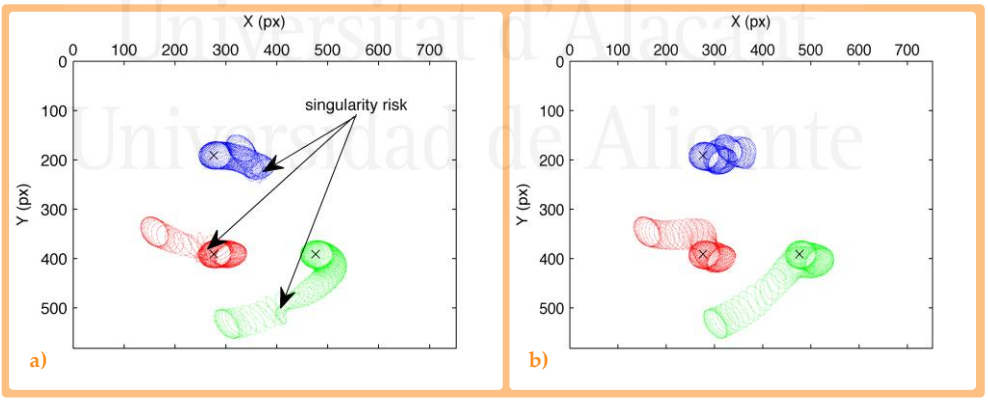

Figure 4.16. Experiment 2. PA10 robot. Image trajectory and dynamic perceptibility ellipses. a) Using the DVS controller. b) Using the DPVS controller.

Figure 4.17 represents the value of the dynamic perceptibility during the experiment. Figure 4.17.a and Figure 4.17.b represent the value of this parameter using the DVS and DPVS controllers respectively. As expected, by using the DPVS,

the system detects the situation where the robot is close to the singularity and the modification of the robot trajectory increases the dynamic perceptibility, avoiding the singularity (a minimum manipulability of 0.04 is obtained in this case, i.e. this parameter is clearly increased).

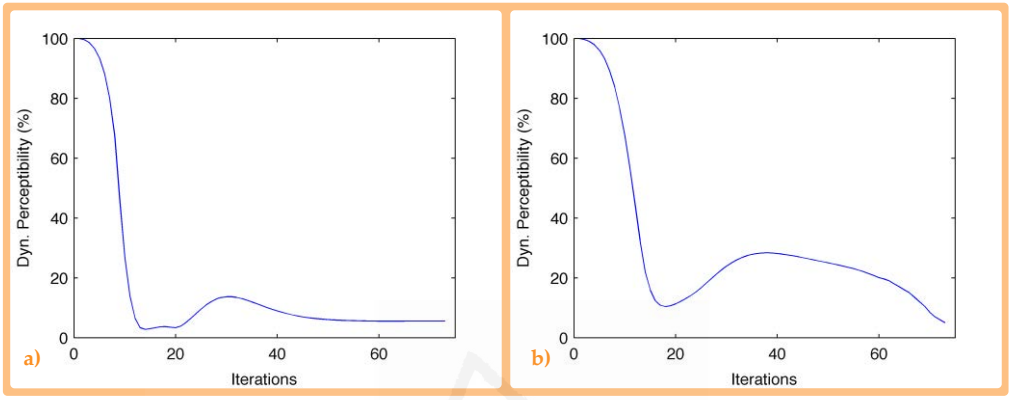

Figure 4.17. Experiment 2. PA10 robot. Dynamic perceptibility. a) Using the DVS controller. b) Using the DPVS controller.

Finally, in Figure 4.18, the robot 3D trajectories obtained from both experiments are shown. This figure represents the modification of the 3D trajectory performed by the end-effector while using the proposed controller to avoid the robot singularity.

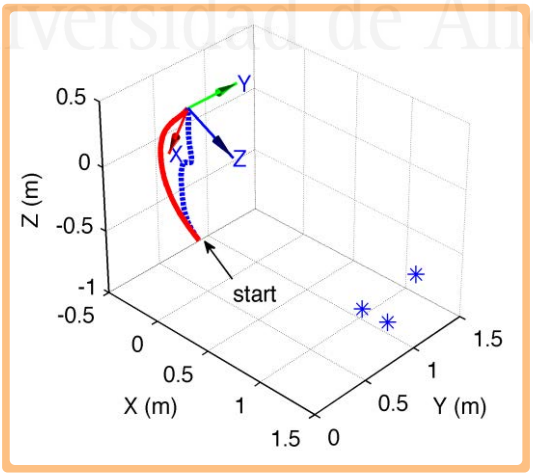

Figure 4.18. Experiment 2. PA10 robot. Obtained robot trajectories. Solid line: DVS controller. Dashed line: DPVS controller.

4.6.3 Visual servoing of a PA10 robot with an image singularity

As previously indicated, the dynamic perceptibility is a measure of the system ability to track objects using a direct visual control system. Therefore, the dynamic perceptibility ellipses provide not only information about the adequate motion to avoid robot singularities taking the robot dynamics into account, but also image information is considered. In this section, an experiment is presented to demonstrate the proposed controller ability to detect and avoid image singularities. In this experiment, a set of three image points are considered as image features to perform the robot guidance. The value of the initial image features extracted in the image are $\boldsymbol{s} = [\boldsymbol{f}_1 = (341, 415), \boldsymbol{f}_2 = (327, 467), \boldsymbol{f}_3 = (540, 254)]$ px and the desired ones are $\boldsymbol{s}_d = [\boldsymbol{f}_{1d} = (429, 483), \boldsymbol{f}_{2d} = (474, 563), \boldsymbol{f}_{3d} = (676, 371)]$ px. Figure 4.19 represents the image trajectory obtained using the proposed DVS controller (Figure 4.19.a) and the DPVS controller (Figure 4.19.b). The desired image features are marked with a X.

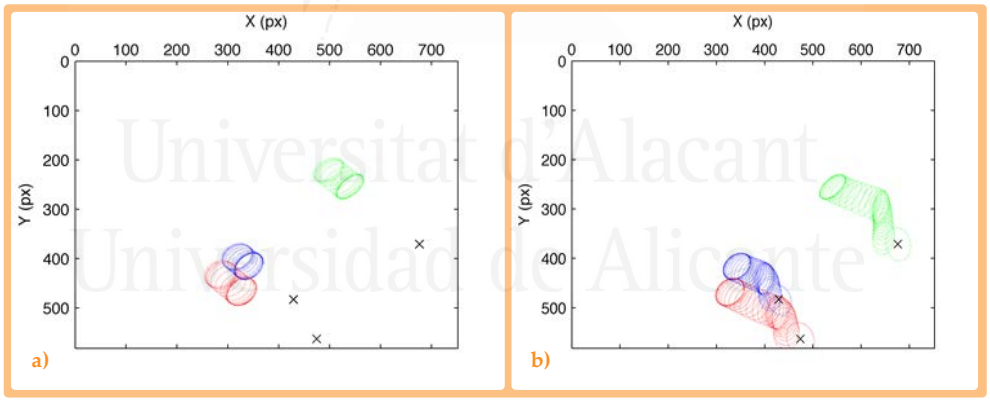

Figure 4.19. Experiment 3. PA10 robot. Image trajectory and dynamic perceptibility ellipses. a) Using the DVS controller. b) Using the DPVS controller.

In Figure 4.20.a the image trajectory begins in the initial image features but the system experiences camera retreat during the first iterations and the robot control stops when an image singularity is achieved. However, by using the image error modification indicated in Equation (4.13), DPVS, the system detects the situation when the robot is near the image singularity and the dynamic perceptibility ellipses guide the robot in a different direction to avoid this situation (in this case

$\mathbf{A} = 0.5I_{3x3}$). Figure 4.20 clearly shows how, by using the proposed controller DPVS, the value of the dynamic perceptibility increases during the tracking.

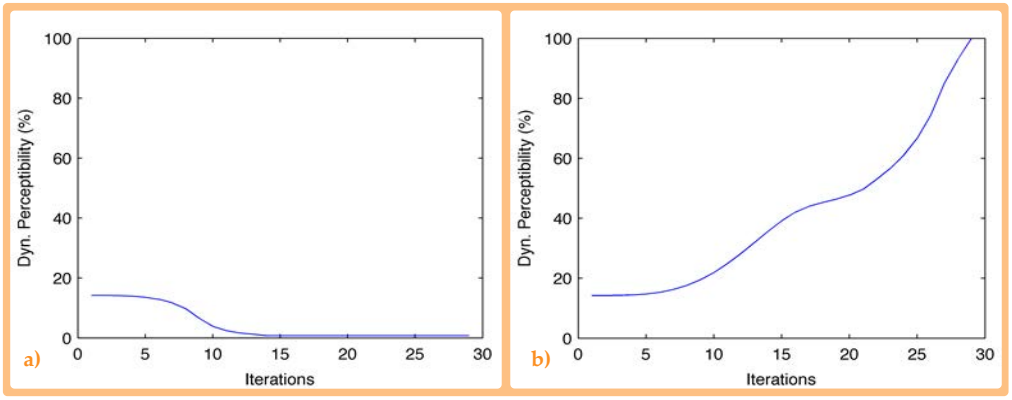

Figure 4.20. Experiment 3. PA10 robot. Dynamic perceptibility. a) Using the DVS controller. b) Using the DPVS controller.

Finally, the 3D trajectories obtained in both cases are represented in Figure 4.21. It can be seen that both trajectories start following the same path but where the DVS controller crashes, the DPVS controller manages to avoid the singularity by changing course and recovering the movement towards the target.

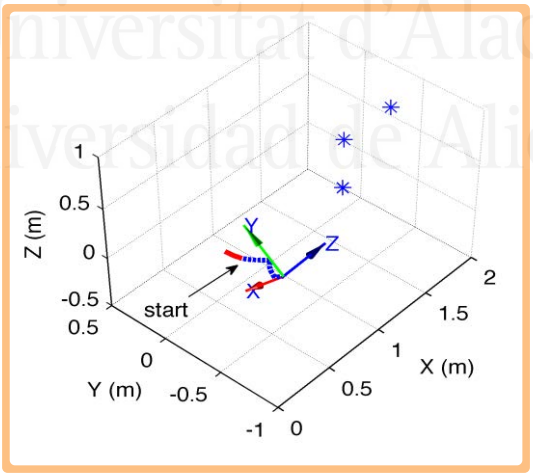

Figure 4.21. Experiment 3. PA10 robot. Obtained robot trajectories. Solid line: DVS controller. Dashed line: DPVS controller.

4.6.4 FPGA implementation of the controller with chaos compensation

With the objective of evaluating the improvements when employing the FPGA-based control architecture, this section compares the behavior when a classic control implementation as described in (Pomares, Perea, & Torres, 2014) is applied, to when the proposed architecture controller with chaos compensation is used. More specifically, this comparison is evaluated during a repetitive trajectory tracking in the image space as described in Figure 4.22.

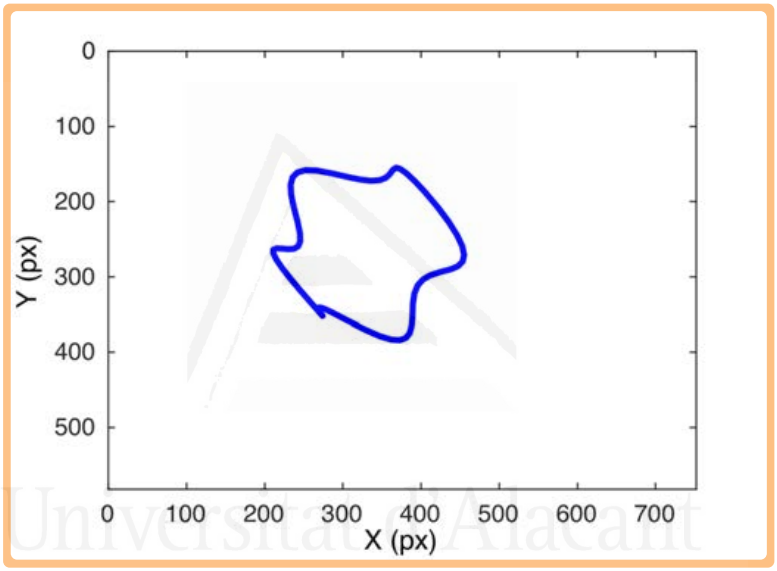

Figure 4.22. Experiment 4. 3 dof robot.
Desired trajectory in image space for the FPGA-based controller.

Figure 4.23 shows the tracking in the image space when the proposed control law (with chaos compensation) when using and not using the proposed FPGA-based architecture. It can be observed that for both cases a correct behavior during the trajectory tracking in the image space is performed. A value of $k = 4.6$ is obtained when using the parameter adjustment method of the delayed feedback controller described in Chapter 3. Although the result is correct for both cases, when using a classic implementation, the average error module in image space is 3.82 pixels, while the value of this parameter for the FPGA-based implementation is 2.55 pixels. The diminishment of this error is due to not only the reduction in

processing times, but also to the possibility of obtaining more constant loops. This last detail allows for a better adjustment and optimization of the delayed feedback controller. It is also worth noting that these parameters adjustment can be done at runtime, without the need to recompiling the program every time that this action needs to be done.

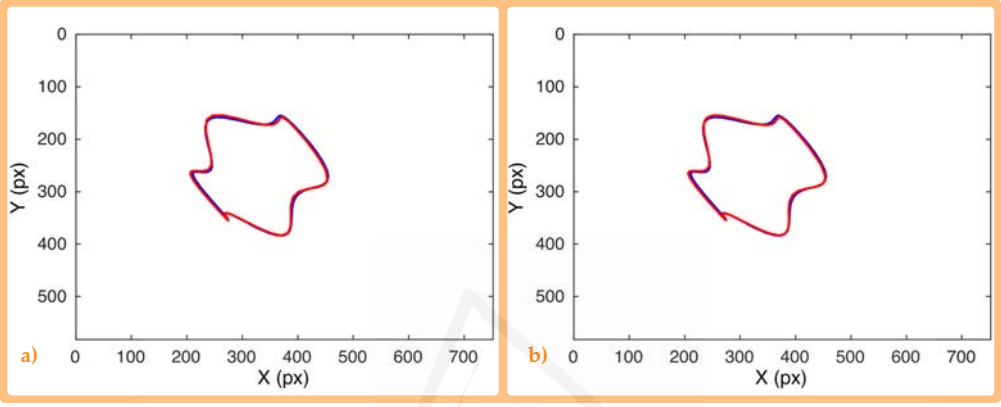

Figure 4.23. Experiment 4. 3 dof robot. Behavior in image space.
a) without using the FPGA-based architecture. b) Using the proposed architecture.

For better observing the improvements, the joint behavior is studied next. Figure 4.24.a represents the joint behavior when using a classic implementation (without FPGA), while Figure 4.24.b shows the same figures but when the proposed architecture is employed. The goal of the controller is to obtain a joint periodic behavior during a periodic trajectory tracking in the image space. During the first cycles, the systems goes through a positioning phase before performing the repetitive trajectory. The behavior is correct when using a classical architecture. However, due to loop time variations in the feedback, the adjustment is not completely correct. As observed in Figure 4.24, by employing the FPGA-based architecture, it is possible to precisely obtain and predict beforehand the feedback delays. This allows for a better adjustment of the controller and for obtaining a more adequate joint behavior.

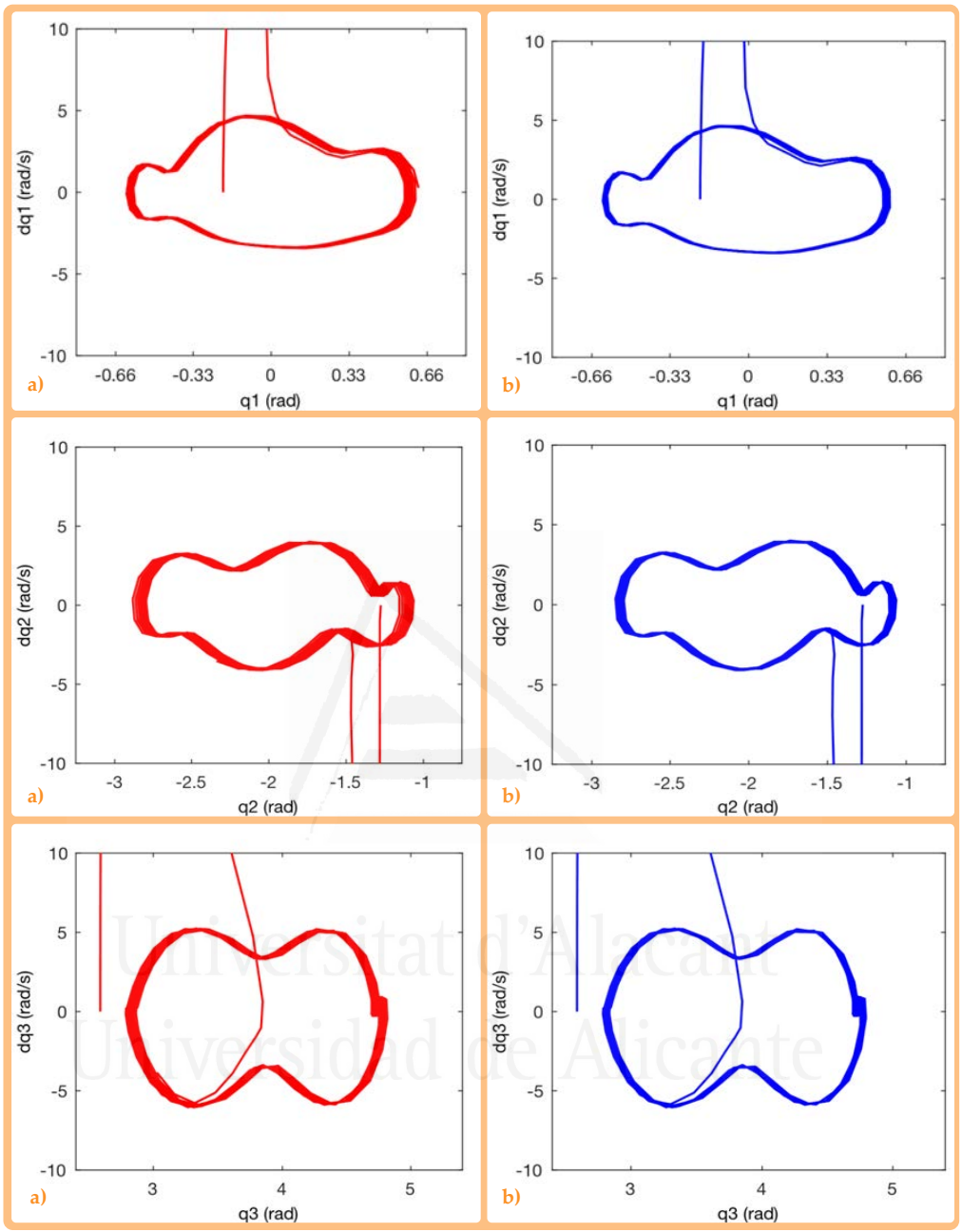

Figure 4.24. Experiment 4. 3 dof robot. Behavior in joint space. a) without using FPGA-based architecture. b) Using FPGA-based architecture.

4.7 Conclusions

The concept of dynamic perceptibility is proposed as a useful parameter to determine the system ability to track objects using a direct visual controller. Also, the possibility of employing this information to avoid both robot and image

singularities determined the integration of this concept into the implemented controller.

Additionally, an FPGA-based direct visual servoing framework to perform the guidance of a robot using an eye-in-hand camera system is proposed. The use of this hardware architecture allows for obtaining constant processing delays and an optimal behavior by carrying out a pipeline processing and the implementation as a framework allows for obtaining different control laws. This gives the possibility of highly adapt and adjust a controller to its task. The Chapter finishes with some experimental results that show the correctness and useful application of the framework.

Up to now, the work described in the Thesis overall focused in the development of an optimal control framework for direct image-based visual servoing control laws for robotic manipulators attached to a fixed structure. Next Chapter develops the framework so it takes into account the dynamics of free-floating robots, like the ones orbiting around earth and where the base is not actively actuated.

5 Visual servoing framework application: Space robotics

An image-based controller for the guidance of a spacecraft is presented in this chapter. The controller utilizes directly the visual features from image frames of a non-cooperative target for calculating both attitude and orbital maneuvers to perform a non-cooperative rendezvous to that object. An image-based controller is derived and its stability is proved analytically. The viability such control scheme is explored through its application to a specific realistic scenario, by taking into account a chasing satellite carrying onboard a zooming camera, 4 reaction wheels and 6 thrusters, as well as by considering the main perturbing factors that characterize the orbital environment during the far and close rendezvous.

Additionally, this chapter proposes the application of the direct image-based visual servoing framework proposed in Chapter 3 to perform the guidance of space free floating manipulators where the base is not actively actuated, and thus, reacting to the movement of the arm.

5.1 Introduction

This chapter describes two different approaches about the application of visual servoing in space robotics: spacecraft guidance and free-floating robot manipulators guidance. The next two subsections describe the state of the art in these two topics and the main contributions of the proposed approaches.

5.1.1 Spacecraft guidance using visual servoing

Space debris is becoming the issue of main concern among the space community because of its repercussion on present and future space missions. Indeed, uncontrolled objects produced by past space mission are currently occupying important orbital slots and they are sources of possible collisions with operative and non-operative satellites (Schaub, Jasper, Anderson, & McKnight, 2015). Despite the recent adoption of some mitigation guidelines (Johnson, 2011) and the development of a network of space debris surveillance and awareness (Donath, Schildknecht, Martinot, & Del Monte, 2010; Flohrer, Schildknecht, & Musci, 2008), the threat of collisions cannot be totally averted. Collisions, as that between Iridium 33 and Cosmos 2251 in 2009 (Wang, 2010), are still probable and they can produce cascade phenomena that may compromise the future utilization of the space (Kessler & Cour, 1978; Liou, 2011; Liou & Johnson, 2008).

Therefore, the need of a remediation to this problem has led the space community to investigate the viability of different active debris removal strategies (Shan, Guo, & Gill, 2016) and the definition and the development of on-orbit servicing missions for satellite rescuing and repairing (Graham & Kingston, 2015). Specifically, the removal of big and dangerous uncontrolled objects seems to be the viable solution for eliminating potential sources of new debris that overcrowd Low Earth Orbit (LEO) orbits. On the other hand, on-orbit service missions have been thought for extend the operational life of satellites which cannot be easily removed by de-orbiting maneuvers but has to be dismissed in graveyard orbits at their end-of-life, i.e. satellites in Geostationary Orbit (GEO).

Preliminary analyses and design concepts of both the mission typologies showed that the close approaches to the debris by the chasing spacecraft are mandatory for the mission's successes, as distance manipulation and touch-less technologies (i.e. electrostatic tug, laser ablation, etc.) could led to requirements not easily implementable onboard of the current platforms (Shan et al., 2016). Indeed, it is evident that, despite of the technology adopted for capturing the uncontrolled debris (i.e. robotic manipulators, nets, harpoons, etc.), the rendezvous of uncooperative objects follows a well-established scheme. Specifically, the chaser has to (a) reach the same orbit of the target satellite, (b) perform phasing orbital maneuvers in order to reduce the distance from the target satellite, (c) synchronize its attitude motion with respect to the target one, (d) perform the rendezvous maneuvers in order to finally (e) allow the on-orbit servicing or the debris grasping and removal operations (Felicetti, Gasbarri, Pisculli, Sabatini, & Palmerini, 2016).

It is worth noting that the visual based approach is one of the most appealing choices for the uncooperative rendezvous, since this technique is considered a low cost, mainly passive and accurate (Palmerini, Sabatini, & Gasbarri, 2016). Furthermore, the technology readiness of space qualified cameras, as well as of the onboard computers, is mature enough that the techniques developed for the control of ground based robots can be easily implemented onboard. An example of automated rendezvous already developed is the Automated Transfer Vehicle (ATV), where the relative position and attitude of the chasing vehicle with respect to the International Space Station (ISS) could be reconstructed by identifying the visual features of a specific target attached to the ISS (De Rosa & Curti, 2006; Pinard, Reynaud, Delpy, & Strandmoe, 2007). Another example is given by the PRISMA mission (Bodin, Noteborn, Larsson, & Chasset, 2011), where two different camera systems have been used during the formation flying demonstration experiment: the Far Range Camera and the Close Range Camera. Specifically, the far range camera has been used as a star-tracker, detecting the target spacecraft as

a bright spot over a diffuse black background. Therefore, only information concerning the line of sight could be used in the guidance, navigation and control loop for reducing the distance down to 20-30m. The close range camera has been used instead for the proximity operations between the spacecraft, extracting more detailed visual features and reconstructing even the attitude of the target platform (Bodin et al., 2012).

The previously mentioned missions demonstrated the viability of vision based Guidance, Navigation, and Control (GNC) loops for the rendezvous of cooperative targets and the actual challenge is represented now by the extension of such techniques to the non-cooperative targets, such as space debris or satellites to be recovered. The main difference between cooperative rendezvous and non-cooperative rendezvous is related to the target that was not designed to perform a rendezvous. Therefore, the target do not send information on its position to the chaser for far rendezvous localization and it does not have specific "target features" for close range approach as well as specific docking system for helping the capture by the chaser. Furthermore, the target satellite attitude motion is a tumbling one, as the target satellite is anymore able to control its attitude during the approach (Bonnal, Ruault, & Desjean, 2013). Specific GNC needs are associated to non-cooperative rendezvous as they are the challenging aspects to be addressed during the mission design. The navigation system should address issues related to the target acquisition and target motion identification by means of specific onboard sensors and real time image processing algorithms. Furthermore, the chaser should be able to obtain information concerning its accurate relative positioning even if, in general, the range is undetermined during the far-distance and angles-only navigation phases (Woffinden & Geller, 2009). Moreover, the guidance system of the chaser should be designed in order to make possible the close approach to the target by taking into account the typology of the capture system as well as the characteristics and performance of the actuation system.

The former mentioned tasks and issues reflect the complexity of this problem, especially if we consider a vision-based system and real control actuators for the automated rendezvous. In both (Petit, Marchand, & Kanani, 2011) and (Gasbarri, Sabatini, & Palmerini, 2014), experimental setups have been settled in order to test the vision-based tracking algorithms to a space-like scenario. The experimental results showed the robustness of the classical algorithms to relative inter frame motions chaser/target orientation variations under different illumination conditions. In (Song, Li, & Ma, 2014), the feasibility of a monocular-based relative navigation for rendezvous and docking of a fully unknown space object has been investigated and successfully verified by using two extended Kalman filters applied to far and close range respectively. Also LIDARs can be used as main sensors for close approaches to uncooperative objects, as shown in (Aghili, Kuryllo, Okouneva, & English, 2011; Opromolla, Fasano, Rufino, & Grassi, 2015; Woods & Christian, 2016). Furthermore, a combined algorithm which uses vision-based predictions and motion planning for the actuation of robotic arms during the pre and post grasping phases is shown in (Aghili, 2012) and the application of visual servoing techniques to a dual arm robotic system is also investigated in (Hafez, Anurag, Shah, Krishna, & Jawahar, 2014). Stereoscopic vision techniques can be also applied for close rendezvous as in (Yu, He, Qiao, & Yu, 2014).

It is worth noting that the problem of vision based rendezvous has been always divided in far and close approach cases. This is essentially due to intrinsic characteristic of the used camera systems: optical system with fixed and predefined focal length have been implemented onboard in both ATV and PRISMA missions, as well as theoretical studies have been focused on the implementation of visual servoing techniques for close approaches and interactions with the target satellites. This chapter proposes the use of a classical camera to perform the guidance of a spacecraft with respect to an observed object using an image-based visual servoing approach. There are not previous research about direct image-based visual servoing systems for the guidance of spacecrafts

taking into account the orbital and attitude dynamics of the spacecraft and the real configuration of employed actuators for attitude and orbital control. This is a contribution of the chapter and a simulation system is proposed to validate the proposed approach.

5.1.2 Free-floating robot manipulators guidance using visual servoing

The research and development of robot manipulators on satellites for space operations has had a remarkable growth within the past few years. These manipulators are especially suited for precise, complex, or even dangerous tasks for astronauts. Currently, the utilization of the robot manipulators mounted on satellites can be summarized into six categories (Flores, Ma, Pham, & Ulrich, 2014): i) assembly, maintenance and repair; ii) spacecraft deployment, release and retrieve; iii) extravehicular activity support; iv) inspection; v) refueling; and vi) multi-arm cooperation. Regarding the base spacecraft, two types of operations are considered and studied (Dubowsky & Papadopoulos, 1993): free-floating case, where the base is completely free and floating in space with no attitude control; and thus, freely reacting to the movements of the manipulator attached to it; and free-flying case, where the base is actively controlled, and thus, the system's attitude and position can be controlled. In this chapter, the free-floating case is considered, where the robot manipulator must be positioned with respect to a tumbling object from which a set of visual features can be extracted by the eye-in-hand camera system. The classical approach to dealing with this kind of situations is divided into four phases (Flores et al., 2014): i) observing and planning; ii) final approaching; iii) impact and capture; and iv) post-capturing stabilization; usually knowing all the parameters of the target object, but there are also some works that deal with the capturing and stabilization of objects with unknown dynamics (Aghili, 2013). The control strategy discussed in this section will focus on observing and approaching the tumbling object. This Thesis presents a new image-based visual servoing approach, using the kinematics and dynamics model of this kind

of robots, not only to achieve a desired location with respect to the observed object in the space, but also to follow a desired trajectory with respect to the tumbling object.

This chapter proposes the use of visual information to perform the guidance of a free-floating satellite-mounted robot (FFSMR). In this case, an image-based approach allows for defining the control law directly in the image space, and does not need precise calibration and modelling (only a set of visual features must be extracted from the observed object as described through the section). This approach is proposed in order to perform the guidance of the FFSMR with respect to space objects, such as orbital debris, small asteroids, or defunct spacecraft. Few proposed image-based controllers take into account the non-linear dynamics model of robotic arms, usually referred to as direct visual servoing. By means of direct visual servoing, the internal control loop of servomotors is removed, so the visual servo control law directly provides the torque to be applied to the robot joints. Additionally, integrating the FFSMR dynamics in the visual controller allows for obtaining a relation between joint speeds and end-effector motion of the robot manipulator taking into account the base attitude disturbance during the tracking. As shown in Section 5.5.3, the use of this approach during the tracking allows for increasing the tracking performance with respect to classical image-based visual servoing systems.

A great number of visual servoing approaches, proposed up to now to perform the guidance of in-orbit robot manipulators, use a position-based approach. In (Petit et al., 2011), a 3D model-based tracking is used for a space rendezvous mission. In this case, a vision-based navigation is proposed using a 2 1/2 D visual servoing approach (Chaumette & Hutchinson, 2007), without considering the system dynamics. In (Petit, Marchand, & Kanani, 2012), the same researchers present a generic tracking and pose estimation method suited for complex, textured or untextured objects in deep space environments, for space rendezvous and space debris removal purposes. Within this last topic we should mention the

work presented in (Yu et al., 2014), where an estimation method of relative pose based on stereo vision is presented for the final phase of the rendezvous and docking of non-cooperative satellites. In (Song et al., 2014), relative navigation method for rendezvous and docking of an unknown tumbling object using a monocular camera is presented. Two extended Kalman filters with different models are used for relative orbit estimation in far range and relative position and attitude estimation in close range. Within this topic, it is worth mentioning the works of Aghili (see e.g. (Aghili, 2012, 2013)), which describe a combined prediction and motion planning approach for robotic arms during the phase of pre- and post-grasping of tumbling objects with unknown dynamics. A Kalman filter is employed to estimate the object dynamics used for the robot path planning. A position-based approach is used utilizing the system dynamics. In order to perform the in-orbit robot guidance without estimating the relative pose between the robot and the observed object, several researchers have proposed the use of image-based approaches. In (Inaba, Oda, & Hayashi, 2003), a classical image-based visual servoing applied to the Japanese Engineering Test Satellite VII (ETSVII) is proposed. As it is described in (Gans, Hu, & Dixon, 2008), multiple tasks can be controlled in a hierarchical manner. The last work presents a priority-based redundancy resolution at the velocity level. This method chooses one task as primary, and projects the other tasks (secondary, tertiary, etc.) into the null space of the primary task derivative. In (Hafez et al., 2014), a classical image-based visual servoing approach is employed for the guidance of a mounted dual-arm space robot. The work is designed to complete the task of servoing the robot's end-effectors to the desired pose, while regulating the orientation of the base-satellite. The visual task is defined as a primary task, while regulating the attitude of the base satellite to zero is defined as a secondary task without considering the system dynamics. Image-based control is also used in the experimental test-bed proposed in (Sabatini, Monti, Gasbarri, & Palmerini, 2013). The paper shows that it is possible to evaluate the elastic properties of a multibody manipulator, thanks to

the analysis of the acquired images. In (Jin, Yang, Xie, Sun, & Liu, 2013), a classical image-based, a position-based, and a switching approach are presented for autonomous satellite capture using an on-board manipulator with binocular hand-eye cameras without considering the system dynamics. In (Shi, Liang, Wang, Xu, & Liu, 2012), the previous approach is simulated taking into account the system dynamics; however, a classical indirect implementation is considered. None of the previous implementations of image-based visual servoing systems for FFSMR considers a direct visual control approach. The need for integrating the system dynamics in the guidance of FFSMR using image information is discussed in works such as (Jin et al., 2013) and (Yang, Jin, Xie, Sun, & Liu, 2014). These works describe a set of ground verification systems, which can experimentally verify and test the reliability of visual servoing control systems and path planning of space robots. In (Ma et al., 2015), a direct image-based visual servoing approach for guiding a FFSMR using an eye-in-hand camera system is proposed. In this case, an inverse dynamics controller is developed to lock the projection of a feature point at a desired constant position on the image plane from an initial one. Contrary to previous papers, using the direct visual servoing approach proposed in this section, the FFSMR is able to track a desired image trajectory with respect to an observed object (not only a positioning task). Additionally, this chapter proposes an optimal control approach to guide the FFSMR using visual information. This approach allows for tracking trajectories considering the optimization of the motor commands with respect to a specified metric. As shown in the experimental results, the use of this controller, jointly with the integration of a chaos compensation technique, allows to increase the tracking precision and to reduce the base attitude disturbance during the tracking. The proposed controller is applied to the direct visual control of a FFSMR during the tracking of image trajectories as shown in (Perez, Emami, & Pomares, 2016; Perez, Pomares, & Emami, 2016).

5.2 Non-cooperative rendezvous modeling

The non-cooperative rendezvous involves a fully operative spacecraft, the chaser, and a non-controllable object, such as space debris to be removed or a damaged spacecraft to be recovered. To analyze the maneuvers, it is necessary to define coordinate frames which help the description and the definition of the system of equations of motion. In the following both the coordinate frames and the equations of motion used are described.

5.2.1 Coordinate frames

Figure 5.1 shows the coordinate frame attached to the body of the chasing spacecraft, named as {B}, and the coordinate frame associated to the object to be chased, named as target coordinate frame {T}. Both of them are orbiting around the Earth, which is also the origin of the Earth Centered Inertial coordinate frame, called {I} in the figure. A Local Vertical Local Horizontal coordinate frame, denoted with the letter {L} in Figure 5.1, is defined by locating its origin in a convenient orbit so that both the chaser and the target motion can be referred by means of relative distances from that, namely:

$$\mathbf{d}_B = \mathbf{r}_B - \mathbf{r}_L \tag{5.1}$$

$$\mathbf{d}_T = \mathbf{r}_T - \mathbf{r}_L \tag{5.2}$$

The $\hat{\mathbf{x}}_L$ axis is directed along the radial direction, the $\hat{\mathbf{z}}_L$ axis is directed as the normal to the orbital plane and the $\hat{\mathbf{y}}_L$ axis forms a right-handed frame with the two other axes.

The main components and coordinate frames associated to the chaser spacecraft and the camera are represented in Figure 5.2. Specifically, the frame {B} is attached to the spacecraft and its origin is coincident with the center of mass G_B. The frame {C} is the camera frame and it is attached to the camera *c*. The 4 reactions wheels, denoted with *rw1*, *rw2*, *rw3* and *rw4*, are displaced in a pyramidal configuration so that their rotation axes are inclined with respect to the $\hat{\mathbf{x}}_B\hat{\mathbf{y}}_B$ body

plane by an angle β. This configuration guarantees a 3 axis stabilization and reliability against the failures of one of the wheels (Hablani, 1994). The spacecraft main thruster is located along the $\hat{\mathbf{z}}_B$ body axis (thz+, pushing along the +z direction) and other 5 small thrusters allow maneuvering along other directions (thz-, thx+, thx-, thy+, thy-). It is assumed that the thrusters do not produce any torque to the spacecraft so that the attitude maneuvers are performed only by using the reactions wheels.

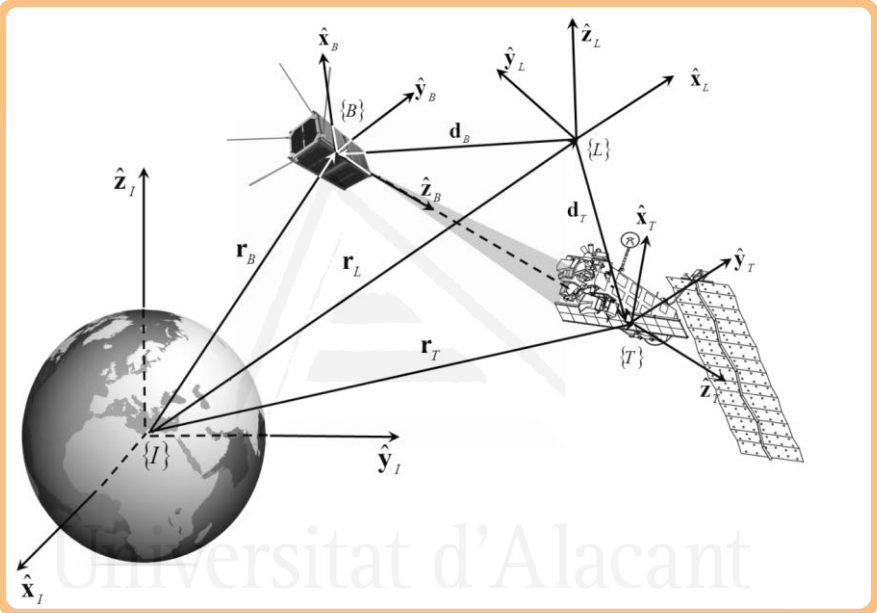

Figure 5.1. Schematic representation of the local vertical local horizontal {L}, of the chasing spacecraft {B} and of the target {T} coordinate frames

5.2.2 System dynamics

Both orbital and attitude dynamics are taken into account for describing the motion of the spacecraft involved in the non-cooperative rendezvous. Concerning the orbital dynamics, it is convenient referring the position of both the chaser spacecraft and target spacecraft with respect to the {L} reference frame and assuming that this frame is moving along in a circular orbit, so that the model for

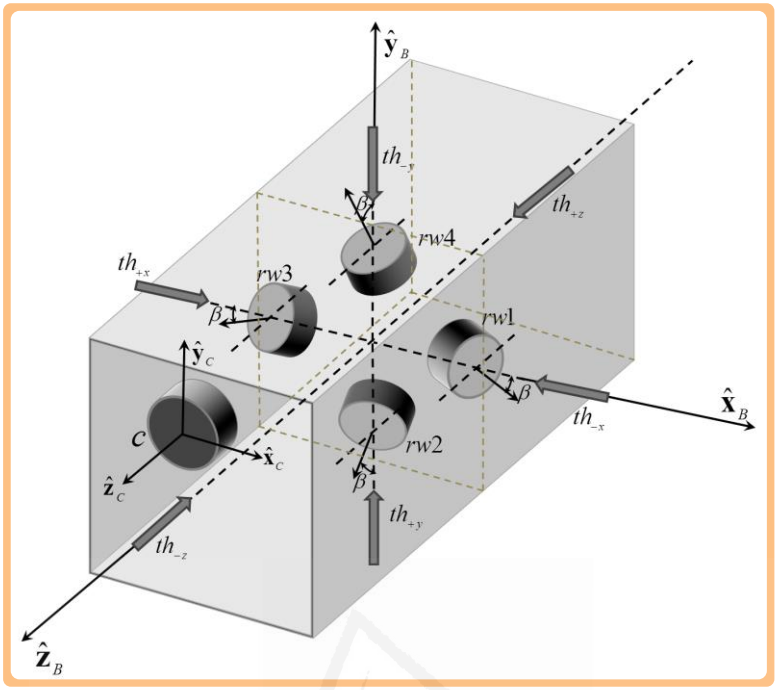

Figure 5.2. Schematic representation of the chaser the associated coordinate frames {B}, the camera frame {C}, the position and directions of the thrusters and of the reaction wheels.

the relative dynamics of the chaser and of the target spacecraft are represented by the Clohessy-Wiltshire equations of motion (Alfriend, Vadali, Gurfil, How, & Breger, 2009):

$$\begin{bmatrix} {}^{L}\dot{\mathbf{d}}_i \\ {}^{L}\dot{\mathbf{v}}_i \end{bmatrix} = \begin{bmatrix} \mathbf{A}_{11} & \mathbf{A}_{12} \\ \mathbf{A}_{21} & \mathbf{A}_{22} \end{bmatrix} \begin{bmatrix} {}^{L}\mathbf{d}_i \\ {}^{L}\mathbf{v}_i \end{bmatrix} + \begin{bmatrix} \mathbf{B}_1 \\ \mathbf{B}_2 \end{bmatrix} \mathbf{u}_{th} \tag{5.3}$$

where ${}^{L}\mathbf{d}_i = \begin{bmatrix} {}^{L}x_i & {}^{L}y_i & {}^{L}z_i \end{bmatrix}^T$ and ${}^{L}\mathbf{v}_i = \begin{bmatrix} {}^{L}\dot{x}_i & {}^{L}\dot{y}_i & {}^{L}\dot{z}_i \end{bmatrix}^T$ are the position and the velocity vectors of the two spacecraft, where the right-subscript i can be substituted with T and B, as per target and chaser spacecraft respectively and the left superscript L means that the components of the vectors are defined in the local horizontal local vertical reference frame. The matrices $\mathbf{A}_{11}, \mathbf{A}_{12}, \mathbf{A}_{21}$ and $\mathbf{A}_{22}$ are defined as follows:

$$\mathbf{A}_{11} = \begin{bmatrix} 0 & 0 & 0 \\ 0 & 0 & 0 \\ 0 & 0 & 0 \end{bmatrix} \quad \mathbf{A}_{12} = \begin{bmatrix} 1 & 0 & 0 \\ 0 & 1 & 0 \\ 0 & 0 & 1 \end{bmatrix}$$
$$\mathbf{A}_{21} = \begin{bmatrix} 3n_L^2 & 0 & 0 \\ 0 & 0 & 0 \\ 0 & 0 & -n_L^2 \end{bmatrix} \quad \mathbf{A}_{22} = \begin{bmatrix} 0 & 2n_L & 0 \\ -2n_L & 0 & 0 \\ 0 & 0 & 0 \end{bmatrix} \tag{5.4}$$

where $n_L = \sqrt{\mu_\oplus / r_L^3}$, $\mu_\oplus = 398600 km^3/s^2$ is the Earth's planetary constant and r_L is the distance between the origins of the L and I coordinate frames. The control action is defined as $\mathbf{u}_{th} = [th_{+x} \quad th_{-x} \quad th_{+y} \quad th_{-y} \quad th_{+z} \quad th_{-z}]^T$ where each element can be only positive or null (a thruster can only push and not pull the spacecraft). It is worth to note that the control applies only in the case of the chaser and which is the only that is provided by on board working thrusters. Therefore the matrices $\mathbf{B}_1$ and $\mathbf{B}_2$ are defined as follows:

$$\mathbf{B}_1 = \begin{bmatrix} 0 & 0 & 0 & 0 & 0 & 0 \\ 0 & 0 & 0 & 0 & 0 & 0 \\ 0 & 0 & 0 & 0 & 0 & 0 \end{bmatrix}$$
$$\mathbf{B}_2 = \frac{1}{m_B} {}^L\mathbf{R}_i \, {}^i\mathbf{D}_{u_{th}} = \frac{1}{m_B} \begin{bmatrix} & {}^L\mathbf{R}_i & \end{bmatrix} \begin{bmatrix} 1 & -1 & 0 & 0 & 0 & 0 \\ 0 & 0 & 1 & -1 & 0 & 0 \\ 0 & 0 & 0 & 0 & 1 & -1 \end{bmatrix} \tag{5.5}$$

where m_B is the mass of the chaser, ${}^L\mathbf{R}_i$ is the cosine direction matrix between the body reference frame and the local horizontal local vertical coordinate frame. The matrix ${}^i\mathbf{D}_{u_{th}}$ distributes the thrusts along the directions towards the thrusters are oriented to with respect to the body coordinate frame.

The chaser model takes into account the mass consumption due to the thrusts. Specifically, the mass chances can be modeled as follows:

$$\dot{m}_B = -\frac{1}{g_0}\left(\frac{th_{+x}}{I_{sp+x}} + \frac{th_{-x}}{I_{sp-x}} + \frac{th_{+y}}{I_{sp+y}} + \frac{th_{-y}}{I_{sp-y}} + \frac{th_{+z}}{I_{sp+z}} + \frac{th_{-z}}{I_{sp-z}}\right) \tag{5.6}$$

where $g_0 = 9.81 m/s^2$ and $I_{sp+x} \ldots I_{sp-z}$ are the specific impulses of the thrusters used as actuators.

The actions provided by the thrusters are defined in the body coordinate frame of the spacecraft (i). Such matrix can be obtained as follows:

$$ {}^{L}\mathbf{R}_{B} = {}^{L}\mathbf{R}_{I}\ {}^{I}\mathbf{R}_{i} = {}^{L}\mathbf{R}_{I}\left({}^{i}\mathbf{R}_{I}\right)^{-1} \tag{5.7} $$

where ${}^{L}\mathbf{R}_{I}$ is the cosine direction matrix between which rotates the coordinates of a vector from the inertial to the local coordinate frame and, for the specific case under concern, is defined as follows:

$$ {}^{L}\mathbf{R}_{I} = \begin{bmatrix} c_{\Omega_L}c_{\nu_L} - c_{i_L}s_{\Omega_L}s_{\nu_L} & s_{\Omega_L}c_{\nu_L} + c_{i_L}c_{\Omega_L}s_{\nu_L} & s_{i_L}s_{\nu_L} \\ -c_{\Omega_L}s_{\nu_L} - c_{i_L}s_{\Omega_L}c_{\nu_L} & -s_{\Omega_L}s_{\nu_L} + c_{i_L}c_{\Omega_L}c_{\nu_L} & s_{i_L}c_{\nu_L} \\ s_{i_L}s_{\Omega_L} & -s_{i_L}c_{\Omega_L} & c_{i_L} \end{bmatrix} \tag{5.8} $$

5.2

where Ω_L is the right ascension of the ascending node of the reference orbit, i_L is the inclination of the reference orbit, $\nu_L = \omega_L + \int_{t_0}^{t} n_L dt$ is the anomaly of the local reference frame and ω_L is the argument of perigee of the reference orbit. In Equation (5.8) the letters s and c represent the sin and the cos functions of the subscripted angle.

The rotation matrix ${}^{i}\mathbf{R}_{I}$ in Equation (5.9) represents the attitude of the spacecraft with respect to the inertial reference frame and can be expressed in terms of quaternions $\mathrm{Q}_i = [\mathrm{q}_i \quad \mathbf{q}_i]^T$ as follows ((Wie, 1998), pp.318-320):

$$ {}^{i}\mathbf{R}_{I} = \left[\left(\mathrm{q}_i^2 - \mathbf{q}_i^T\mathbf{q}_i\right)\mathbf{E} + 2\mathbf{q}_i\mathbf{q}_i^T - 2\mathrm{q}_i\tilde{\mathbf{q}}_i\right] \tag{5.9} $$

where $\mathbf{E}$ is the identity matrix and $\tilde{\mathbf{q}}_i$ is the skew-symmetric matrix of the vector part of the quaternion. Indeed, the kinematic equations concerning the attitude are integrated by using quaternions. Specifically, the following equation is used:

$$ \dot{\mathrm{Q}}_i = \frac{1}{2}\boldsymbol{\Omega}(\boldsymbol{\omega}_i)\mathrm{Q}_i = \frac{1}{2}\begin{bmatrix} \tilde{\boldsymbol{\omega}}_i & \boldsymbol{\omega}_i \\ -\boldsymbol{\omega}_i^T & 0 \end{bmatrix}\begin{bmatrix} \mathbf{q}_i \\ \mathrm{q}_i \end{bmatrix} \tag{5.10} $$

where $\boldsymbol{\omega}$ is the angular velocity of the spacecraft.

Furthermore, the attitude dynamics of the satellite can be modeled as follows (Turner, 1997):

$$\dot{\boldsymbol{\omega}}_i = -\boldsymbol{I}_i^{-1}(\boldsymbol{\omega}_i \times \boldsymbol{I}_i\boldsymbol{\omega}_i) - \boldsymbol{I}_i^{-1}(\boldsymbol{\omega}_i \times \boldsymbol{h}_w) + \boldsymbol{I}_i^{-1}\boldsymbol{T}_w + \boldsymbol{I}_i^{-1}\boldsymbol{T}_e \tag{5.11}$$

where $\boldsymbol{I}_i$ is the moment of inertia matrix of the spacecraft, $\boldsymbol{h}_w$ is the angular momentum of the wheels, $\boldsymbol{T}_w$ is the torque provided by the reaction wheels' acceleration and $\boldsymbol{T}_e$ is the external disturbing torque applied to the satellite, such as the gravity gradient torque, modeled by means of (Turner, 1997):

$$\boldsymbol{T}_e = \frac{3\mu_{\oplus}}{r_i^3}\hat{\boldsymbol{r}} \times \boldsymbol{I}_i\hat{\boldsymbol{r}} \tag{5.12}$$

On the other side, the torque provided by the reaction wheel increases the angular momentum of the wheels and this effect should be taken into account by means of the following equation:

$$\dot{\boldsymbol{h}}_w = -\boldsymbol{T}_w \tag{5.13}$$

It is worth to note that the only platform which can be controlled in this problem is the chaser spacecraft. For the debris, both the thrusts and the reaction wheels torques do not apply and have to be set equal to zero in the simulations.

The torque T_w, provided by the reaction wheels of the chaser, is obtained by considering the following relation (Turner, 1997):

$$\boldsymbol{T}_w = \boldsymbol{D}_{sw}\boldsymbol{U}_w = \begin{bmatrix} cos\beta & 0 & -cos\beta & 0 \\ 0 & cos\beta & 0 & -cos\beta \\ sin\beta & sin\beta & sin\beta & sin\beta \end{bmatrix} \begin{bmatrix} u_{w1} \\ u_{w2} \\ u_{w3} \\ u_{w4} \end{bmatrix} \tag{5.14}$$

where u_{w1}, u_{w2}, u_{w3} and u_{w4} are the control torques applied to each reaction wheel. Optimized algorithms for torque distribution among the wheels are well known (as them showed in (Turner, 1997) or (Hablani, 1994)), and in this Thesis the torque needed will be distributed as follows:

$$\boldsymbol{U}_w = \boldsymbol{D}_{sw}^T\left(\boldsymbol{D}_{sw}\boldsymbol{D}_{sw}^T\right)^{-1}\boldsymbol{T}_w \tag{5.15}$$

Therefore, the complete set of differential equations for the chaser spacecraft is represented by Equations (5.3),(5.6),(5.10),(5.11), and (5.13), while for the debris Equations (5.6) and (5.13) are not used. However, we can consider a reduced set of equations of motion even in the case of the chaser dynamics, that will be used for demonstrating the stability of the adopted visual servoing strategy. In particular, we can consider only the equations representing the pure dynamics of the system (i.e. the lower partition of Equation (5.3) and Equation (5.11)), so that the equations of motion of the chaser satellite can be written as:

$$\boldsymbol{F}_{\mathrm{B}} + \boldsymbol{F}_{\mathrm{E}} = \boldsymbol{I}_i\ddot{\boldsymbol{x}}_{\mathrm{c}} + \boldsymbol{C}_{\mathrm{b}} \tag{5.16}$$

where $\ddot{\boldsymbol{x}}_{\mathrm{c}} = [\dot{\boldsymbol{v}}_{\mathrm{c}}^{\mathrm{T}} \quad \dot{\boldsymbol{\omega}}_{\mathrm{c}}^{\mathrm{T}}]^{\mathrm{T}} \in \Re^6$ denotes the absolute linear and angular accelerations of the spacecraft expressed in the inertial coordinate frame, $\boldsymbol{C}_{\mathrm{b}} \in \Re^6$ is a velocity/displacement-dependent, non-linear terms for the satellite, $\boldsymbol{F}_{\mathrm{B}} \in \Re^6$ is the force and moment exerted on the satellite, and $\boldsymbol{F}_{\mathrm{E}} \in \Re^6$ external / disturbing torque applied to the satellite (gravity gradient).

5.2.3 Spacecraft visual servoing

A set of k image points can be extracted from the target object $\boldsymbol{s} = [\boldsymbol{f}_1, \boldsymbol{f}_2, \ldots, \boldsymbol{f}_{\mathrm{k}}]^{\mathrm{T}} \in \Re^{2\mathrm{k}}$, and the coordinates of an image point in pixels are $\boldsymbol{f}_i = [f_{ix}, f_{iy}]^{\mathrm{T}} \in \Re^2$. Therefore, the image-based visual controller must perform the guidance of the spacecraft to track the desired trajectory in the image space, $\boldsymbol{s}^*(t)$.

The visual control system has to generate the required linear and angular accelerations on the spacecraft during the approach to an observed object. In this section, we consider that the proposed visual servoing approach allows the control of the spacecraft using k visual features, using an eye-in-hand configuration, where a camera is mounted on the spacecraft.

From the definition of interaction matrix (Equation (3.4)), the following relation can be obtained differentiating with respect to the time:

$$\ddot{\mathbf{s}}_r = \mathbf{L}_s\ddot{\boldsymbol{x}}_c + \dot{\mathbf{L}}_s\dot{\boldsymbol{x}}_c \tag{5.17}$$

where $\dot{\boldsymbol{x}}_c \in \Re^6$ is the linear and angular velocity of the camera in the inertial frame and $\mathbf{L}_s \in \Re^{2k\times 6}$ is the classical interaction matrix that relates image feature points velocity and camera velocity. As previously described, the spacecraft is considered performing a tracking of a desired image trajectory. Solving (5.17) for the desired spacecraft accelerations, $\ddot{\boldsymbol{x}}_c$, from the reference image accelerations, $\ddot{\mathbf{s}}_r$:

$$\ddot{\boldsymbol{x}}_c = \mathbf{L}_s^{+}\left(\ddot{\mathbf{s}}_r - \dot{\mathbf{L}}_s\dot{\boldsymbol{x}}_c\right) \tag{5.18}$$

where $\ddot{\mathbf{s}}_r$ will be obtained from the desired image trajectory (see Equation (3.14)). As stated, the variable $\ddot{\mathbf{s}}_r$ denotes the reference image accelerations of the proposed image-based controller. The desired spacecraft accelerations are obtained from (5.18), therefore, the control law is given by:

$$\boldsymbol{F}_B + \boldsymbol{F}_E = \boldsymbol{I}_i\mathbf{L}_s^{+}\left(\ddot{\mathbf{s}}_r - \dot{\mathbf{L}}_s\dot{\boldsymbol{x}}_c\right) + \boldsymbol{C}_b \tag{5.19}$$

Considering the previous assumptions, the closed-loop behavior is computed from Equation (5.19) as:

$$\boldsymbol{I}_i\ddot{\boldsymbol{x}}_c = \boldsymbol{I}_i\mathbf{L}_s^{+}\left(\ddot{\mathbf{s}}_r - \dot{\mathbf{L}}_s\dot{\boldsymbol{x}}_c\right) \tag{5.20}$$

This last equation can be simplified by pre-multiplying by $\mathbf{L}_s\,\boldsymbol{I}_i^{-1}$:

$$\mathbf{L}_s\,\ddot{\boldsymbol{x}}_c = \ddot{\mathbf{s}}_r - \dot{\mathbf{L}}_s\dot{\boldsymbol{x}}_c \tag{5.21}$$

Considering the value of the reference image acceleration given in Equation (5.14), and using the relation given in (5.17), Equation (5.21) is equal to:

$$\ddot{\boldsymbol{e}}_s = -\boldsymbol{K}_D\dot{\boldsymbol{e}}_s - \boldsymbol{K}_P\boldsymbol{e}_s \tag{5.22}$$

Therefore, an asymptotic tracking is achieved by the visual servo controller expressed in Equation (5.19) for the tracking of an image trajectory.

Next section describes the application of the framework proposed in Chapter 3 for the guidance of an FFSMR.

5.3 Kinematics and dynamics of the FFSMR

5.3.1 System architecture and assumptions

Figure 5.3 represents the main components of the FFSMR. With $\boldsymbol{q} \in \Re^n$ are represented the generalized joint coordinates of the robot manipulator (in our case, n=4). Frame {B} is attached to the base satellite. The inertial coordinate frame is called {I}. The end-effector frame, {E}, is attached to the manipulator end-effector, and frame {C} is the camera frame (attached to the camera). The camera extracts k visual feature points from the observed object. Therefore, the image-based direct visual controller must perform the FFSMR guidance to track the desired trajectory in the image space, $\boldsymbol{s}_d(t)$.

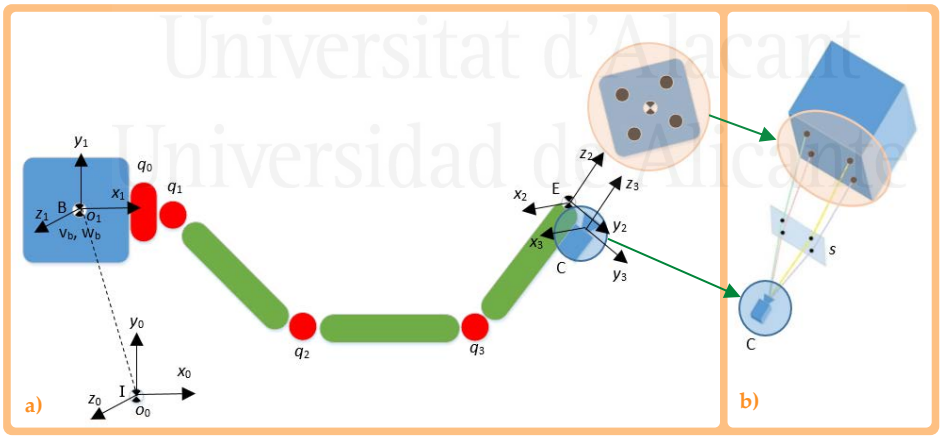

Figure 5.3. Schematic representation of a) the FFSMR, b) the vision system

As previously indicated, this Chapter defines a direct visual servoing system applied to a FFSMR for the tracking of image trajectories. Additionally, we assume that:

- The FFSMR will track an image trajectory defined with respect to a target object from which four visual features points can be extracted, i.e., k=4. The presented controller can be easily extended to employ other kinds of visual primitive to perform the guidance (only the interaction matrix employed throughout the Thesis depends on the considered primitive (Chaumette & Hutchinson, 2006)).
- An eye-in-hand camera system is employed; therefore, a constant relation between the camera coordinate frame and the robot end-effector frame is considered.
- The target undergoes constant linear and angular motion and its angular momentum is known in advance. An estimation can be obtained using previous works such as (Hillenbrand & Lampariello, 2005; Lichter & Dubowsky, 2004).
- There are no external forces acting on the entire system. No gas-jet thrusters are used on the base satellite.
- The capturing phase is not considered, therefore, there are no interaction forces between the FFSMR and the observed object.

5.3.2 FFSMR dynamics

The equations of motion of an n-degree-of-freedom FFSMR can be written as (Yoshida, 2003):

$$\begin{bmatrix}\mathbf{F}_b\\ \boldsymbol{\tau}\end{bmatrix} = \begin{bmatrix}\mathbf{M}_{bb} & \mathbf{M}_{bm}\\ \mathbf{M}_{bm}^T & \mathbf{M}_{mm}\end{bmatrix}\begin{bmatrix}\ddot{\boldsymbol{x}}_b\\ \ddot{\boldsymbol{q}}\end{bmatrix} + \begin{bmatrix}\boldsymbol{c}_b\\ \boldsymbol{c}_m\end{bmatrix} \tag{5.23}$$

where $\ddot{\boldsymbol{q}} \in \Re^n$ is the set of joint accelerations, $\ddot{\boldsymbol{x}}_b = [\dot{\boldsymbol{v}}_b^T \quad \dot{\boldsymbol{\omega}}_b^T]^T \in \Re^6$ denotes the absolute linear and angular accelerations of the base satellite expressed in the inertial coordinate frame, $\mathbf{M}_{bb} \in \Re^{6\times6}$ is the inertia matrix of the satellite, $\mathbf{M}_{bm} \in \Re^{6\times n}$ is the coupled inertia matrix of the satellite and the manipulator, $\mathbf{M}_{mm} \in \Re^{n\times n}$ is the inertia matrix of the manipulator; $\boldsymbol{c}_b$ and $\boldsymbol{c}_m \in \Re^6$ are a velocity/displacement-dependent, non-linear terms for the base and manipulator,

respectively, $\mathbf{F}_b \in \Re^6$ is the force and moment exerted on the base satellite, and $\boldsymbol{\tau} \in \Re^n$ is the applied joint torque on the robot manipulator. The FFSMR is freely floating in space; therefore, the external wrench on the satellite and the manipulator end-effector is assumed to be zero. The motion of the FFSMR is governed only by the applied torque on the manipulator joints, $\mathbf{F}_b = 0$. Hence, Equation (5.23) can be written in the following compact form:

$$\mathbf{M}^*_{mm}\ddot{\boldsymbol{q}} + \mathbf{H}^* = \boldsymbol{\tau} \tag{5.24}$$

where $\mathbf{M}^*_{mm} \in \Re^{n\times n}$ is the generalized inertia matrix and $\mathbf{H}^* \in \Re^n$ is the generalized Coriolis and centrifugal matrix, defined explicitly as:

$$\mathbf{M}^*_{mm} = \mathbf{M}_{mm} - \mathbf{M}^T_{bm}\mathbf{M}^{-1}_{bb}\mathbf{M}_{bm} \tag{5.25}$$

$$\mathbf{H}^* = \boldsymbol{c}_m - \mathbf{M}^T_{bm}\mathbf{M}^{-1}_{bb}\boldsymbol{c}_b \tag{5.26}$$

The linear and angular momenta of the system $(\boldsymbol{\ell}^T, \boldsymbol{\Psi}^T)^T \in \Re^6$ are equal to:

$$\begin{bmatrix}\boldsymbol{\ell}\\ \boldsymbol{\Psi}\end{bmatrix} = \mathbf{M}_{bb}\dot{\boldsymbol{x}}_b + \mathbf{M}_{bm}\dot{\boldsymbol{q}} \tag{5.27}$$

where $\dot{\boldsymbol{q}} \in \Re^n$ represents the robot manipulator joint speeds, and $\dot{\boldsymbol{x}}_b = [\boldsymbol{v}_b^T \quad \boldsymbol{\omega}_b^T]^T \in \Re^6$ denotes the absolute linear and angular velocities of the base satellite expressed in the inertial coordinate frame. The relationship between the joint speeds and the corresponding end-effector's absolute linear and angular velocities can be expressed through differential kinematics:

$$\dot{\boldsymbol{x}}_e = \mathbf{J}_m\dot{\boldsymbol{q}} + \mathbf{J}_b\dot{\boldsymbol{x}}_b \tag{5.28}$$

where $\dot{\boldsymbol{x}}_e \in \Re^6$ is the linear and angular velocity of the manipulator end-effector in the inertial frame, $\mathbf{J}_m \in \Re^{6\times n}$ is the manipulator Jacobian matrix, and $\mathbf{J}_b \in \Re^{6\times 6}$ is the Jacobian matrix for the base satellite. Combining (5.28) and (5.27) yields an

equation directly relating the joint speeds and end-effector motion of the robot manipulator (Yoshida, 2003):

$$\dot{\boldsymbol{x}}_e = \mathbf{J}_g \dot{\boldsymbol{q}} + \dot{\boldsymbol{x}}_{ge} \tag{5.29}$$

$$\mathbf{J}_g = \mathbf{J}_m - \mathbf{J}_b \mathbf{M}_{bb}^{-1} \mathbf{M}_{bm} \tag{5.30}$$

$$\dot{\boldsymbol{x}}_{ge} = \mathbf{J}_b \mathbf{M}_{bb}^{-1} \begin{bmatrix} \boldsymbol{\ell} \\ \boldsymbol{\psi} \end{bmatrix} \tag{5.31}$$

where $\mathbf{J}_g$ is the Generalized Jacobian Matrix, and $\dot{\boldsymbol{x}}_{ge}$, is an offset velocity due to the non-zero momentum. The visual servoing control techniques allow for the control of manipulator joints using k visual features, typically using an eye-in-hand configuration, where a camera is held by the end-effector. The relationship between velocities in the camera image space, $\dot{s}_r$, and end-effector motion, $\dot{\boldsymbol{x}}_e$, is expressed by:

$$\dot{\boldsymbol{s}}_r = \mathbf{L}_s \dot{\boldsymbol{x}}_e \tag{5.32}$$

where $\mathbf{L}_s \in \Re^{2k \times 6}$ is the interaction matrix, and $\boldsymbol{s}_r = [f_{1x}, f_{1y}, f_{2x}, f_{2y}, \dots, f_{kx}, f_{ky}]^T \in \Re^{2k}$ is a vector of the k extracted image feature points. From (5.32) and (5.29), the image space velocity $\dot{\boldsymbol{s}}_r$ can be related to joint speeds $\dot{\boldsymbol{q}}$ by means of the following relationship:

$$\dot{\boldsymbol{s}}_r = \mathbf{L}_s \mathbf{J}_g \dot{\boldsymbol{q}} + \mathbf{L}_s \dot{\boldsymbol{x}}_{ge} = \mathbf{L}_J \dot{\boldsymbol{q}} + \dot{\boldsymbol{s}}_{ge} \tag{5.33}$$

where $\mathbf{L}_J$ is the Jacobian matrix mapping from joint space to image space. This matrix relates differential changes in joint configuration of the robot to differential changes in the observed image feature parameters. Additionally, $\dot{\boldsymbol{s}}_{ge}$ is considered as the projection in the image space of the velocity $\dot{\boldsymbol{x}}_{ge}$. The image acceleration or second derivative of $\boldsymbol{s}_r$ is obtained by differentiating Equation (5.33) with respect to time:

$$\ddot{\mathbf{s}}_r = \mathbf{L}_J \ddot{\boldsymbol{q}} + \dot{\mathbf{L}}_J \dot{\boldsymbol{q}} + \ddot{\mathbf{s}}_{ge} \tag{5.34}$$

The variable $\ddot{\mathbf{s}}_r$ denotes the reference image accelerations that will be employed by the optimal controller proposed in Section 3.

5.4 Optimal control approach

5.4.1 Direct control of the FFSMR

As described in Chapter 3, a system with m constrains that represent the task for the FFSMR to be executed is considered. The time derivate of these constraints is represented by the following equation:

$$\mathbf{A}(\boldsymbol{q}, \dot{\boldsymbol{q}}, t)\ddot{\boldsymbol{q}} = \boldsymbol{b}(\boldsymbol{q}, \dot{\boldsymbol{q}}, t) \tag{5.35}$$

where $\mathbf{A}(\boldsymbol{q}, \dot{\boldsymbol{q}}, t) \in \Re^{m \times n}$ and $\boldsymbol{b}(\boldsymbol{q}, \dot{\boldsymbol{q}}, t) \in \Re^{m \times 1}$. In order to reduce the energy and fuel required for performing the visual servoing task, the proposed optimal controller is designed to minimize the control torque for the FFSMR, taking into account the following function cost:

$$\boldsymbol{\Omega}(t) = \boldsymbol{\tau}^T \mathbf{W}(t) \boldsymbol{\tau} \tag{5.36}$$

where $\mathbf{W}(t)$ is a time-dependent weight matrix. By defining $\boldsymbol{z} = \mathbf{W}^{1/2}\boldsymbol{\tau} = \mathbf{W}^{1/2}(\mathbf{M}^*_{mm}\ddot{\boldsymbol{q}} + \mathbf{H}^*)$, it is possible to derive the joint accelerations $\ddot{\boldsymbol{q}} = (\mathbf{M}^*_{mm})^{-1}\left(\mathbf{W}^{-1/2}\boldsymbol{z} - \mathbf{H}^*\right)$. Taking into account the constraints defined in Equation (5.35):

$$\mathbf{A}(\mathbf{M}^*_{mm})^{-1}\mathbf{W}^{-1/2}\boldsymbol{z} = \boldsymbol{b} + \mathbf{A}(\mathbf{M}^*_{mm})^{-1}\mathbf{H}^* \tag{5.37}$$

The vector $\boldsymbol{z}$ which minimizes $\boldsymbol{\Omega}(t) = \boldsymbol{z}^T\boldsymbol{z}$ while fulfilling Equation (5.37) is given by $\boldsymbol{z} = \left(\mathbf{A}(\mathbf{M}^*_{mm})^{-1}\mathbf{W}^{-1/2}\right)^+(\boldsymbol{b} + \mathbf{A}(\mathbf{M}^*_{mm})^{-1}\mathbf{H}^*)$, and as the joint torque is given by $\boldsymbol{\tau} = \mathbf{W}^{-1/2}\boldsymbol{z}$. To conclude, the control law that minimizes $\boldsymbol{\Omega}(t)$ of the

FFSMR based on the dynamics model expressed in Equation (5.24), while performing the task described in Equation (5.35), is given by:

$$\boldsymbol{\tau} = \mathbf{W}^{-1/2}\left(\mathbf{A}(\mathbf{M}^{*}_{mm})^{-1}\mathbf{W}^{-1/2}\right)^{+} \cdot (\boldsymbol{b} + \mathbf{A}(\mathbf{M}^{*}_{mm})^{-1}\mathbf{H}^{*}) \tag{5.38}$$

As it can be seen in Equation (5.38), the matrix $\mathbf{W}$ is an important factor in the control law determining how the control efforts are distributed over the joints.

Equation (5.34), which relates the visual servoing task with the joint space, can be expressed into the form of Equation (5.35) as:

$$\mathbf{L}_J\ddot{\boldsymbol{q}} = \ddot{\boldsymbol{s}}_r - \dot{\mathbf{L}}_J\dot{\boldsymbol{q}} - \ddot{\boldsymbol{s}}_{ge} \tag{5.39}$$

This way, the task constrains are defined by the following relationships:

$$\begin{aligned} \mathbf{A} &= \mathbf{L}_J \\ \boldsymbol{b} &= \ddot{\boldsymbol{s}}_r - \dot{\mathbf{L}}_J\dot{\boldsymbol{q}} - \ddot{\boldsymbol{s}}_{ge} \end{aligned} \tag{5.40}$$

Therefore, with the given definition of $\mathbf{A}$ and $\boldsymbol{b}$, the optimal control will minimize the control torque for the joints while performing a tracking in the image space. The final control law can be obtained replacing these variables into the function that minimizes the motor signals described by Equation (5.38):

$$\boldsymbol{\tau} = \mathbf{W}^{-1/2}\left(\mathbf{L}_J(\mathbf{M}^{*}_{mm})^{-1}\mathbf{W}^{-1/2}\right)^{+} \cdot \left(\ddot{\boldsymbol{s}}_r - \dot{\mathbf{L}}_J\dot{\boldsymbol{q}} - \ddot{\boldsymbol{s}}_{ge} + \mathbf{L}_J(\mathbf{M}^{*}_{mm})^{-1}\mathbf{H}^{*}\right) \tag{5.41}$$

As it can be seen, the visual controller represented by (5.41) implicitly depends on the weighting matrix $\mathbf{W}$, and different values of this matrix can simplify the product $\mathbf{L}_J(\mathbf{M}^{*}_{mm})^{-1}\mathbf{W}^{-1/2}$, and consequently the control law. A proper choice practically would be $\mathbf{W} = (\mathbf{M}^{*}_{mm})^{-1}$.

The optimal control approach described in this section will be employed to track an image trajectory, taking into account the FFSMR dynamics. As discussed,

the tracked trajectory is defined and expressed as a set of constraints following Equation (5.35) (see Equation (5.40)).

Substituting Equation (5.14) into the dynamic visual servo controller, Equation (5.41), the control law is set by the following relationship:

$$\begin{aligned}\boldsymbol{\tau} = \ & \mathbf{W}^{-1/2}\left(\mathbf{L}_J(\mathbf{M}^*_{mm})^{-1}\mathbf{W}^{-1/2}\right)^+ \\ \cdot & \left(\ddot{\boldsymbol{s}}_d + \mathbf{K}_D\dot{\boldsymbol{e}}_s + \mathbf{K}_P\boldsymbol{e}_s - \dot{\mathbf{L}}_J\dot{\boldsymbol{q}} - \ddot{\boldsymbol{s}}_{ge} + \mathbf{L}_J(\mathbf{M}^*_{mm})^{-1}\mathbf{H}^*\right)\end{aligned} \tag{5.42}$$

In order to demonstrate the asymptotic tracking of the control law (5.42), some operations must be done. First, the closed-loop behavior is computed using Equation (5.24) as:

$$\begin{aligned}\mathbf{M}^*_{mm}\ddot{\boldsymbol{q}} + \mathbf{H}^* = \ & \mathbf{W}^{-1/2}\left(\mathbf{L}_J(\mathbf{M}^*_{mm})^{-1}\mathbf{W}^{-1/2}\right)^+\left(\ddot{\boldsymbol{s}}_d + \mathbf{K}_D\dot{\boldsymbol{e}}_s + \mathbf{K}_P\boldsymbol{e}_s\right. \\ & \left. - \dot{\mathbf{L}}_J\dot{\boldsymbol{q}} - \ddot{\boldsymbol{s}}_{ge} + \mathbf{L}_J(\mathbf{M}^*_{mm})^{-1}\mathbf{H}^*\right)\end{aligned} \tag{5.43}$$

Equation (5.43) can be simplified by pre-multiplying its left and right sides by $\left(\mathbf{L}_J(\mathbf{M}^*_{mm})^{-1}\mathbf{W}^{-1/2}\right)\mathbf{W}^{1/2}$:

$$\mathbf{L}_J\ddot{\boldsymbol{q}} = \ddot{\boldsymbol{s}}_d + \mathbf{K}_D\dot{\boldsymbol{e}}_s + \mathbf{K}_P\boldsymbol{e}_s - \dot{\mathbf{L}}_J\dot{\boldsymbol{q}} - \ddot{\boldsymbol{s}}_{ge} \tag{5.44}$$

Using the relationship expressed in (5.39), it can be concluded that:

$$\ddot{\boldsymbol{e}}_s = -\mathbf{K}_D\dot{\boldsymbol{e}}_s - \mathbf{K}_P\boldsymbol{e}_s \tag{5.45}$$

Therefore, when $\mathbf{L}_J$ is full-rank an asymptotic tracking is achieved by the visual servo controller expressed in Equation (5.41) for the tracking of an image trajectory.

5.4.2 Optimal control of the FFSMR with chaos compensation

As previously stated, chaos compensation was integrated in classical direct visual controllers to obtain a periodic joint trajectory when the robot's end-effector also tracks a periodic image trajectory. This last aspect guarantees a smoother joint

behavior, and increases the safety by obtaining predictable trajectories. In this section, the chaos compensation is also integrated in the FFSMR controller in order to decrease the torque required to perform the guidance, consequently reducing the base attitude disturbance. To do this, a DFC method will be integrated in the controller. The DFC method generates a perturbation proportional to the difference between the current joint velocities and the joint velocities delayed by one period. The control action or perturbation of the DFC controller vanishes when the stabilization of the target orbit is achieved. The resulting control law with chaos compensation is:

$$\boldsymbol{\tau} = \mathbf{M}^*_{mm}\lambda\big(\boldsymbol{q}(t-\varepsilon)-\boldsymbol{q}(t)\big) + \mathbf{W}^{-1/2}\big(\mathbf{L}_J(\mathbf{M}^*_{mm})^{-1}\mathbf{W}^{-1/2}\big)^{+} \cdot \big(\ddot{\boldsymbol{s}}_d + \mathbf{K}_D\dot{\boldsymbol{e}}_s + \mathbf{K}_P\boldsymbol{e}_s - \dot{\mathbf{L}}_J\dot{\boldsymbol{q}} - \ddot{\boldsymbol{s}}_{ge} + \mathbf{L}_J(\mathbf{M}^*_{mm})^{-1}\mathbf{H}^*\big) \tag{5.46}$$

where λ is a constant gain to be determined, and ε is the feedback time-delay. The adjustment of the constants λ and ε is performed by using the algorithm described in Chapter 3. Using these values, the system under control automatically settles on the target periodic motion, and the stability of this motion is maintained with only small perturbations.

5.5 Simulations

5.5.1 Simulation of the spacecraft visual servoing

A simulation campaign was performed in order to analyze the performance of the proposed direct visual servo controller. A debris removal mission was simulated in order to check the viability of such technique to a realistic scenario, including real properties and characteristics of the chaser and of the debris objects. Specifically, the target of the selected mission is to perform rendezvous maneuver to the Envisat satellite. Indeed, Envisat represents the most immediate target that is being considered for the active debris removal by the European Space Agency, because of its mass, size and threat of collisions with other objects in orbit. In order to safely remove such a massive object from its orbit, a capturing system process

followed by a controlled reentry maneuver is necessary. Therefore it appears evident that an image based rendezvous maneuver represents a mandatory task for any mission for the removal of such debris. In the following subsections a description of the parameters of the objects, of the actuators and of the sensors used in the simulations are provided, as well as the simulation results. Three different cases are considered, that can be used during different phases of the debris removal mission: a lateral translation maneuver, a straight approach maneuver, an approach maneuver with attitude changes.

The mass properties and the orbital parameters that characterize the target object under concern are reported in Table 5.1. The chaser is a small size satellite whose mass, sizes and inertia properties are reported in Table 5.2. The main characteristics of the onboard actuators and camera systems are reported in Table 5.3. The initial positions, velocities, quaternions and angular velocities for the chaser and target spacecraft are reported in Table 5.4.

Table 5.1. Mass, Size and Orbital Parameters of the Envisat Satellite

Mass (kg)	Moments of Inertia (kg m2)	Center of Mass (m)
$m_T = 7827.8$	$\mathbf{I}_T = \begin{bmatrix} 17023.2 & 397.1 & -2171.4 \\ 397.1 & 124825.7 & 344.2 \\ -2171.4 & 344.2 & 129112.2 \end{bmatrix}$	$CoM_T = \begin{bmatrix} -3.9 \\ 0.0 \\ 0.0 \end{bmatrix}$
Length (m)	**Width (m)**	**Height (m)**
$l_T = 26.0$	$w_T = 10.0$	$h_T = 26.0$
Semi-Major	**Eccentricity**	**RAAN (deg)**
$a_T = 7144.9$	$a_T = 7144.9$	$a_T = 7144.9$
Inclination (deg)	**Argument of Perigee (deg)**	**Initial True**
$i_T = 98.4$	$\omega_T = 83.3$	$\nu_{0T} = 0.0$

Table 5.2. Mass, Size and Orbital Parameters of the Chaser Satellite

Mass (kg)	Moments of Inertia (kg m2)	Center of Mass (m)
$m_B = 200.0$	$\mathbf{I}_B = \begin{bmatrix} 230.4 & 0.0 & 0.0 \\ 0.0 & 259.2 & 0.0 \\ 0.0 & 0.0 & 288.0 \end{bmatrix}$	$CoM_B = \begin{bmatrix} 0.0 \\ 0.0 \\ 0.0 \end{bmatrix}$
Length (m)	**Width (m)**	**Height (m)**
$l_B = 2.6$	$w_B = 1.2$	$h_B = 1.2$

Table 5.3. Onboard Reaction Wheels Properties (from ("https://www.cubesatshop.com/," n.d.))

Max Torque (Nm)	Saturation Angular Momentum (Nms)	Wheel speed (rpm)
0.055	$4.0 - 12.0$	6000

Table 5.4. Initial Conditions for the Target and Chaser Spacecraft

Target Position (m)	Target Velocity (m/s)	Target Quaternions	Target Angular Velocity (rad/s)
$d_T = \begin{bmatrix} 0.0 \\ 0.0 \\ 0.0 \end{bmatrix}$	$v_T = \begin{bmatrix} 0.0 \\ 0.0 \\ 0.0 \end{bmatrix}$	$Q_T = \begin{bmatrix} -0.2241 \\ -0.4830 \\ 0.1294 \\ 0.08365 \end{bmatrix}$	$\omega_T = \begin{bmatrix} 0.0 \\ 0.0 \\ 0.0 \end{bmatrix}$
Chaser Position (m)	**Chaser Velocity (m/s)**	**Chaser Quaternions**	**Chaser Angular Velocity (rad/s)**
$d_B = \begin{bmatrix} 0.0 \\ -20.0 \\ 0.0 \end{bmatrix}$	$v_B = \begin{bmatrix} 0.0 \\ 0.0 \\ 0.0 \end{bmatrix}$	$Q_B = \begin{bmatrix} 0.1830 \\ -0.500 \\ -0.500 \\ 0.6830 \end{bmatrix}$	$\omega_B = \begin{bmatrix} 0.0 \\ 0.0 \\ 0.0 \end{bmatrix}$

5.5.2 Results

5.5.2.1. Maneuver 1. Lateral translation

During this first maneuver, the chaser spacecraft has to perform translational maneuver in order to move perpendicularly to its line of sight with respect to the target spacecraft. Therefore, the desired trajectory of the visual features in the image plane is a linear trajectory between the initial image points $\boldsymbol{s} = [\boldsymbol{f}_1 = (495, 469), \boldsymbol{f}_2 = (495, 550), \boldsymbol{f}_3 = (575, 550), \boldsymbol{f}_4 = (575, 469)]^T$ pix. and the final desired ones $\boldsymbol{s}^* = [\boldsymbol{f}_1^* = (588, 562), \boldsymbol{f}_2^* = (588, 642), \boldsymbol{f}_3^* = (668, 642), \boldsymbol{f}_4^* = (668, 562)]^T$ pix. The proportional and derivative gain matrices are $\mathbf{K}_P = 0.001\mathbf{I}$ and $\mathbf{K}_D = 0.01\mathbf{I}$ respectively. Figure 5.4 represents the obtained behavior of the system during the maneuver. Figure 5.4.a and Figure 5.4.b represent the initial and final poses of the chaser spacecraft with respect the target one, respectively. In these figures, the selected visual features are highlighted by means of red points. It is worth noting that the maneuver produces a lateral translation of the chaser with respect to the target while the relative distance between the two spacecraft is maintained constant. In Figure 5.5 the trajectories of the visual features during the maneuver are represented in the image plane. As it can be observed in this last figure, the tracking of the desired trajectory has been correctly performed by the chaser spacecraft.

Figure 5.6 represents the thrust profiles applied during the maneuver. Specifically, it is worth noting that the main thrusts are applied in the x-y plane. During the first 2 minutes the –x and –y thrusters are activated, producing a movement of the visual features from the bottom-left side to the upper-right side of the image plane. Then, a thrust directed in the opposite direction is applied in order to stop the motion of the chaser in the desired position. The thrusters aligned to the z direction are only used for small corrections in order to maintain a

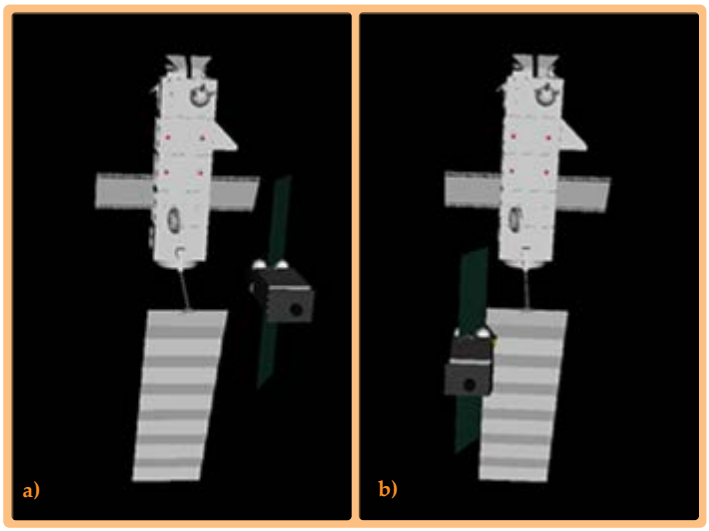

Figure 5.4. Obtained trajectory during the maneuver 1. a) Initial pose of the chasing and target spacecraft. b) Final pose of the chasing and target spacecraft.

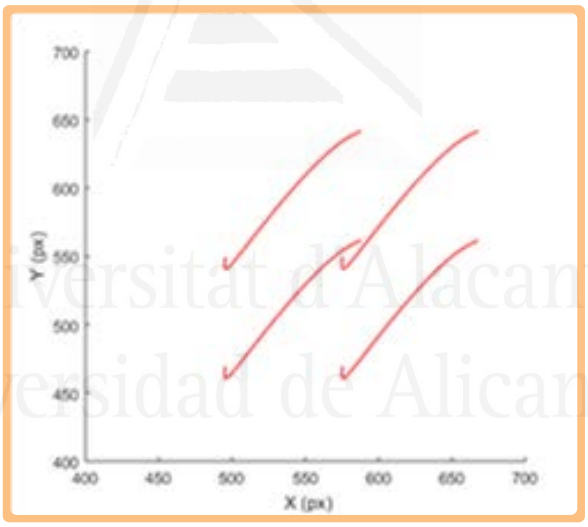

Figure 5.5. Obtained image trajectory during the maneuver 1.

constant distance between the spacecraft, specifically only the –z thruster is activated to counteract the effects of the gravity gradient between the two bodies while the +z thruster is not used. The resulting behavior of position and velocity of the chaser spacecraft is represented in Figure 5.7. The angular velocity and the torques on the wheels are negligible during this maneuver.

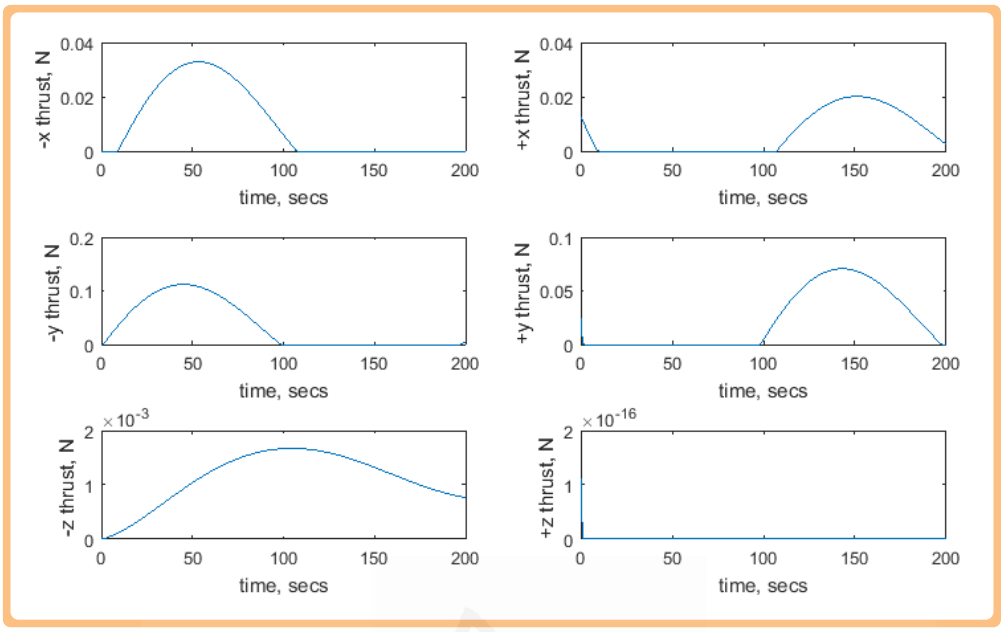

Figure 5.6. Thrust forces during the maneuver 1.

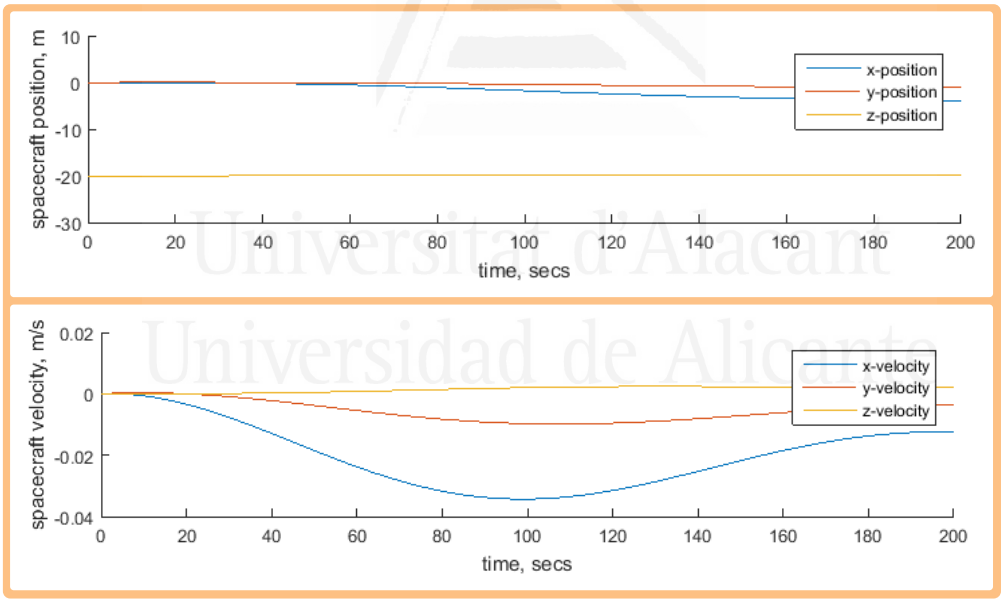

Figure 5.7. Position and velocity of the chaser spacecraft during the maneuver 1.

5.5.2.2. Maneuver 2. Straight Rendezvous

During the maneuver 2, the chaser spacecraft has to decrease its distance with respect to the debris. For this reason, the desired trajectories of the visual features

change linearly from an initial condition $\boldsymbol{s} = [\boldsymbol{f}_1 = (495, 469), \boldsymbol{f}_2 = (495, 550), \boldsymbol{f}_3 = (575, 550), \boldsymbol{f}_4 = (575, 469)]^T$ px. to the desired ones $\boldsymbol{s}^* = [\boldsymbol{f}_1^* = (455, 389), \boldsymbol{f}_2^* = (455, 630), \boldsymbol{f}_3^* = (696, 630), \boldsymbol{f}_4^* = (696, 389)]^T$ px. in the image plane. The proportional and derivative gain matrices are $\mathbf{K}_P = 0.001\mathbf{I}$ and $\mathbf{K}_D = 0.05\mathbf{I}$ respectively. Figure 5.8 represents the initial and final poses obtained for the target and chaser spacecraft, and Figure 5.9 shows the corresponding image trajectories of the selected visual features during the maneuver. It is worth noting that, the reduction of the distance between the two bodies is obtained by increasing the size of the shape of the debris seen in the image plane of the camera.

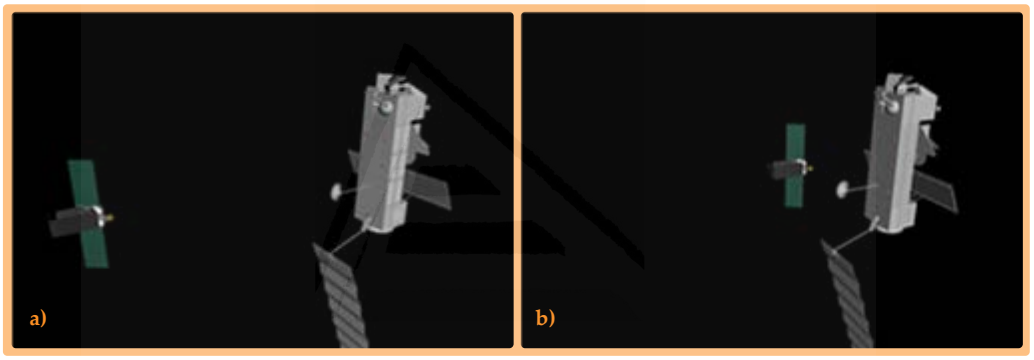

Figure 5.8. Obtained trajectory during the maneuver 2. a) Initial pose of the chasing and target spacecraft. b) Final pose of the chasing and target spacecraft.

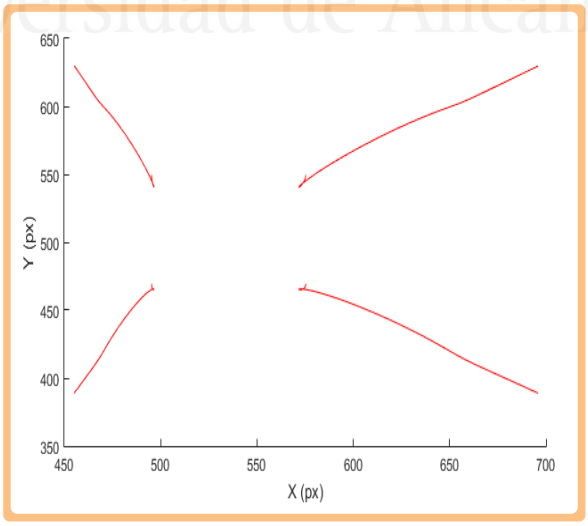

Figure 5.9. Image trajectory during the maneuver 2.

The visual servoing controller is then able to compute the thrust profiles necessary to perform the maneuver, as that shown in Figure 5.10. In this case the main thrust is provided by the +z and –z thrusters that have to provide forces up to 1N. The specific maneuver is obtained by bang-bang like thrust profile, where the chaser first compensates the action of the gravity gradient, which tend to let the two bodies separate each other and then it is accelerated towards the debris until it reaches the desired relative position with respect to the debris, when a thrust along the –z axis reduces the relative velocity between the bodies.

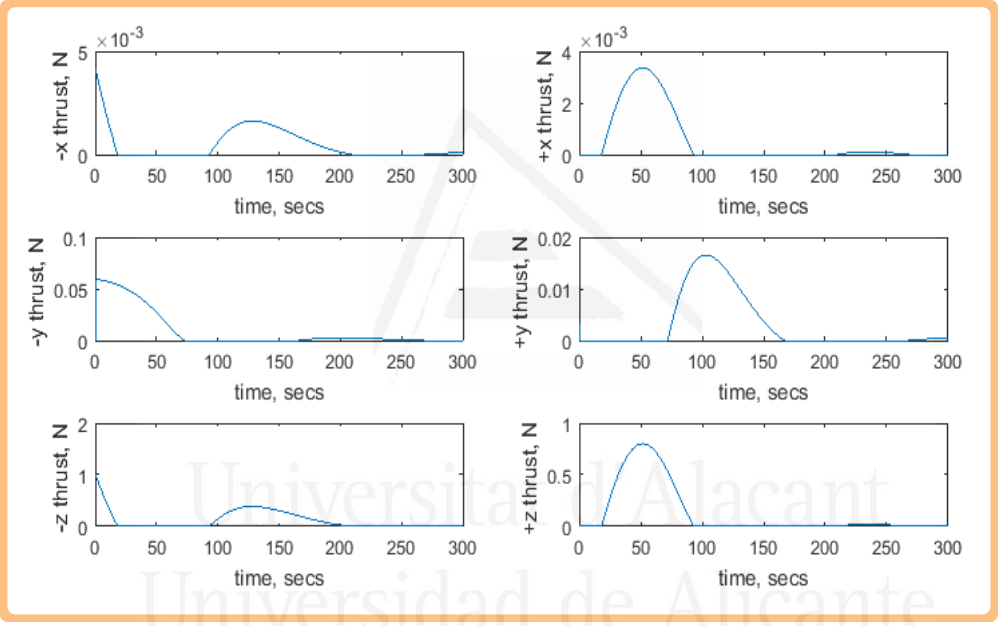

Figure 5.10. Thrust forces during the maneuver 2.

The corresponding position and velocity of the chaser spacecraft are represented in Figure 5.11, respectively. It is worth noting that the distance between the two bodies decreases from 20 m down to 7m. In this maneuver, the angular velocity and the torques produced by the reaction wheels are negligible and they are not represented.

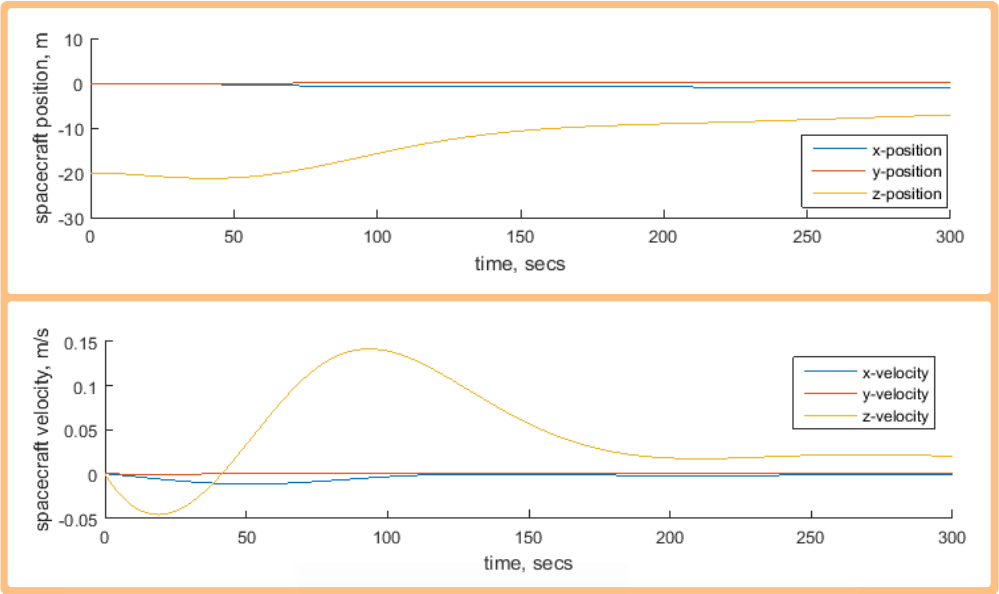

Figure 5.11. Position and velocity of the chaser spacecraft during the maneuver 2.

5.5.2.3. Maneuver 3. Rendezvous with change in the relative attitude

In the previous two maneuvers, the relative attitude between the spacecraft has been maintained constant. However, by using the proposed visual servoing technique, it is possible also to command changes on the relative attitude of the chaser with respect to the debris. The following maneuver has been set in order to verify the viability of such control strategy on performing also attitude corrections. In the following, a specific maneuver, where the chaser spacecraft has to perform a close rendezvous by changing also its attitude, is proposed. The desired trajectory of the visual features of the debris with respect to the camera field of view have to change linearly from $\boldsymbol{s} = [\boldsymbol{f}_1 = (495, 469), \boldsymbol{f}_2 = (495, 550), \boldsymbol{f}_3 = (575, 550), \boldsymbol{f}_4 = (575, 469)]^T$ to the desired ones $\boldsymbol{s}^* = [\boldsymbol{f}_1^* = (424, 400), \boldsymbol{f}_2^* = (424, 620), \boldsymbol{f}_3^* = (648, 630), \boldsymbol{f}_4^* = (648, 390)]^T$. The proportional and derivative gain matrices are $\mathbf{K}_P = 0.001\mathbf{I}$ and $\mathbf{K}_D = 0.08\mathbf{I}$ respectively.

Figure 5.12 shows two different perspectives of the initial and final positions of the spacecraft in this maneuver, where both the changes in range and attitude are evident. The tracking of the desired trajectories of the visual features in the image plane is successfully accomplished as is shown in Figure 5.13. Figure 5.14

represents the thrusts forces applied during this maneuver and the position and velocity of the chaser spacecraft. The changes in the attitude configuration of the chaser spacecraft are represented in Figure 5.15, where the quaternion and the angular velocity of the chaser spacecraft show that the sensibly modifies the relative orientation of the chaser with respect to the debris. Finally, the computed torques and the angular momentum of the wheels are shown in Figure 5.16. It is worth noting that, within this maneuver, the chaser attitude changes of 14deg in 10 min with a peak torque provided by the reaction wheels of 0.05 Nm, that is largely inside the operational working ranges typical for this kind of actuators.

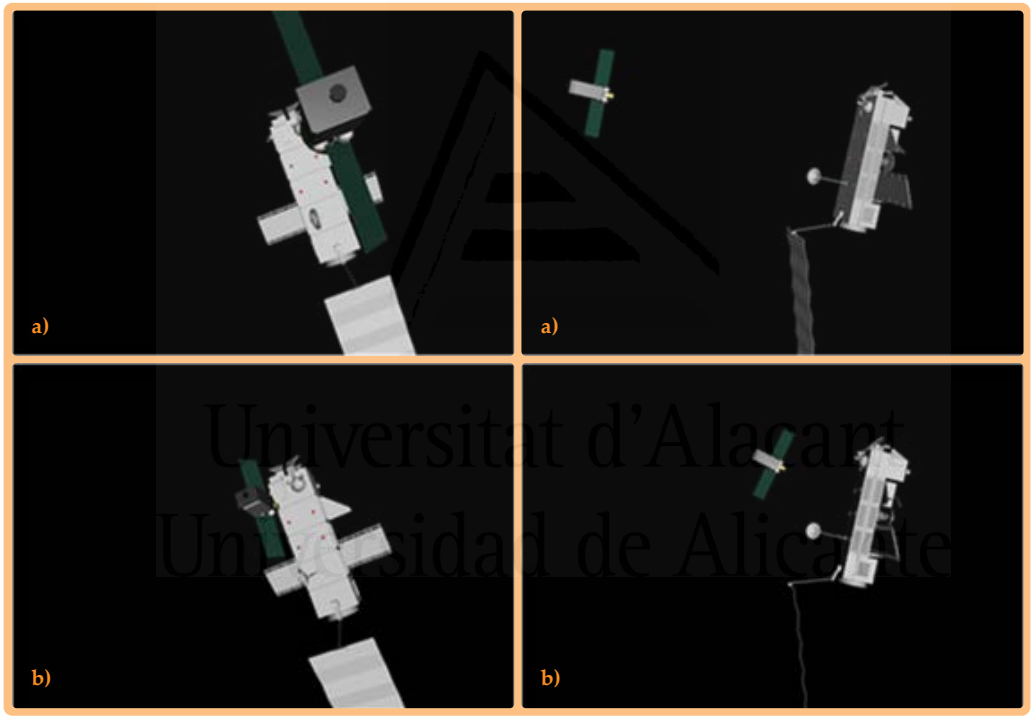

Figure 5.12. Obtained trajectory during the maneuver 3. a) Initial position of the chasing and target spacecraft. b) Final position of the chasing and target spacecraft

Even the angular momentum stored by the reaction wheels is largely inside the common working ranges of common attitude actuators.

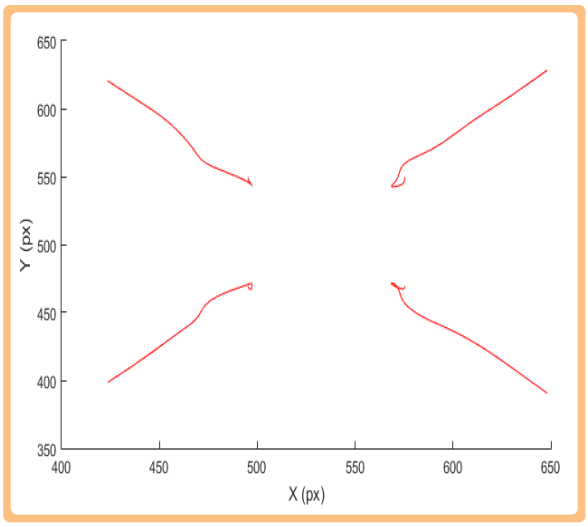

Figure 5.13. Image trajectory during the maneuver 3.

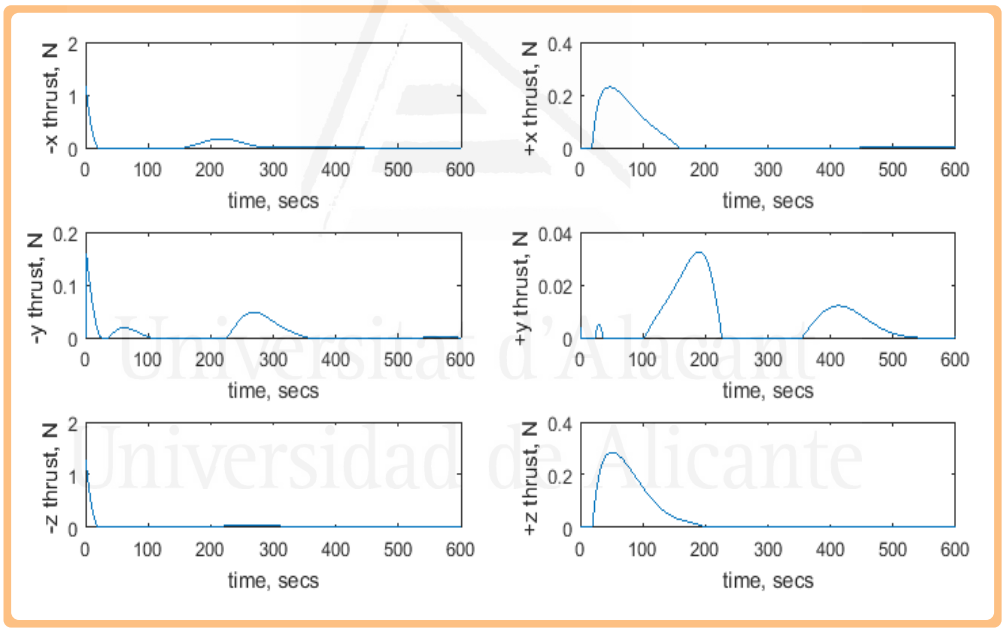

Figure 5.14. Thrust forces during the maneuver 3.

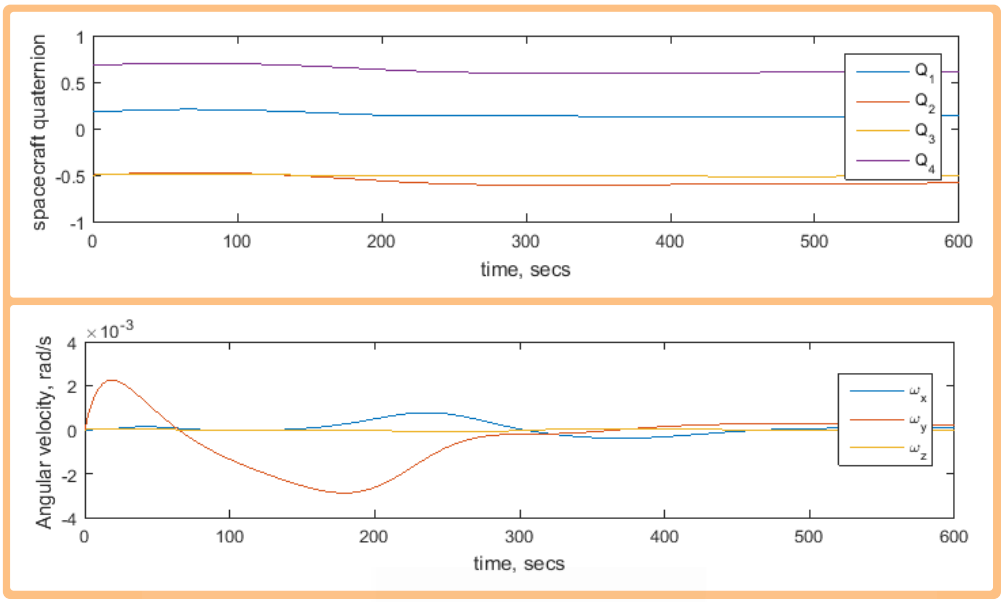

Figure 5.15. Quaternion and angular velocity of the chaser spacecraft during the maneuver 3.

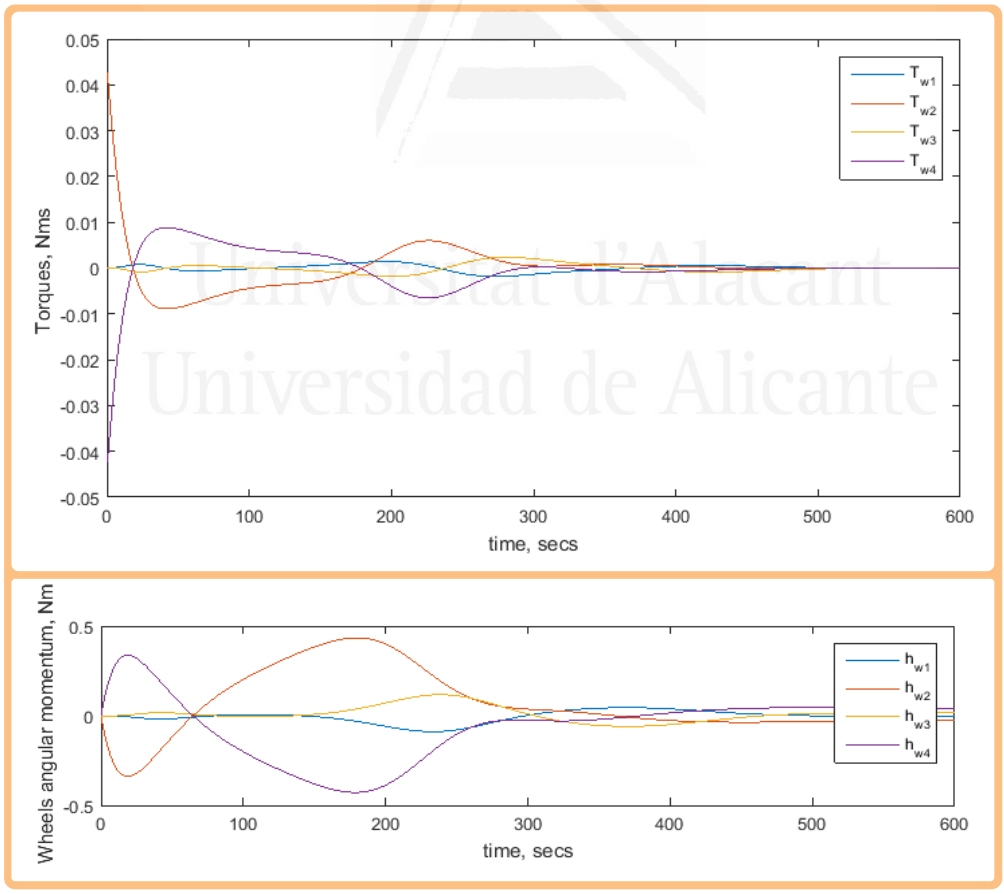

Figure 5.16. Angular momentum and torques on reaction wheels during the maneuver 3.

5.5.3 Simulation of the FFSMR visual servoing

This section describes simulations for the tracking of image trajectories considering the proposed direct visual servo controller for the FFSMR (Equation (5.46)). Table 5.5 lists the dynamic parameters employed in the simulation of the FFSMR. The robot manipulator's dynamic parameters are extracted from the three-degrees-of-freedom robot described in (Pomares, Perea, Jara, García, & Torres, 2013). The robot is guided by an eye-in-hand camera system. The parameters of a Gigabit Ethernet TM6740GEV camera is considered, which acquires 200 images every second with a resolution of 1280x1024 pixels. The eye-in-hand camera extracts four visual features from the workspace. The proportional and derivative matrices employed in the experiments are $\mathbf{K}_P = 0.1\mathbf{I}$ and $\mathbf{K}_D = 0.5\mathbf{I}$. Additionally, the weighting matrix is selected as $\mathbf{W} = (\mathbf{M}^*_{mm})^{-1}$. These values are considered in all the simulations presented in this section.

Table 5.5. Dynamic parameters of the FFSMR

Base	Mass (kg)	Side (m)	Inertia (kg·m²)		
			I_x	I_y	I_z
	60	0.3	22.5	22.5	22.5
Arm	**Mass (kg)**	**Side (m)**	**Inertia (kg·m2)**		
			I_x	I_y	I_z
Link 1	5	0.012	0.01	0.031	0.031
Link 2	1.75	0.124	0.002301	0.000981	0.002601
Link 3	0.8	0.152	0.001673	0.001656	0.001902
Link 4	0.5	0.099	0.0004802	0.0002	0.000546

5.5.4 Results

5.5.4.1 Tracking of an image trajectory

This experiment evaluates the tracking of the desired image trajectory indicated in Figure 5.17. This figure represents the trajectory to be tracked for the four visual features extracted by the eye-in-hand camera system. Using the proposed controller, the end-effector trajectory in the 3D space represented in Figure 5.18.a is obtained. In the beginning of the experiment, the robot's end-effector is not located at the desired trajectory. Therefore, the robot converges during the first iterations towards it (approaching phase) and continues the tracking of the desired trajectory. Figure 5.18.b represents in blue the image error module during the experiment, $\boldsymbol{e} = \boldsymbol{s} - \boldsymbol{s}_d$. From Figure 5.18, the error remains low and decreases during the tracking. In order to highlight the necessity of integrating the system dynamics in the controller, a classical indirect visual servoing system (Pomares et al., 2013) is also employed for the tracking of the trajectory presented in Figure 5.17. Figure 5.18.b represents, in red, the image error module obtained during the tracking by using the classical controller. As shown, the error is greater because the classical controller does not take into account the system dynamics and the base attitude disturbance during the tracking. The torque generated by the proposed direct controller during the tracking is shown in Figure 5.19.a. Figure 5.19.b represents the FFSMR during the tracking of the trajectory.

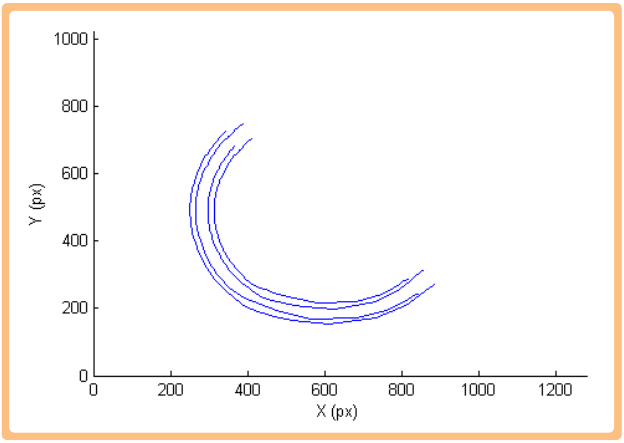

Figure 5.17. Desired image trajectory. Experiment 1.

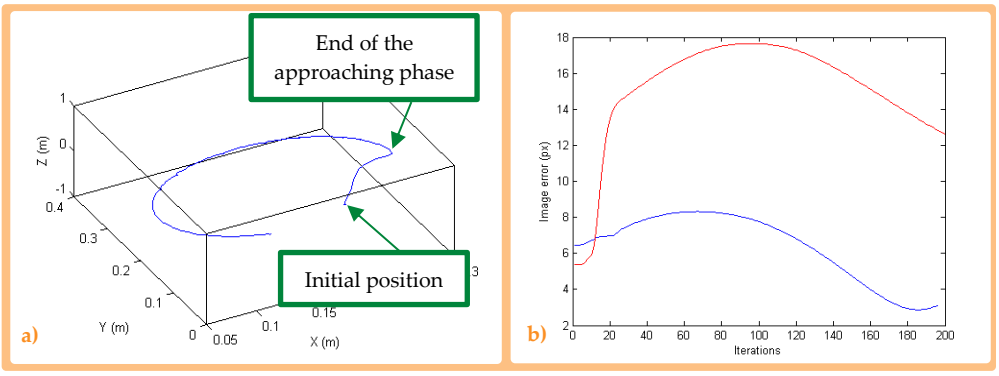

Figure 5.18. Experiment 1. a) 3D trajectory of the manipulator end-effector during the tracking. b) Image error using the proposed approach (blue) and using classical image-based control (red).

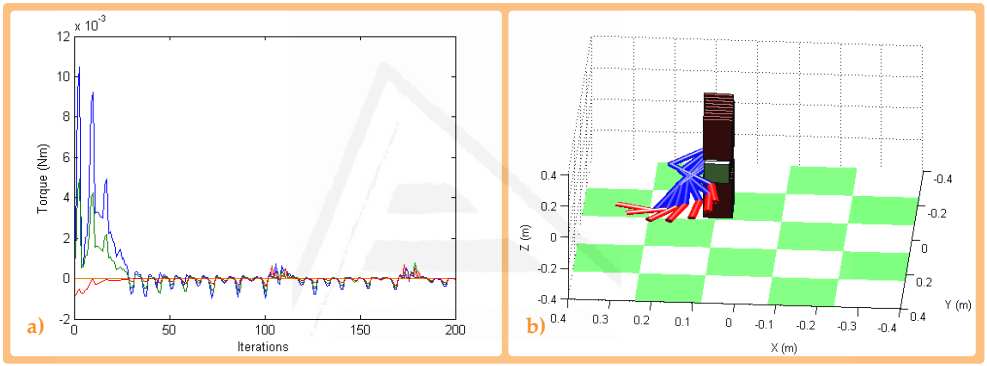

Figure 5.19. Experiment 1. a) Torque during the tracking. b) 3D trajectory of the FFSMR.

5.5.4.2 Tracking of a circular trajectory

This experiment evaluates the tracking of a planar and circular trajectory for the robot end-effector defined by the following equation:

$$\begin{bmatrix} x_{xd} \\ y_{yd} \end{bmatrix} = \begin{bmatrix} 0.2 + 0.01\cos(0.02\pi) \\ 0.02 + 0.01\sin(0.02\pi) \end{bmatrix} \tag{5.47}$$

The tracking of this circular trajectory allows for evaluating the controller with and without the integration of the chaos controller. Figure 5.20.a represents the circular 3D trajectory described by the robot end-effector during the experiment. To observe the tracking precision more clearly, Figure 5.20.b and Figure 5.20.c

show the image error module and the 3D Cartesian error module during the experiment, respectively.

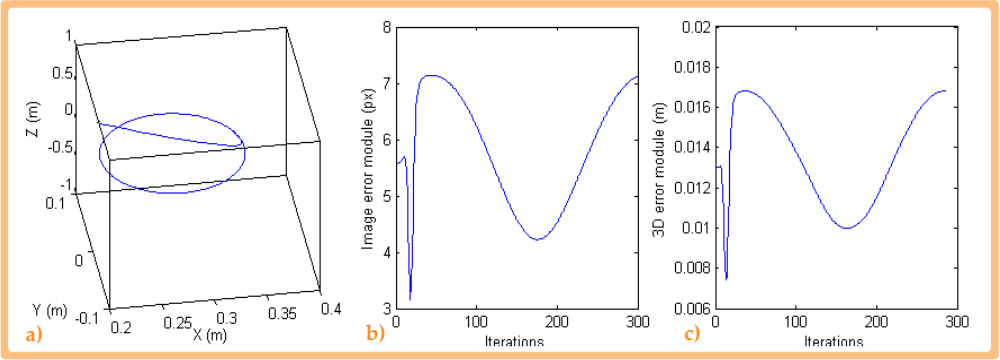

Figure 5.20. Experiment 2. a) 3D trajectory of the robot manipulator end-effector. b) Image error module. c) 3D error module.

5.5

As it can be seen, these errors remain low during the experiment, and a correct tracking is carried out. These results are obtained by integrating the chaos controller. Similar results are obtained without the integration of the chaos controller. In order to observe the difference between these two strategies more clearly, the joint behavior is shown in Figure 5.21 and Figure 5.22.

Figure 5.21 represents the joint torque generated by the controller with and without chaos control. As it can be seen, lower torque values are obtained by integrating the chaos compensation in the controller. This effect can also be observed in the 3D trajectory described by the FFSMR during the tracking (Figure 5.22). Figure 5.22.a represents a sampling of the robot joint configurations employed during the tracking. As this figure shows, the joint configuration varies and a chaotic and unpredictable behavior is obtained in the joint space. A smoother and repetitive joint behavior is obtained in Figure 5.22.b with the use of the chaos compensation.

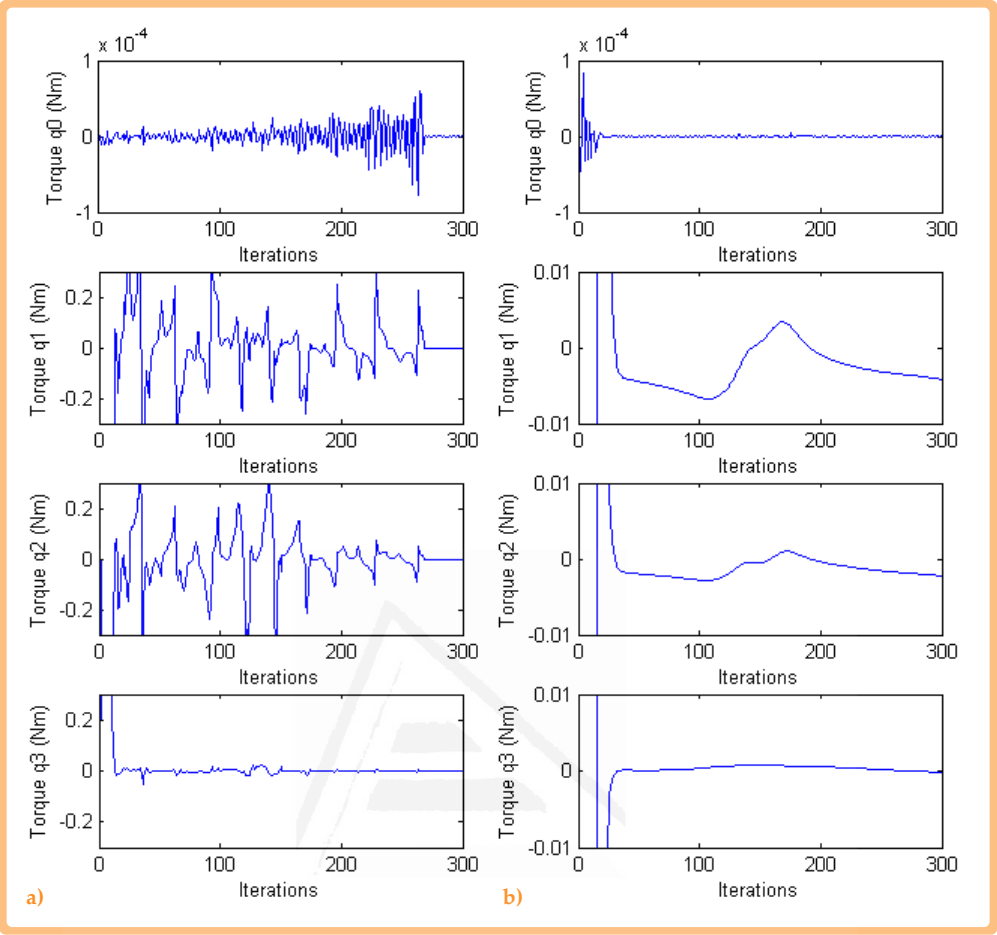

Figure 5.21. Experiment 2. Torque during the tracking.
a) Without chaos control. b) With chaos control.

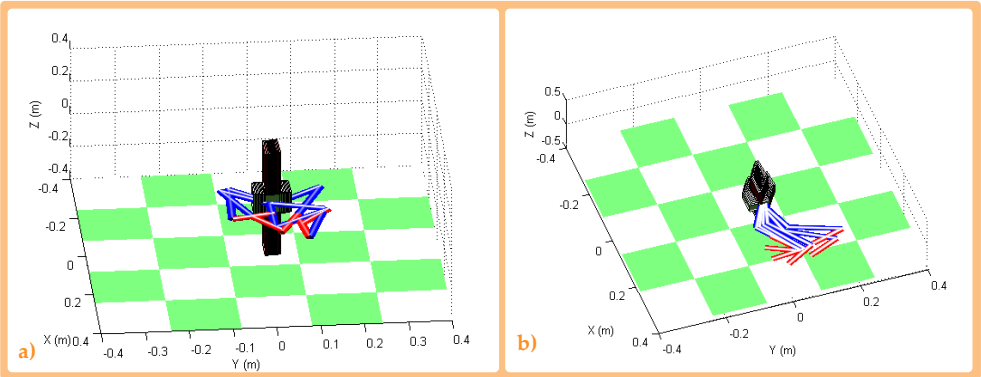

Figure 5.22. Experiment 2. 3D trajectory of the FFSMR.
a) Without chaos control. b) With chaos control.

5.5.4.3 Tracking of a repetitive and irregular trajectory

This experiment consists of the tracking of the repetitive and irregular trajectory in the image space that is shown in Figure 5.23. From the control law stated in Equation (5.42), when $\mathbf{W} = (\mathbf{M}_{mm}^{*})^{-2}$, the following expression can be obtained for the controller, which represents a direct visual controller using inversion of the dynamic model:

$$\boldsymbol{\tau} = \mathbf{M}_{mm}^{*}\left(\mathbf{L}_J\right)^{+} \cdot \left(\ddot{\mathbf{s}}_d + \mathbf{K}_D\dot{\boldsymbol{e}}_s + \mathbf{K}_P\boldsymbol{e}_s - \dot{\mathbf{L}}_J\dot{\boldsymbol{q}} - \ddot{\mathbf{s}}_{ge} + \mathbf{L}_J(\mathbf{M}_{mm}^{*})^{-1}\mathbf{H}^{*}\right) \tag{5.48}$$

Figure 5.24 evaluates the tracking of the desired image trajectory represented in Figure 5.23 using both controllers, the one stated in Equation (5.48) and the one used in the previous experiments (Equation (5.42) and $\mathbf{W} = (\mathbf{M}_{mm}^{*})^{-1}$). In both cases, the chaos compensation method is integrated. As Figure 5.24 shows, lower image and 3D errors are obtained using the proposed controller, $\mathbf{W} = (\mathbf{M}_{mm}^{*})^{-1}$, with respect to the one obtained when $\mathbf{W} = (\mathbf{M}_{mm}^{*})^{-2}$. Both controllers achieve the correct tracking, but a better image and 3D behavior is obtained with the proposed controller.

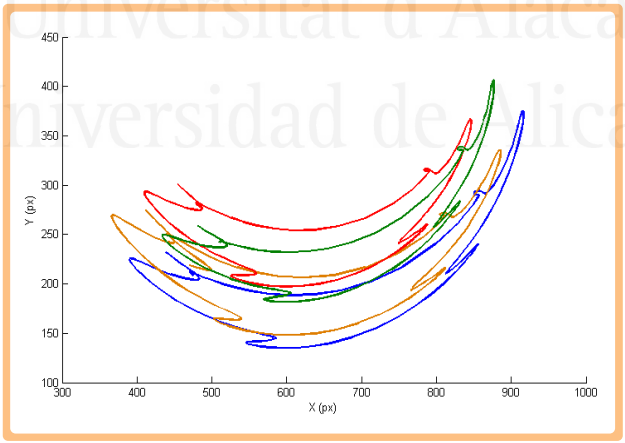

Figure 5.23. Experiment 3. Desired image trajectory.

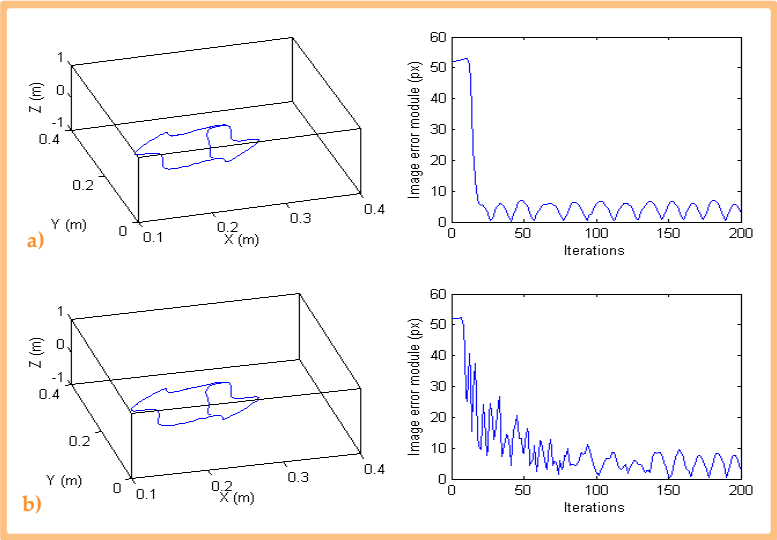

Figure 5.24. Experiment 3. 3D trajectory during the tracking of the desired image trajectory and image error module. a) $W=(M^{*}_{mm})^{-1}$. b). $W=(M^{*}_{mm})^{-2}$.

5.6 Conclusions

This Chapter deals with strategies for guiding two different space systems, a direct image-based controller for guiding spacecrafts to perform maneuvers like approaching and rendezvous, and a free-floating satellite mounted robot, where the base is not actuated and thus reacting to the movement of the arm.

In contrast with the previous indirect image-based visual servoing approaches proposed up to now to perform the guidance of space robots, this chapter presents a new direct image-based visual servoing system that takes into account the system kinematics and dynamics. An adaptive and flexible tool is obtained, allowing for a concurrent control of both attitude and orbit of the chasing spacecraft during all phases of a non-cooperative rendezvous. The viability of the controller has been tested in a variety of test case maneuvers, including approaches with and without attitude and the lateral changes, as well as far and close rendezvous, and in all such cases the maneuvers have been accomplished, despite the perturbing actions due to the gravity gradient forces and torque. Also, the proposed controller allows the spacecraft not only to achieve a given location from

an initial one, but also to perform the tracking of a desired image trajectory. Three different experiments with three different scenarios were developed for each of the two types of robots, and the proposed controller worked properly for all of them. For the actuated satellite robot, the first experiment illustrates a lateral translation when performing the visual servoing task. The second one shows the behavior when dealing with a straight rendezvous. The third experiment represents a rendezvous with change in the relative attitude.

For the FFSMR, the first experiment illustrates the tracking of a non-repetitive image trajectory. The second one illustrates the tracking of a circular trajectory performed by the end-effector, where the chaotic movement of the joints was avoided by using the chaos compensator. Even though movements in 3D Cartesian space of the end-effector were very similar, when studying the torque applied to the joints, and thus, the evolution of the positions of the links, a great improvement was achieved, avoiding high fuel consumption due to sudden, fast, chaotic movements of the links. In the third experiment, the tracking of an abrupt trajectory was examined with the optimal control strategy with chaos compensation but with different values of the weight matrix.

6 Conclusions

This last Chapter describes the most prominent conclusions about the research carried out and presented throughout this Thesis. The main results accomplished with this research are published in several scientific media. This Chapter briefly describes the most important contributions for each one of them. Lastly, different ideas for improving the proposed control schemes are presented. Described next are possible future works that allow for extending direct visual servoing systems to manipulating tasks where two manipulator robots with two robotic hands with tactile sensory systems are implied.

6.1 Conclusions

The research presented throughout the Thesis was focused on the development of an image-based visual servoing framework based in optimal control and its extension for singularity avoidance as well as its application to a variety of different robot manipulators like free-floating manipulators. The framework as well as the developed extensions constitute the main contributions that are synthetized in the next paragraphs together with the main conclusions obtained throughout the Thesis.

An optimal framework to define new dynamic visual controllers to carry out the guidance of robot manipulators is proposed. The proposed general method employs optimal control to define the desired behaviour in the joint space based on an indicated cost function which determines how the control effort is distributed over the joints. The proposed approach allows to derive well known

direct image-based visual servoing systems such as these based on inverse dynamics. However, new direct visual controllers can be obtained with different precision and dynamical properties. Once the framework is defined, it is extended for allowing it to perform the control of redundant manipulator robots. This extension allows for integrating different additional weight functions with the objective of avoiding robot singularities, image singularities, or even avoiding the chaotic joint behavior typical of such systems. First of all, the concept of manipulability for solving robot redundancy is employed. After controlling the redundancy, different controllers can be generated depending on the weight function W. As indicated throughout the Thesis, the best behavior occurs when $\mathbf{W} = \mathbf{M}^{-1}$. In contrast, when $\mathbf{W} = \mathbf{I}$ the controller is much simpler and easy to implement. The use of $\mathbf{W} = \mathbf{D}$ allows for indicating what joints support the strongest torques. The framework also allows for adjusting diverse trajectory tracking behaviors for adapting them to every situation.

Another important contribution of the Thesis is the concept of dynamic perceptibility. This parameter allows for detecting situations where the robot is close to an image or joint singularity. Dynamic perceptibility is represented as ellipses and indicate the robot's movement capacity for each feature point in the image when performing the visual servoing. The concept of dynamic perceptibility allows for integrating the robot's dynamic information in a way that ellipses show which directions of the movement are more suitable according to kinematic and dynamic restrictions, as well as the features configuration in the image for every moment. The shape of the ellipses permits to have information of, for example, the closeness of the robot to a singular configuration in the joint space as well as in the image space. This information is employed by the designed controllers with the purpose of not only detecting but also avoiding singularities during the tracking.

A chaotic joint behavior happens when an unpredictable and non-periodic movement in the joint space is computed by the controller when performing a

repetitive trajectory tracking in the image. A chaos controller is also integrated in the proposed framework so that it is capable of determining the best references for the robot's end-effector and joints to behave in a correct manner (a periodic and repetitive behavior at joint level). Results show that dynamic controllers not only correctly achieve the tracking of periodic trajectories in the Cartesian space but that are also capable of avoiding the chaotic behavior present in such systems.

The last phase of the Thesis was performed in collaboration with the group of "Onboard space systems" from Luleå University of Technology in Sweden. This research consisted in the extension of the framework for the direct visual servoing of spacecraft and free-floating space manipulators. The dynamics of such systems is integrated into the framework for later evaluate their behavior for trajectory tracking. It is worth noting that for obtaining a correct simulation of the behavior of these robots is necessary to take into account not only its dynamics but also the orbital dynamics in which the task is being performed.

6.2 Publications

This Section cites all different publications produced by the research presented in this Thesis: four journal papers included in JCR (first quartile), two contributions to international conferences, and five national conferences.

6.2.1 Journal papers included in JCR

- "**FPGA-based architecture for direct visual control robotic systems**". Alabdo, A.; Pérez, J.; García, G.J.; Pomares, J.; Torres, F.; Mechatronics, 39, pp. 2014-216, 2016.

This paper describes the framework for rapidly developing FPGA-embedded dynamic visual servoing systems described more in detail in this Thesis in Chapters 3, 4, and 5. The parallel design of algorithms increments the precision of these type of controllers, while minimizing the response time. Direct image-

based visual servoing systems derived from this framework allow for the tracking of trajectories by obtaining different dynamic behaviors depending on the weighting matrix. A new method for compensating the chaotic behavior of these systems is also added to the derived controllers from the weighting matrix. For checking the viability of this proposed FPGA-based framework, and for demonstrating the effects of the metrics, some of the derived controllers are evaluated during the image tracking. This development does not only imply the obtaining of the first FPGA based direct visual servoing controller, but also permits to convert the control system into a real-time control system taking advantage of reconfigurable characteristics of FPGAs. This strategy allows to have a more stable control cycle and with a known timing. The paper shows the main contributions and final experimental results of the public project for emerging groups of the University of Alicante "Control visual embebido de robots manipuladores utilizando hardware reconfigurable FPGA" (GRE12-17), to which the author of this Thesis was a collaborator.

This paper was published in "Mechatronics" journal, in November, 2016. In 2016, the journal had an impact factor in 'Journal Citation Reports' from 'ISI Web of Knowledge' of 2.496, and was located at position 29 out of a total of 130 in the 'Engineering, Mechanical' category, being above the first quartile. The impact index of 'Mechatronics' journal remained stable since 2013, year in which it had an impact factor of 1.823, always rising since 2010 (0.994).

- "**FPGA-based visual control system using dynamic perceptibility**". Perez, J.; Alabdo, A.; Pomares, J; Garcia, G.J.; Torres, F.; Robotics and Computer Integrated Manufacturing, 41 pp. 13-22, 2016.

This publication presents the concept of dynamic perceptibility, that provide information about the system's capability for performing the tracking of an object with a direct visual servoing strategy. This concept is integrated in the proposed controllers and implemented in the architecture for avoiding robot joint singularities as well as image singularities. For this, an optimal direct visual

servoing framework for robots that integrated dynamic perceptibility is detailed. This paper presents the formulation for the optimal framework and details the implementation of one of the derived controllers in the FPGA-based architecture. The paper describes how the framework implemented in a FPGA for developing direct visual servoing systems can be reconfigured in an easy way for testing new controllers or simply for adding new functionalities to the already implemented controllers. Following the same idea as the journal paper published in 'Mechatronics', this paper integrates a new term that allows to take the dynamic perceptibility into account. The little time required for implementing this new controller represents a big step forward in the design and testing of new direct visual servoing systems embedded in a real-time system thanks to FPGAs.

This paper was published in the journal 'Robotics and Computer-Integrated Manufacturing' in October, 2016. In 2016, the journal had an impact factor in 'Journal Citation Reports' of 'ISI Web of Knowledge' of 2.846, and was in position 11 out of a total of 44 in the category of 'Engineering, Manufacturing', belonging to the first quartile. Impact index of journal 'Robotics and Computer-Integrated Manufacturing' increased since 2011, when it had an impact factor of 1.173.

- **"Direct image-based visual servoing of free-floating space manipulators".** Perez, J., Emami, M. R., & Pomares, J. Aerospace Science and Technology, 55, 1–9. 2016

This paper presents an image-based controller to perform the guidance of a free-floating robot manipulator. The manipulator has an eye-in-hand camera system, and is attached to a base satellite. The base is completely free and floating in space with no attitude control, and thus, freely reacting to the movements of the robot manipulator attached to it. The proposed image-based approach uses the system's kinematics and dynamics model, not only to achieve a desired location with respect to an observed object in space, but also to follow a desired trajectory with respect to the object. To do this, the paper presents an optimal control approach to guiding the free-floating satellite-mounted robot, using

visual information and considering the optimization of the motor commands with respect to a specified metric along with chaos compensation. The proposed controller is applied to the visual control of a four-degree-of-freedom robot manipulator in different scenarios.

This paper was recently published in the journal 'Aerospace Science and Technology' in August 2016. In 2016, the journal had an impact factor in 'Journal Citation Reports' of 'ISI Web of Knowledge' of 2.057, and was in position 3 out of a total of 31 in the category of 'Engineering, Aerospace', belonging to the first quartile. Impact index of journal 'Aerospace Science and Technology' increased since 2012, when it had an impact factor of 0.873.

- "**Direct visual servoing framework based on optimal control for redundant joint structures**". Pomares, J.; Jara, C.A.; Pérez, J.; Torres, F.; International Journal of Precision Engineering and Manufacturing 16(2), pp. 267-274. 2015.

This paper describes the optimal control-based framework for the generation of direct visual servoing control laws. Not only the framework is described but also the controller precision is studied. This precision varies depending on the weighting matrix **W** for different types of trajectories.

This paper was published in the journal 'International Journal of Precision Engineering and Manufacturing' in April, 2015. In 2015, the journal had an impact factor in 'Journal Citation Reports' of 'ISI Web of Knowledge' of 1.075, belonging to the first quartile in the category of 'Engineering, Manufacturing' and 'Engineering, Mechanical'. Since its publication, the paper has been cited a total of two times according to 'ISI Web of Knowledge' and 'Google Scholar'.

6.2.2 International conferences

- "**Image-based control of satellite-mounted robot manipulators”**, Perez, J., Pomares, J., & Emami, M. R. In 2016 7th International Conference on Mechanical and Aerospace Engineering (ICMAE) (pp. 346–351). London, UK. 2016

This paper describes an optimal strategy for a controller for trajectory tracking for robotic arms mounted on a free-floating system while controlling its chaotic behavior. This allows to optimize the movement of the system and thus the fuel/energy consumption.

- **“FPGA-based visual control of robot manipulators using dynamic perceptibility**", J. Pérez, A. Alabdo, G. J. García, J. Pomares, F. Torres., In Proceedings of the International Conference on ReConFigurable Computing and FPGAs (ReConFig). Cancun, Mexico. 2015.

This paper describes the proposed controller based on inverse dynamics for trajectory tracking as well as its implementation in the FPGA. Also, the concept of dynamic perceptibility is described as a criterion for detecting not only robot singularities but also image singularities. Both contributions are integrated with the objective of allowing trajectory tracking in the image while avoiding possible singularities that might appear during said tracking.

- **“FPGA-based Framework for Dynamic Visual Servoing of Robot Manipulators”,** A. Alabdo, J. Pérez, J. Pomares, G.J. Garcia, F. Torres., in Proceedings of the IEEE International Conference on Emerging Technologies and Factory Automation. Luxemburgo. 2015.

This paper describes the optimal control-based framework for the guidance of robot manipulators. Said framework allows for generating direct image-based visual servoing laws with different behaviors depending on the weighting matrix employed. The implementation of the proposed FPGA-based architecture is

detailed after describing the framework and all different components of the controller.

6.2.3 National conferences

- "**Control visual dinámico basado en FPGA de un robot manipulador de 6 grados de libertad**", A. Alabdo, J. Pérez, J. Pomares, G. J. García, F. Torres., En Proceedings de las XXXVII Jornadas de Automática, Madrid, Spain, September 2016.

This paper describes the fundamentals of different hardware components that make up the architecture employed for the implementation of different proposed controllers throughout the Thesis. The main elements of a direct image-based visual servoing system and how they can be implemented in an FPGA are described. The controller is applied for the guidance of a 6 degree of freedom Mitsubishi PA-10 robot.

- **"ViSeC-Matlab: Una herramienta para el aprendizaje de sistemas de control visual sobre Matlab",** J. Pérez, A. Alabdo, G. J. García, J. Pomares, F. Torres., En Proceedings de las XXXVI Jornadas de Automática, Bilbao, Spain, September 2015.

This paper presents the tool ViSeC developed for evaluating all different controllers defined throughout the Thesis by simulation. This tool is based on Matlab's robotics toolbox and allows for easily introduce new visual controllers and evaluate their behavior, generating graphs such as image error, control actions, robot's trajectory, image trajectory, among others. It also allows for easily define the visual servoing task, making simpler the debugging process before the implementation.

6.3 Future works

Research performed throughout the Thesis opened new lines of research that can be addressed with the experience and developments carried out. Within this

future lines of research, it is worth mentioning the design of visual servoing systems for the guidance of robotic hands. Today, research to drove this Thesis focus are being applied to the project "Sistema robótico multisensorial con manipulación dual para tareas asistenciales humano-robot" (DPI2015-68087-R) funded by Ministerio de Economía y Competitividad y FEDER funds. The project's fundamental objective is the development of a multisensorial robotic torso and its application to human-robot assistance tasks. This robotic torso is made up by two manipulators, each one of them with a robotic hand. Developments presented throughout the Thesis allow for the guidance of both robotics manipulators by using artificial vision. However, implemented controllers cannot perform the guidance of robotic hands as described throughout the Thesis. These controllers can be extended to include kinematic and dynamic characteristics of these robotic hands. This way, the experience obtained with this Thesis opens a new promising line of research like the guidance of manipulating systems based on robotic hands by employing direct visual servoing.

Another line of research is the extension of direct visual servoing systems for the case of bimanual control. For this case, the controller not only has to compute the guidance of the corresponding manipulators and robotic hands, but also coordinate the movement among them. Also, when performing manipulation tasks, not only visual information from the environment needs to be considered, but also tactile information that states the interaction force applied to the manipulated object by each finger. The extension of the proposed controllers for considering tactile information is another line of research derived from the Thesis in a close future.

For this Thesis, a computer vision system composed of a single camera situated at the manipulator's end-effector is considered. The use of an artificial vision system for human-robot collaboration tasks with only one camera usually implies that the information provided by such camera is simply not enough due

to occlusions. The use of different artificial vision systems is proposed as future works. This way, developed controllers must use multiple vision systems located in the workspace for using the most adequate one depending on which one is more convenient for the positioning of the robot. It becomes necessary to determine which criterion is best for determining what vision system is the most adequate, at the same time that the controller coordinates the control actions from the information obtained by the vision system for computing the final movement.

Lastly, and within the collaboration carried off with "Onboard space systems" research group that belongs to Luleå University of Technology in Sweden, the visual controllers are being extended for guiding robotic manipulators mounted on actuated satellites. This way, the visual controller must be capable of guiding the robotic manipulator as well as actuating the thrusters for performing satellite-robot rendezvous.

6 Conclusiones

Este último capítulo describe las conclusiones más destacadas sobre la investigación realizada y presentada a lo largo de esta Tesis. Los principales resultados obtenidos con esta investigación se publican en varios medios científicos. Este capítulo describe brevemente las contribuciones más importantes para cada una de ellas. Por último, se presentan diferentes ideas para mejorar los esquemas de control propuestos. Finalmente, se describen los posibles trabajos futuros que permitirían que los sistemas de control visual directos se apliquen en tareas de manipulación con dos robots equipados con dos manos robóticas con sensores táctiles.

6.1 Conclusiones

La investigación presentada a lo largo de la Tesis se ha enfocado en el desarrollo de un *framework* de control visual basado en imagen basado en un control óptimo y su extensión para la evitación de singularidades, así como su aplicación a una variedad de robots manipuladores diferentes, como manipuladores flotantes. Tanto el *framework*, como las extensiones desarrolladas, constituyen las principales aportaciones que se sintetizan en los próximos párrafos, junto con las principales conclusiones obtenidas a lo largo de la Tesis.

Se propone un *framework* óptimo para definir nuevos controladores visuales dinámicos para llevar a cabo el guiado de robots manipuladores. El método general propuesto emplea un control óptimo para definir el comportamiento deseado en el espacio articular, basado en una función de coste indicada que

determina cómo se distribuye el esfuerzo de control sobre las articulaciones. El enfoque propuesto permite derivar sistemas de control visual directo basado en imagen conocidos, tales como el basado en dinámica inversa. Sin embargo, se pueden obtener nuevos controladores visuales directos con diferentes propiedades dinámicas y de precisión. Una vez que se ha definido el *framework*, se amplía para permitir que realice el control de robots manipuladores redundantes. Esta extensión permite integrar diferentes funciones de peso adicionales, con el objetivo de evitar singularidades del robot, singularidades de la imagen, o incluso evitar el comportamiento caótico de las articulaciones típico de tales sistemas. En primer lugar, se emplea el concepto de manipulabilidad para resolver la redundancia del robot. Después de controlar la redundancia, se pueden generar diferentes controladores dependiendo de la función de peso $\mathbf{W}$. Como se indica a lo largo de la Tesis, el mejor comportamiento ocurre cuando $\mathbf{W} = \mathbf{M}^{-1}$. En contraste, cuando $\mathbf{W} = \mathbf{I}$ el controlador es mucho más simple y fácil de implementar. El uso de $\mathbf{W} = \mathbf{D}$ permite indicar qué articulaciones soportarán los pares más fuertes. El *framework* también permite ajustar diversos comportamientos de seguimiento de trayectorias para adaptarlos a cada situación.

Otra importante contribución de la Tesis es el concepto de perceptibilidad dinámica. Este parámetro permite detectar situaciones en las que el robot está cerca de una singularidad en la imagen o en el robot. La perceptibilidad dinámica se representa como elipses, e indica la capacidad de movimiento del robot para cada punto característico en la imagen cuando se realiza el control visual. El concepto de perceptibilidad dinámica permite integrar la información dinámica del robot, de manera que las elipses muestren qué direcciones del movimiento son más adecuadas según las restricciones cinemáticas y dinámicas, así como la configuración de las características en la imagen para cada momento. La forma de las elipses permite tener información, por ejemplo, de la proximidad del robot a una configuración singular tanto en el espacio de la articulación como en el

espacio de la imagen. Esta información es empleada por los controladores diseñados con el propósito de no solo detectar sino también evitar singularidades durante el seguimiento.

Un comportamiento caótico articular ocurre cuando, al realizar una trayectoria repetitiva de la trayectoria en la imagen, el regulador calcula un movimiento imprevisible y no periódico en el espacio articular. En el framework propuesto se integra también un término controlador de caos con el objetivo de determinar las mejores referencias para que el efector final del robot y sus articulaciones se comporten de manera correcta (un comportamiento periódico y repetitivo a nivel de conjunto). Los resultados muestran que los controladores dinámicos no sólo logran correctamente el seguimiento de trayectorias periódicas en el espacio Cartesiano, sino que también son capaces de evitar el comportamiento caótico presente en tales sistemas.

La última fase de la Tesis se realizó en colaboración con el grupo de "Onboard space systems" de la Luleå University of Technology en Suecia. Esta investigación consistió en la extensión del *framework* para el control visual directo de satélites espaciales y robots manipuladores en el espacio. La dinámica de tales sistemas se integra en el *framework* para, posteriormente, evaluar su comportamiento para el seguimiento de trayectorias. Cabe señalar que para obtener una simulación correcta del comportamiento de estos robots es necesario tener en cuenta no sólo su dinámica, sino también la dinámica orbital en la que se realiza la tarea.

6.2 Publicaciones

Esta sección cita las diferentes publicaciones producidas por la investigación presentada en esta Tesis: cuatro artículos de revistas incluidas en el JCR (primer cuartil), dos contribuciones a conferencias internacionales y cinco conferencias nacionales.

6.2.1 Artículos en revistas incluidas en el JCR

- "**FPGA-based architecture for direct visual control robotic systems**". Alabdo, A.; Pérez, J.; García, G.J.; Pomares, J.; Torres, F.; Mechatronics, 39, pp. 2014-216, 2016.

En este trabajo se describe el *framework* para el desarrollo rápido de sistemas de control visual dinámico integrados en FPGA, descritos con mayor detalle en esta Tesis en los Capítulos 3, 4 y 5. El diseño paralelo de algoritmos incrementa la precisión de este tipo de controladores, minimizando el tiempo de respuesta. Los sistemas de control visual directo basado en imagen derivados de este *framework* permiten el seguimiento de trayectorias mediante la obtención de diferentes comportamientos dinámicos dependiendo de la matriz de ponderación. También se añade un nuevo método para compensar el comportamiento caótico de estos sistemas a los controladores derivados de la matriz de ponderación. Para comprobar la viabilidad de este *framework* basado en FPGA propuesto, y para demostrar los efectos de las métricas, algunos de los controladores derivados se evalúan durante el seguimiento de trayectorias en la imagen. Este desarrollo no sólo implica la obtención del primer controlador de control visual directo basado en FPGA, sino que también permite convertir el sistema de control en un sistema de control en tiempo real, aprovechando las características reconfigurables de las FPGAs. Esta estrategia permite tener un ciclo de control más estable y con un tiempo conocido. El trabajo muestra las principales aportaciones y resultados experimentales finales del proyecto público para grupos emergentes de la Universidad de Alicante "Control visual embebido de robots manipuladores utilizando hardware FPGA reconfigurable" (GRE12-17), del que el autor de esta tesis fue colaborador.

Este artículo fue publicado en la revista "Mechatronics", en noviembre de 2016. En 2016 la revista tuvo un factor de impacto en el 'Journal Citation Reports' del 'ISI Web of Knowledge' de 2.496, y se localizó en la posición 29 de un total de 130 en la categoría "Ingeniería mecánica", dentro del primer cuartil. El índice de

impacto de la revista 'Mechatronics' se ha mantenido estable desde el año 2013, año en el que tuvo un factor de impacto de 1.823, siempre aumentando desde 2010 (0.994).

- "**FPGA-based visual control system using dynamic perceptibility**". Perez, J.; Alabdo, A.; Pomares, J; Garcia, G.J.; Torres, F.; Robotics and Computer Integrated Manufacturing, 41 pp. 13-22, 2016.

Esta publicación presenta el concepto de perceptibilidad dinámica, que proporciona información sobre la capacidad del sistema para realizar el seguimiento de un objeto con una estrategia de control visual directo. Este concepto se integra en los controladores propuestos y se implementa en la arquitectura para evitar las singularidades articulares del robot, así como las singularidades de la imagen. Para ello, se detalla un *framework* óptimo de control visual directo para robots que integra perceptibilidad dinámica. Este artículo presenta la formulación para el *framework* óptimo y detalla la implementación de uno de los controladores derivados en la arquitectura basada en FPGA. El documento describe cómo el *framework* implementado en una FPGA para el desarrollo de sistemas de control visual directo puede ser reconfigurado de una manera fácil, para probar nuevos controladores, o simplemente para agregar nuevas funcionalidades a los controladores ya implementados. Siguiendo la misma idea que el artículo publicado en 'Mechatronics', este trabajo integra un nuevo término que permite tener en cuenta la perceptibilidad dinámica. El poco tiempo requerido para la implementación de este nuevo controlador representa un gran paso adelante en el diseño y prueba de nuevos sistemas de control visual directo incorporados en un sistema de tiempo real gracias a las FPGAs.

Este artículo fue publicado en la revista 'Robotics and Computer-Integrated Manufacturing' en octubre de 2016. En 2016, la revista tuvo un factor de impacto en el 'Journal Citation Reports' del 'ISI Web of Knowledge' de 2.846, y estaba en la posición 11 de un total de 44 en la categoría de "Engineering, Manufacturing", perteneciente al primer cuartil. El índice de impacto de la revista 'Robotics and

Computer-Integrated Manufacturing' ha aumentado de manera continua desde 2011, cuando tuvo un factor de impacto de 1.173.

- **"Direct image-based visual servoing of free-floating space manipulators".** Perez, J., Emami, M. R., & Pomares, J. Aerospace Science and Technology, 55, 1–9. 2016

Este artículo presenta un controlador basado en imágenes para realizar el guiado de un robot manipulador con base flotante. El manipulador tiene un sistema de cámara *'eye-in-hand'*, y se une a un satélite base. La base es totalmente libre y flota en el espacio sin control de la altitud y, por lo tanto, reacciona libremente a los movimientos del robot manipulador unido a él. El enfoque basado en imagen propuesto utiliza el modelo cinemático y dinámico del sistema, no sólo para lograr una ubicación deseada con respecto a un objeto observado en el espacio, sino también para seguir una trayectoria deseada con respecto al objeto. Para ello, el artículo presenta un enfoque de control óptimo para guiar al robot montado en el satélite de libre flotación, utilizando información visual, y considerando la optimización de los comandos del motor con respecto a una métrica especificada junto con la compensación del caos. El controlador propuesto se aplica al control visual de un robot manipulador de cuatro grados de libertad en diferentes escenarios.

Este artículo fue publicado en la revista 'Aerospace Science and Technology' en agosto de 2016. En 2016, la revista tuvo un factor de impacto en el 'Journal Citation Reports' del 'ISI Web of Knowledge' de 2.057, y estaba en la posición 3 de un total de 31 en la categoría de "Ingeniería, Aeroespacial", perteneciente al primer cuartil. El índice de impacto de la revista 'Ciencia y Tecnología Aeroespacial' ha aumentado desde 2012, cuando tuvo un factor de impacto de 0,873.

- "**Direct visual servoing framework based on optimal control for redundant joint structures**". Pomares, J.; Jara, C.A.; Pérez, J.; Torres,

F.; International Journal of Precision Engineering and Manufacturing 16(2), pp. 267-274. 2015.

Este artículo describe el *framework* basado en el control óptimo para la generación de leyes de control visual directo. No sólo se describe el *framework*, sino que también se estudia la precisión del controlador. Esta precisión varía dependiendo de la matriz de ponderación **W** para diferentes tipos de trayectorias.

Este artículo fue publicado en la revista 'International Journal of Precision Engineering and Manufacturing' en abril de 2015. En 2015, la revista tuvo un factor de impacto en el 'Journal Citation Reports' del 'ISI Web of Knowledge' de 1.075, perteneciente al primer cuartil en la categoría de 'Engineering and Manufacturing' y 'Ingeniería Mecánica'. Desde su publicación, el documento ha sido citado un total de dos veces según 'ISI Web of Knowledge' y 'Google Scholar'.

6.2.2 Congresos internacionales

- "**Image-based control of satellite-mounted robot manipulators”**, Perez, J., Pomares, J., & Emami, M. R. In 2016 7th International Conference on Mechanical and Aerospace Engineering (ICMAE) (pp. 346–351). London, UK. 2016

Este artículo describe una estrategia óptima para un controlador para el seguimiento de trayectorias con brazos robóticos montados sobre un sistema de flotación libre mientras se controla su comportamiento caótico. Esto permite optimizar el movimiento del sistema y, por lo tanto, el consumo de combustible/energía.

- **“FPGA-based visual control of robot manipulators using dynamic perceptibility**", J. Pérez, A. Alabdo, G. J. García, J. Pomares, F. Torres., In Proceedings of the International Conference on

ReConFigurable Computing and FPGAs (ReConFig). Cancun, Mexico. 2015.

Este artículo describe el controlador propuesto basado en la dinámica inversa para el seguimiento de trayectorias, así como su implementación en la FPGA. Además, el concepto de perceptibilidad dinámica se describe como un criterio para detectar no sólo las singularidades del robot sino también las singularidades de la imagen. Ambas contribuciones están integradas con el objetivo de permitir el seguimiento de trayectorias en la imagen evitando al mismo tiempo posibles singularidades que pudieran aparecer durante dicho seguimiento.

- **"FPGA-based Framework for Dynamic Visual Servoing of Robot Manipulators",** A. Alabdo, J. Pérez, J. Pomares, G.J. Garcia, F. Torres., in Proceedings of the IEEE International Conference on Emerging Technologies and Factory Automation. Luxemburgo. 2015.

Este artículo describe el *framework* basado en el control óptimo para el guiado de robots manipuladores. Dicho *framework* permite generar leyes de control visual basado en imagen directo con comportamientos diferentes dependiendo de la matriz de ponderación empleada. La implementación de la arquitectura basada en FPGA propuesta se detalla después de describir el *framework* y todos los diferentes componentes del controlador.

6.2.3 Congresos nacionales

- "**Control visual dinámico basado en FPGA de un robot manipulador de 6 grados de libertad**", A. Alabdo, J. Pérez, J. Pomares, G. J. García, F. Torres., En Actas de las XXXVII Jornadas de Automática, Madrid, Septiembre 2016.

Este artículo se describen los fundamentos de los diferentes componentes de hardware que componen la arquitectura utilizada para la implementación de los diferentes controladores propuestos a lo largo de la Tesis. Se describen los elementos principales de un sistema de control visual basado en imagen directo,

y cómo se pueden implementar en un FPGA. El controlador se aplica en el guiado de un robot Mitsubishi PA-10 de 6 grados de libertad.

- **"ViSeC-Matlab: Una herramienta para el aprendizaje de sistemas de control visual sobre Matlab",** J. Pérez, A. Alabdo, G. J. García, J. Pomares, F. Torres., En Actas de las XXXVI Jornadas de Automática, Bilbao, Septiembre 2015.

Este artículo presenta la herramienta ViSeC, desarrollada para la evaluación de todos los diferentes controladores definidos a lo largo de la Tesis por simulación. Esta herramienta se basa en la *toolbox* de robótica de Matlab, y permite introducir fácilmente nuevos controladores visuales y evaluar su comportamiento, generando gráficas como error de imagen, acciones de control, trayectoria del robot o trayectoria en la imagen, entre otras. También permite definir fácilmente la tarea de control visual, simplificando el proceso de depuración antes de la implementación.

6.3 Trabajos futuros

La investigación realizada a lo largo de la Tesis ha permitido abrir nuevas líneas de investigación que se pueden abordar con la experiencia y los desarrollos realizados. Dentro de estas futuras líneas de investigación, vale la pena mencionar el diseño de sistemas de control visual para el guiado de manos robóticas. Hoy en día, las investigaciones desarrolladas en esta Tesis se están aplicando al proyecto "Sistema robótico multisensorial con manipulación dual para tareas asistenciales humano-robot" (DPI2015-68087-R), financiado por los fondos del Ministerio de Economía y Competitividad y FEDER. El objetivo fundamental del proyecto es el desarrollo de un torso robótico multisensorial y su aplicación a las tareas de asistencia humano-robot. Este torso robótico está compuesto por dos manipuladores, cada uno de ellos con una mano robótica. Los desarrollos presentados a lo largo de la Tesis permiten el guiado de ambos

manipuladores robóticos mediante el uso de la visión artificial. Sin embargo, los controladores implementados no pueden realizar el guiado de las manos robóticas como se describe a lo largo de la Tesis. Estos controladores pueden extenderse para incluir características cinemáticas y dinámicas de estas manos robóticas. De esta manera, la experiencia obtenida con esta Tesis abre una nueva línea prometedora de investigación como el guiado de sistemas de manipulación basados en manos robóticas mediante el empleo de control visual directo.

Otra línea de investigación es la extensión de sistemas de control visual directo para el caso del control bimanual. Para este caso, el controlador no sólo tiene que calcular el guiado de los manipuladores correspondientes y las manos robóticas, sino también coordinar el movimiento entre ellos. Además, cuando se realizan tareas de manipulación, no sólo se debe considerar la información visual del entorno, sino también la información táctil que indica la fuerza de interacción aplicada al objeto manipulado por cada dedo. La extensión de los controladores propuestos para considerar la información táctil es otra línea de investigación derivada de la Tesis en un futuro cercano.

Para esta Tesis, se considera un sistema de visión por ordenador compuesto por una sola cámara situada en el efector final del manipulador. El uso de un sistema de visión artificial para tareas de colaboración humano-robot con una sola cámara suele implicar que la información proporcionada por dicha cámara simplemente no sea suficiente debido a las oclusiones. El uso de diferentes sistemas de visión artificial se propone como trabajos futuros. De esta manera, los controladores desarrollados deben utilizar sistemas de visión múltiples ubicados en el espacio de trabajo para usar el más adecuado dependiendo de cuál sea más conveniente para el posicionamiento del robot. Se hace necesario determinar qué criterio es mejor para determinar qué sistema de visión es el más adecuado, al mismo tiempo que el controlador coordina las acciones de control a partir de la información obtenida por el sistema de visión para calcular el movimiento final.

Por último, y dentro de la colaboración llevada a cabo con el grupo de investigación "Onboard space systems" que pertenece a la Luleå University of Technology en Suecia, los controladores visuales se están extendiendo para guiar manipuladores robóticos montados en satélites actuados. De esta manera, el controlador visual debe ser capaz de guiar al manipulador robótico, así como de accionar los propulsores para realizar el rendezvous del satélite robot.

7 References

7.1 References

Aghili, F. (2012). A Prediction and Motion-Planning Scheme for Visually Guided Robotic Capturing of Free-Floating Tumbling Objects With Uncertain Dynamics. *IEEE Transactions on Robotics*, *28*(3), 634–649. http://doi.org/10.1109/TRO.2011.2179581

Aghili, F. (2013). Pre- and post-grasping robot motion planning to capture and stabilize a tumbling/drifting free-floater with uncertain dynamics. In *2013 IEEE International Conference on Robotics and Automation* (pp. 5461–5468). IEEE. http://doi.org/10.1109/ICRA.2013.6631360

Aghili, F., Kuryllo, M., Okouneva, G., & English, C. (2011). Fault-Tolerant Position/Attitude Estimation of Free-Floating Space Objects Using a Laser Range Sensor. *IEEE Sensors Journal*, *11*(1), 176–185. http://doi.org/10.1109/JSEN.2010.2056365

Agravante, D. J., Claudio, G., Spindler, F., & Chaumette, F. (2017). Visual Servoing in an Optimization Framework for the Whole-Body Control of Humanoid Robots. *IEEE Robotics and Automation Letters*, *2*(2), 608–615. http://doi.org/10.1109/LRA.2016.2645512

Alfriend, K., Vadali, S. R., Gurfil, P., How, J., & Breger, L. (2009). *Spacecraft formation flying: Dynamics, control and navigation* (Vol. 2). Butterworth-Heinemann.

Allen, P. K., Yoshimi, B., & Timcenko, A. (1991). Real-time visual servoing. In *Proceedings. 1991 IEEE International Conference on Robotics and Automation* (pp. 851–856). IEEE Comput. Soc. Press. http://doi.org/10.1109/ROBOT.1991.131694

Andolfatto, L., Lavernhe, S., & Mayer, J. R. R. (2011). Evaluation of servo, geometric and dynamic error sources on five-axis high-speed machine tool. *International Journal of Machine Tools and Manufacture*, *51*(10), 787–796. http://doi.org/10.1016/j.ijmachtools.2011.07.002

Bodin, P., Noteborn, R., Larsson, R., & Chasset, C. (2011). System test results from the GNC experiments on the PRISMA in-orbit test bed. *Acta Astronautica*, *68*(7), 862–872. http://doi.org/10.1016/j.actaastro.2010.08.021

Bodin, P., Noteborn, R., Larsson, R., Karlsson, T., D'Amico, S., Ardaens, J. S., … Berges, J. C. (2012). The prisma formation flying demonstrator: Overview and conclusions from the nominal mission. *Advances in the Astronautical Sciences*, *144*(2012), 441–460.

Bonnal, C., Ruault, J. M., & Desjean, M. C. (2013). Active debris removal: Recent progress and current trends. *Acta Astronautica*, *85*, 51–60. http://doi.org/10.1016/j.actaastro.2012.11.009

Bourquardez, O., Mahony, R., Guenard, N., Chaumette, F., Hamel, T., & Eck, L. (2009). Image-Based Visual Servo Control of the Translation Kinematics of a Quadrotor Aerial Vehicle. *IEEE Transactions on Robotics*, *25*(3), 743–749. http://doi.org/10.1109/TRO.2008.2011419

Cervera, E., Berry, F., & Martinet, P. (2001). Stereo Visual Servoing with a Single Point: a Comparative Study. In *IEEE International Conference on Advanced Robotics* (pp. 213–218).

Cervera, E., & del Pobil, A. P. (2002). Sensor-based learning for practical planning of fine motions in robotics. *Information Sciences*, *145*(1–2), 147–168. http://doi.org/10.1016/S0020-0255(02)00228-1

Cervera, E., Garcia, N., Martinez, E., Nomdedeu, L., & del Pobil, A. P. (2008). Safety for a robot arm moving amidst humans by using panoramic vision. In *Robotics and*

Automation, 2008. ICRA 2008. IEEE International Conference on (pp. 2183–2188). http://doi.org/10.1109/ROBOT.2008.4543530

Chaumette, F. (1990). *La Relation Vision-Commande: Théorie Et Application À Des Tâches Robotiques*. University of Rennes.

Chaumette, F. (1998). Potential problems of stability and convergence in image-based and position-based visual servoing. In *The confluence of vision and control* (pp. 66–78). London.

Chaumette, F., & Hutchinson, S. (2006). Visual servo control. I. Basic approaches. *IEEE Robotics & Automation Magazine*, *13*(4), 82–90. http://doi.org/10.1109/MRA.2006.250573

Chaumette, F., & Hutchinson, S. (2007). Visual servo control. II. Advanced approaches [Tutorial]. *IEEE Robotics & Automation Magazine*, *14*(1), 109–118. http://doi.org/10.1109/MRA.2007.339609

Chaumette, F., Rives, P., & Espiau, B. (1993). Classification and realization of the different vision-based tasks. *Visual Servoing*, *7*, 199–228.

Cheah, C. C., Hou, S. P., Zhao, Y., & Slotine, J. J. E. (2010). Adaptive Vision and Force Tracking Control for Robots With Constraint Uncertainty. *IEEE/ASME Transactions on Mechatronics*, *15*(3), 389–399. http://doi.org/10.1109/TMECH.2009.2027115

Cheah, C. C., Liu, C., & Slotine, J. J. E. (2007). Adaptive Vision based Tracking Control of Robots with Uncertainty in Depth Information. In *Proceedings 2007 IEEE International Conference on Robotics and Automation* (pp. 2817–2822). http://doi.org/10.1109/ROBOT.2007.363898

Chen, J., Dawson, D. M., Dixon, W. E., & Behal, A. (2005). Adaptive homography-based visual servo tracking for a fixed camera configuration with a camera-in-hand extension. *IEEE Transactions on Control Systems Technology*, *13*(5), 814–825. http://doi.org/10.1109/TCST.2005.852150

Chesi, G., & Hashimoto, K. (2010). *Visual Servoing via Advanced Numerical Methods*.

Chesi, G., Hashimoto, K., Prattichizzo, D., & Vicino, A. (2004). Keeping features in the field of view in eye-in-hand visual servoing: a switching approach. *IEEE Transactions on Robotics*, *20*(5), 908–914. http://doi.org/10.1109/TRO.2004.829456

Corke, P. I., & Hutchinson, S. A. (2001). A new partitioned approach to image-based visual servo control. *IEEE Transactions on Robotics and Automation*, *17*(4), 507–515. http://doi.org/10.1109/70.954764

David, P., DeMenthon, D., Duraiswami, R., & Samet, H. (2004). SoftPOSIT: Simultaneous Pose and Correspondence Determination. *International Journal of Computer Vision*, *59*(3), 259–284. http://doi.org/10.1023/B:VISI.0000025800.10423.1f

De Luca, A., Ferri, M., Oriolo, G., & Giordano, P. R. (2008). Visual servoing with exploitation of redundancy: An experimental study. In *2008 IEEE International Conference on Robotics and Automation* (pp. 3231–3237). IEEE. http://doi.org/10.1109/ROBOT.2008.4543703

De Rosa, D., & Curti, F. (2006). Visual Monitoring of Space Rendezvous: A Structure From Motion Problem. In *AIAA/AAS Astrodynamics Specialist Conference and Exhibit*. American Institute of Aeronautics and Astronautics. http://doi.org/doi:10.2514/6.2006-6762

Dementhon, D. F., & Davis, L. S. (1995). Model-based object pose in 25 lines of code. *International Journal of Computer Vision*, *15*(1–2), 123–141. http://doi.org/10.1007/BF01450852

Dhipa, M., Jeyakkannan, N., & Chandrasekar, A. (2015). Hardware accelerated stereo imaging for visual servoing. In *2015 Online International Conference on Green Engineering and Technologies (IC-GET)* (pp. 1–4). http://doi.org/10.1109/GET.2015.7453786

Donath, T., Schildknecht, T., Martinot, V., & Del Monte, L. (2010). Possible European systems for space situational awareness. *Acta Astronautica*, *66*(9), 1378–1387. http://doi.org/10.1016/j.actaastro.2009.10.036

Dong, G., & Zhu, Z. H. (2015). Position-based visual servo control of autonomous robotic manipulators. *Acta Astronautica*, *115*, 291–302. http://doi.org/10.1016/j.actaastro.2015.05.036

Dubowsky, S., & Papadopoulos, E. (1993). The kinematics, dynamics, and control of free-flying and free-floating space robotic systems. *IEEE Transactions on Robotics and Automation*, *9*(5), 531–543. http://doi.org/10.1109/70.258046

Espiau, B. (1994). Effect of camera calibration errors on visual servoing in robotics. In T. Yoshikawa & F. Miyazaki (Eds.), *Experimental Robotics III: The 3rd International Symposium, Kyoto, Japan, October 28--30, 1993* (pp. 182–192). Berlin, Heidelberg: Springer Berlin Heidelberg. http://doi.org/10.1007/BFb0027594

Fang, Y., Behal, A., Dixon, W. E., & Dawson, D. M. (2002). Adaptive 2.5D visual servoing of kinematically redundant robot manipulators. In *Decision and Control, 2002, Proceedings of the 41st IEEE Conference on* (Vol. 3, pp. 2860–2865 vol.3). http://doi.org/10.1109/CDC.2002.1184282

Felicetti, L., Gasbarri, P., Pisculli, A., Sabatini, M., & Palmerini, G. B. (2016). Design of robotic manipulators for orbit removal of spent launchers' stages. *Acta Astronautica*, *119*, 118–130. http://doi.org/10.1016/j.actaastro.2015.11.012

Flohrer, T., Schildknecht, T., & Musci, R. (2008). Proposed strategies for optical observations in a future European Space Surveillance network. *Advances in Space Research*, *41*(7), 1010–1021. http://doi.org/10.1016/j.asr.2007.02.018

Flores, A., Ma, O., Pham, K., & Ulrich, S. (2014). A review of space robotics technologies for on-orbit servicing. *Progress in Aerospace Sciences*. Elsevier Ltd.

Gans, N. R., Hu, G., & Dixon, W. E. (2008). Keeping Objects in the Field of View: An Underdetermined Task Function Approach to Visual Servoing. In *2008 IEEE*

International Symposium on Intelligent Control (pp. 432–437). IEEE. http://doi.org/10.1109/ISIC.2008.4635969

Garcia, G. J., Corrales, J. A., Pomares, J., & Torres, F. (2009). Survey of visual and force/tactile control of robots for physical interaction in Spain. *Sensors*, *9*(12), 9689–9733.

García, G. J., Jara, C. A., Pomares, J., Alabdo, A., Poggi, L., & Torres, F. (2014). A Survey on FPGA-Based Sensor Systems: Towards Intelligent and Reconfigurable Low-Power Sensors for Computer Vision, Control and Signal Processing. *Sensors*, *14*(4), 6247–6278. http://doi.org/10.3390/s140406247

Garcia, G. J., Pomares, J., & Torres, F. (2004). Control visual de robots manipuladores. Una herramienta para su diseño y aprendizaje.

Garcia, N., Perez, C., Sabater, J. M., Morales, R., & Badesa, F. J. (2011). Robust and cooperative image-based visual servoing system using a redundant architecture. *Sensors*, *11*(12), 11885–11900.

Gasbarri, P., Sabatini, M., & Palmerini, G. B. (2014). Ground tests for vision based determination and control of formation flying spacecraft trajectories. *Acta Astronautica*, *102*, 378–391. http://doi.org/10.1016/j.actaastro.2013.11.035

Graham, A. R., & Kingston, J. (2015). Assessment of the commercial viability of selected options for on-orbit servicing (OOS). *Acta Astronautica*, *117*, 38–48. http://doi.org/10.1016/j.actaastro.2015.07.023

Hablani, H. B. (1994). Sun-tracking commands and reaction wheel sizing with configuration optimization. *Journal of Guidance, Control, and Dynamics*, *17*(4), 805–814. http://doi.org/10.2514/3.21270

Hadj, H., Mezouar, Y., Martinet, P., & Chaumette, F. (2008). Catadioptric Visual Servoing From 3-D Straight Lines. *IEEE Transactions on Robotics*, *24*(3), 652–665. http://doi.org/10.1109/TRO.2008.919288

Hafez, A. H. A., Anurag, V. V., Shah, S. V., Krishna, K. M., & Jawahar, C. V. (2014). Reactionless visual servoing of a dual-arm space robot. In *2014 IEEE International Conference on Robotics and Automation (ICRA)* (pp. 4475–4480). IEEE. http://doi.org/10.1109/ICRA.2014.6907512

Han, J., Campbell, N., Jokinen, K., & Wilcock, G. (2012). Investigating the use of Non-verbal Cues in Human-Robot Interaction with a Nao robot. In *2012 IEEE 3rd International Conference on Cognitive Infocommunications (CogInfoCom)* (pp. 679–683). http://doi.org/10.1109/CogInfoCom.2012.6421937

Hill, J., & Park, W. T. (1979). Real Time Control of a Robot with a Mobile Camera. *Proceedings of the 9th. International Symposium on Industrial Robots, Washington, DC, USA*, 233–246.

Hillenbrand, U., & Lampariello, R. (2005). Motion and parameter estimation of a free-floating space object from range data for motion prediction. In *8th International Symposium on Artificial Intelligence, Robotics, and Automation in Space*.

Hirai, K., Hirose, M., Haikawa, Y., & Takenaka, T. (1998). The development of Honda humanoid robot. In *Proceedings. 1998 IEEE International Conference on Robotics and Automation (Cat. No.98CH36146)* (Vol. 2, pp. 1321–1326 vol.2). http://doi.org/10.1109/ROBOT.1998.677288

Horaud, R., Dornaika, F., & Lamiroy, B. (1997). Object Pose: The Link between Weak Perspective, Paraperspective, and Full Perspective. *International Journal of Computer Vision*, *22*(2), 173–189. http://doi.org/10.1023/A:1007940112931

https://www.cubesatshop.com/. (n.d.).

Hu, J. S., Chang, N. Y. C., & Yang, J. J. (2011). FPGA-based embedded visual servoing platform for quick response visual servoing. *… (ASCC), 2011 8th …*, 263–268. Retrieved from http://ieeexplore.ieee.org/xpls/abs_all.jsp?arnumber=5899082

Huang, P., Zhang, F., Cai, J., Wang, D., Meng, Z., & Guo, J. (2017). Dexterous Tethered Space Robot: Design, Measurement, Control and Experiment. *IEEE*

Transactions on Aerospace and Electronic Systems, *PP*(99), 1. http://doi.org/10.1109/TAES.2017.2671558

Inaba, N., Oda, M., & Hayashi, M. (2003). Visual Servoing of Space Robot for Autonomous Satellite Capture. *Transactions of the Japan Society for Aeronautical and Space Sciences*, *46*(153), 173–179. http://doi.org/10.2322/tjsass.46.173

Ismail, Z., & Varatharajoo, R. (2010). A study of reaction wheel configurations for a 3-axis satellite attitude control. *Advances in Space Research*, *45*(6), 750–759. http://doi.org/10.1016/j.asr.2009.11.004

Janabi, F., & Marey, M. (2010). A Kalman-Filter-Based Method for Pose Estimation in Visual Servoing. *IEEE Transactions on Robotics*, *26*(5), 939–947. http://doi.org/10.1109/TRO.2010.2061290

Jara, C. A., Pomares, J., Candelas, F. A., & Torres, F. (2014). Control framework for dexterous manipulation using dynamic visual servoing and tactile sensors' feedback. *Sensors (Basel, Switzerland)*, *14*(1), 1787–1804. http://doi.org/10.3390/s140101787

Jin, M., Yang, H., Xie, Z., Sun, K., & Liu, H. (2013). The ground-based verification system of visual servoing control for a space robot. In *2013 IEEE International Conference on Mechatronics and Automation* (pp. 1566–1570). IEEE. http://doi.org/10.1109/ICMA.2013.6618147

Johnson, N. L. (2011). Space Debris Mitigation Guidelines. *Space Debris*. Retrieved from http://hdl.handle.net/2060/20110014989

Jorstad, A., Burlina, P., Wang, I. J., Lucarelli, D., & DeMenthon, D. (2008). Model-based pose estimation by consensus. In *2008 International Conference on Intelligent Sensors, Sensor Networks and Information Processing* (pp. 569–574). IEEE. http://doi.org/10.1109/ISSNIP.2008.4762050

Kelly, R., Cervantes, I., Alvarez-Ramirez, J., Bugarin, E., & Monroy, C. (2008). On Transpose Jacobian Control for Monocular Fixed-Camera 3D Direct Visual Servoing. In *Robot Manipulators*. InTech. http://doi.org/10.5772/6208

Kessler, D. J., & Cour, B. G. (1978). Collision frequency of artificial satellites: The creation of a debris belt. *Journal of Geophysical Research*, *83*(A6), 2637. http://doi.org/10.1029/JA083iA06p02637

Khatib, O. (1983). Dynamic Control of Manipulators in Operational Space. In *6th IFTOMM Congress on Theory of Machines and Mechanisms* (pp. 1–10).

Kosmopoulos, D. I. (2011). Robust Jacobian matrix estimation for image-based visual servoing. *Robotics and Computer-Integrated Manufacturing*, *27*(1), 82–87. http://doi.org/10.1016/j.rcim.2010.06.013

Kumar, N., Borm, J. H., Panwar, V., & Chai, J. (2012). Tracking control of redundant robot manipulators using RBF neural network and an adaptive bound on disturbances. *International Journal of Precision Engineering and Manufacturing*, *13*(8), 1377–1386. http://doi.org/10.1007/s12541-012-0181-5

Kung, Y. S., & Shu, G. S. (2005). Development of a FPGA-based Motion Control IC for Robot Arm. In *2005 IEEE International Conference on Industrial Technology* (pp. 1397–1402). IEEE. http://doi.org/10.1109/ICIT.2005.1600854

Li, X., & Cheah, C. C. (2012). Adaptive regional feedback control of robotic manipulator with uncertain kinematics and depth information. In *2012 American Control Conference (ACC)* (pp. 5472–5477). http://doi.org/10.1109/ACC.2012.6315007

Li, X., & Cheah, C. C. (2013). Global task-space adaptive control of robot. *Automatica*, *49*(1), 58–69. http://doi.org/10.1016/j.automatica.2012.07.003

Lichter, M. D., & Dubowsky, S. (2004). State, shape, and parameter estimation of space objects from range images. *IEEE International Conference on Robotics and*

Automation, 2004. Proceedings. ICRA '04. 2004, *3*(April), 2974–2979. http://doi.org/10.1109/ROBOT.2004.1307513

Lin, C. J. (2004). Motion planning of redundant robots by perturbation method. *Mechatronics*, *14*(3), 281–297. http://doi.org/10.1016/S0957-4158(03)00032-1

Liou, J. C. (2011). An active debris removal parametric study for LEO environment remediation. *Advances in Space Research*, *47*(11), 1865–1876. http://doi.org/10.1016/j.asr.2011.02.003

Liou, J. C., & Johnson, N. L. (2008). Instability of the present LEO satellite populations. *Advances in Space Research*, *41*(7), 1046–1053. http://doi.org/10.1016/j.asr.2007.04.081

Lippiello, V., Siciliano, B., & Villani, L. (2003). Robust visual tracking using a fixed multi-camera system. In *IEEE International Conference on Robotics and Automation* (Vol. 3, pp. 3333–3338).

Lippiello, V., Siciliano, B., & Villani, L. (2007a). A Position-Based Visual Impedance Control for Robot Manipulators. In *Proceedings 2007 IEEE International Conference on Robotics and Automation* (pp. 2068–2073). IEEE. http://doi.org/10.1109/ROBOT.2007.363626

Lippiello, V., Siciliano, B., & Villani, L. (2007b). Position-Based Visual Servoing in Industrial Multirobot Cells Using a Hybrid Camera Configuration. *IEEE Transactions on Robotics*, *23*(1), 73–86. http://doi.org/10.1109/TRO.2006.886832

Lippiello, V., Siciliano, B., & Villani, L. (2007c). Robot force/position control with force and visual feedback. In *Control Conference (ECC), 2007 European* (pp. 3790–3795).

Liu, Z., Li, L., & Zhang, H. (2007). Control chaos in a spatially redundant manipulator with flexible link. In *Proceedings of 12th world congress in mechanism and machine science*.

Liyanage, M. H., & Krouglicof, N. (2014). A single time scale visual servoing system for a high speed SCARA type robotic arm. In *2014 IEEE International Conference on Robotics and Automation (ICRA)* (pp. 4153–4160). IEEE. http://doi.org/10.1109/ICRA.2014.6907463

Ma, G., Jiang, Z., Li, H., Gao, J., Yu, Z., Chen, X., … Huang, Q. (2015). Hand-eye servo and impedance control for manipulator arm to capture target satellite safely. *Robotica*, *33*(4), 848–864. http://doi.org/10.1017/S0263574714000587

MacCleery, B., & Kassas, Z. M. (2008). New Mechatronics Development Techniques for FPGA-Based Control and Simulation of Electromechanical Systems. *IFAC Proceedings Volumes*, *41*(2), 4434–4439. http://doi.org/10.3182/20080706-5-KR-1001.00748

Mahony, R., Kumar, V., & Corke, P. (2012). Multirotor Aerial Vehicles: Modeling, Estimation, and Control of Quadrotor. *IEEE Robotics & Automation Magazine*, *19*(3), 20–32. http://doi.org/10.1109/MRA.2012.2206474

Malis, E., & Rives, P. (2003a). Robustness of image-based visual servoing with respect to depth distribution errors. In *Robotics and Automation, 2003. Proceedings. ICRA '03. IEEE International Conference on* (Vol. 1, pp. 1056–1061 vol.1). http://doi.org/10.1109/ROBOT.2003.1241732

Malis, E., & Rives, P. (2003b). Uncalibrated active affine reconstruction closing the loop by visual servoing. In *Intelligent Robots and Systems, 2003. (IROS 2003). Proceedings. 2003 IEEE/RSJ International Conference on* (Vol. 1, pp. 498–503 vol.1). http://doi.org/10.1109/IROS.2003.1250678

Mansard, N., Khatib, O., & Kheddar, A. (2009). A Unified Approach to Integrate Unilateral Constraints in the Stack of Tasks. *IEEE Transactions on Robotics*, *25*(3), 670–685. http://doi.org/10.1109/TRO.2009.2020345

Marchand, E., Chaumette, F., & Rizzo, A. (1996). Using the task function approach to avoid robot joint limits and kinematic singularities in visual servoing. In

Intelligent Robots and Systems '96, IROS 96, Proceedings of the 1996 IEEE/RSJ International Conference on (Vol. 3, pp. 1083–1090 vol.3). http://doi.org/10.1109/IROS.1996.568954

Mariottini, G. L., & Prattichizzo, D. (2008). Image-based Visual Servoing with Central Catadioptric Cameras. *The International Journal of Robotics Research*, *27*(1), 41–56. http://doi.org/10.1177/0278364907084320

Mezouar, Y., & Chaumette, F. (2002). Avoiding self-occlusions and preserving visibility by path planning in the image. *Robotics and Autonomous Systems*, *41*(2), 77–87. http://doi.org/10.1016/S0921-8890(02)00277-4

Mezouar, Y., & Chaumette, F. (2003). Optimal Camera Trajectory with Image-Based Control. *The International Journal of Robotics Research*, *22*(10), 781–803. http://doi.org/10.1177/027836490302210001

Mishra, A., Ghosh, R., Goyal, A., Thakor, N. V., & Kukreja, S. L. (2016). Real-time robot tracking and following with neuromorphic vision sensor. In *2016 6th IEEE International Conference on Biomedical Robotics and Biomechatronics (BioRob)* (pp. 13–18). http://doi.org/10.1109/BIOROB.2016.7523451

Miyazaki, F., & Masutani, Y. (1990). Robustness of sensory feedback control based on imperfect Jacobian. In *Robotic research: The fifth international symposium* (pp. 201–208). Cambridge, MA: MIT Press.

Muthuramalingam, A., Himavathi, S., & Srinivasan, E. (2008). Neural Network Implementation Using FPGA: Issues and Application. *International Journal of Electrical, Computer, Energetic, Electronic and Communication Engineering*, *2*(2), 2801–2808 EM–amrlingam@hotmail.com, hima_pondy@y. Retrieved from http://citeseerx.ist.psu.edu/viewdoc/download?doi=10.1.1.131.9059&rep=rep1&type=pdf

Nakanishi, J., Cory, R., Mistry, M., Peters, J., & Schaal, S. (2008). Operational Space Control: A Theoretical and Empirical Comparison. *The International Journal of Robotics Research*, *27*(6), 737–757. http://doi.org/10.1177/0278364908091463

Nematollahi, E., & Janabi, F. (2009). Generalizations to control laws of image-based visual servoing. *International Journal of Optomechatronics*, *3*(3), 167–186.

Oberkampf, D., DeMenthon, D. F., & Davis, L. S. (1993). Iterative pose estimation using coplanar points. In *Proceedings of IEEE Conference on Computer Vision and Pattern Recognition* (pp. 626–627). IEEE Comput. Soc. Press. http://doi.org/10.1109/CVPR.1993.341055

Opromolla, R., Fasano, G., Rufino, G., & Grassi, M. (2015). Uncooperative pose estimation with a LIDAR-based system. *Acta Astronautica*, *110*, 287–297. http://doi.org/10.1016/j.actaastro.2014.11.003

Osornio, R. A., de Jesús Romero, R., Herrera, G., & Castañeda, R. (2009). FPGA implementation of higher degree polynomial acceleration profiles for peak jerk reduction in servomotors. *Robotics and Computer-Integrated Manufacturing*, *25*(2), 379–392. http://doi.org/10.1016/j.rcim.2008.01.002

Ott, E., Grebogi, C., & Yorke, J. A. (1990). Controlling chaos. *Phys. Rev. Lett.*, *64*(11), 1196–1199. http://doi.org/10.1103/PhysRevLett.64.1196

Ozawa, R., & Chaumette, F. (2011). Dynamic visual servoing with image moments for a quadrotor using a virtual spring approach. In *2011 IEEE International Conference on Robotics and Automation* (pp. 5670–5676). http://doi.org/10.1109/ICRA.2011.5979645

Palmerini, G. B., Sabatini, M., & Gasbarri, P. (2016). Guidelines for active removal of non-functional targets designed to assist rendezvous and capture. In *2016 IEEE Aerospace Conference* (pp. 1–13). http://doi.org/10.1109/AERO.2016.7500709

Papanikolopoulos, N. P. (1995). Selection of features and evaluation of visual measurements during robotic visual servoing tasks. *Journal of Intelligent & Robotic Systems*, *13*(3), 279–304. http://doi.org/10.1007/BF01424011

Park, D. H., Kwon, J. H., & Ha, I. J. (2012). Novel Position-Based Visual Servoing Approach to Robust Global Stability Under Field-of-View Constraint. *IEEE Transactions on Industrial Electronics*, *59*(12), 4735–4752. http://doi.org/10.1109/TIE.2011.2179270

Park, J., Chung, W., & Youm, Y. (1999). Computation of gradient of manipulability for kinematically redundant manipulators including dual manipulators system. *Transactions on Control, Automation and Systems Engineering*, *1*(1), 8–15.

Park, J. H., & Jong, Y. (2003). Robust visual servoing for motion control of the ball on a plate. *Mechatronics*, *13*(7), 723–738. http://doi.org/10.1016/S0957-4158(02)00039-9

Pérez, C. (2008). *Control de robots manipuladores usando información visual: Aplicación a la estimación del movimiento del objeto*. University of Elche.

Perez, J., Alabdo, A., Pomares, J., Garcia, G. J., & Torres, F. (2016). FPGA-based visual control system using dynamic perceptibility. *Robotics and Computer-Integrated Manufacturing*, *41*, 13–22. http://doi.org/10.1016/j.rcim.2016.02.005

Perez, J., Emami, M. R., & Pomares, J. (2016). Direct image-based visual servoing of free-floating space manipulators. Aerospace Science and Technology, 55, 1–9. http://doi.org/10.1016/j.ast.2016.05.012

Perez, J., Pomares, J., & Emami, M. R. (2016). Image-based control of satellite-mounted robot manipulators. In 2016 7th International Conference on Mechanical and Aerospace Engineering (ICMAE) (pp. 346–351). http://doi.org/10.1109/ICMAE.2016.7549564

Petit, A., Marchand, E., & Kanani, K. (2011). Vision-based space autonomous rendezvous: A case study. In *2011 IEEE/RSJ International Conference on Intelligent Robots and Systems* (pp. 619–624). IEEE. http://doi.org/10.1109/IROS.2011.6094568

Petit, A., Marchand, E., & Kanani, K. (2012). Tracking complex targets for space rendezvous and debris removal applications. In *2012 IEEE/RSJ International Conference on Intelligent Robots and Systems* (pp. 4483–4488). IEEE. http://doi.org/10.1109/IROS.2012.6386083

Pinard, D., Reynaud, S., Delpy, P., & Strandmoe, S. E. (2007). Accurate and autonomous navigation for the ATV. *Aerospace Science and Technology*, *11*(6), 490–498. http://doi.org/10.1016/j.ast.2007.02.009

Pomares, J., Corrales, J. A., Garcia, G. J., & Torres, F. (2011a). Direct visual Servoing to track trajectories in human-robot cooperation. *International Journal of Advanced Robotic Systems*, *8*(4), 129–138.

Pomares, J., García, G. J., Perea, I., Corrales, J. A., Jara, C. A., & Torres, F. (2011b). Visual control of a multi-robot coupled system: Application to collision avoidance in human-robot interaction. In *Computer Vision Workshops (ICCV Workshops), 2011 IEEE International Conference on* (pp. 1045–1051). http://doi.org/10.1109/ICCVW.2011.6130366

Pomares, J., Jara, C. A., Perez, J., & Torres, F. (2015). Direct visual servoing framework based on optimal control for redundant joint structures. *International Journal of Precision Engineering and Manufacturing*, *16*(2), 267–274. http://doi.org/10.1007/s12541-015-0035-z

Pomares, J., Perea, I., Jara, C. A., García, G. J., & Torres, F. (2013). Dynamic visual servo control of a 4-axis joint tool to track image trajectories during machining complex shapes. *Robotics and Computer-Integrated Manufacturing*, *29*(4), 261–270. http://doi.org/10.1016/j.rcim.2013.01.008

Pomares, J., Perea, I., & Torres, F. (2014). Dynamic Visual Servoing With Chaos Control for Redundant Robots. *IEEE/ASME Transactions on Mechatronics*, *19*(2), 423–431. http://doi.org/10.1109/TMECH.2013.2243160

Prats, M., Martínez, E., Sanz, P. J., & del Pobil, A. P. (2008). The UJI librarian robot. *Intelligent Service Robotics*, *1*(4), 321–335. http://doi.org/10.1007/s11370-008-0028-1

Pyragas, K. (1992). Continuous control of chaos by self-controlling feedback. *Physics Letters A*, *170*(6), 421–428. http://doi.org/10.1016/0375-9601(92)90745-8

Pyragas, K. (2006). Delayed feedback control of chaos. *Philosophical Transactions. Series A, Mathematical, Physical, and Engineering Sciences*, *364*(1846), 2309–34. http://doi.org/10.1098/rsta.2006.1827

Sabatini, M., Monti, R., Gasbarri, P., & Palmerini, G. (2013). Deployable space manipulator commanded by means of visual-based guidance and navigation. *Acta Astronautica*, *83*, 27–43. http://doi.org/10.1016/j.actaastro.2012.10.015

Sakagami, Y., Watanabe, R., Aoyama, C., Matsunaga, S., Higaki, N., & Fujimura, K. (2002). The intelligent ASIMO: system overview and integration. In *IEEE/RSJ International Conference on Intelligent Robots and Systems* (Vol. 3, pp. 2478–2483 vol.3). http://doi.org/10.1109/IRDS.2002.1041641

Samson, C., Espiau, B., & Borgne, M. L. (1991). *Robot Control: The Task Function Approach*. Oxford University Press.

Sanderson, A. C., & Weiss, L. E. (1980). Image-Based Visual Servo Control Using Relational Graph Error Signals. *Proceedings of the IEEE International Conference on Cybernetics and Society, Cambridge, MA, USA*, 1074–1077.

Schaub, H., Jasper, L. E. Z., Anderson, P. V., & McKnight, D. S. (2015). Cost and risk assessment for spacecraft operation decisions caused by the space debris environment. *Acta Astronautica*, *113*, 66–79. http://doi.org/10.1016/j.actaastro.2015.03.028

Schramm, F., & Morel, G. (2006). Ensuring visibility in calibration-free path planning for image-based visual servoing. *IEEE Transactions on Robotics*, *22*(4), 848–854. http://doi.org/10.1109/TRO.2006.878955

Shamsuddin, S., Yussof, H., Ismail, L., Hanapiah, F. A., Mohamed, S., Piah, H. A., & Zahari, N. I. (2012). Initial response of autistic children in human-robot interaction therapy with humanoid robot NAO. In *2012 IEEE 8th International Colloquium on Signal Processing and its Applications* (pp. 188–193). http://doi.org/10.1109/CSPA.2012.6194716

Shan, M., Guo, J., & Gill, E. (2016). Review and comparison of active space debris capturing and removal methods. *Progress in Aerospace Sciences*, *80*, 18–32. http://doi.org/10.1016/j.paerosci.2015.11.001

Sharma, R., & Hutchinson, S. (1997). Motion perceptibility and its application to active vision-based servo control. *IEEE Transactions on Robotics and Automation*, *13*(4), 607–617. http://doi.org/10.1109/70.611333

Shi, Y., Liang, B., Wang, X., Xu, W., & Liu, H. (2012). Modeling and simulation of space robot visual servoing for autonomous target capturing. In *2012 IEEE International Conference on Mechatronics and Automation* (pp. 2275–2280). IEEE. http://doi.org/10.1109/ICMA.2012.6285698

Siciliano, B., Villani, L., Lippiello, V., & De Santis, A. (2010). Force and Visual Control for Safe Human-Robot Interaction. In J. Angeles, B. Boulet, J. J. Clark, J. Kövecses, & K. Siddiqi (Eds.), *Brain, Body and Machine: Proceedings of an International Symposium on the Occasion of the 25th Anniversary of the McGill University Centre for Intelligent Machines* (pp. 1–16). Berlin, Heidelberg: Springer Berlin Heidelberg. http://doi.org/10.1007/978-3-642-16259-6_1

Siegwart, R., Nourbakhsh, I. R., & Scaramuzza, D. (2011). *Introduction to autonomous mobile robots*. *MIT Press*.

Silani, E., & Lovera, M. (2005). Magnetic spacecraft attitude control: a survey and some new results. *Control Engineering Practice*, *13*(3), 357–371. http://doi.org/10.1016/j.conengprac.2003.12.017

Song, L., Li, Z., & Ma, X. (2014). Autonomous rendezvous and docking of an unknown tumbling space target with a monocular camera. In *Proceedings of 2014 IEEE Chinese Guidance, Navigation and Control Conference* (pp. 1008–1013). IEEE. http://doi.org/10.1109/CGNCC.2014.7007346

Song, W., Wang, G., Xiao, J., Wang, G., & Hong, Y. (2012). Research on multi-robot open architecture of an intelligent CNC system based on parameter-driven technology. *Robotics and Computer-Integrated Manufacturing*, *28*(3), 326–333. http://doi.org/10.1016/j.rcim.2011.10.002

Soria, C., Roberti, F., Carelli, R., & Sebastián, J. M. (2008). Control Servo-Visual de un Robot Manipulador Planar Basado en Pasividad. *Revista Iberoamericana de Automática E Informática Industrial RIAI*, *5*(4), 54–61. http://doi.org/10.1016/S1697-7912(08)70177-8

Strom, J., Slavov, G., & Chown, E. (2010). Omnidirectional Walking Using ZMP and Preview Control for the NAO Humanoid Robot. In J. Baltes, M. G. Lagoudakis, T. Naruse, & S. S. Ghidary (Eds.), *RoboCup 2009: Robot Soccer World Cup XIII* (pp. 378–389). Berlin, Heidelberg: Springer Berlin Heidelberg. http://doi.org/10.1007/978-3-642-11876-0_33

Sun, Q., & Gao, F. (2016). An online gait planner of hexapod robot to safely pass through crowded environment based on tactile sense and virtual dynamic model. In *2016 9th International Conference on Human System Interactions (HSI)* (pp. 176–182). http://doi.org/10.1109/HSI.2016.7529628

Tahri, O., Mezouar, Y., Andreff, N., & Martinet, P. (2009). Omnidirectional Visual-Servo of a Gough #x2013;Stewart Platform. *IEEE Transactions on Robotics*, *25*(1), 178–183. http://doi.org/10.1109/TRO.2008.2008745

Takegaki, M., & Arimoto, S. (1981). A New Feedback Method for Dynamic Control of Manipulators. *Journal of Dynamic Systems, Measurement, and Control*, *103*(2), 119. http://doi.org/10.1115/1.3139651

Tatlicioglu, E., Braganza, D., Burg, T. C., & Dawson, D. M. (2009). Adaptive control of redundant robot manipulators with sub-task objectives. *Robotica*, *27*(6), 873. http://doi.org/10.1017/S0263574708005274

Thuilot, B., Martinet, P., Cordesses, L., & Gallice, J. (2002). Position based visual servoing: keeping the object in the field of vision. In *Proceedings 2002 IEEE International Conference on Robotics and Automation (Cat. No.02CH37292)* (Vol. 2, pp. 1624–1629). IEEE. http://doi.org/10.1109/ROBOT.2002.1014775

Tu, Y. W., & Ho, M. T. (2011). Design and implementation of robust visual servoing control of an inverted pendulum with an FPGA-based image co-processor. *Mechatronics*, *21*(7), 1170–1182. http://doi.org/10.1016/j.mechatronics.2011.07.011

Turner, R. F. (1997). Spacecraft Dynamics and Control. A Practical Engineering Approach. *Proceedings of the Institution of Mechanical Engineers*, *211*(6), 431.

Udwadia, F. E. (2003). A new perspective on the tracking control of nonlinear structural and mechanical systems. *Proceedings of the Royal Society A: Mathematical, Physical and Engineering Sciences*, *459*(2035), 1783–1800. http://doi.org/10.1098/rspa.2002.1062

Wang, S., Ye, A., Guo, H., Gu, J., Wang, X., & Yuan, K. (2016). Autonomous pallet localization and picking for industrial forklifts based on the line structured light. In *2016 IEEE International Conference on Mechatronics and Automation* (pp. 707–713). http://doi.org/10.1109/ICMA.2016.7558649

Wang, T. (2010). Analysis of Debris from the Collision of the Cosmos 2251 and the Iridium 33 Satellites. *Science & Global Security*, *18*(2), 87–118. http://doi.org/10.1080/08929882.2010.493078

Wang, Y. (2016). *A Visual Servoing Approach to Human-Robot Interactive Object Transfer*. BoD.

Wang, Y., Lang, H., & de Silva, C. W. (2009). A robust mobile robot manipulation system using a switch-based visual-servo controller. In *Industrial Mechatronics and Automation, 2009. ICIMA 2009. International Conference on* (pp. 364–367). http://doi.org/10.1109/ICIMA.2009.5156638

Wang, Y., Thunberg, J., & Hu, X. (2012). A transformation of the Position Based Visual Servoing Problem into a convex optimization problem. In *2012 IEEE 51st IEEE Conference on Decision and Control (CDC)* (pp. 5673–5678). IEEE. http://doi.org/10.1109/CDC.2012.6426022

Wie, B. (1998). *Space vehicle dynamics and control*. Aiaa.

Wilson, W. J., Williams, C. C., & Bell, G. S. (1996). Relative end-effector control using Cartesian position based visual servoing. *IEEE Transactions on Robotics and Automation*, *12*(5), 684–696. http://doi.org/10.1109/70.538974

Woffinden, D. C., & Geller, D. K. (2009). Observability Criteria for Angles-Only Navigation. *IEEE Transactions on Aerospace and Electronic Systems*, *45*(3), 1194–1208. http://doi.org/10.1109/TAES.2009.5259193

Woods, J. O., & Christian, J. A. (2016). Lidar-based relative navigation with respect to non-cooperative objects. *Acta Astronautica*, *126*, 298–311. http://doi.org/10.1016/j.actaastro.2016.05.007

Xian, B., De Queiroz, M. S., Dawson, D., & Walker, I. (2004). Task-space tracking control of robot manipulators via quaternion feedback. *IEEE Transactions on Robotics and Automation*, *20*(1), 160–167. http://doi.org/10.1109/TRA.2003.820932

Xie, W. F., Li, Z., Tu, X. W., & Perron, C. (2009). Switching Control of Image-Based Visual Servoing With Laser Pointer in Robotic Manufacturing Systems. *IEEE Transactions on Industrial Electronics*, *56*(2), 520–529. http://doi.org/10.1109/TIE.2008.2003217

Yang, H., Jin, M., Xie, Z., Sun, K., & Liu, H. (2014). Ground verification of space robot capturing the free-floating target based on visual servoing control with time delay. *Industrial Robot: An International Journal*, *41*(6), 543–556. http://doi.org/10.1108/IR-05-2014-0339

Yoshida, K. (2003). Engineering Test Satellite VII Flight Experiments for Space Robot Dynamics and Control: Theories on Laboratory Test Beds Ten Years Ago, Now in Orbit. *The International Journal of Robotics Research*, *22*(5), 321–335. http://doi.org/10.1177/0278364903022005003

Yoshikawa, T. (1985a). Dynamic manipulability of robot manipulators. In *Proceedings. 1985 IEEE International Conference on Robotics and Automation* (Vol. 2, pp. 1033–1038). Institute of Electrical and Electronics Engineers. http://doi.org/10.1109/ROBOT.1985.1087277

Yoshikawa, T. (1985b). Manipulability of Robotic Mechanisms. *The International Journal of Robotics Research*, *4*(2), 3–9. http://doi.org/10.1177/027836498500400201

Yu, F., He, Z., Qiao, B., & Yu, X. (2014). Stereo-Vision-Based Relative Pose Estimation for the Rendezvous and Docking of Noncooperative Satellites. *Mathematical Problems in Engineering*, *2014*, 1–12. http://doi.org/10.1155/2014/461283

Zergeroglu, E., Dawson, D. D., Walker, I. W., & Setlur, P. (2004). Nonlinear tracking control of kinematically redundant robot manipulators. *IEEE/ASME Transactions on Mechatronics*, *9*(1), 129–132. http://doi.org/10.1109/TMECH.2004.823890

Zhang, L., Slaets, P., & Bruyninckx, H. (2012). An open embedded hardware and software architecture applied to industrial robot control. In *2012 IEEE International Conference on Mechatronics and Automation* (pp. 1822–1828). http://doi.org/10.1109/ICMA.2012.6285098

Zhang, L., Slaets, P., & Bruyninckx, H. (2014). An open embedded industrial robot hardware and software architecture applied to position control and visual servoing application. *International Journal of Mechatronics and Automation*, *4*(1), 63. http://doi.org/10.1504/IJMA.2014.059775

Universitat d'Alacant
Universidad de Alicante

ED|UA Escola de Doctorat
Escuela de Doctorado

edua.ua.es